Biogéochimie du fer et des éléments associés : Exemple de l'arsenic (V)

Mohamad Fakih

N° ORDRE : 3788
de la thèse

THÈSE

Présentée

DEVANT L'UNIVERSITÉ DE RENNES 1

pour obtenir

Le grade de : ***DOCTEUR DE L'UNIVERSITÉ DE RENNES 1***

Mention : **Sciences de la Terre**

PAR

Mohamad FAKIH

Équipe d'accueil: **Géosciences Rennes**

École Doctorale : **Sciences de la Matière**

Composante universitaire: **UFR Structure et Propriétés de la Matière**

Biogéochimie du fer et des éléments associés : exemple de l'arsenic (V)

Soutenue le 24 octobre 2008 devant la commission d'examen

COMPOSITION DU JURY :

Rapporteurs	Danielle Fortin	Université d'Ottawa (Canada)
	Oleg Pokrovsky	Université de Toulouse
Examinateurs	Guillaume Morin	Universités Paris 6 et 7 - IPGP
	Bernd Nowack	EMPA – St. Gallen (Suisse)
Directeurs de thèse	Aline Dia	Université de Rennes 1
	Mélanie Davranche	Université de Rennes 1
	Xavier Châtellier	Université de Rennes 1

REMERCIEMENT

Je tiens à remercier toutes les personnes qui sont intervenues d'une manière directe ou indirecte au cours de cette thèse.

C'est un plaisir de remercier Aline Dia, Mélanie Davranche et Xavier Châtellier pour m'avoir confié ce sujet de thèse. Merci à tous les trois pour votre confiance, votre disponibilité et votre enthousiasme. Je ne vous remercierai jamais assez.

Aline, milles merci pour ta direction pour la thèse, ta disponibilité, mais aussi pour ta gentillesse, ta patience, grâce à toi j'ai réussi de rester très bien orienter vers les objectifs de la thèse.

Mélanie, tu m'as fait découvrir le monde de terrain et la réduction du fer, je te remercie très profondément pour ton encadrement, ton intelligence, tes immenses connaissances dans ces domaines, tes belles critiques scientifiques et tes suggestions innombrables qui m'ont beaucoup servi.

Xavier, tu m'as fait découvrir le monde scientifique de l'autre bout de la terre mais aussi la biominéralisation, milles merci pour tes conseils avisés, et ton soutien permanent.

J'exprime également toute ma gratitude à Danielle Fortin et Oleg Pokrovsky pour avoir accepter d'être rapporteurs de ce mémoire.

Je remercie les membres du jury, Bernd Nowack et Guillaume Morin qui m'ont fait l'honneur de juger ce travail, mais aussi à leurs aides précieuses concernant les analyses minéralogiques XRF, DRX et XANES, les discussions scientifiques et leurs remarques.

J'exprime toute ma reconnaissance à toutes les personnes qui à un moment ou un autre, se sont intéressées à mes recherches. Parmi celles-ci je cite notamment tout le personnel du laboratoire de Géosciences Rennes à l'Université de Rennes1. Mais surtout tous les membres de l'équipe «Biogéochimie». J'ai eu un grand plaisir de travailler à leur côté dans une ambiance très agréable et conviviale. Je tiens à remercier Gérard Gruau pour ses conseils et les discussions passionnées et pour les renseignements précieux. Je remercie également Emilie Jardé, Anne-Catherine Pierson-Wickmann pour les discussions scientifiques.

Cette thèse, qui a un important volet expérimental, n'aurait pas pu voir le jour sans un fort appui technique. Je tiens à remercier Patrice Petitjean, d'abords pour sa compagnie de terrain, les montages et les mis en point de colonne du sol, la synthèse des plaquettes, la préparation du terrain et surtout pour les discussions scientifiques intéressantes et son amitié. Mille mercis à Odile et Martine pour les analyses analytiques (Chromatographie et ICP-MS) et pour leurs discussions

toujours enrichissantes. Je remercie également Jean-Pierre Caudal pour la fabrication des plaquettes.

Mes reconnaissances à Olivier Dauteuil et Nathalie Celton pour leurs aides et leurs soutiens.

Je remercie Chris Daugney de m'avoir accueilli à Taupo (Nouvelle-Zélande) à Geology and Nuclear Science (GNS) pour le séjour scientifique très enrichissant, ainsi que pour les discussions scientifiques.

Je remercie également toutes les personnes extérieures au laboratoire qui ont contribué à l'avancement de mes travaux : Yohan Wang (IMPMC- Universités Paris 6 et 7) pour le traitement de donnée XANES, Yannick Benard (INRA-Agrocampus Rennes) pour l'induration de la colonne du sol, Xavier Le Coz pour la préparation de plaquettes pour le NanoSIMS, Thomas Delhaye pour les analyses des échantillons au NanoSIMS. Un grand merci à Jo Le Lannic et Sandra Casale du CMEBA, Université de Rennes 1, pour les observations microscopiques et les analyses élémentaires.

Merci pour les collocs de bureau et de labo pour leurs soutiens, Olivier, Gocha, Mathieu (bonne chance pour la fin de ta thèse), Raul, Selva, Dominique, Emilie, Jennifer, Jessy, Nicolas, Rémi, Thibault, Rita, Emmanuel, Vincent, Chrystelle, Jo, Loïc, et ceux que j'oublie.

Merci pour mes amis en France, A. Chamas, A. Lhaf, F. Assi, J. Dakhlalah, M.A. Noureddine, M. Hoteit, M. Mroué, R. Makké, S. Nahlé, et ceux que j'oublie.

Je remercie ma famille et surtout ma mère, qui ont toujours cru en moi depuis le début, et qui m'ont toujours été présents lorsque j'en ai eu besoin.

Enfin, je réserve une mention particulière à Hiba.

A tous, MERCI…

TABLE DES MATIERES

Introduction générale

I. INTRODUCTION

1. CONTEXTE

1.1. Le fer dans le milieu naturel

Le fer (Fe), 4ème élément de la croûte terrestre, 2ème métal le plus abondant dans la Terre (Schwertmann et Cornell, 1991), est présent dans les sols, essentiellement dans les minéraux primaires issus de la roche mère ou secondaires formés lors de l'altération des roches (oxydes, silicates, carbonates, sulfures, phosphates). Le fer est un élément qui présente une très forte réactivité grâce à ses capacités de sorption et ses propriétés rédox. Ainsi les cycles biogéochimiques de nombreux éléments (*e.g.* As, P, Pb) sont contrôlés par sa spéciation. En milieu réduit, la dissolution des phases minérales riches en fer (oxydes, hydroxydes, oxyhydroxydes…) peut augmenter la mobilité des éléments qui lui sont associés. Au contraire, en milieu oxydant, leur mobilité est réduite par 'piégeage' à la surface en réponse à des processus d'adsorption ou dans la structure du solide par coprécipitation. De plus, si l'on considère que la plupart des réactions de dissolution ou précipitation du fer se produit par voie microbienne, la disponibilité et la transformation du fer jouent un rôle essentiel sur le cycle global du carbone.

Dans les sols et les environnements sédimentaires, la stabilité, la surface spécifique, la porosité, le taux de dissolution, et la cinétique de transformation des oxydes de fer sont contrôlés par leur structure cristalline (Cornell et Schwertmann, 1996). La précipitation et la dissolution de ces oxydes de Fe sont dépendantes des conditions de pH, de l'état d'oxydo-réduction du milieu et de la présence de ligands organiques (McBride, 1994). Les paramètres chimiques et physico-chimiques (pH, Eh, présence de ligands, température et régime hydrique) sont eux-mêmes souvent sous la dépendance des activités microbiennes qui les modifient en permanence.

Le fer ferrique est en général insoluble, mais il présente une très faible solubilité exceptée dans certaines conditions acides, réduites ou en présence de ligands. Par hydrolyse, les ions Fe^{3+} peuvent précipiter sous la forme d'oxydes de fer cristallisés comme la goethite, l'hématite, l'akaganéite et nanocristallins comme la ferrihydrite (Fig. I.1). La solubilisation du fer aboutit le plus souvent à la formation de fer ferreux ionique ou complexé, sauf en milieu très acide. Dans le milieux naturel, le Fe(II) peut s'adsorber sur les surfaces minérales ou microbiennes présentes ou précipitées en milieu oxydant pour former des solides riches en Fe peu cristallisés, cristallisés ou mixtes de type hydroxydes de magnétite ($Fe^{II}Fe^{III}{}_2O_4$), vivianite ($Fe(PO_4)_2.nH_2O$), Fe(II) et Fe(III) (rouilles vertes), sidérite ($FeCO_3$), hydroxyde de carbonate ferreux ($Fe^{II}{}_2(OH)_2CO_3$) et amakinite ($(Fe^{2+},Mg)(OH)_2$) (Lovley et al., 1987 ; Lovley et Phillips, 1988 ; Mortimer et Coleman, 1997 ; Fredrickson et al., 1998 ; Cooper et al., 2000 ; Ona-Nguema et al., 2002 ; 2004 ; 2008 soumis ; Zachara et al., 2002 ; Fredrickson et al., 2003). Ces solides peuvent eux-mêmes évoluer, en fonction des conditions du milieu, vers des structures cristallisées comme la lépidocrocite, la feroxyhite, la maghémite et l'hématite (Schwertmann et Cornell, 2000) (Fig. I.1).

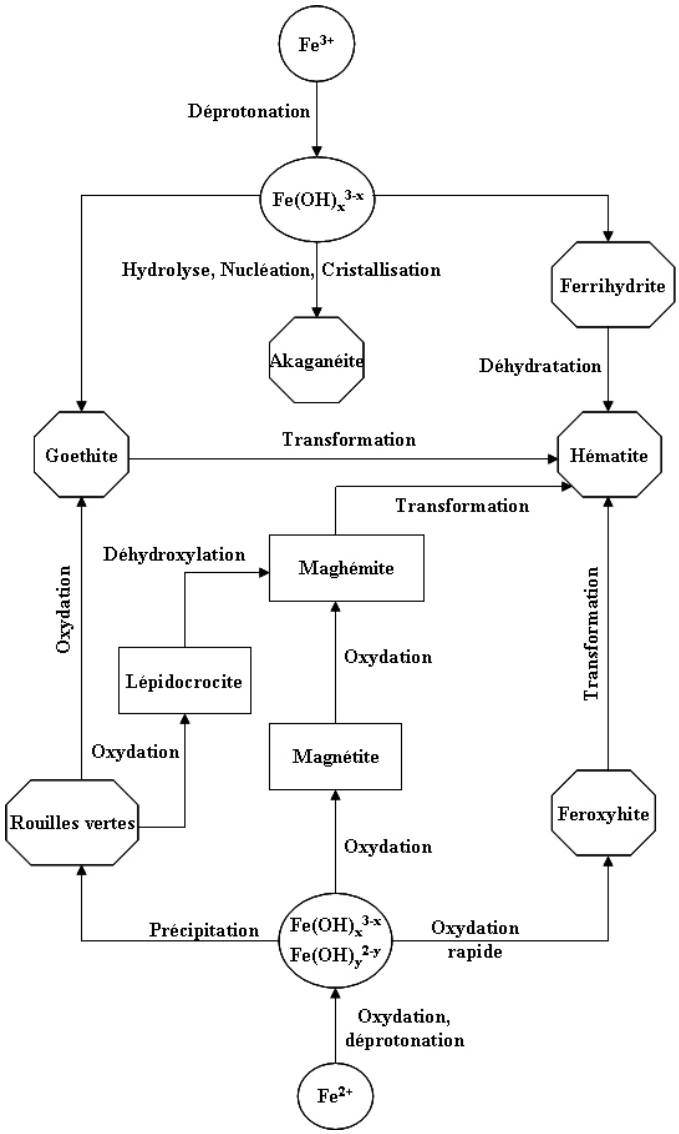

Figure I.1. Présentation schématique des voies de transformations des oxydes de fer les plus fréquentes (Schwertmann et Cornell, 2000).

1.2. Les oxyhydroxydes de fer

Les oxyhydroxydes de fer sont des phases minérales ubiquistes dans les sols. Leurs solubilités contrôlent la biodisponibilité du fer. Leur stabilité thermodynamique est elle-même fonction de leur structure cristalline (Cornell et Schwertmann, 2003). Il existe une grande variété d'oxyhydroxydes de Fe qui présentent des tailles de cristaux différents (Cornell et Schwertmann, 2003). A l'état naturel, ils se trouvent très rarement sous forme de phases pures. Le tableau I.1 regroupe les oxyhydroxydes les plus communément étudiés dans la littérature ainsi que leurs propriétés physico-chimiques. La solubilité des oxyhydroxydes augmente en général dans l'ordre goethite<lépidocrocite<ferrihydrite.

Les oxyhydroxydes de fer sont formés à partir de l'hydrolyse de Fe(III) ou de l'oxydation abiotique ou biotique de Fe(II) (Ehrenreich and Widdel, 1994; Emerson and Moyer, 1997; Cornell and Schwertmann, 2003). De plus, en fonction des conditions du milieu et de leur stabilité, certains oxyhydroxydes peuvent se transformer en d'autres oxyhydroxydes souvent plus stables. Par exemple, la ferrihydrite qui est thermodynamiquement métastable peut se

transformer en goethite ou hématite en conditions oxiques (Cornell and Schwertmann, 2003). Cependant, les cinétiques de transformation sont lentes en l'absence de catalyseurs. Certains cations, anions ou molécules neutres peuvent modifier les taux de dissolution ou de transformation (Cornell and Schwertmann, 2003).

Tableau I.1. Propriétés physico-chimiques des oxyhydroxydes de fer les plus étudiés dans la littérature.

	Ferrihydrite	Lépidocrocite	Goethite
Formule	$Fe_{10}O_{14}(OH)_2$	γ-FeOOH	α-FeOOH
Système cristallin	Hexagonal	Orthorhombique	Orthorhombique
Morphologie principale	--	Ecailles	Aiguilles
Surace spécifique moyenne ($m^2.g^{-1}$)	100-700	15-260	8-200
Energie libre standard ($KJ.mol^{-1}$)	-699	-477.7	-488.6
Produit de solubilité (25°C) (log Kso)	-39	-39.5	-40.7

Etant donnée leur ubiquité et leur réactivité, les oxyhydroxydes de fer jouent un rôle important dans le contrôle de la mobilité des éléments traces (nutriments, métaux toxiques…). Ces éléments peuvent être adsorbés à leur surface retardant ainsi la dissolution lors des processus de dissolution réductrice par exemple. Ils peuvent également être mis en jeu dans des substitutions isomorphiques aux sein des structures cristallines des oxyhydroxydes de Fe(III) influençant ainsi leur morphologie, la taille des cristaux, leur surface spécifique, leur réactivité de surface et en conséquence leur taux de dissolution en milieux acides ou réduits (Schwertmann et Latham, 1986 ; Fisher, 1988 ; Rajot, 1992 ; Bousserrhine, 1995 ; Trolard et Tardy, 1989 ; Davranche et Bollinger, 2000a ; Cornell and Schwertmann, 2003**).** La plupart des métaux substitués au sein des oxyhydroxydes de Fe(III) modifie la solubilité des oxydes et ralentit leur transformation en un autre oxyde de fer par rapport à leur homologue pur (Trolard et Tardy, 1989 ; Cornell and Schwertmann, 2003).

1.3. L'oxydo-réduction du fer

La mobilisation du fer est très fortement contrôlée par les conditions oxydo-réductrices du milieu (Fig. I.2). En conditions oxydantes et à des pH élevés, le fer ferreux est rapidement oxydé en fer ferrique (Stumm et Morgan, 1996) alors qu'en condition réductrices, le fer est sous forme Fe(II) soluble. Ces processus de dissolution/précipitation peuvent être biotiques ou abiotiques. Les micro-organismes peuvent transformer le fer par bio-oxydation (aboutissant à une biominéralisation) ou bio-réduction (aboutissant à une biodissolution) soit, par voie directe (transformation enzymatique ou fixation à des protéines spécifiques) soit de manière indirecte en modifiant les conditions d'oxydoréduction du milieu (pH et/ou Eh) par production d'acides, de complexants ou de réducteurs (Francis, 1988 ; Ehrlich, 1990 ; Lovley, 1991 ; Bousserrhine, 1995).

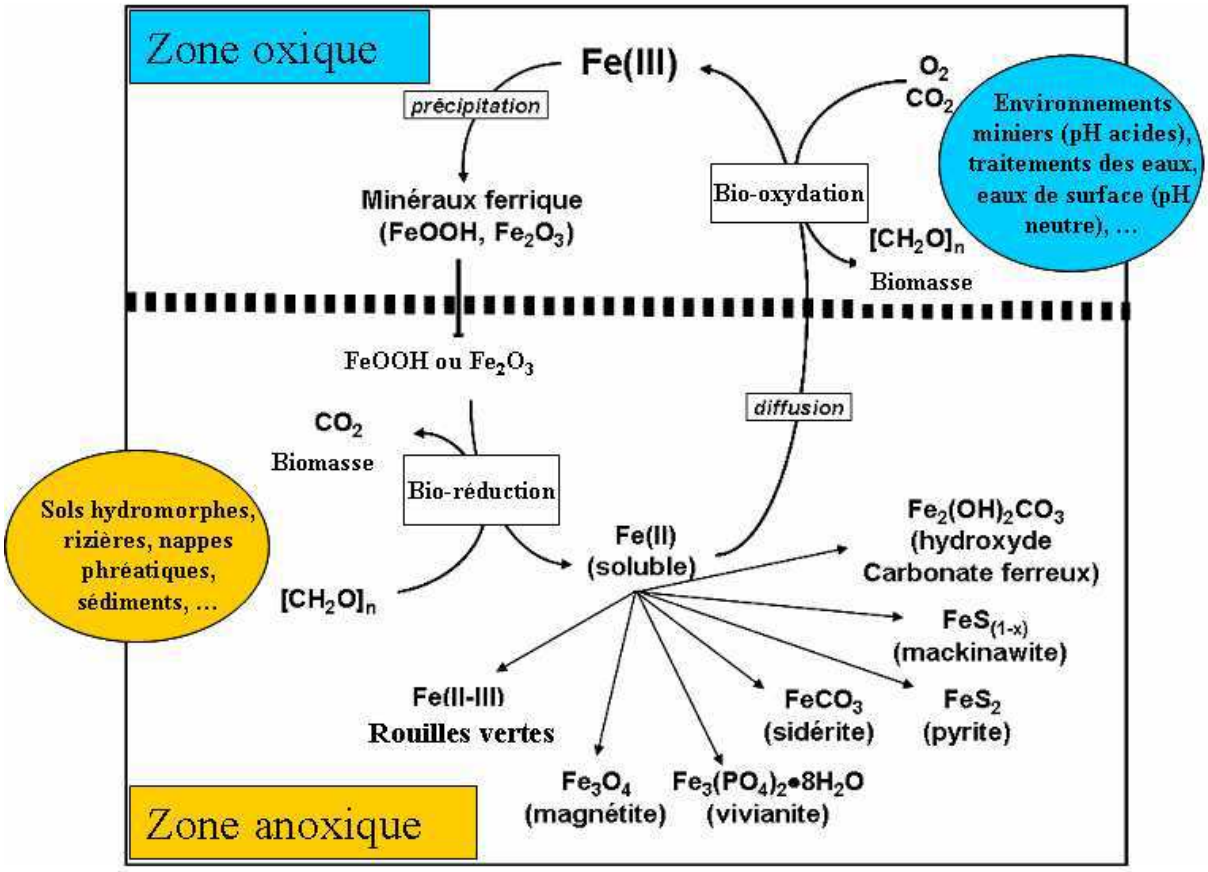

Figure I.2. Modèle du cycle rédox biogéochimique du fer dans les sols. Figure modifiée d'après Ona-Nguema (2003).

1.3.1. La bio-oxydation/biominéralisation

Dans les lacs, les zones humides et les sédiments, des épisodes d'oxydation du fer se produisent périodiquement, notamment en fin de cycle hydrologique, lorsque les zones humides s'assèchent (réoxydation du Fe(II)). Certaines bactéries comme *Gallionella ferruginea* et *Leptothrix* (Widdel et al., 1993) peuvent, en présence d'oxygène induire l'oxydation du Fe^{2+} pour des pH proches de la neutralité et comme *Acidithiobacillus ferrooxidans*, pour des pH acides. Très récemment, plusieurs auteurs ont montré que certaines bactéries étaient même capables de produire des oxydes de Fe en milieu anaérobie (Widdel et al., 1993 ; Straub et al., 1996, 2004 ; Kappler et Newman, 2004).

Les particules d'oxydes de fer peuvent être produites soit, en surface des cellules bactériennes soit, à l'intérieur de ces cellules. Les oxydes de fer formés à la surface et à l'intérieur sont appelés respectivement minéraux biogéniques extracellulaires et intracellulaires (Fortin et Langley, 2005) (Fig. I.3).

Les processus de biominéralisation sont dépendants : (a) de la croissance de phases minérales, (b) de la présence de molécules structurantes, (c) de l'espace disponible (matrice, vésicule), et (d) des cellules microbiennes elles-mêmes (surface, concentration, propriétés de surface….) (Fortin et Langley, 2005). Les micro-organismes sont capables d'associer intimement leurs constituants organiques cytoplasmiques ou extracellulaires à divers minéraux, qui se retrouvent ainsi soit, intégrés au sein des cellules soit, plus ou moins intimement associés à des matrices extracellulaires souvent très spécifiques. Dans les deux

cas, il apparaît clairement que ce sont les activités biologiques cellulaires qui contrôlent directement ou indirectement la production, le dépôt, voire parfois la résorption des biominéraux. Ce contrôle est intégré de façon à la fois hiérarchique et globale, depuis l'activité de la cellule individuelle jusqu'au déterminisme de la morphologie de l'organisme entier (Ricqlès et Livage, 2004).

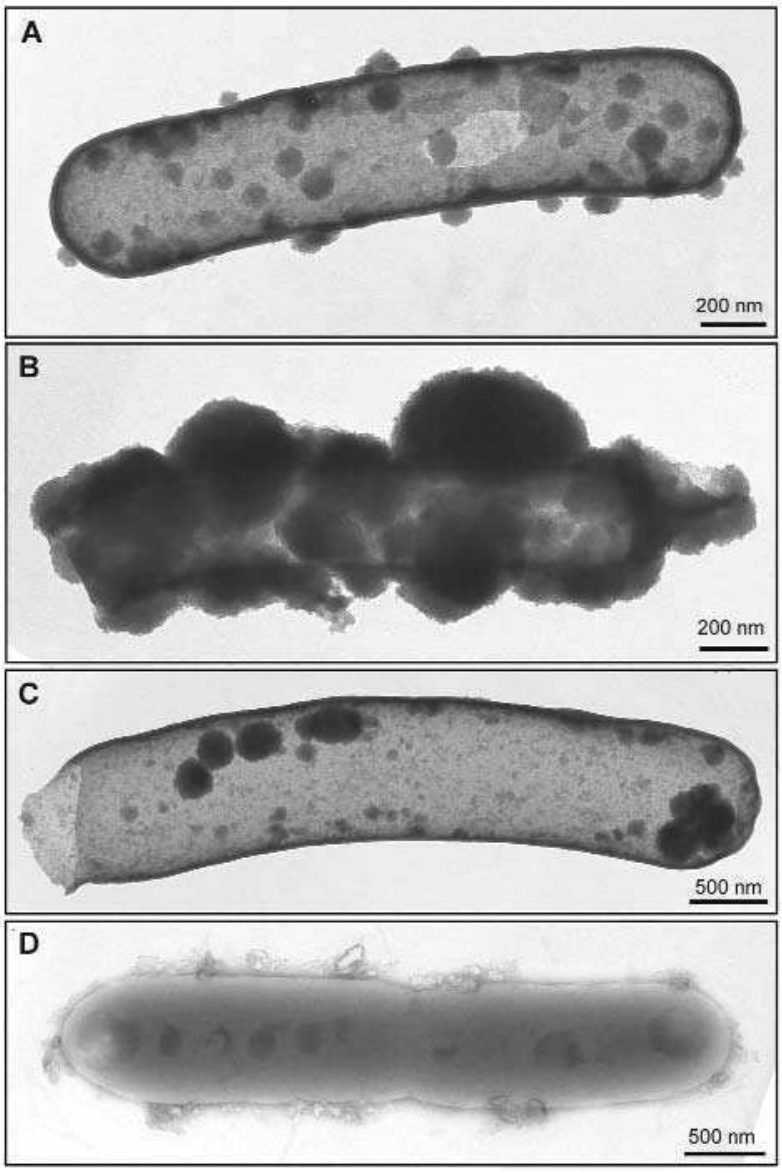

Figure I.3. Observations réalisées au microscopique eletronique à transmission (MET) des oxydes de fer amorphes intra- (A et B) et extracellulaire (C) sur des bactéries. La formation des aggrégats des minéraux amorphes ont été observé à la surface cellulaire des bactéries ferro-oxydantes cultivées aux laboratoires (D). (Belkova et al., 2004).

1.3.2. La bio-réduction ou biodissolution

Dans les environnements anoxiques, comme les lacs, les marais, les sols hydromorphes, certains micro-organismes sont capables, en absence d'oxygène, de réduire les oxyhydroxydes de fer par un processus de respiration dissimilatrice couplé à l'oxydation de la matière organique (e.g. Lovley et al., 1987 ; Lovley et Phillips, 1988 ; Roden et Lovley,

1993 ; Loveley, 2000 ; Zachara et al., 2001 ; 2002 ; Roden, 2006) (Fig. I.4). Le Fe(II) est alors mobile ou peut à son tour précipiter pour former des minéraux secondaires dans les sols et les sédiments. Les principaux minéraux observés en conditions réductrices sont la magnétite ($Fe^{II}Fe^{III}{}_2O_4$), vivianite ($Fe(PO_4)_2.nH_2O$), Fe(II) et Fe(III) (rouilles vertes), sidérite ($FeCO_3$), hydroxyde de carbonate ferreux ($Fe^{II}{}_2(OH)_2CO_3$) et amakinite ($(Fe^{2+},Mg)(OH)_2$) (Lovley et al., 1987 ; Lovley et Phillips, 1988 ; Mortimer et Coleman, 1997 ; Fredrickson et al., 1998 ; Cooper et al., 2000 ; Ona-Nguema et al., 2002 ; 2004 ; 2008 soumis ; Zachara et al., 2002 ; Fredrickson et al., 2003).

Les oxydes de fer nano-cristallins sont plus facilement réduits par les micro-organismes que les oxydes de fer cristallisés (Ehrlich, 1990 ; Lovley et Phillips, 1986a ; Munch et Ottow, 1980). La dissolution microbienne des oxydes de fer se produit selon plusieurs mécanismes. Des mécanismes directs, nécessitant un contact entre le métal et les micro-organismes et des mécanismes indirects, où la transformation chimique du métal s'effectue à distance par l'intermédiaire de produits du métabolisme microbien (Pelmont, 1993).

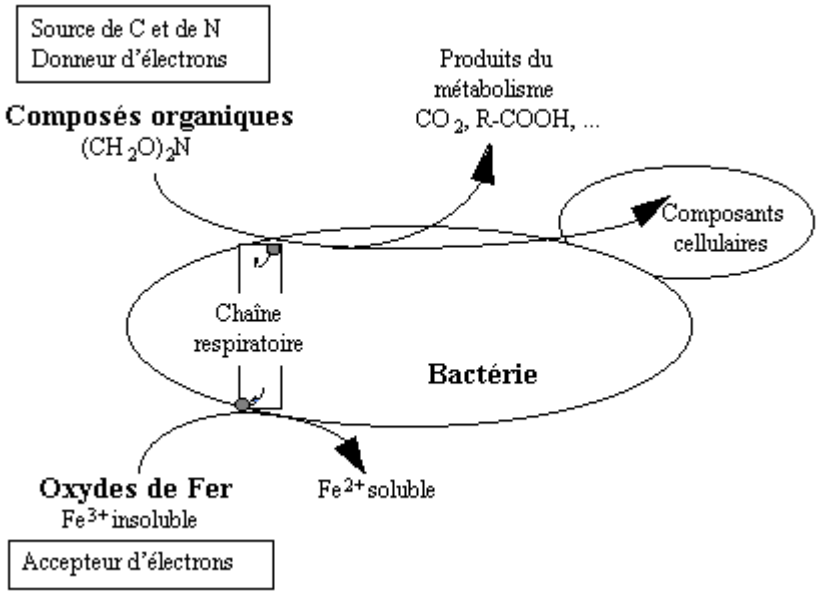

Figure I.4. Schéma fonctionnel d'une bactérie ferri-réductrice.

Le phénomène de réduction dissimilatrice s'accompagne de l'oxydation complète de la matière organique utilisée, jusqu'au stade CO_2, avec réduction d'une quantité correspondante de Fe(III). Sans ce métabolisme le fer joue le rôle d'accepteur final d'électrons soit, principal dans le cas de processus de respiration anaérobie. Il existe aussi des métabolismes où le Fe(III) joue le rôle d'accepteur d'éléctron annexe au cours de processus de fermentation (Lovley, 1991 ; Bousserrhine, 1995). Dans les deux cas, l'oxydation a lieu au détriment de l'hydrogène, de l'acétate, d'acides organiques et de nombreux produits aromatiques issus de la décomposition de végétaux (Pelmont, 1993 ; Ehrlich, 1990). Bien que ces métabolismes aient été très largement étudiés, la biochimie et les mécanismes de réduction du Fe(III) restent mal connus. Les mécanismes proposés actuellement sont en partie enzymatiques et varient en fonction de la nature du milieu. Dans certain cas, il a été montré que le contact entre la bactérie et l'oxyde de fer est nécessaire à la réduction (Arnold et al., 1990 ; Bousserrhine, 1995).

Dans le cas des mécanismes indirects, les micro-organismes produisent des agents réducteurs dans le milieu (oxalate, pyruvate...) (Francis, 1988 ; Lovley, 1991 ; Bousserhine, 1995) ou encore utilisent les vavettes à éléctron, molécules qui transportent les éléctrons

(substances humiques) (Lovvley, 1991). Pour cela, il est nécessaire que les bactéries puissent trouver une source de carbone fermentescible (substances humiques, catéchols, hydroxyquinones...). Dans certains cas, le profit d'un tel mécanisme pour la bactérie est minime. Les oxydes métalliques sont utilisés comme réceptacles des réducteurs intracellulaires sécrétés lors de la croissance en milieu anaérobie (Brown et al., 1999).

1.4. Le cycle du fer et des éléments associés

L'ubiquité du fer dans les milieux continentaux, couplée à ses différents degrés d'oxydation et à sa spéciation, en fait un facteur important de contrôle de la mobilité des éléments dans le milieu. Bien que représentant une faible partie du poids sec du matériel particulaire (entre 1 et 5%) et souvent mal cristallisés dans les environnements de surface, les oxyhydroxydes de fer possèdent en effet de très grandes surfaces spécifiques sur lesquelles les cations métalliques ou les anions (phosphates ou nitrates, par exemple) peuvent se fixer (Stumm et Morgan, 1996 ; Sigg et al. 2000). Les éléments peuvent soit s'adsorber à leur surface soit dans certains cas être séquestrés par co-précipitation (Cr, V, Co…) (Stumm et Morgan, 1996 ; Warren et Haack, 2001).

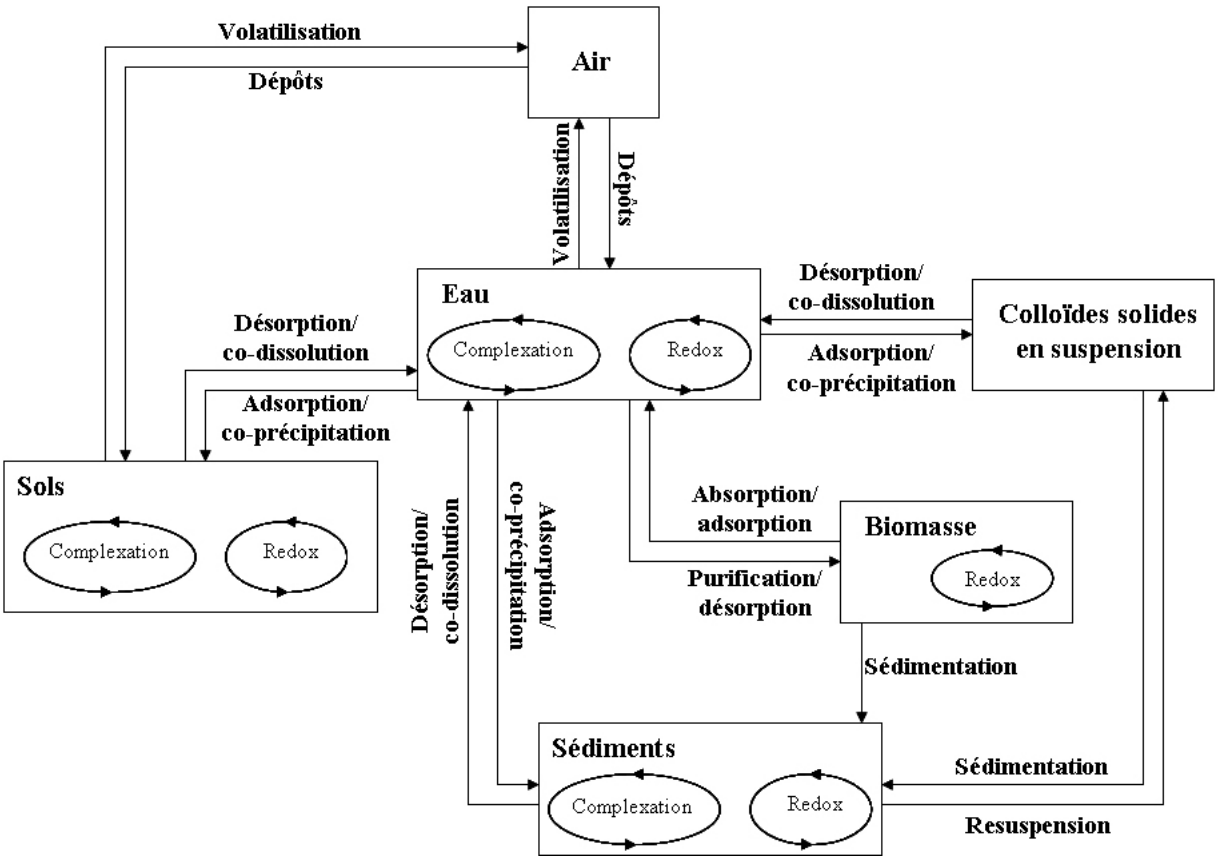

Figure I .5. Schéma des processus qui contrôlent le cycle biogéochimique des métaux dans les environnements aquatiques (Hering et Kraemer, 1998)

Si les processus biogéochimiques gouvernent la distribution des métaux dans différents compartiments environnementaux (Fig. I.5), la part respective des différents mécanismes impliqués dans la séquestration des métaux varie d'un milieu à l'autre. Ainsi, l'adsorption des métaux sur les oxyhydroxydes de fer est un processus important dans les sols et les aquifères puisque la faible biomasse qu'elles contiennent, rend les processus d'adsorption ou de

complexation par la matière organique négligeable (Freeze et Cherry, 1979). Il a été proposé que dans les eaux de surface océaniques ou lacustres, la dynamique des métaux est régulée par la séquestration biologique phytoplanctonique et/ou l'adsorption par des surfaces alguales (Gordon et al., 1982). En réalité la situation est beaucoup plus complexe et on connait mal l'importance relative des formes organiques et minérales des métaux dans les eaux de surface. Dans les milieux anoxiques (zones humides, fonds de lacs, sédiments…), la solubilité du Fe(II) issu de la réduction biotique ou abiotique d'oxyhydroxydes de Fe(III), est contrôlée par des minéraux contenant du fer réduit comme des hydroxydes et sulfures de Fe(II)/Fe(III). Néanmoins, la distribution et les conditions de formation de ces minéraux parfois peu stables (rouilles vertes) dans les sols restent mal contraintes. Ces minéraux représentent pourtant une étape clé du cycle biogéochimique du fer et donc des éléments traces associés.

Les oxyhydroxydes de fer, peuvent également servir de catalyseurs dans le cycle de métaux rédox sensibles comme l'arsenic ou le chrome (Deng et Stumm, 1994). Dans le milieu naturel, les minéraux de fer peuvent jouer un rôle réel de 'détoxification' dans les eaux, les sols, et les sédiments au travers de réactions rédox. A titre d'exemple, il a été montré que la réduction du Cr(VI), espèce toxique en Cr(III) était accélérée par la présence de goethite et de lépidocrocite, le transfert d'électrons étant facilité par l'adsorption de Fe^{2+} à la surface des solides. De même, la ferrihydrite transforme le Sb(III) toxique en Sb(V) plus inoffensif (Belzile et al., 2001). Dans les eaux de drainage d'exploitations minières abandonnées, des oxydes de fer amorphes peuvent précipiter entraînant avec eux un certain nombre d'éléments comme le Sr, Cs, Pb ou U. En revanche, la réduction biotique de l'U(VI) mobile en U(IV) insoluble peut être diminuée par la présence d'oxydes de fer réduits préférentiellement à l'uranium (Wielinga et al., 2000). Le Co(III) peut lui, se substituer au fer dans la goethite lors de la précipitation. Ensuite lors d'une réduction biotique, le Co(II) reste adsorbé sur la goethite restante (Zachara et al., 2001). Le nickel co-précipite avec les oxyhydroxydes de fer et il a été montré que sa présence, même en faible quantité, retardait la bio-réduction de la ferrihydrite (Fredrickson et al., 2001).

Ces quelques exemples non exhaustifs, montrent donc, que les cycles biogéochimiques d'un certain nombre d'éléments traces, dont les métaux, sont intimement liés au cycle du fer et à la capacité de séquestration des oxyhydroxydes de fer. A ce titre, au-delà des connaissances fondamentales, les enjeux environnementaux liés à la compréhension des dynamiques spatio-temporelles des oxyhydroxydes de fer, portent sur la dépollution et la remédiation des milieux naturels ou les problèmes de traitements des eaux à des fins de potabilisation et concernent des éléments traces variés (Hg, As, Sb, Se, Cu, Zn, Pb, U, Ni, Co, Cr, Cd…).

2. CIBLES D'ETUDE

2.1. Les surfaces bactériennes et la bio-oxydation du fer

Les minéraux biogéniques sont des minéraux qui se forment en présence de micro-organismes. Les plus fréquents dans l'environnement sont les oxydes de fer et de manganèse, les sulfures (de métaux lourds), les silicates, et les minéraux carbonatés (Fortin, 2004 ; Fortin et Langley, 2005 ; Fortin et al., 1998, 2007). Leur formation peut être passive ou active (Fortin, 2004). Le fer (III) qui s'adsorbe très fortement sur les surfaces bactériennes, forme fréquemment des précipités d'oxydes de fer insolubles sur les surfaces bactériennes (Mayers et Beveridge, 1989 ; Ferris et al., 1989 ; Konhauser et Ferris, 1996). Les mécanismes actifs sont reliés à l'activité métabolique des bactéries qui engendre des gradients chimiques

pouvant mener à la sursaturation de la solution et à la précipitation de minéraux. Les mécanismes passifs sont eux, reliés à la réactivité de la paroi cellulaire des bactéries (Daughney et Fortin, 2006 ; Fortin et Langley, 2005 ; Châtellier et Fortin, 2004 ; Fortin, 2004 ; Fortin et Beveridge, 2000 ; Fortin et al., 1997 ; Châtellier et al., 2001, 2004). Ce sont précisément ces mécanismes passifs, ou plus exactement les réactions non métaboliques qui nous intéressent dans la première partie du travail. Il a souvent été montré que les bactéries, du fait de la présence de groupements chimiques réactifs à leur surface, catalysaient l'oxydation du fer et la précipitation d'oxydes de fer (Ferris et al., 1989). Warren et Ferris (1998) ont montré lors d'une étude de l'hydrolyse du Fe(III) en présence et en absence de bactéries que les taux d'extraction du fer dans les systèmes biotiques étaient plus élevés que dans les systèmes abiotiques. Ils ont alors émis l'hypothèse que la précipitation du fer était influencée par la présence de sites de nucléation à la surface des bactéries et par conséquent que la précipitation du fer était une conséquence directe de son adsorption. De plus, les observations des cellules biominéralisées dans le milieu naturel suggèrent que les cellules ou les polymères exocellulaires qu'elles sécrètent servent de surfaces ou de lignes de nucléation (Fortin et al., 1998). Châtellier et al., (2001, 2004) ont également montré qu'une oxydation rapide de Fe(II) en présence de bactéries provoquait la formation de lépidocrocite et de ferrihydrite sur et près de la surface des cellules (Fig. I.3).

La présence de bactéries affecte également la morphologie des cristaux de lépidocrocite comparée à celle observée dans des systèmes abiotiques (Châtellier et al., 2001). Cependant, des études menées en présence de bactéries, de Fe et de Si, SO_4^{2-} ou PO_4^{3-} en concentrations typiques de celles des eaux naturelles ont montré que la présence de bactéries avait un effet minime sur la morphologie des oxydes suggérant que la présence des anions était le facteur dominant de la nucléation et de la précipitation des oxydes (Fortin et Langley, 2005). Ces différentes études montrent qu'il est actuellement difficile de savoir si les surfaces bactériennes jouent le rôle de matrice pour la formation des oxydes de fer dans l'environnement. Concernant la bio-oxydation du fer, plusieurs points restent également à éclaircir. En effet, si Châtellier et al. (2001 ; 2004) ont montré que l'oxydation de Fe(II) en présence de bactéries provoquait la précipitation d'oxydes de fer à la surface des bactéries, le mécanisme de cette précipitation n'a pas encore été clairement mis en évidence. Le Fe(II) s'oxyde t-il en solution ou à la surface des bactéries? Si l'oxydation a lieu en solution, l'apparition de nano-cristaux correspond-elle à une adsorption de Fe(III) suivie d'une hydrolyse ou les nano-cristaux de fer se forment-ils en solution et se lient-ils ensuite à la surface?

Pour répondre à ces questions nous avons réalisé dans cette thèse des cinétiques d'oxydation du fer dans des conditions contrôlées de pH, de température, de concentration en oxygène et de conductivité, en la présence et en l'absence de bactéries. Pour quantifier les processus microscopiques impliqués, nous avons complété ce volet par une étude de la cinétique d'oxydation du Fe(II) adsorbé à la surface d'une bactérie *Bacillus subtilis*.

2.2. Etude in situ de la bio-réduction (biodissolution)

Depuis ces dernières années, de nombreuses études se sont intéressées à la bio-réduction du fer. Cependant, la plupart de ces travaux ont porté sur des descriptions qualitatives des phénomènes, en particulier sur les mécanismes minéralogiques ou biogéochimiques de destruction ou de formation de minéraux (e.g., Loveley et al., 1987, Roden et Lovley, 1993, Roden et Zachara, 1996, Kukkadapu et al., 2001, Pedersen et al., 2006). Les principaux facteurs influençant le processus de bio-réduction sont aujourd'hui mieux connus, et incluent : la nature et la qualité de la biomasse, la nature de l'oxyde (structure minéralogique et surface

spécifique), l'influence des sous-produits de réaction (réadsorption de Fe(II) à la surface de l'oxyde ou des surfaces bactériennes) (Roden et Urrutia, 2002 ; Roden, 2003 ; Bonneville et al., 2004, Châtellier et Fortin, 2004). Cependant, moins d'attention a été accordée à la description quantitative du processus de bio-réduction. L'un des principaux enjeux de recherche concernant la bio-réduction du fer est donc de développer des stratégies de quantification de la réduction par voie biologique (par exemple à l'aide de modèles) et des processus géochimiques associés dans les systèmes naturels. L'objectif de la présente étude n'est pas de mettre au point des modèles, mais de quantifier *in situ* le processus de bio-réduction des oxyhydroxydes de fer, c'est-à-dire directement dans un sol naturel, et d'identifier et de quantifier les mécanismes tels que la réadsorption, la reprécipitation, la redistribution d'éléments, qui sont associés à ce processus. Jusqu'à présent, la bio-réduction du fer a été essentiellement étudiée en laboratoire à l'aide d'oxydes synthétiques ou naturels (e.g. Lovley et Phillips, 1986a ; Lovley et al., 1987 ; Francis and Dodge, 1990; Roden et Lovley, 1993 ; Roden and Wetzel, 2002 ; Roden et Zachara, 1996 ; Kukkadapu et al., 2001). Si la plupart de ces études ont permis de comprendre et de caractériser les mécanismes de la biodissolution réductrice, elles ont été réalisées dans des conditions très éloignées des systèmes naturels, c'est à dire sans tenir compte de l'influence des différents composants des sols, des flux d'eau au sein des sols, des variations bioclimatiques. L'étude menée dans le cadre de cette thèse consiste donc à développer une technologie capable de quantifier et de caractériser la biodissolution du fer directement dans un sol.

Cependant, développer une telle technique pose un certain nombre de problèmes liés à des verrous méthodologiques. Par exemple, comment évaluer le taux de dissolution d'oxyhydroxydes de fer spécifiques, dans la matrice hétérogène d'un sol naturel? Comment extraire ou isoler un oxyhydroxyde afin étudier l'évolution de sa minéralogie au cours d'un processus de réduction? Comment quantifier la réadsorption éventuelle des éléments associés ? Pour pallier à ces difficultés, nous avons développé en collaboration avec Bernd Nowack (EMPA, Suisse) une nouvelle technique qui consiste à insérer directement dans différents horizons de sol des supports inertes (acrylique) recouverts d'oxyhydroxydes de fer synthétiques dopés ou non en As(V). Cette méthodologie originale offre la possibilité de mettre directement en contact des oxydes de fer, un horizon de sol et sa solution sans perte de matériel et sans avoir la difficulté, ensuite, de séparer les oxydes de fer du reste de la matrice. Cette technique nous a permis d'aborder des questions plus spécifiques comme :

- Le rôle de la cristallographie des oxydes, de la nature de l'horizon de sol choisi et des conditions rédox y régnant sur la cinétique et le taux de réduction en conditions naturelles des oxyhydroxydes de fer,
- La nature des produits secondaires de la réduction et leur impact sur la mobilité des éléments associés,
- L'effet de la présence d'ions substitués sur les taux de dissolutions des oxydes de Fe ,
- Le rôle des colonisations bactériennes sur le processus de bio-réduction.

3. ORGANISATION DU MEMOIRE DE THESE

Outre l'introduction qui commence le document et les conclusions et perspectives qui le concluent, ce mémoire se divise en deux grands chapitres qui se décomposent comme suit.

Le chapitre I concerne une étude de la biominéralisation et de l'oxydation du Fe(II) en présence des bactéries. Ce chapitre est lui même divisé en deux parties. La première partie est constituée d'un article paru en 2008 dans la revue Environmental Science and Technology (Volume 42, pages 3194 à 3200). Cet article est intitulé '*Bacillus subtilis* bacteria hinder the oxidation and hydrolysis of Fe^{2+} ions'. Dans une deuxième partie, cette étude est complétée

par une étude de la cinétique d'oxydation du Fe(II) adsorbé à la surface de bactéries *Bacillus subtilis.*

Le chapitre II concerne l'étude *in situ* de la bio-réduction d'oxyhydroxydes de fer synthétiques (ferrihydrite et lépidocrocite) dopés ou non en As(V). Il est composé de trois parties, dont deux articles. Le premier de ces articles est intitulé 'A new tool for *in situ* monitoring of Fe-mobilization in soils'. La version révisée a été soumise en Juillet 2008 à la revue Applied Geochemistry. Cet article est complété d'une étude de la dissolution réductrice de lépidocrocite dopée en As(V) dans un sol hydromorphe : étude cinétique de terrain. La troisième partie de ce chapitre correspond à un second article intitulé 'Environmental impact of As(V)-Fe oxyhydroxide reductive dissolution: an experimental insight from in situ monitoring'. Cet article a été soumis en Juin 2008 à la revue Chemical Geology.

Cette thèse s'inscrit dans le cadre d'un projet "Biogéochimie du fer et des contaminants associés (As, Cr, Cd)", financé par le programme national « ECCO » ECOSPHERE CONTINENTALE : Processus et Modélisation. Ce projet associe l'UMR 6118 Géosciences Rennes, l'UMR 7590 Institut de Minéralogie et Physique des Milieux Condensés (IMPMC), le groupe ITO de l'ETH Zurich (Suisse) et l'UMR 6553 Ecobio Rennes. Le site de l'étude est localisé dans le bassin versant expérimental de Kervidy-Naizin qui fait partie de l'ORE AgrHys, labellisé par le Ministère de la Recherche et l'INRA.

II. CHAPITRE I

Biominéralisation - Oxydation du Fe(II)

Ce chapitre est composé de deux parties, la première partie traite le rôle joué par Bacillus subtilis dans l'oxydation et l'hydrolyse des ions Fe^{2+}. Cette partie a donné lieu à une publication parue dans « Environmental Science and Technology ». Le format de l'article a été légèrement modifié pour que les détails des méthodes employées apparaissent directement dans le texte et non plus dans une partie 'supporting informations'. La deuxième partie est un complément qui porte sur la comparaison de cinétiques d'oxydation du fer à différentes pH en présence de Bacillus subtilis (réactions non métaboliques). Dans la première partie, nous avons montré que dans des conditions de saturation des surfaces, l'oxydation des cations Fe^{2+} en présence de bactéries conduit à la formation d'oxydes ferriques. Dans la deuxième partie, des conditions de sous-saturation des surfaces ont été adoptées, afin de déterminer si les cations Fe^{2+}, adsorbés pour la plupart d'entre eux, s'oxydaient et à quelle vitesse.

1. ROLE JOUE PAR LES BACTERIES DANS L'OXYDATION ET L'HYDROLYSE DES IONS FE^{2+} : LE CAS DE BACILLUS SUBTILIS

Mohamad Fakih
Xavier Châtellier
Mélanie Davranche
Aline Dia

Cette partie est extraite de 'Environmental Science and Technology', Mohamad Fakih, Xavier Châtellier, Mélanie Davranche, and Aline Dia (2008) *Bacillus subtilis* bacteria hinder the oxidation and hydrolysis of Fe^{2+} ions. Volume 42: 3194–3200.

RÉSUMÉ

Les bactéries sont souvent étroitement associées aux oxydes de fer dans le milieu naturel. Cependant, leur rôle exact dans le processus de précipitaion des ces oxydes est encore mal connu. Dans cette étude, des ions Fe^{2+} ont été progressivement ajoutés à différentes concentrations de cellules de *Bacillus subtilis* en conditions aérobies constantes, tout en maintenant le pH à 6,5 par ajout de NaOH. Les synthèses abiotiques produisent des nano-cristaux de lépidocrocite et la cinétique de précipitation est largement autocatalytique. Les synthèses biotiques ont produit des petites particules mal cristallisées pour les concentrations intermédiaires en cellules bactériennes. Par contre, la formation de ces particules est totalement inhibée pour de fortes concentrations en cellules bactériennes. L'effet autocatalytique est retardé, et son intensité est réduite. Dans les deux cas, l'oxydation et l'hydrolyse des ions Fe^{2+} sont plus lentes.

ABSTRACT

Bacteria are known to associate closely with secondary iron oxides in natural environments, but it is still unclear whether they catalyze their precipitation. Here Fe^{2+} ions were progressively added to various concentrations of *Bacillus subtilis* bacteria in permanently oxic conditions, while maintaining the pH at 6.5 by adding a NaOH solution at a monitored rate. The iron/bacteria precipitates were characterized by wet chemistry, SEM and XRD. Abiotic syntheses produced nanolepidocrocite and their kinetics displayed a strong autocatalytic effect. Biotic syntheses led to the formation of tiny and poorly crystallized particles at intermediate bacterial concentrations and to a complete inhibition of particle formation at high bacterial concentrations. The occurrence of the autocatalytic effect was delayed and its intensity was reduced. Both the oxidation and the hydrolysis of Fe^{2+} ions were hindered.

1.1 INTRODUCTION

Bacteria affect the cycling of metals by sorption processes (Fein et al., 1997; Daughney and Fein, 1998; Burnett et al., 2006a; Guine et al., 2006). They also influence the formation and dissolution of minerals, including iron oxides, which can themselves adsorb many organic and inorganic molecules (Randall et al., 1999; Ferris et al., 2000; Gao and Mucci, 2001; Dixit and Hering, 2003; Spadini et al., 2003). Specific bacteria thrive in environments where iron oxides massively precipitate, such as iron springs or acid mine drainage (Fortin et al., 1996; Emerson et al., 1999; Emerson, 2000; Anderson and Pedersen, 2003; Baker and Banfield, 2003; James and Ferris, 2004). More generally, secondary iron oxides are commonly found in close association with all sorts of microorganisms through non-metabolic processes (Fortin et al., 1993; Schultze-Lam et al., 1996; Fortin and Ferris, 1998; Jackson et al., 1999). It has been suggested that bacterial cell walls or exopolymers act as templates, which catalyze the nucleation and growth of iron oxide crystals with specific properties (Ferris et al., 1989; Schultze-Lam et al., 1996; Fortin et al., 1997; Fortin and Ferris, 1998; Warren and Ferris, 1998; Mavrocordatos and Fortin, 2002; Chan et al., 2004; Fortin, 2004). A few laboratory studies investigated the exposition of bacterial cells to Fe^{3+} ions (Châtellier et al., 2001, 2004; Chan et al., 2004). A continuum between sorption and precipitation of various bacterial cells exposed to Fe^{3+} ions was observed, with mixed

conclusions as to whether the cells were favoring or not the precipitation of the Fe oxides. The study of the effect of natural organic matter on the kinetics of oxidation of Fe(II) has also led to different conclusions, depending on the type of ligands considered (Rancourt et al., 2005; Wightman and Fein, 2005). Here, we exposed increasing concentrations of *Bacillus subtilis*, a model Gram-positive bacterium, which has been used in several studies investigating the interactions between Fe and bacterial surfaces (Beveridge and Murray, 1980; Santana-Casiano et al., 2000; Châtellier et al., 2001, 2004; Rose and Waite, 2002; Châtellier and Fortin, 2004; Chan et al., 2004), to progressive additions of Fe^{2+} ions at constant pH. In addition to the characterization of the precipitates by SEM and XRD, we measured here over time several parameters related to the kinetics of the reaction, such as the rate of proton release and the redox potential. The dissolved organic carbon (DOC) and Fe(II)/Fe(III) concentrations were determined at selected times. Although metabolic effects were not the focus of this study, we also monitored cell death through enumerations.

1.2. MATERIALS AND METHODS

1.2.1. Synthesis of the Fe/bacteria composite suspensions

Bacillus subtilis cells (ATCC 168) were grown in Tryptic Soy Broth (Difco, 30 $g.L^{-1}$) with yeast extract (Difco, 5 $g.L^{-1}$), at 37°C under mild agitation according to a protocol adapted from Daughney and Fein (1998). A preculture of 100 ml was first inoculated from a Petri dish and incubated for 24 hours. 2 erlenmeyer flasks of 2 liters containing each one 1 liter of growth medium were then inoculated using 6 ml of preculture per flask. Cultures were harvested after 7.5 hours, while in exponential phase. The 2 liters of bacterial culture were mixed together and washed 3 times in 500 ml of a 0.01M NaCl solution, using centrifugations at 10000 g. They were then left to rest overnight at 5°C, washed again twice in 500 ml of 0.01M NaCl, and finally once in 100 ml of 0.01M NaCl. An aliquot of 10 ml was sampled from the stock suspension and dried for a week at 70°C. After a week, the dry weight of the sample was recorded, the weight corresponding to the NaCl salt was subtracted, and the dry weight of biomass present in the stock suspension was thus determined. In parallel, and in order to obtain an immediate estimation of the biomass concentration, the optical density at 600 nm (OD_{600}) of the suspension was measured. Preliminary tests indicated the dry biomass concentration c_b in the suspension was related to OD_{600} by the linear relationship "c_b ($g.L^{-1}$) = 0.286 OD_{600}", which we used throughout our study to determine how much stock suspension was needed in each experiment.

A Fe(II) stock solution was prepared in 2.5×10^{-3} M HCl ($[FeCl_2] = 1.25 \times 10^{-2}$ M, or 0 for the blank experiments). The bacterial stock suspension was diluted to the desired concentration (c_b = 0, 0.135, 0.350 or 1.30 dry $g.L^{-1}$) in 500 ml of 0.01M NaCl solution, and introduced in a thermostated beaker set at 25°C. Starting at the time t = 0, 20 ml of the Fe(II) stock solution were added to the suspension at a rate of 0.05 ml/min, using an automated burette (Titrino 794, Metrohm). In parallel, the pH was continuously maintained at 6.5 by adding progressively 4.9 ± 0.7 ml of a 0.1 M NaOH solution, using a second automated burette programmed in a pH stat mode. The total final concentration of Fe was thus equal to approximately 480 µM. After the end of the addition of the Fe(II) solution (t = 24000 s), the suspension was left in contact with the atmosphere at pH 6.5 for another 56000 s. Each synthesis was replicated six times, using independently grown bacterial cultures. Three blank experiments were also performed at a bacterial concentration of 1.30 $g.L^{-1}$. In one experiment for each type of synthesis, the O_2 concentration and the redox potential were recorded.

1.2.2. Scanning Electron Microscopy (SEM), X-Ray Diffraction (XRD), wet chemistry and enumerations

Dissolved organic carbon was measured by filtering the suspensions using 0.2 µm cellulose acetate filters (Sartorius). The filtrates were diluted with ultra-pure water in order to reach a carbon concentration in the 0-10 $mg.L^{-1}$ range, and measured using a Shimadzu TOC-5050A carbon analyzer.

Dissolved Fe(II) concentrations were measured using a protocol adapted from Viollier et al. (2000), by adding 0.5 ml of a 10^{-2} M ferrozine solution and 0.5 ml of a 10^{-1} M ammonium acetate solution to 4 ml of the filtrate of the suspension and recording the absorbance at 562 nm. For the total dissolved Fe concentrations, 0.5 ml of the ferrozine solution, 0.5 ml of a 10^{-1} M ammonium acetate solution, and 1 ml of a hydroxylamine hydrochloride solution (10^{-1} M hydroxylamine hydrochloride, 2M HCl) were reacted with 4 ml of the filtrate overnight. Then 0.5 ml of an ammonium acetate buffer solution (10 M ammonium acetate, pH 9.5) was added and the absorbance was recorded at 562 nm. The linear relationship between absorbance and Fe concentration was obtained by calibrating this experimental protocol with standard $FeCl_2$ and $FeCl_3$ solutions. Since Châtellier et al. have demonstrated that Fe^{2+} sorption onto *Bacillus subtilis* cells was reversible when the pH is lowered (Châtellier and Fortin, 2004), the total Fe(II) concentration was estimated by adding 0.5 ml of a 1 M HCl solution to 4 ml of the unwashed suspension, which brought the pH down to 2.0 ± 0.2. After 1 hour at pH 2, the suspensions were filtered and the filtrate was added to 0.4 ml of the ferrozine solution and to 0.4 ml of a 10^{-1} M ammonium acetate solution. The absorbance of the solution was then measured at 562 nm. In Table II.1.1, the percentage of Fe in the +II oxidation state was estimated by dividing the total Fe(II) concentration by the total Fe concentration, which was equal in all systems to 480 µm.

For the bacterial enumerations, 100 µl of the suspension were sampled either right at the time when the culture was harvested in late exponential phase or at t = 0, t = 25000 s and t = 80000 s. Different dilutions were prepared in sterile growth medium using a laminar biosafety cabinet (Bioair, Safeflow, Class II) and sterile conditions (autoclaved beakers, pipette tips,…). For each dilution, 100 µl of the suspension was spread on a tryptic soy agar Petri dish and 6 drops of 20 µl of the suspension were dropped on another Petri dish. For some dilutions, replicate Petri dishes were made. The Petri dishes were incubated for 20 hours at 37°C. Then the number of colonies was counted. The morphology of *Bacillus subtilis* colonies is somewhat characteristic. Based on this, contamination by other strains was found to be negligible. The numbers of colonies counted on each Petri dish are presented in Table II.1.1. They were used to estimate the order of magnitude of the number of colony forming units per dry g of bacteria in the bacterial suspension at the different sampling times. Those are presented in Table II.1.1. The dry weight of the bacterial suspension at the time when the bacteria were harvested was calculated by assuming that no bacteria were lost during the washing steps. This assumption likely led to a relatively precise estimation since the supernatants during the washing steps were transparent.

At the end of the reaction, aliquots of the Fe/bacteria suspensions were also sampled, washed 5 times in acetone in microtubes (6000g, 10 min), dried at the critical point (Balzers Instruments, CPD010, Liechtenstein), and observed by SEM. The samples were observed after being coated, or not, with Au-Pd nanoparticles by cathodic deposition with a JEOL JFC 1100 sputter. The equipment used was a JEOL JSM-6301F Field Emission Gun Scanning Electron Microscope operated at 5, 7 or 9kV. The suspensions were washed 5 times in ultra-pure water (10300g, 10 min, 5°C), frozen, and then lyophilized at 0.120 mbar (Alpha 1-4,

Christ, Osterode, Germany). The dried samples were analyzed by X-Ray Diffraction. XRD measurements were performed with a Philips X'Pert diffractometer, using a Cu source operating at 45 kV and 40 mA, and a Kevex Si(Li) solid-state detector. All samples were run in a step-scan mode for the angle 2Θ, at 0.04°/30s from 8.5° to 90°.

Table II.1.1. Number of colonies per Petri dish. For each dilution, the first and second lines correspond to Petri dishes inoculated with 100 µl of suspension, spread on the agar, and with 6 unspread drops of 20 µl of suspension, respectively. Thick characters correspond to the data selected for the calculation of the number of colony forming units (c.f.u.) per ml of the original undiluted suspension, which was obtained by averaging the selected numbers and taking the dilution into account. m is the approximate number of c.f.u. per dry g of bacteria selected for Table II.1.2.

	Exponential Phase (c_b = 0.85 g.L^{-1})	**Blank experiment (c_b = 1.30 g.L^{-1})**			**Iron experiment (c_b = 1.30 g.L^{-1})**		
Time (seconds)	< 0	0	25000	80000	0	25000	80000
10^8 dilution	0; 0 0; 0						
10^7 dilution	0; 3 1; 4	0 1			0 1		
10^6 dilution	**28; 29** **29; 42**	8; 11 5; 9	0; 0 1; 0		2; 1 10; 6	0; 0 0; 0	
10^5 dilution		**58** **78**	10 6; 6	1 2	**46** **51**	1 0; 0	0 0
10^4 dilution			**104;118** **61; 61**	14 27; 21		0; 0 0; 1	1; 0 0; 1
10^3 dilution			> 200 > 200	**193** **102; 121**		**5; 1** **2; 1**	3; 2 5; 7
10^2 dilution				> 200 > 200			**27** **35; 39**
10^1 dilution							> 200 > 200
Per ml	2.9×10^8	6.1×10^7	8.1×10^6	1.3×10^6	4.4×10^7	2.1×10^4	3.0×10^4
Per dry g	3.4×10^{11}	4.7×10^{10}	6.2×10^9	9.7×10^8	3.4×10^{10}	1.6×10^7	2.3×10^7
m	3×10^{11}	4×10^{10}	6×10^9	1×10^9	4×10^{10}	2×10^7	2×10^7

1.2.3. Kinetics and stoichiometry

The normalized rate of proton release v(t), averaged for each period of 1000 seconds, was calculated as:

$$v(t) = \frac{N(OH^-) - N(H^+)}{N(Fe^{2+})} \qquad \text{(II.1.2.3.1)}$$

where $N(H^+)$ and $N(OH^-)$ were the number of moles of H^+ and OH^- added during the period of 1000 seconds considered, and $N(Fe^{2+}) = 1.04 \times 10^{-5}$ was the number of moles of Fe^{2+} added per 1000 seconds for t < 24000 s. The final stoichiometry of the reaction was also calculated by determining how many OH^- had been added per introduced Fe^{2+} cation, after having subtracted the effect of the acid in the $FeCl_2$ solution. The reaction of oxidation/hydrolysis of the protons reads:

$$Fe^{2+} + \frac{1}{4}O_2 + 2OH^- \rightarrow FeOOH + \frac{1}{2}H_2O \qquad \text{(II.1.2.3.2)}$$

In a system where reaction (2) would be occurring, the final stoichiometry of the reaction n would be equal to 2. Were it to occur completely and instantaneously for all the introduced Fe^{2+} ions, v(t) would also be equal to 2 at any time.

1.3. RESULTS AND DISCUSSION

1.3.1. Blank experiments

As shown in Figure II.1.1 in the three blank experiments, $|v(t)|$ was at most times t < 60000 s lower than 0.1. In the following, v(t) will be presented and discussed for t < 60000 s.

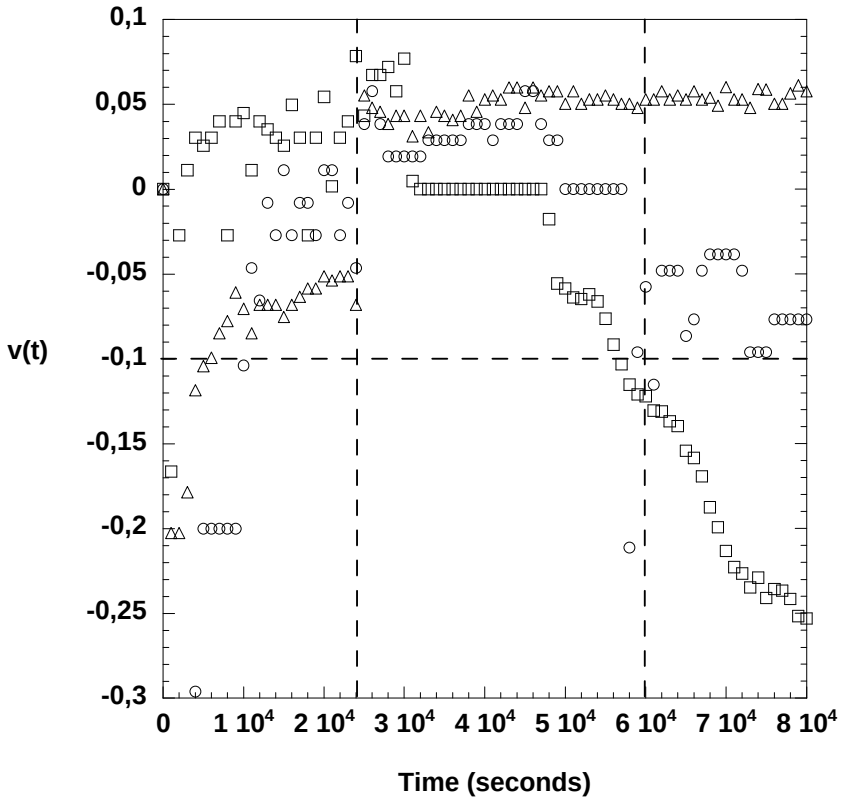

Figure II.1.1. Rate of base addition as a function of time in the blank experiments (c_b = 1.30 $g.L^{-1}$, no Fe added). Each symbol corresponds to an independent experiment. Vertical dashed lines correspond to t = 24000 s (the end of the period of addition of the HCl 0.0025 N solution) and to t = 60000 s (the end of the period selected for Figure II.1.5).

Enumerations of the c.f.u. are detailed in Table II.1 and summarized in Table II.1.2. They indicated that most cells died over time. This was paralleled by an increase of the DOC, which was possibly related to cell lysis (Table II.1.2). However, the percentage of organic carbon in the dissolved phase remained lower than 10% in all systems at all times. In contrast, in an autoclaved suspension, this percentage reached 27%.

Upon SEM observation, most cells looked intact and the DOC remained visually insignificant (Fig. II.1.2f). The cells were about 2 μm long at least, and often occurred as

attached dimers. Hence they did not undergo sporulation, as *B. subtilis* spores are known to be at most around 1.4 µm long and to occur as monomers (Santo and Doi, 1974; Cliff et al., 2005). The dissolved organic molecules were possibly an assemblage of polysaccharides, proteins and nucleic acids (Bura et al., 1998). We did not investigate here their chemical nature, and they will be referred to collectively thereafter as bacterial exuded molecules.

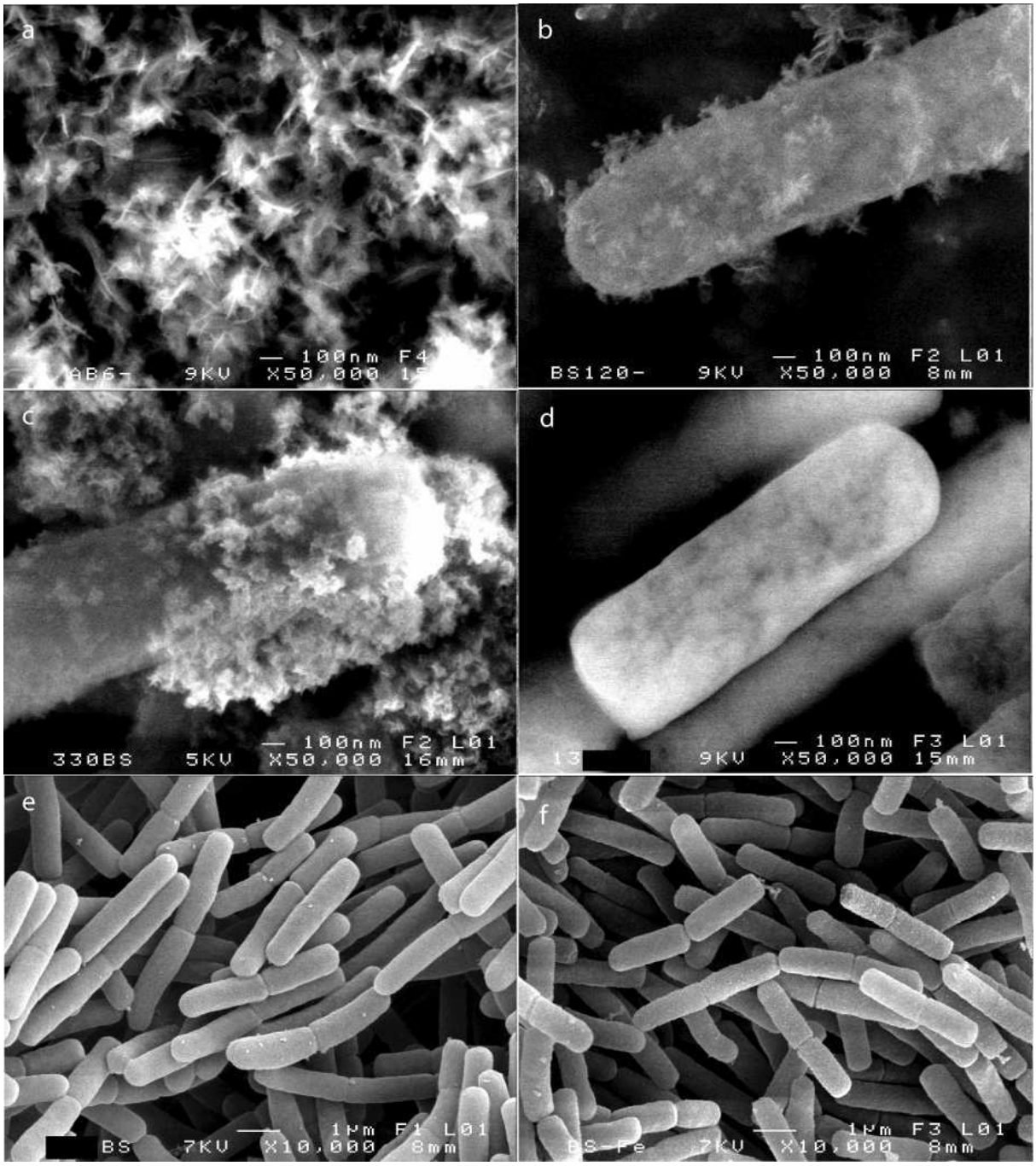

Figure II.1.2. SEM micrographs of bacteria from: abiotic Fe oxides (a); Fe/bacteria suspensions prepared with a *B. subtilis* dry weight concentration of 0.135 $g.L^{-1}$ (b), 0.350 $g.L^{-1}$ (c), and 1.30 $g.L^{-1}$ (d and e); blank experiment (f). Samples were coated with Au-Pd nanoparticles in Figures II.1.2e and II.1.2f.

Table II.1.2. Chemical and bacteriological analyzes of the suspensions and final stoichiometries of the syntheses (n.a.: not applicable or not available).

Sampling Time (seconds)	**Abiotic**	**c_b = 0.135** $g.L^{-1}$	**c_b = 0.350** $g.L^{-1}$	**c_b = 1.30** $g.L^{-1}$	**Blank (c_b = 1.30** $g.L^{-1}$**)**
	Number of colony forming units per dry g of bacteria (exponential phase: 3×10^{11})				
0	n.a.	n.a.	n.a.	4×10^{10}	4×10^{10}
25000	n.a.	n.a.	n.a.	6×10^{9}	2×10^{7}
80000	n.a.	n.a.	n.a.	1×10^{9}	2×10^{7}
	Dissolved Organic Carbon ($mg.L^{-1}$)				
0	n.a.	1.6	3.1	9.0	7.8
25000	n.a.	2.4	5.6	24	14
80000	n.a.	4.1	8.5	39	15
Autoclaved	n.a.	n.a.	n.a.	140	154
	% of Organic Carbon in the dissolved phase				
0	n.a	2.7 %	2.0 %	1.6 %	1.4 %
25000	n.a	4.1 %	3.7 %	4.2 %	2.5 %
80000	n.a	6.9 %	5.6 %	6.9 %	2.6 %
Autoclaved	n.a.	n.a.	n.a.	25 %	27 %
	Dissolved Fe(II) (µM)				
25000	1.0	1.2	11	51	< 0.5
80000	< 0.5	< 0.5	0.8	5.0	< 0.5
	Dissolved Fe (µM)				
25000	2.7	7.3	16	153	4.0
80000	1.8	1.9	9.3	132	2.3
	Total Fe(II) (µM)				
25000	1.7	8.5	42	189	2.5
80000	1.1	3.2	11	39	1.3
	% of Fe in the +II oxidation state (using Total Fe = 480 µM)				
25000	0.3 %	1.8 %	8.8 %	39 %	n.a.
80000	0.2 %	0.7 %	2.3 %	8.1 %	n.a.
	% of Fe(II) in the dissolved phase				
25000	n.a.	14%	26%	27%	n.a.
80000	n.a.	< 15%	7%	13%	n.a.
	% of Fe in the dissolved phase (using Total Fe = 480 µM)				
25000	0.6 %	1.5 %	3.3 %	32 %	n.a.
80000	0.4 %	0.4 %	1.9 %	27 %	n.a.
	Average of the final stoichiometry n				
80000	2.04	1.94	1.83	1.60	-0.10

1.3.2. Inhibition of the Fe oxide precipitation by the bacteria

The abiotic iron-oxides were characterized by an average final stoichiometry n = 2.04 (Table II.1.2), in good agreement with the formation of an iron oxyhydroxide solid (reaction

2). As observed by SEM, they occurred as clumps of thin sheet-like particles aggregated into macroscopic structures (Fig. II.1.2a). The characteristic size for each clump was 200 ± 100 nm. Because of their very thin thickness, the sheet-like particles were not completely opaque to electrons. As a result, many "needles" could be observed in Figure II.1.1a, corresponding to the thin edge of the particles. These needles were about 150 ± 50 nm long and at most about 10 nm wide. The third dimension of the sheet-like particle, when it could be measured, was on the order of 70 ± 30 nm. The particles were identified by XRD as poorly crystalline lepidocrocite. Similar lepidocrocite crystals have already been observed in natural environments or produced in the laboratory, in conditions where Fe^{2+} ions are oxidized at neutral or slightly acidic pH (Schwertmann and Taylor, 1979; Beveridge and Murray, 1980; Fortin et al., 1993; Châtellier and Fortin, 2004). For the biotic samples, the XRD pattern displayed peaks at 1.18, 1.20, 1.26, 1.39, 1.53, 1.62, 1.73, 1.85, 1.93, 2.09, 2.37, 2.49, 3.30, and 6.9 Å, which are consistent with the d-spacings of lepidocrocite (Cornell and Schwertmann, 2003). The patterns of the biotic samples all displayed a very broad peak around 4.5 Å, which is characteristic of the presence of the bacterial cells (Châtellier et al., 2001). On the pattern of the system prepared with a bacterial concentration of 0.135 $g.L^{-1}$, most of the peaks present in the pattern of the abiotic system could be distinguished.

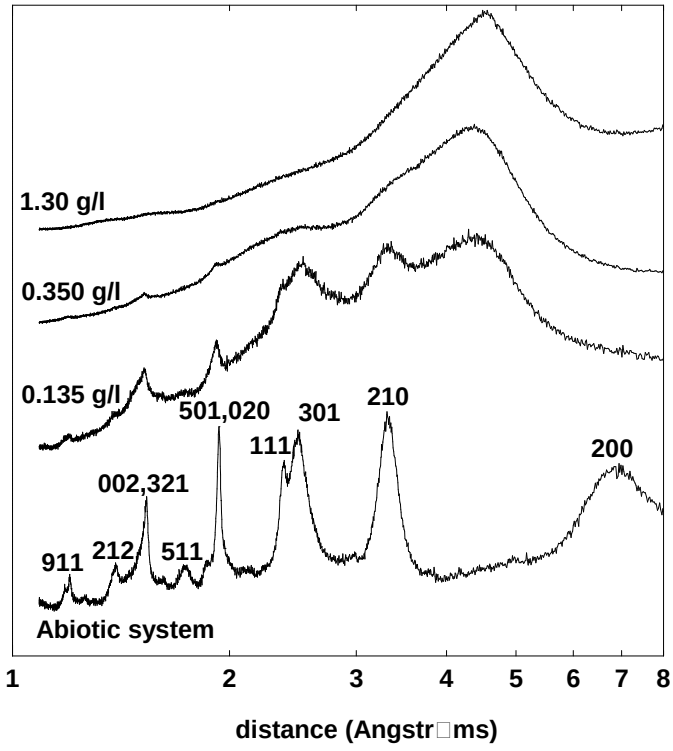

Figure II.1.3. XRD patterns of abiotic Fe oxides and of Fe/bacteria suspensions prepared with a *B. subtilis* dry weight concentration of 0.135, 0.350 and 1.30 $g.L^{-1}$. The hkl identification of the peaks is given as in reference (Cornell and Schwertmann, 2003).

However, the 200 reflection at about 6.9 Å was absent and some of the minor peaks were barely or not detectable. This pattern was similar to those published in a previous study, where the effect of the presence of *B. subtilis* bacterial surfaces on the oxidation of Fe^{2+} ions was investigated at a similar bacteria/Fe ratio (Châtellier et al., 2001). On the XRD pattern of the system prepared with a bacterial concentration of 0.350 $g.L^{-1}$, the reflections at 1.52 and 1.92 Å appeared as tiny peaks barely rising above the background, while two broad humps were detected around 2.5 and 3.3 Å. This suggests that the iron-oxide particles prepared in this sample were less crystalline than in the abiotic sample and in the sample prepared at a

bacterial concentration of 0.135 $g.L^{-1}$. However, the higher concentration of bacterial cells present with respect to the iron oxide particles also likely contributed to hide the signal of the iron-oxide particles. At the higher bacterial concentration of 1.30 $g.L^{-1}$, the XRD pattern of the sample did not display any peak other than that of the bacterial cells at 4.5 Å.

In the biotic syntheses, the average final stochiometries were equal to 1.94, 1.83, and 1.60 for bacterial concentrations of 0.135, 0.350, and 1.30 $g.L^{-1}$ respectively (Table II.1.1, Fig. II.1.4). This suggests that the reaction of oxidation/hydrolysis of the introduced Fe(II) remained incomplete. Figures II.1.2b and II.1.2c display SEM micrographs of iron-bacteria composite suspensions prepared using bacterial concentrations of 0.135 $g.L^{-1}$ and 0.350 $g.L^{-1}$. As in the blank experiments, the cells appeared to be intact and did not sporulate. Iron-oxide particles could be observed in these systems. Most of them were in close association with the bacterial cell walls. The sheet-like morphology, observed in the abiotic systems for the iron-oxide particles, could still be distinguished, but much less clearly. Particles were smaller and the system was best described as fractal-like in the 10-200 nm length scale range. In those samples, the XRD patterns of the iron-bacteria composite suspensions were still indicative of the presence of a very poorly crystalline lepidocrocite phase. At the higher bacterial concentration of 1.30 $g.L^{-1}$, the XRD pattern did not display any reflection, and no iron-oxide particles could be observed by SEM (Figs. II.1.2d and II.1.2e). Introduced Fe atoms thus remained adsorbed on the surface of the cells or associated to bacterial exuded molecules as monomers of Fe(II) or Fe(III), or as oligomers or polymers of Fe(III).

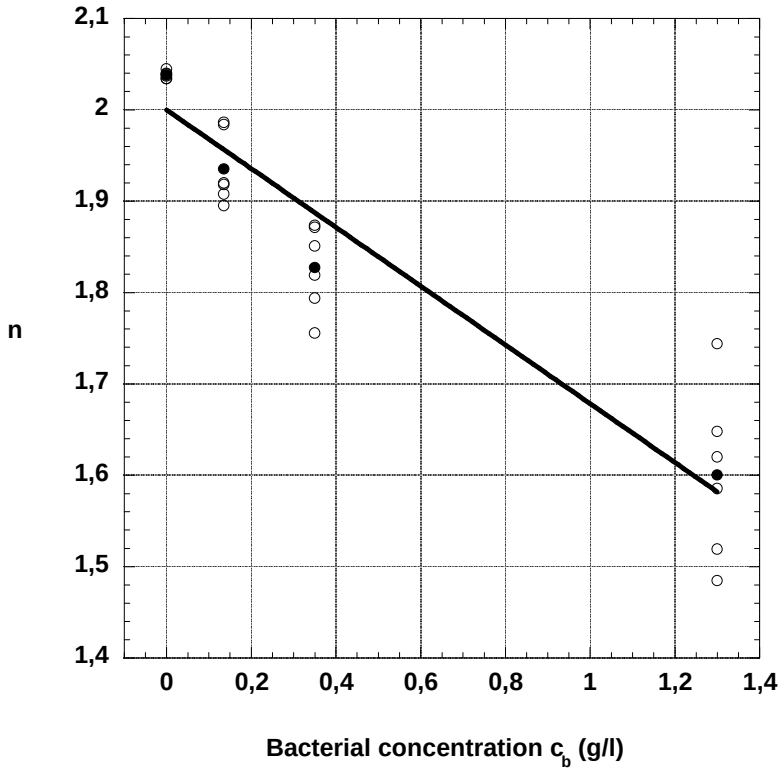

Figure II.1.4. Stoichiometry n of all syntheses as a function of the bacterial concentration (open symbols). The best linear fit corresponds to $n = 2.00 - 0.32 \times c_b$ ($R = 0.93$). The average stoichiometry for each bacterial concentration is shown as full symbols. The three blank experiments led to stoichiometries of -0.16, -0.17, +0.03 (average: -0.10).

It has been shown previously that bacteria can adsorb significant amount of ferrous and ferric ions (Urrutia and Roden, 1998; Châtellier et al., 2001; Daughney et al., 2001; Liu et al., 2001; Rose and Waite, 2002; Roden and Urrutia, 2002). At neutral pH, *B. subtilis* can adsorb within minutes up to about 3.5×10^{-4} moles of Fe^{2+} ions per dry g of bacteria (Rose and

Waite, 2002), and probably about the same amount of Fe^{3+} ions (Châtellier et al., 2001) . This is equivalent to Fe concentrations of about 45, 120, and 440 μM for bacterial concentrations of 0.135, 0.350 and 1.30 $g.L^{-1}$ respectively, and should be compared to the total Fe concentration of about 480 μM in our experiments. In the biotic syntheses prepared using concentrations of 0.135 or 0.350 $g.L^{-1}$, the bacterial surfaces were loaded with more Fe(II) than they could adsorb. Most of the Fe was oxidized and hydrolyzed in the form of precipitates accumulating on the surface of the cells, as observed by SEM. In contrast, in the syntheses prepared with 1.30 $g.L^{-1}$ of bacteria, the cell surfaces capacity for Fe(II) sorption was barely reached. Altogether, our SEM, XRD and stoichiometric results indicated that the reactive groups present on the cell walls and on the exuded molecules of the *B. subtilis* bacteria were able to stabilize Fe in monomeric form or at least in a low coordination number, thereby preventing the precipitation of Fe oxides. In addition, in the case where the reactive groups were saturated with Fe, the crystallization of the particles being formed was hindered by the bacteria, as already demonstrated earlier (Beveridge and Murray, 1980; Châtellier and Fortin, 2004). Common observations of bacteria encrusted with iron oxides are thus not indicative of a catalytic nucleation of the crystals directly on the cell walls. Rather, they likely simply reflect the affinity of bacterial cell walls for iron, in conditions of oversaturation.

1.3.3. Inhibition of the oxidation of Fe(II) by the bacteria

In the abiotic system, the total Fe(II) and dissolved Fe concentrations were lower than 3 μM at $t \geq 25000$ s (Table II.1.2), indicating that the reaction of oxidation/hydrolysis was nearly complete even only 1000 seconds after the end of the addition of the $FeCl_2$ solution. At a bacterial concentration of 0.135 g/, the total Fe(II) and dissolved Fe concentrations were still lower than 10 μM at $t \geq 25000$ s, i.e., they represented less than 2% of the total Fe concentration. However, the percentage of Fe in the +II oxidation state at t = 25000 s increased to 8.8% for c_b = 0.350 $g.L^{-1}$ and to 39% for c_b = 1.30 $g.L^{-1}$. At t = 80000 s, it was still equal to 8.1% in the system prepared with 1.30 $g.L^{-1}$ of bacteria. Hence, our chemical analyzes demonstrate that the bacterial cell walls and exuded molecules were able to retard significantly the oxidation of the Fe(II).

1.3.4. Role of the exuded molecules

The cells exuded bacterial organic molecules in solution, possibly in relation to cell lysis. Enumerations indicated that the number of c.f.u. was significantly smaller in the Fe experiment, suggesting that Fe^{2+} ions had a toxic effect on the cells, which was additive to that of the treatment applied to the cells in the blank experiment (Table II.1.2). DOC concentrations increased with time and bacterial concentration in the biotic systems, from about 1.6 $mg.L^{-1}$ at t = 0 for c_b = 0.135 $g.L^{-1}$ to 39 $mg.L^{-1}$ at t = 80000 s for c_b = 1.30 $g.L^{-1}$ (Table II.1.1). Correspondingly, the dissolved Fe(II) and Fe concentrations increased with bacterial concentration. However, they decreased with time. In all the biotic systems, even though the DOC concentration was increasing over time, the percentage of Fe(II) in the dissolved phase decreased, suggesting that the reactive groups present on the cell walls may have been able to retard the oxidation of the Fe(II) more efficiently than those present on the exuded molecules. For the bacterial concentrations c_b = 0.135 $g.L^{-1}$ and c_b = 0.350 $g.L^{-1}$, the amount of Fe in the dissolved phase decreased to less than 2% at t = 80000 s, indicating that the exuded molecules were unable to prevent the precipitation of Fe oxide particles. However, they may have played a role on crystal growth, as suggested recently (Châtellier et al., 2004).

In contrast, in the system at 1.30 $g.L^{-1}$ of bacteria, the dissolved Fe concentrations decreased only slightly over time and remained elevated, representing about 30% of the total Fe. In this system, where the hydrolysis of the Fe remained largely incomplete (see also SEM observations), the bacterial exuded molecules thus played a significant role in the stabilization of the Fe(III) monomers or oligomers. In this way, they also contributed to help preventing the saturation of the surfaces from occurring.

1.3.5. Kinetics of the reactions

The kinetics of the reaction were investigated by observing the rate of proton release v(t) (Fig. II.1.5), the redox potential (Fig. II.1.6), and the O_2 concentrations. The latter remained in all cases quite stable over time and are presented in Figure II.1.7.

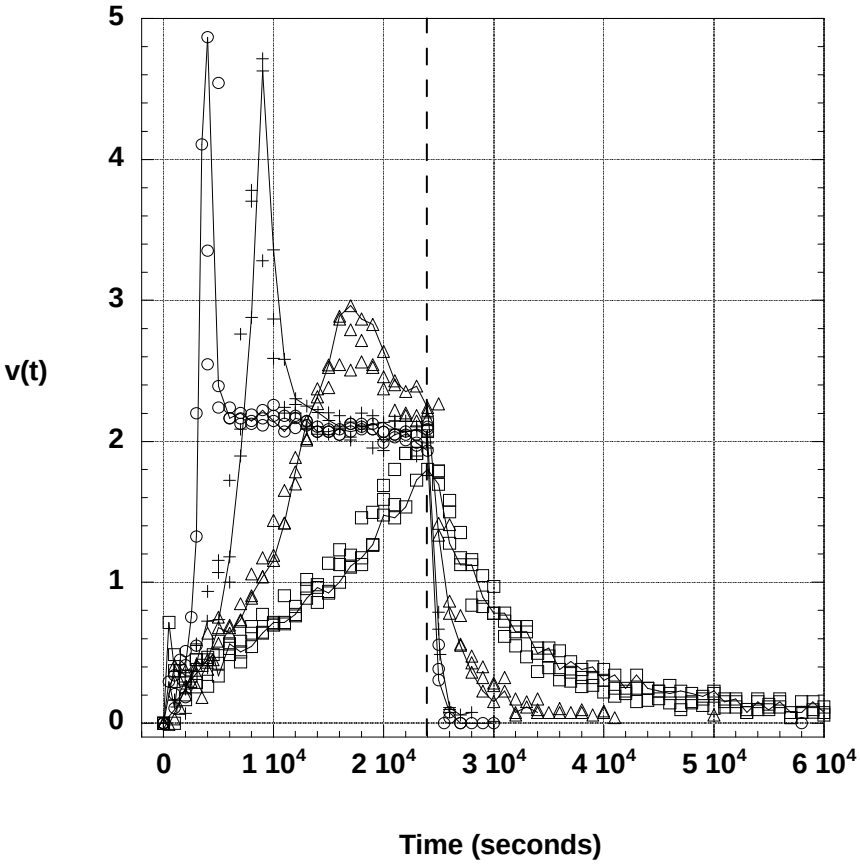

Figure II.1.5. Characteristic kinetic curves for iron oxides syntheses prepared in the presence of various concentrations c_b of bacteria. c_b = 0 (circles), 0.135 $g.L^{-1}$ (crosses), 0.350 $g.L^{-1}$ (triangles), and 1.30 $g.L^{-1}$ (squares). For the sake of clarity, for each bacterial concentration, only three individual experiments are presented and a line is drawn between data points for only one of these three experiments. The vertical dashed line correspond to t = 24000 s.

As seen on Figure II.1.5, during the first 2000 seconds, v(t) remained in all cases significantly smaller than the reference value of 2, as it was equal to v(t) = 0.2 ± 0.2. In the abiotic syntheses, v(t) increased sharply to about 4.5 ± 1.5 between t = 2000 s and t = 4000 s, it decreased to a value of 2.1 ± 0.2 between t = 4000 s and t = 6000 s, and it stayed in this range until t = 24000 s, i.e., the end of the period during which the $FeCl_2$ solution was added. For t > 24000 s, v(t) decreased rapidly and reached a value equal to 0 within less than 2000 s. Hence, the kinetics of the abiotic syntheses were characterized by a slow start, which was

consistent with the slightly acidic pH and an initial Fe(II) concentration in the reaction vessel equal to zero.

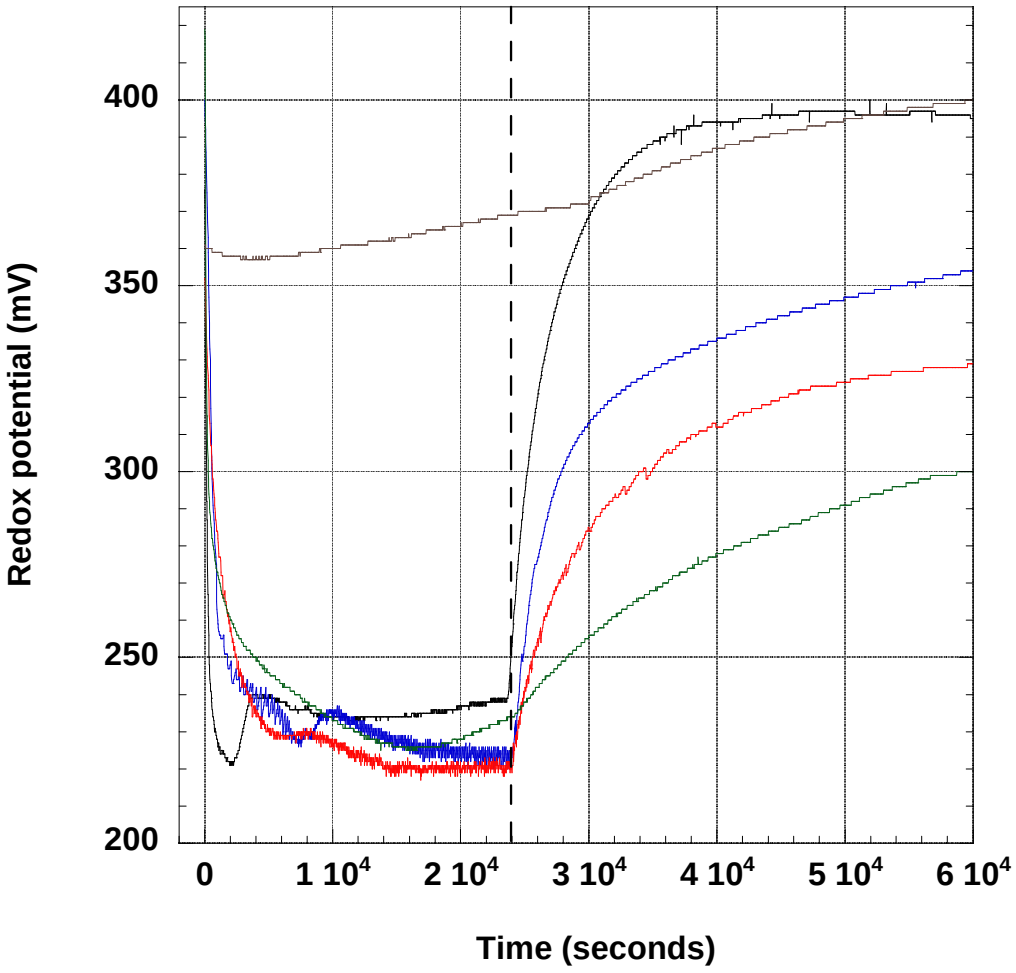

Figure II.1.6. Redox potential over time in the blank experiment (brown line) and as a function of the bacterial concentration: c_b = 0 (black line), 0.135 $g.L^{-1}$ (blue line), 0.350 $g.L^{-1}$ (red line), and 1.30 $g.L^{-1}$ (green line). The vertical dashed line correspond to t = 24000 s.

As time increased, the Fe(II) concentration in the reaction vessel built up. This was corroborated by the measurement of the redox potential, which decreased sharply during the first 2000 seconds from 376 mV to 221 mV (Fig. II.1.6). The rate of homogeneous Fe(II) oxidation increases linearly with the Fe(II) concentration (Cornell and Schwertmann, 2003). However, at t ≈ 2000 s, v(t) increased exponentially in the abiotic systems. The autocatalytic acceleration of the oxidation of Fe^{2+} ions by iron oxyhydroxide nuclei has been known for some time (Tamura et al., 1980; Tüfekci and Sarikaya, 1996). Direct evidence for a Fe(II)-Fe(III) electron transfer at the oxide interface has been provided more recently (Williams and Scherer, 2004).

At the light of these previous studies, we interpret that the initial regime of homogeneous nucleation in solution was followed by a regime of crystal growth during which the rapid oxidation of the Fe(II) occurred primarily at the oxide interface. The overshoot observed in the kinetic curves of Figure II.1.2 corresponded to the onset of the regime, when most Fe^{2+} ions accumulated in the solution were quickly consumed. This was paralleled by an increase of the redox potential from 221 mV to 240 mV (Fig. II.1.6). After the overshoot, introduced Fe(II) ions were rapidly adsorbed and oxidized onto the precipitates, and v(t) stabilized at a value close to 2 (reaction 2). Between t = 4000 s and t = 24000 s, the redox potential was

almost stable, in the 233-240 mV range. At t > 24000 s, v(t) decreased to zero within 2000 seconds. The redox potential also increased rapidly. For instance, from t = 24000 s to t = 25000 s, it displayed an increase of 42 mV, from 239 mV to 281 mV. This was consistent with a rapid oxidation and hydrolysis of the introduced Fe^{2+} ions characteristic of the regime, which prevailed after t = 2000 s.

The oxygen concentration was recorded using an electrode (Fisher Scientific Bioblock). Examples of oxygen concentrations curves as a function of time are given in Figure II.1.7.

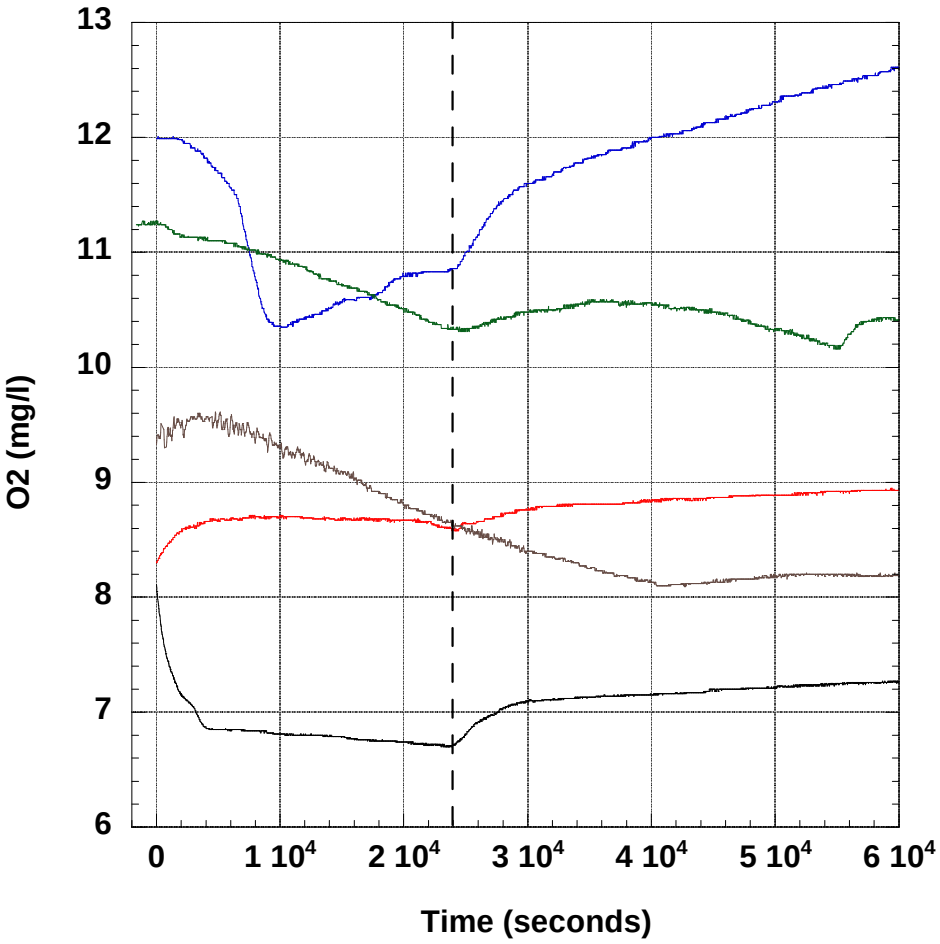

Figure II.1.7. Oxygen concentration over time in the blank experiment (brown line) and as a function of the bacterial concentration: c_b = 0 (black line), 0.135 $g.L^{-1}$ (blue line), 0.350 $g.L^{-1}$ (red line), 1.30 $g.L^{-1}$ (green line). The vertical dashed line correspond to t = 24000.

Although an important variability of about ± 3 $mg.L^{-1}$ was observed among independent experiences, which we attribute mainly to calibration difficulties and/or matrix effects, the recorded oxygen concentrations were consistent with the solubility of oxygen in water, which is on the order of 8-9 $mg.L^{-1}$ at 25°C. In most instances, the slight variations of the oxygen concentration could be correlated with the different stages of the reaction. For instance, it can be seen in Figure II.1.7 for the curve corresponding to the bacterial concentration of 0.135 $g.L^{-1}$ that the decrease of the oxygen concentration stopped at the end of the overshoot. And for all curves except in the blank experiment, the oxygen concentration rebounded at t = 24000 s, when the addition of the $FeCl_2$ solution was ended, which corresponded to a rapid decrease in the rate of the reaction. In some other instances, the variations of the oxygen concentration may have reflected instabilities or drifts of the electrode. In all experiments, the

variations of the oxygen concentration over time were limited to ± 2 $mg.L^{-1}$ or less. This demonstrates that quite stable oxic conditions were maintained throughout the syntheses in the reaction vessel.

The biotic syntheses were characterized by noticeably different kinetics, even in the system prepared with the lowest bacterial concentration. As it can be seen in Figure II.1.5, above t = 3000 s, the kinetics of the various abiotic and biotic syntheses split. As in the abiotic syntheses, an overshoot such as v(t) > 2 was reached in all syntheses performed with a bacterial concentration equal to 0.135 $g.L^{-1}$ or 0.350 $g.L^{-1}$. However, the time at which the peak of the overshoot was reached was larger than in the abiotic systems, and it increased with the bacterial concentration. In addition, as the bacterial concentration increased, the intensity of the overshoot decreased, and its duration increased. For instance, in the syntheses performed with 0.350 $g.L^{-1}$ of bacteria, the maximal rate of proton release was equal to 2.75 ± 0.2, and it remained higher than 2.3 from t = 15000 s until t = 20000 s. Because of the delayed occurrence of the overshoot, the duration of the stationary regime was significantly decreased in the biotic syntheses corresponding to a bacterial concentration of 0.135 $g.L^{-1}$. And the stationary regime was barely reached in the systems prepared with 0.350 $g.L^{-1}$ of bacteria. For t > 24000 s, v(t) decreased in the biotic systems, but more slowly than in the abiotic syntheses. The extent of time needed to reach v(t) < 0.1 increased with the bacterial concentration. Whereas it was equal to 1000-2000 seconds for the abiotic syntheses, it increased to about 2000 and 10000 seconds for the syntheses prepared with 0.135 and 0.350 $g.L^{-1}$ of bacteria respectively. The biotic syntheses prepared with 1.30 $g.L^{-1}$ were characterized by particularly slow kinetics. At t = 24000 s, v(t) was still smaller than 2. For t > 24000 s, v(t) decreased much more slowly than in any of the other systems. At t = 50000 s, it was larger than 0.1. The measurements of the redox potential in the biotic systems were consistent with the results displayed on Figure II.1.2 for the rate of proton release. Initially the rapid decrease of the redox potential in all systems was suggestive of a build up of the dissolved Fe(II) concentration in the solution. However, sorption processes and the reactions of oxidation and of hydrolysis of the Fe led to a stabilization of the redox potential, which was in all cases comprised between 215 mV and 250 mV for 4000 s < t < 24000 s. Between t = 24000 s and t = 25000 s, the redox potential sprang back of 30, 23, and 4 mV, for the syntheses prepared with 0.135, 0.350 and 1.30 $g.L^{-1}$ respectively, in comparison with a jump of 42 mV for the abiotic system. In agreement with the chemical analyzes, this suggests that residual Fe(II) lingered for longer periods of time in the biotic systems and that its oxidation was increasingly slowed by the presence of increasing concentrations of bacteria.

Complexation of the Fe^{2+} ions onto the bacterial reactive sites of the cell walls or of the exuded molecules inhibited their quick build-up as free ions in solution. This explains at least to some extent the retardation of the overshoot in the biotic kinetic curves, as well as the slow ending of the reaction at t > 24000 s. Complexation is regulated by a reversible thermodynamic equilibrium. Hence, as free Fe cations were reacting irreversibly with the iron oxide nuclei or crystals, the equilibrium was moving in favor of the dissociation of still complexed Fe^{2+} cations. As the bacterial concentration was increasing, the number of bacterial reactive sites was also increasing, moving the equilibrium in favor of the complexation of the Fe^{2+} or Fe^{3+} cations and thereby retarding the reactions of hydrolysis with the iron oxide nuclei or particles. Our study indicates that the complexation of Fe^{2+} cations onto bacterial reactive sites can drastically affect their kinetics of oxidation and hydrolysis, which can be retarded by many hours.

At a bacterial concentration of 0.135 $g.L^{-1}$, the kinetic curve was similar to the abiotic curve, except that it was shifted in time by about 5000 seconds, which corresponded to a Fe addition of about 100 μM. The bacterial surfaces were able to adsorb around 45 μM of Fe at most (Rose and Waite, 2002). On the other hand, the measured dissolved Fe concentration at t

= 25000 s was equal to only 7.3 μM in the system at 0.135 $g.L^{-1}$, in comparison with 2.7 μM for the abiotic system. Since the DOC concentrations were higher at t = 25000 s than at t = 0, this suggests that the exuded molecules initially present in the suspensions at 0.135 $g.L^{-1}$ were able to immobilize at most 5-10 μM of Fe. Hence, Fe^{2+} complexation was likely able to immobilize at most about 55 μM of Fe and to delay the kinetic curves by at most about 3000 s. Hence other processes also possibly played a significant retardation role on the reaction kinetics of the biotic syntheses at 0.135 $g.L^{-1}$. For instance, newly formed iron oxide nuclei might have adhered onto and interacted with the bacterial cell walls. In this case, their reactive sites were unavailable or less easily accessible to dissolved Fe ions for the reaction of hydrolysis. In addition, the physical immobilization of the Fe(III) monomers or oligomers on the cell walls also reduced their ability to react with each other. These two suggestions are supported by the SEM observations, which indicated that most of the iron oxide particles were in close association with the cell walls (Figure II.1.2). In the case of the biotic syntheses at 1.30 $g.L^{-1}$, the inhibiting effect of the cell walls on the growth of the crystal nuclei was particularly spectacular. However, even though the stoichiometry of those syntheses was significantly lower than 2, it was still equal to 1.60. Since Fe^{2+} complexation onto bacteria is known to be a relatively rapid phenomenon (Rose and Waite, 2002), and since Fe(II) oxidation alone consumes protons (Cornell and Schwertmann, 2003), the addition of a significant fraction of the base over a long period of time after the end of the addition of the Fe(II) suggests that the hydrolysis of the Fe(III) had proceeded to a significant extent at t = 80000 s in the systems prepared with c_b = 1.30 $g.L^{-1}$. We thus believe that Fe in those systems occurred probably mainly as oligomers of Fe(III) atoms. Further work, using for instance EXAFS of Mössbauer spectroscopy, would be interesting to characterize more precisely the speciation of the Fe immobilized by the bacterial cells walls and exuded molecules.

2. INTERACTIONS NON METABOLIQUES ENTRE LES SURFACES BACTERIENNES ET LE FER : EXEMPLE DE LA CINETIQUE D'OXYDATION DU FER(II) ADSORBE A LA SURFACE DE *BACILLUS SUBTILIS*

2.1. INTRODUCTION

Si nous avons pu démontrer que la présence de surfaces bactériennes ralentissait les processus d'oxydation et d'hydrolyse du Fe^{2+} (Fakih et al., 2008a ; pratie II.1.3.3), il reste à quantifier directement les cinétiques et les processus microscopiques impliqués. Pour atteindre cet objectif, nous avons réalisé une étude de la cinétique d'oxydation du Fe(II) adsorbé à la surface de *Bacillus subtilis.* Cette étude a été effectuée à deux pH différents 6,5 et 7,5. Une concentration élevée en cellules bactériennes par rapport à la concentration en Fe(II) a été choisie pour garantir que l'adsorption de Fe(II) ait lieu. Des isothermes d'adsorption et de désorption ont également été réalisées afin de vérifier que les modèles de Châtellier et Fortin (2004) pouvaient s'appliquer aux conditions expérimentales choisies ici. Ces modèles montrent que l'adsorption des ions Fe^{2+} est réversible à la surface des cellules de *Bacillus subtilis*, et que la concentration des sites réactifs de surface capables d'adsorber le Fe^{2+} est de 3.5×10^{-4} mol.g^{-1} (poids sec des bactéries). En fin, cette étude a permis de commencer à fixer des contraintes sur les mécanismes en jeu, mais elle reste préliminaire et nécessite d'être complétée.

2.2. MATERIELS ET METHODES

2.2.1. Préparation de la suspension bactérienne

Les suspensions bactériennes utilisées ont été préparées en adaptant le protocole de culture décrit dans la partie II (paragraphe II. 1. 2. 1)

2.2.2. Isothermes d'adsorption/désorption

Une solution de $FeCl_2.4H_2O$ ($1,2\ 10^{-2}$ M) a été préparée à pH 3 à l'aide de HCl (2,5 mM) pour prévenir l'oxydation du Fe(II) (Fakih et al., 2008a ; partie II.1.2.1). La suspension mère bactérienne est diluée dans NaCl (10^{-2} M), pour obtenir 100 ml d'une suspension à 5 g (poids sec).L^{-1} de bactéries (Châtellier et al., 2001, 2004 ; Fakih et al. ; 2008a, partie II.1.2.1).

2.2.2.1. Isotherme d'adsorption

La suspension bactérienne (99 mL) a été introduite dans un réacteur de 100 ml thermostaté à 25°C et hermétique à l'oxygène atmosphérique. La suspension a été agitée à l'aide d'un barreau aimanté. Des conditions strictement anaérobiques ont été obtenues par bullage de N_2 dans la suspension pendant 1,5 h. Le taux d'oxygène dissous et le pH ont été mesurés en continu, respectivement à l'aide d'une sonde à oxygène (Fisher Scientific

Bioblock) et d'une électrode pH (Metrohm : 6.0259.100). Le réacteur était connecté à deux burettes asservies de HCl et $FeCl_2$ (Titrino 794, Metrohm). Initialement, le pH de la suspension a été fixé à 2 par ajout d'HCl (10^{-1} M) afin d'empêcher l'oxydation du fer. Un ml de la solution de $FeCl_2$ a été ajouté, pour obtenir une concentration de fer de 10^{-4} M. La suspension a ensuite été stabilisée dans ces conditions pendant 1 h. Le pH de la suspension bactérienne a été progressivement augmenté jusqu'à pH 6,5 par ajout de NaOH (1 M). A chaque fois que le pH a augmenté d'une demie-unité, la suspension a reposé 1h, puis 3 ml ont été prélevés. L'échantillon a été immédiatement filtré à 0,2 µm. Puis 200 µl de ferrozine ont été ajoutés au filtrat, afin de déterminer la concentration en Fe(II) en solution (Viollier et al., 2000 ; Châtellier et al., 2004).

2.2.2.2. Isotherme de désorption

Afin d'évaluer la réversibilité de l'isotherme d'adsorption du Fe, une isotherme de désorption du Fe a été réalisée. Au cours de la désorption, le même protocole a été suivi mais en diminuant le pH de demie-unité en demie-unité de pH 6,5 à 2. Un prélèvement a été effectué par demie-unité de pH afin de déterminer la concentration en Fe(II) en solution selon le protocole décrit dans le paragraphe précédent.

2.2.3. Cinétique d'oxydation abiotique de Fe(II)

Un mL d'une solution de $FeCl_2.4H_2O$ (10^{-2} M) a été ajouté à 99 mL d'une solution NaCl (10^{-2} M) à pH 2 en conditions anaérobies dans un réacteur thermostaté (25 ± 1º C). Le pH de la suspension a été maintenu constant par l'ajout de HCl (10^{-1} M) ou de NaOH (10^{-1} M) à l'aide de deux burettes asservies (Titrino 794, Metrohm). Le pH a ensuite été augmenté rapidement à pH 6,5 ou 7,5 par ajout de NaOH (1 M). Les conditions anaérobiques ont alors été interrompues par ouverture du réacteur et la cinétique d'oxydation a été suivie en mesurant la quantité de NaOH (10^{-1} M) ajoutée en fonction du temps, en considérant que pour chaque mole de fer oxydé, 2 moles de NaOH étaient consommées (Eq. II.1.2.3.2).

$$Fe^{2+} + \frac{1}{4}O_2 + 2OH^- \rightarrow FeOOH + \frac{1}{2}H_2O \qquad \text{(II.1.2.3.2)}$$

2.2.4. Cinétique d'oxydation de Fe(II) à la surface de Bacillus subtilis

Une suspension bactérienne a été réalisée en ajoutant 5 $g.L^{-1}$ de cellules bactériennes à 99 ml d'une solution de NaCl (10^{-2} M) en anaérobie. Le pH initial de la suspension bactérienne variant entre 6,5 et 6,7, le pH a été ajusté à 4 par ajout de HCl (1 M). Un ml d'une solution de $FeCl_2.4H_2O$ (10^{-2} M) a ensuite été ajouté à cette suspension pour obtenir une concentration en Fe(II) de 10^{-4} M. Le système s'est équilibré pendant 10 mn, 1,5 ml de la suspension ont été prélevés afin de déterminer la concentration en Fe(II) dissous. Ensuite la suspension a été mise en aérobie et le pH a été ajusté à 5 par l'ajout de NaOH (1 M). Après une mise à l'équilibre de 10 min, 1,5 ml de la suspension ont été à nouveau prélevés. Enfin, le pH a été augmenté à 6,5 ou 7,5 après une mise à l'équilibre de 10 min, 1,5 ml de la suspension ont été prélevés.

Cette augmentation progressive, mais néanmoins assez rapide du pH, visait à éviter qu'une partie trop importante du Fe(II) ne s'oxyde avant de s'adsorber. En effet, à pH > 6,

l'oxydation du Fe(II) dissous peut être rapide. Le pH a ensuite été maintenu constant grâce à un titrateur. Au cours de la première heure, un prélèvement de 3 ml a été effectué toutes les 15 minutes, puis les prélèvements ont été progressivement espacés. L'expérience a été stoppée au bout de 24 h.

La moitié de chaque prélèvement (1,5 mL) a été immediatement filtrée à 0,2 µm, 100 µl de ferrozine ont ensuite été ajoutés au filtrat afin de déterminer la concentration de Fe(II) en solution. Dans un deuxième temps, 100 µl de HCl (1 M) ont été ajoutés au 1,5 mL non filtrés restant afin de désorber le Fe(II) de la surface des cellules bactériennes et de déterminer la concentration en fer adsorbé sur les bactéries. Au bout d'une heure, cette suspension a été filtrée à 0,2 µm, et 100 µl de ferrozine ont ensuite été ajoutés au filtrat afin de déterminer la concentration de Fe(II).

2.3. RESULTATS

2.3.1. Isothermes d'adsorption et de désorption

L'isotherme d'adsorption présentée dans la Figure II.1.1, montre qu'au fur et à mesure de l'augmentation de pH, la concentration de fer adsorbé à la surface des cellules bactériennes croît. Au dessus de pH 4, la pente de l'isotherme d'adsorption augmente rapidement. Cette augmentation correspond à une augmentation de la concentration en Fe(II) adsorbé. A partir de pH 6, quasiment tout le fer est adsorbé à la surface des cellules. L'étude de la cinétique d'oxydation du Fe(II) adsorbé à la surface des bactéries a débuté dans ces conditions.

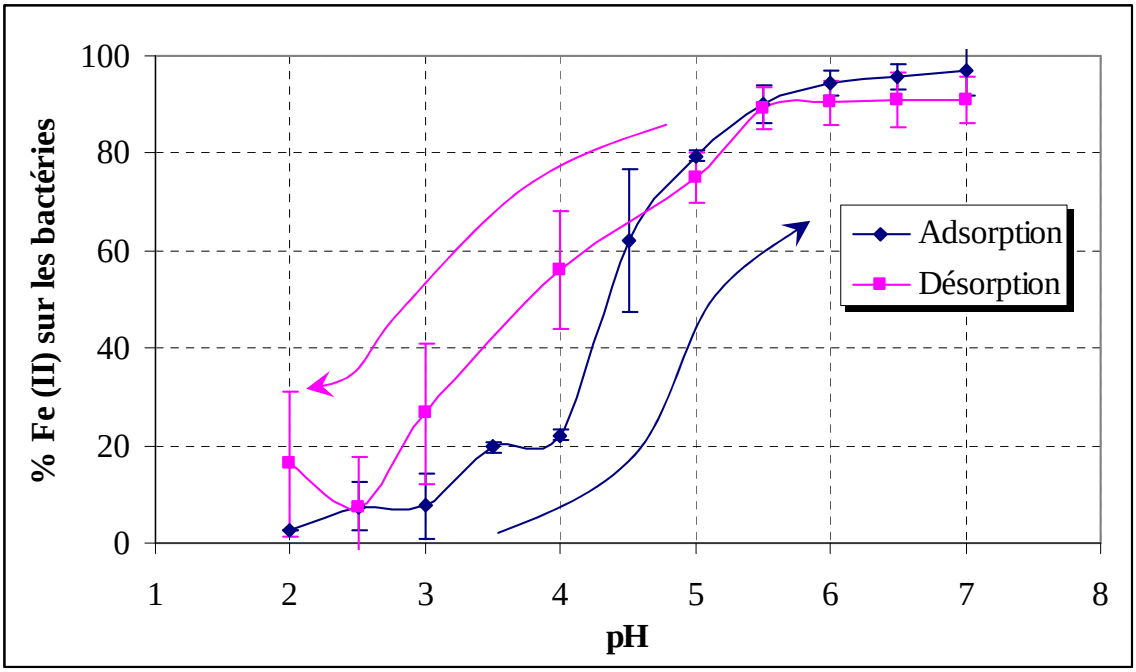

Figure II.2.1. Isothermes d'adsorption et désorption des ions Fe(II) (10^{-4} M) à la surface de *Bacillus subtilis* (5 $g.L^{-1}$). Les barres d'erreur correspondent à cinq répétitions de l'expérience avec cinq suspensions bactériennes différentes.

Malgré quelques écarts, les deux isothermes d'adsorption et de désorption sont assez semblables suggérant que l'adsorption est un phénomène réversible. Cependant à pH 2, 83% du Fe(II) total est présent dans la phase dissoute. 17 ± 15% en moyenne du Fe(II) sont donc restés lié à la phase particulaire correspondant aux cellules. Des imprécisions expérimentales peuvent également être en partie responsables de cette différence à l'issue de la désorption. Néanmoins, même si cette question n'est pas résolue cette différence ne remet pas en cause la quasi-réversibilité de l'adsorption de Fe(II) à la surface de *Bacillus subtilis* dans la mesure où la majorité du Fe(II) est libérée dans la solution à pH 2.

2.3.2. Cinétique d'oxydation de Fe(II) à pH 6,5 et 7,5

2.3.2.1. Cinétique d'oxydation abiotique de Fe(II) à pH 6,5 et 7,5

L'oxydation abiotique de Fe(II) à pH 6,5 est très rapide puisque le Fe(II) est libre dans la solution. Le Fe(II) est ajouté en en début d'expérience en une seule fois. Le volume de NaOH ajouté augmente progressivement pour se stabiliser vers 0,2 mL au bout de 1500 s (Fig. II.2.2). Ce volume correspond à la quantité de base ajoutée pour oxyder et hydrolyser les 10^{-5} moles de Fe(II) introduites dans le réacteur (Eq. II.1.2.3.2).

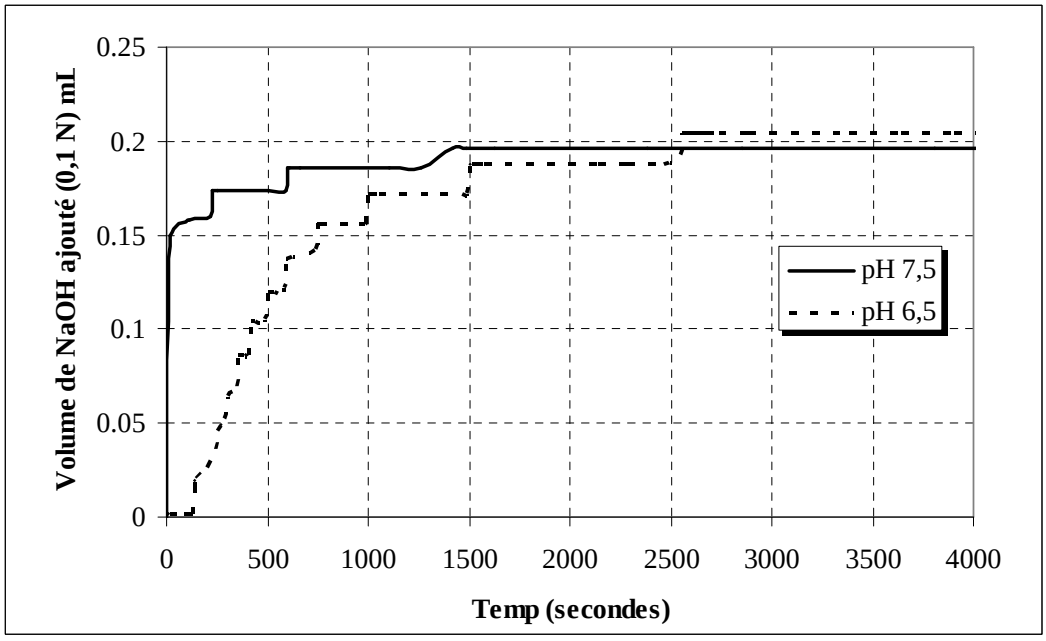

Figure II.2.2. Cinétique d'oxydation abiotique de Fe(II) (10^{-4} M) à pH 6,5 et à pH 7,5.

La cinétique abiotique d'oxydation de Fe(II) à pH 7,5 est encore plus rapide, puisque environ 75% de Fe(II) sont oxydés en moins de 20 s. Après 500 s, quasiement tout le Fe est oxydé. Dès les premières secondes, le volume de NaOH ajouté augmente à 0,18 ml et, se stabilise ensuite à 0,2 ml au bout de 1500 s (Fig. II.2.2).

2.3.2.2. Cinétique d'oxydation de Fe(II) à pH 6,5 et 7,5 en présence de bactéries

Cette cinétique d'oxydation a été mesurée par le suivi de la quantité de Fe(II) adsorbé à la surface des cellules bactériennes. La quantité de Fe(II) adsorbée diminue avec le temps alors que la concentration en Fe(II) dans la solution est en dessous de la limite de détection de la méthode de dosage à la ferrozine. Pour des conditions experimentales equivalentes, quand le Fe(II) n'est pas préalablement adsorbé à la surface des cellules bactériennes, du Fe(II) est présent et mesuré dans la solution (Fakih et al., 2008a ; partie II.1.3.2). La diminution de la concentration en Fe(II) adsorbé à la surface bactérienne dans notre expérience ne correspond donc pas à un processus de désorption. Aucune précipitation de Fe(III) n'est d'ailleurs observée dans la suspension. Il est donc possible d'assumer que le Fe(II) s'oxyde en Fe(III) à la surface des cellules bactériennes. Wightman et Fein, (2005), ont d'ailleurs montré que la désorption de Fe(III) est très difficile à cause de la forte stabilité du complexe Fe-surface bactérienne même à pH acide (1,5-2). L'oxydation peut cependant être expliquée par une seconde hypothèse qui consisterait en une désorption du Fe(II) induite par son oxydation très rapide dans la solution suivie d'une réadsorption à la surface des cellules bactériennes.

Le tableau II.2.1 montre l'évolution du pourcentage en Fe(II) adsorbé et oxydé dans les suspensions bactériennes en fonction du pH. La Figure II.2.3 représente les cinétiques d'adsorption/oxydation du Fe(II) en présence de bactéries pour des suspensions maintenues à pH 6,5 et 7,5. L'oxydation du Fe(II) débute entre pH 5 et pH 6,5 (Tableau II.2.1). Environ 20% et 30% du fer ont été oxydés durant cette première étape pour les expériences 1 et 2.

Tableau II.2.1. Moyenne et écart-type du pourcentage de Fe(II) adsorbé à la surface de *Bacillus subtilis* pendant la phase de l'augmentation de pH à 6,5 et à 7,5 avant de lancer la cinétique d'oxydation pour les deux expériences. L'écart type correspond à l'erreur de la réplication pour 5 expériences.

	% moyen de Fe (II) oxydé	**Ecart-type**		**% moyen de Fe (II) oxydé**	**Ecart- type**
Expérience 1			**Expérience 2**		
pH 4	-0,38	1,81	pH 4	3,17	4,86
pH 5	5,94	5,41	pH 5	15,35	3,24
pH 6,5 (t_0)	21,47	1,96	pH 6,5	22,36	6,37
			pH 7,5 (t_0)	31,82	7,89

Dans le cas de l'expérience 1, où l'étude cinétique s'est déroulée à pH 6,5, 40% du Fe(II) se sont oxydés dans les trois premières heures et 30% dans les 6 heures suivantes. Au bout de 21 heures, il ne reste plus que 10% de fer non oxydé et adsorbé (Tableau II.2.1, Fig. II.2.3).

Pour l'expérience 2 d'oxydation menée à pH 7,5, il y avait un risque que Fe(II) s'oxyde avant son adsorption sur les surfaces bactériennes. Le pH a donc été augmenté plus progressivement au début de l'expérience afin de favoriser l'adsorption. Le tableau II.2.1 montre que 30% du Fe(II) sont néanmoins oxydés durant la première étape de l'expérience 2. Ensuite, l'essentiel de l'oxydation se réalise durant la première heure. Au bout de quatre heures, seuls 6,6 ± 5,5% de Fe(II) restent non oxydés et adsorbés sur les surfaces bactériennes (Fig. II.2.3).

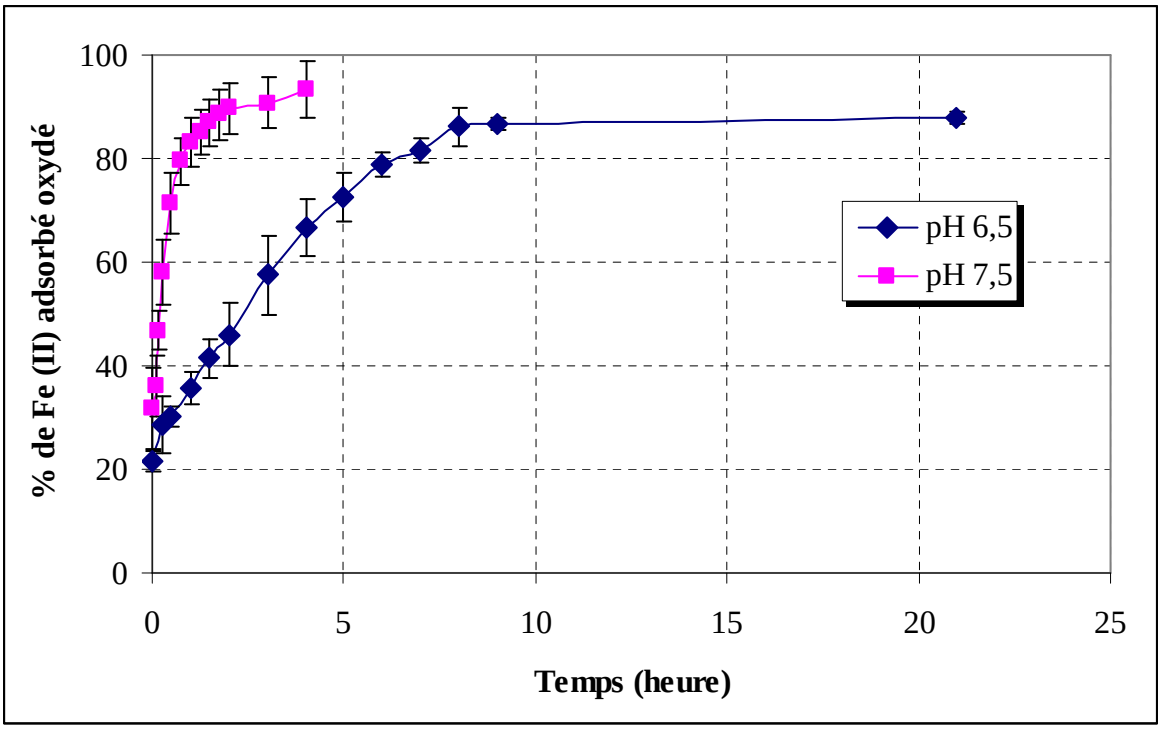

Figure II.2.3. Cinétique d'oxydation du Fe(II) (10^{-4} M) à la surface de *Bacillus subtilis* (5 $g.L^{-1}$) à pH 6,5 et 7,5. T0 correspond aux moments où les conditions anaérobiques ont été interrompues.

2.4. DISCUSSION

2.4.1. Isothermes d'adsorption et de désorption

Châtellier et Fortin (2004) ont observé que l'adsorption de Fe(II) à la surface de *Bacillus subtilis* était un phénomène rapide qui atteignait l'équilibre thermodynamique en quelques dizaines de minutes. La concentration des sites d'adsorption à pH neutre pour les ions Fe^{2+} a été estimée à environ 3,5 x 10^{-4} $moles.g^{-1}$ de bactéries sèches (Châtellier et Fortin, 2004). Dans nos expériences, les surfaces des bactéries sont sous-saturées, et elles ne devraient donc pas avoir de difficulté à adsorber l'ensemble du Fe(II), à des pH proches de la neutralité.

L'augmentation de la concentration de Fe(II) adsorbé à la surface des bactéries avec le pH est expliquée par le fait que les sites réactifs vis-à-vis de Fe(II) sont des groupements acido-basiques (Fein et al., 1997 ; Châtellier et Fortin, 2004 ; Rancourt et al., 2005). Au fur et à mesure que le pH augmente, les protons en solution deviennent moins nombreux, et sont donc moins compétitifs vis-à-vis de Fe(II) pour former des complexes de surface. De plus, la déprotonation de l'ensemble des groupements acido-basiques à la surface des cellules tend à leur conférer une charge négative qui favorise une attraction électrostatique des cations.

La valeur du pH au niveau du saut de l'isotherme (Fig. II.2.1) dépend de plusieurs paramètres, tels que la concentration en cellules bactériennes ou encore l'affinité de Fe(II) pour les différentes fonctions de surface. Nos résultats sont cohérents avec ceux de Châtellier et Fortin (2004). Ils montrent notamment que, si l'on ajoute 10^{-4} M de $FeCl_2$ dans une suspension de bactéries *Bacillus subtilis* à 5 $g.L^{-1}$, presque tout le fer est adsorbé à la surface des cellules à des pH > 6.

2.4.2. Effets non métaboliques de la surface bactériennes sur la cinétique d'oxydation de Fe(II)

Dans notre expérience d'oxydation abiotique, l'oxydation du Fe(II) se produit rapidement, encore plus à pH 7,5 qu'à pH 6,5. De ce fait, l'effet autocatalytique de l'oxydation n'a pu être mis en évidence, car il s'est manifesté trop rapidement pour être détecté.

Dans l'expérience d'oxydation biotique, l'oxydation du fer à pH 7,5 est beaucoup plus rapide (Tableau II.2.1, Fig. II.2.3). Lorsque les surfaces bactériennes sont sur-saturées en Fe(II), l'oxydation des cations Fe(II) en présence des bactéries conduit à la formation d'oxydes ferriques (Warren et Ferris, 1998). Cependant, lorsque les surfaces sont sous-saturées et le Fe(II) préalablement adsorbé, quel est l'impact de la présence des bactéries sur la vitesse d'oxydation de Fe(II)? L'expérience d'oxydation du Fe(III) en présence des bactéries, montre un fort ralentissement de cette cinétique d'oxydation du fer.

Trente pourcents des ions ferreux sont oxydés durant la première étape de l'expérience d'oxydation biotique 2 à pH 7,5. A ce pH, l'oxydation est plus rapide alors que la plupart des ions sont adsorbés à la surface des cellules comme l'ont montré les expériences d'adsorption. Si les ions ferreux s'oxydent malgré leur adsorption à la surface des bactéries, l'oxydation de Fe(II) est donc complètement dépendante du processus d'adsorption. C'est donc la cinétique désorption du Fe(II) qui contrôle sa cinétique d'oxydation.

Comme précédemment émise, une deuxième hypothèse serait que le Fe(II) s'oxyde très rapidement en solution après s'être désorbé et avant de se réadsorber sour forme de Fe(III) à la surface des bactéries puisque le Fe(III) présente une forte affinité pour ce type de surface ou si la cinétique d'oxydation du complexe est très lente (Wightman et Fein, 2005). Le Fe(III) préférentielement adsorbé au Fe(II) induirait sa libération dans la solution puis son oxydation et ainsi de suite. Cette hypothèse repose sur une oxydation quasi-instantanée du Fe(II), ce qui semble plausible au regard des résultats obtenus par les expériences d'oxydation abiotiques à pH 7,5. Dans cette hypothèse, ce serait la réaction de désorption qui controlerait la vitesse d'oxydation de Fe(II).

2.5. CONCLUSIONS

Nous nous sommes ici efforcés de mieux caractériser certains des processus non métaboliques impliquant le fer et les bactéries. Dans un intervalle de pH de 2 à 6,5, nous avons étudié la réversibilité de l'adsorption des ions Fe(II) à la surface de *Bacillus subtilis*. Malgré la possibilité d'une fraction d'adsorption irréversible, nos résultats présentent une bonne cohérence avec les résultats obtenus par Châtellier et Fortin (2004) qui montrent que l'adsorption des ions ferreux sur les surfaces bactériennes est un phénomène réversible.

Dans une seconde phase, la cinétique d'oxydation des ions Fe(II) adsorbés sur les surfaces bactériennes a été étudiée à pH 6,5 et 7,5. L'oxydation des ions ferreux dans ces conditions est un phénomène bien plus lent que dans des conditions abiotiques équivalentes. Deux hypothèses peuvent expliquer ces résultats : (1) l'oxydation de Fe(II) en Fe(III) se produit à la surface des cellules bactériennes, la cinétique d'oxydation est donc contrôlée par la cinétique de la réaction d'adsorption. (2) Les ions Fe(II) se désorbent de la surface des cellules bactériennes, s'oxydent rapidement en solution puis se réadsorbent. La cinétique d'oxydation est donc contrôlée par la cinétique de la réaction de désorption.

Cependant, il est important de noter que cette étude reste une étude préliminaire qui devra être complétée. En effet, afin de prouver sans équivoque que le Fe(II) s'oxyde en milieu

biotique, il est nécessaire de déterminer la concentration totale en Fe en solution (via des analayses par GFAAS ou ICP-MS), la concentration en Fe(III) étant alors obtenue par différence entre l'analyse du fer total et l'analyse du Fe(II). Le degré d'oxydation du fer adsorbé à la surface des bactéries doit être également déterminé. Il faudra utiliser, à ces fins, des techniques de spectroscopie fine comme la spectroscopie Mössbauer ou de radiations synchrotrons comme le XANES.

III. CHAPITRE II

Biodissolution - Réduction du Fe(III)

Ce chapitre est composé de trois parties. La première partie est constituée d'une étude de développement d'un 'outil' de suivi in situ de la dissolution d'oxydes de fer dopés en As(V) dans un sol hydromorphe. Cette partie a donné lieu à une publication soumise à la revue Applied Geochemistry en Avril 2008. Elle est complétée d'une étude de la dissolution de lépidocrocite dopée en As(V) dans ce même sol. La troisième partie présente et discute les résultats obtenus, en utilisant ces nouveaux dispositifs expérimentaux pour l'étude de la dissolution réductrice de ferrihydrite et lépidocrocite dopées en arsenic en colonnes de sols anaérobies. Cette troisième partie est présentée sous la forme d'un article scientifique soumis à la revue Chemical Geology en Juin 2008.

1. DEVELOPPEMENT D'UN 'OUTIL' DE SUIVI *IN SITU* DE LA MOBILISATION DU FER DANS LES SOLS

Mohamad Fakih
Mélanie Davranche
Aline Dia
Bernd Nowack
Patrice Petitjean
Xavier Châtellier
Gérard Gruau

Cette partie correspond à un article resoumis en version révisée à la revue Applied Geochemistry :' A new tool for *in situ* monitoring of Fe-mobilization in soils' (Juillet - 2008)

RÉSUMÉ

L'objectif de cette étude est de développer et tester une nouvelle technique d'étude qualitative et quantitative *in situ* de la dissolution réductrice d'oxydes de fer dopés en As(V) dans un sol hydromorphe. L'outil se compose de plaquettes acrylique ($2 \times 2 \times 0{,}2$ cm) striées. Dans ces stries sont fixées des particules de ferrihydrite pure (Fh) ou dopées en As(V) (Fh-As). Ces supports ont ensuite été insérés dans deux horizons (organo-minéral et albique), d'un sol de zone humide qui connait régulièrement des alternances des conditions rédox. La dissolution de la ferrihydrite et la solubilisation de l'As ont été quantifiées par spectrométrie de fluorescence des rayons-X (FRX). L'évolution minéralogique de la ferrihydrite a été caractérisée par microscope électronique à balayage équipé d'un spectromètre en énergie dispersive (SEM-EDS). Après plusieurs mois d'incubation, la ferrihydrite a été dissoute à des taux comparables à ceux mesurés dans les études de laboratoire, dans une gamme de 1 à 10.10^{-12} mol. Fe m^{-2}. s^{-1}. Les observations microscopiques (SEM) indiquent que les plaquettes sont fortement colonisées par les bactéries et que des biofilms se sont formés à leur surface dans l'horizon organo-minéral suggérant l'intervention d'un processus biologique plus marqué dans l'horizon organo-minéral que dans l'horizon albique. Après sept mois d'incubation des sulfures de fer se sont formés aux dépens de la ferrihydrite presque totalement dissoute dans l'horizon albique.

ABSTRACT

The aim of this study was to design and test a new tool for (i) the quantitative *in situ* monitoring of Fe(III) reduction in soils and (ii) the tracking of the potential mineralogical changes of Fe-oxides. The tool consists of small ($2 \times 2 \times 0.2$ cm) striated polymer plates coated with synthetic pure ferrihydrite or arsenic-doped ferrihydrite (Fh-As). These slides were then inserted within two different horizons (organo-mineral and albic) located in a wetland soil with alternating redox conditions. Dissolution was quantified by X-ray fluorescence (XRF) analyses of total metal contents before and after insertion into the soil. The crystallographic evolution of Fe oxides was characterized by scanning electron microscope equipped with an energy-dispersive spectrometer (SEM-EDS). Over the months, the ferrihydrite progressively disappeared, at rates comparable to those previously measured in laboratory studies, i.e. in the $1\text{-}10.10^{-12}$ mol. Fe m^{-2}. s^{-1} range. SEM observations indicate that the supports were highly colonized by bacteria and biofilms in the organo-mineral horizon, suggesting a biological-mediated process, while the albic horizon appeared to be characterized by a mostly chemical-mediated process. In the albic horizon, iron sulfide and other micro-precipitates were formed after seven months of incubation in balance with a quasi dissolution of initial Fe-oxides.

1.1. INTRODUCTION

Iron (III) oxides are common mineral components of soils, sediments, aquifers and geological materials. Trace metals commonly associate with Fe(III) oxides as adsorbed or co-precipitated species. Consequently the biogeochemical cycles and fate of Fe and trace metals are closely linked (Francis and Dodge, 1988; Lovley, 1991). Sorption and redox chemistry of Fe(III) oxides have been widely studied because of the recognition that they control water chemistry and contaminant behaviour in near-surface geochemical systems (Charlatchka and

Cambier, 2000; Davranche and Bollinger, 2000a; Davranche et al., 2003; Bonneville et al., 2004; Grybos et al., 2007). The stability of iron phases in soils exerts a major control on the mobility of both organic (Avena and Koopal, 1998) and inorganic pollutants (Ahmann et al., 1997; Zobrist et al., 2000; Zachara et al., 2001). Under oxic conditions, crystallized or amorphous Fe(III) mineral phases are able to incorporate or scavenge toxic trace elements such as As, Cr, Cd or Pb (Bousserrhine et al., 1999; Morin et al., 1999; Brown and Sturchio, 2002; Morin et al., 2002a; Bonneville et al., 2004). By contrast, the reduction of Fe(III) has been termed as the most important change that takes place in the development of anaerobic soils when the oxygen content decreases (Lovley, 1991). As a direct consequence the resulting reductively dissolved Fe(II) and associated trace metals can be released into soil solution (Schwertmann and Taylor, 1989; Lovley and Coates, 1997; Davranche and Bollinger, 2000a; Quantin et al., 2001; Zachara et al., 2001).

Iron reduction has thus to be considered as a key biogeochemical process that can affect metal geochemistry in soils through both direct and indirect mechanisms (Cooper et al., 2006). Iron (III) oxides can be reductively dissolved either by abiotic (e.g. Davranche and Bollinger, 2000a, b; Davranche et al., 2003; Chatain et al., 2005) or microbial pathways (e.g. Lovley and Phillips, 1986a ; Francis and Dodge, 1990; Roden and Wetzel, 2002; Zachara et al., 2001). However, biological reduction of iron oxides in natural environments is probably the major process governing Fe(III) reduction (Francis and Dodge, 1990; Grybos et al., 2007) since Fe(III) acts as terminal electron acceptor for bacteria-mediated organic matter oxidation to carbon dioxide (Lovley and Phillips, 1986a; Francis and Dodge, 1990; Chuan et al., 1996; Charlatchka and Cambier, 2000; Green et al., 2003; Quantin et al., 2001, 2002; Grybos et al., 2007).

Numerous studies have been dedicated to the understanding of the impact of Mn- and Fe-oxyhydroxides reduction on trace metal mobility in soils. Among them, incubation experiments - using synthesized iron oxides or natural soil samples - were performed using a series of chemical reducing agents (such as hydroxylamine, ascorbate or sodium borohydride) (Davranche and Bollinger, 2000a, b; Davranche et al., 2003; Chatain et al., 2005). Microbial-mediated reduction experiments of synthetic iron oxides co-precipitated with Pb, Cr, Ni, Zn and Cd (Francis and Dodge, 1990; Zachara et al., 2001) or natural samples (Charlatchka and Cambier, 2000; Chuan et al., 1996; Quantin et al., 2001; Quantin et al., 2002) were also conducted. However, experimental studies carried out with natural samples were lacking information on newly precipitated minerals. By contrast, experiments performed with synthesized iron oxides did not yield information on the impact of the soil matrix. For instance, the true impact of the other solid phases naturally occurring in soils, such as organic matter or clays, both known to be strong scavengers of Fe(II) and trace metals, is not considered, since the soil matrix is absent. And when present, the soil structure is usually strongly disturbed. In addition, the soil solution composition and its flow are usually not adequately reproduced. Recently though, Benner et al. (2002) and Hansel et al. (2003) showed, by studying the reductive dissolution of iron oxides in dynamic system, that both solution flow and solute release strongly influence the dissolution rate and the nature of newly formed minerals.

To overcome the inherent limitations of laboratory experiments, several authors developed recently techniques to study *in situ* mineral dissolution in soils (Jorgensen and Willems, 1987; Voegelin et al., 2002; Birkefeld et al., 2005, 2006, 2007; Jenkinson and Franzmeier, 2006). As an example, Jenkinson and Franzmeier (2006) have built specific captors dedicated to the identification of the reduction conditions that could occur in natural soils. Iron oxides were fixed by air-flow heat on tubes that could be directly inserted into soils. Reduction was visually assessed by the observation of the depletion of the oxide coating on the tube surface. Although this technique ensures that the solids can be totally recovered at

the end of the incubation time, it can be only applied to a specific type of iron oxide (the one formed during the iron fixation by the air-flow heat system). Birkefeld et al. (2005) also developed an *in situ* method to monitor the transformation of metallic oxides in soils. They fixed particles on polymer supports with a thin film of epoxy resin. Thereby, the particles were not only in direct contact with the soil matrix but the designed supports could also be easily recovered and analyzed.

Because most previous experimental approaches studying *in situ* the evolution of minerals in soil suffered from drawbacks, this study was focussed on a further development of the support technique designed by Birkefeld et al. (2005) for the use with iron oxides. Iron oxide particles were fixed onto inert polymer slides at low temperature by precipitating directly the Fe-oxide particles onto the slides. The slides were then inserted into two different horizons of a wetland soil, bringing the iron oxide particles in direct contact with the soil matrix. To investigate the alteration of the iron oxide particles over time, the slides were recovered after 1, 3 or 7 months and they were examined by XRF and SEM-EDS. The goals of this work were beyond the test of the technique itself, to quantify the reductive dissolution of iron oxides in anaerobic soils, to study the mineralogical evolution of the iron oxides and the formation of secondary phases and finally to evaluate the impact of the reductive dissolution on the release of an associated trace element, arsenic.

1.2. MATERIALS AND METHODS

All chemicals used in this study were of analytical grade. All solutions were prepared with doubly de-ionised water (Milli-Q system, Millipore). All containers used in this study were first soaked in 10% ultrapure HNO_3 for 48 h at 60°C to remove all possible contaminants, rinsed with Milli-Q water for 24 h at 60°C, and finally dried at 30°C.

1.2.1. Polymer Supports

The principle of the polymer support-method is to bind iron oxides irreversibly on polymer plates. Considering its peculiar properties, Poly(methyl methacrylate) (PMMA) polymer (Plexiglas/Acrylite) was chosen as material for the slides. PMMA is highly resistant against weathering and is characterized by sturdy mechanical and chemical properties (Schwarz, 2002). The PMMA supports can stay for long times (up to years) in soils under environmental conditions without any aging (Birkefeld et al., 2005).

The support size of 2×2 cm $\times$ 0.2 was chosen to fit the sample holder of the X-Ray fluorescence (XRF) instrument. The thickness of the plates was selected to be 2-mm-wide to avoid both torsion and bending of the support (Fig. III.1.1). In a first attempt, inspired by Birkefeld et al. (2005), iron coated quartz grains were fixed with epoxy resin onto a 4-cm^2-size polymer support. However, a major problem was encountered during mineralogical analyses. The X-ray diffraction (XRD) spectra corresponded to the quartz spectra since the iron oxide amount was much smaller than that of the quartz.

In an alternative procedure the iron oxides were directly fixed onto the slide surface, beforehand treated to allow iron oxide particles binding. Without surface treatment, indeed, iron oxide could not hold on to the slide. Four different procedures were tested to optimize the immobilization of the iron oxides on the PMMA: (1) sandpapering of the support surface using a coarse grain sandpaper (100-µm-diameter), (2) stripes made by a cutter, spaced less than 2 mm apart; (3) a regular series of 0.5-mm-deep holes with 0.9 mm diameter regularly spaced from each other at 2 mm using a robot (Charlyrobot, France), (4) 0.1-mm-deep

parallel stripes, spaced 1 mm apart using a robot (Charlyrobot, France) (Fig. III.1.1). All supports were washed and dried according to the herebelow described washing procedure. The polymer supports were (i) soaked in 10% ultrapure HNO_3 for 48 h at 60°C to remove all possible contaminants, (ii) rinsed with Milli-Q water for 24 h at 60°C, and (iii) finally dried at 30°C. Pure ferrihydrite (Fh) and ferrihydrite associated with As (Fh-As) (1% of coprecipitated As) were synthesized (Schwertmann and Cornell, 2000) in the presence of the PMMA slides. At the end of the synthesis, the suspension containing iron precipitate and slides were centrifuged at 4500 rpm for 15 minutes not only to separate the solid from the solution but also to get a better contact of Fh with the slides. The supports were dialysed using a 12 kDa dialysis bag. The external solution was regularly removed and replaced with milli-Q water until the solution conductivity became lower than 15 $\mu S.cm^{-1}$. The slides were dried during 24 hours at 35°C, and then stroked with a paintbrush to eliminate the weakly bound iron oxides at the slide surface.

a)

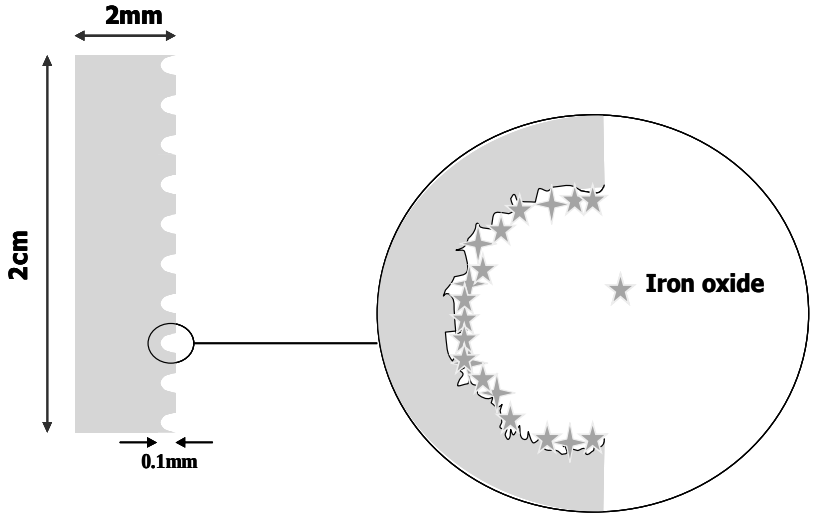

b)

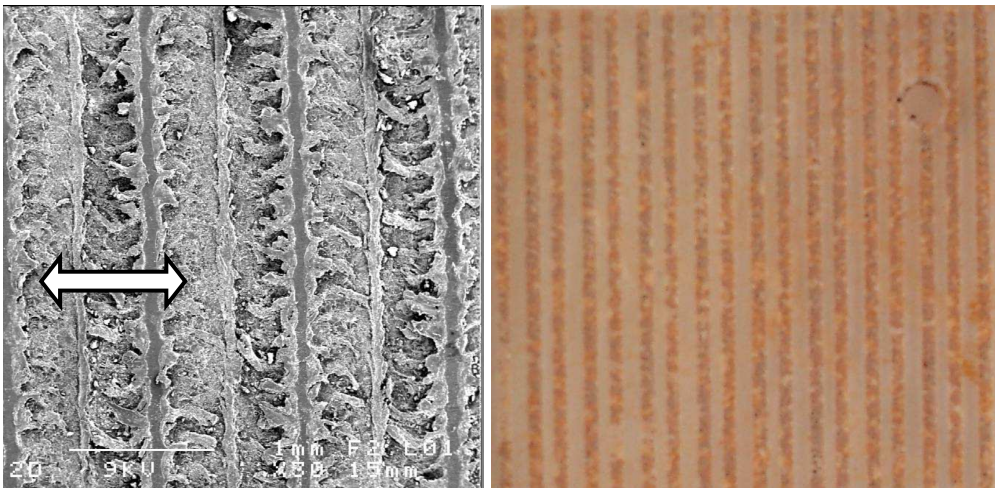

Figure III.1.1. a) Scheme of the Fe-oxide fixation onto the stripes. b) (Left) SEM picture of a type (4) PMMA slide after coating with HFO, the arrow indicates the stripe width. (Right) Digital picture of a bare PMMA slide.

In order to determine the amount of iron oxides covering the four different slide types, optical and scanning electron microscope (SEM) observations and weight analyses were conducted. The slide types (2) and (3) were rejected since they presented a large surface

heterogeneity. Ferrihydrite tended to form micro-blocks during the drying process. The slides of type (1) reached an average value of 0.87 mg Fe-oxide per support with a variation coefficient of 26.4%. The slides of the types (4) displayed an average of 1.01 mg per support with a variation coefficient of 0.16%. Type (4) slides were finally chosen after microscopic studies and quantification of the Fe bound to 60 type (4) slides. The initial amounts of Fe attached to each individual slide were determined by XRF (See the herebelow section III.1.2.4).

1.2.2. Stability of iron oxide fixation onto slide

Abrasion test were carried out to quantify the potential falling off of iron oxides when the slides were introduced and recovered from the soil matrix. Polymer supports covered by Fh were introduced into a mixture of 50/50 (by weight) of humidified sand (sand from Fontainebleau (France), 150-300 µm in diameter, VWR) and glass marbles (2mm in diameter) to model a soil matrix. These two components were beforehand washed with concentrated HCl and then rinsed 5 times in milli-Q water. The slides were left 10 days in contact with the moist mixture. The polymer supports were then extracted by hand and the sand/marble mixture washed with 20 mL of concentrated HCl. The presence of iron in the solution was then analyzed by an Agilent Technologies HP4500 ICP-MS instrument (Dia et al., 2000; Yeghicheyan et al., 2001; Davranche et al., 2005; Pourret et al., 2007). It can be noted that the Fe content measured in the solution leaching the sand and glass marble mixture was lower than the ICP-MS detection limit for iron (20 $\mu g.kg^{-1}$).

1.2.3. Calibration of X-Ray Fluorescence (XRF) and Fe concentration quantification

XRF analyses were conducted before and after contact with the soil to determine the amount of fixed Fe and associated elements on a Spectro X-Lab 2000 (Germany) instrument. The XRF technique allowed a non destructive analysis of the slides. A custom-made calibration was performed for the various iron oxides. A set of 7 supports was stirred in various HCl concentrations to obtain slides with variable iron amounts. Pure Fh and Fh-As slides were stirred with 0, 0.1, 0.2, 0.3, 0.4, 0.5 and 1N of HCl for 30 minutes at 250 rpm. HCl concentrations and required time of incubation were selected after preliminary test experiments. The supports were then dried and analyzed by XRF. The remaining particles were completely dissolved by stirring the supports with 6N HCl for 1 hour at 250 rpm. The iron and As concentrations in the solution were then analyzed by AAS (SOLAAR M6 F-AAS, Thermo). Plotting of XRF data and absolute amount of Fe and As on each slide allowed to make a calibration to transform XRF results into Fe and As concentrations per slide.

1.2.4. SEM/EDS Scanning Electron Microscopy with X-ray microanalysis

The slides devoted to the SEM/EDS observations were maintained in anaerobic conditions until they were brought to the SEM facility. SEM combined with Energy Dispersive X-ray Spectroscopy (EDS) was used to analyze surface mineral modifications as well as to identify the elemental composition of eventually newly formed phases. Before insertion into the soil, a first series of samples was directly observed by SEM. This allowed a comparison of the morphology of the iron oxides before and after exposure to the soil. A second series of incubated slides was dried at critical point following the herebelow described procedure and

then metallised. The drying at the critical point was used to preserve the biological structure of the biofilm and bacteria. The slides were submerged for 48 hours in a bath of 2.5% glutaraldehyde adjusted with 0.1M NaOH to pH 7.2 (Anderson, 1951), then washed three times during 10 min in anaerobic water adjusted with 0.1M NaOH to pH 7.2. They were then dehydrated during 10 min in successive ethanol solutions (30%, 60%, 80%, 90%, 95%, and 100%). The slide surfaces were observed by SEM with a JEOL JSM-6301F Field Emission Gun Scanning Electron Microscope operating at 9kV after being coated with Au-Pd nanoparticles by cathodic deposition with a JEOL JFC 1100 sputter. The elemental composition of individual particles or agglomerates of particles was investigated by Energy Dispersive X-ray Spectroscopy (EDS) using an Oxford Link-Isis Si/Li analyzer. Some slides were also examined by SEM and EDS after their incubation in the soil horizons without drying at critical point.

1.2.5. Field experiments within soil

The slides were inserted in two different horizons in the wetland soil of the Kervidy-Naizin catchment, Western France. This wetland was selected because of the evidence of periodical iron reduction events (Fe(II) release into soil solution) during temporal flooding in winter and spring. Dissolved Fe(II) concentrations were found to increase from 0 (< 0.01 $mg.L^{-1}$, detection limit) in late fall (beginning of the flooded period) to 11.5 $mg.L^{-1}$ in spring (end of the waterlogged period) (Bourrié et al., 1999; Dia et al., 2000; Olivié-Lauquet et al., 2001; Gruau et al., 2004).

The slides were inserted into the organo-mineral horizon (0 to 15 cm) and the albic horizon (15 to 30 cm). Fifteen pure Fh slides and 15 Fh-As slides were inserted into each horizon. One should mention that the Fe-oxides fixed on slides did not chemically disturb the soil system since the amount of fixed Fe-oxides on slides was low compared to the total concentration in iron in the soil (Table III.1.1). The polymer supports were vertically inserted into the soils with the help of a small stainless steel lancet. The bottom of the lancet was flattened to allow the penetration into the soil. In order to locate the slides in the soil for retrieval, a thin nylon thread was fixed on the support. The slide insertion did not much disturb the soil system at scales of more than a few mm. The impact of the slides on the natural flow of the soil solution did possibly not differ from the effect of small rocks or debris naturally present in the soil.

At each sampling campaign, five slides were removed from each soil horizon. The slides were removed from soil after a period of 1, 3 or 7 months. Within a few seconds after being exposed to the air, the slides were stored in anaerobic and hermetically sealed bottles, which were immediately flushed with nitrogen. Later on, the slides were rinsed with anaerobic Ultra-pure water in order to remove the loosely attached soil particles in Jacomex isolator glove box under purifications (< 10 ppm of O_2 and H_2O). Two slides were also dried under anaerobic conditions at the critical point for SEM observations (see section III.1.2.6). This procedure is required to observe possible organo-mineral associations and analyze surface changes as well as to evidence eventual new minerals. One other slide was cleaned with water and dried at room temperature overnight for quantitative analysis by XRF. Finally, two slides were cleaned and dried under anaerobic conditions in the isolator glove box for XRD analyses.

Soil samples were collected at both depths and dried at ambient temperature. Total concentrations of major and trace elements were analyzed by ICP-MS (trace elements) and ICP-AES (minor elements) following a lithium metaborate fusion. The loss of ignition was measured as an indicator of the carbon content. The major element concentrations in the soil

are given in Table III.1.1. The organo-mineral horizon contained 1.03% of iron while the albic horizon contained only 0.61%. The concentration of As was 7.47 $\mu g.g^{-1}$ in the organo-mineral horizon and 3.66 $\mu g.g^{-1}$ in the albic horizon.

Table III.1.1. Bulk chemical composition (major and trace elements) of the two investigated soil horizons from the wetland of the Kervidy-Naizin catchment (North-western France).

Major elements (%)	**Si**	**Al**	**Fe**	**Mn**	**Mg**	**Ca**	**Na**	**K**	**Ti**	**P**	**LOI**
Organo-mineral horizon	28	3.5	1.03	0.01	0.28	0.13	0.14	1.00	0.49	0.02	**19.1**
Albic horizon	33	4.3	0.61	0.00	0.26	0.04	0.16	1.32	0.63	0.01	**6.2**
Trace elements ($\mu g.g^{-1}$)	As	Cd	Co	Cr	Cu	Ni	Pb	Zn	REE		
Organo-mineral horizon	7.48	0.29	5.38	76.61	8.52	17.01	22.53	38.78	128.27		
Albic	3.66	0.17	3.36	92.04	3.95	17.22	15.64	31.55	134.26		

1.2.6. Soil solution sampling and chemical analyses

During the incubation times, about 20 ml of solution were sampled once a month under nitrogen flux using a water trap (Bourrié et al., 1999) inserted in the two soil horizons. The samples were filtered through a 0.2 µm cellulose acetate membrane (Millipore) and divided into several aliquots for the analysis of Fe(II), SO_4^{2-} and NO_3^-. Iron (II) was directly complexed by 1.10 phenantroline following the AFNOR NF T90-017 methodology (AFNOR, 1997), and analysed using an UV-visible spectrophotometer (UVIKON XS, Bio-Tek) with a precision of ±5%. NO_3^- and SO_4^{2-} concentrations were analysed by ion chromatography (Dionex, model X120), with a precision of about ±4%.

1.3. RESULTS

1.3.1. Support stability

The amount of released iron during the abrasion test was lower than the ICP-MS detection limit for iron (20 $\mu g.kg^{-1}$), the loss due to abrasion can therefore been considered as less than 0.08 % (in weight). Hence, the supports can be considered as not sensitive to mechanic abrasion during insertion, exposure and retrieval. Test with leaching of the supports in water showed no decrease in the Fe content over time. The tested iron oxides on the supports were therefore stable when pH or redox conditions did not change.

1.3.2. XRF calibration curve

The XRF signal was linearly related to the amount of Fe-oxides and As on the plates (Fig. III.1.2). The calibration curve for pure Fh had a correlation coefficient of 0.98, for Fh-As of 0.98 for Fe and 0.96 for As. These three correlation coefficients correspond to those previously determined by Birkefeld et al. (2005) for other metal particles.

1.3.3. Soil solution composition during incubation

The pH remained constant at 6.05 ± 0.2 in both soil horizons during the seven months of incubation. The Fe(II) concentrations in the organo-mineral horizon soil solution during the incubation in the wetland soils increased from 0.21 $mg.L^{-1}$ to 2.58 $mg.L^{-1}$, NO_3^- concentrations decreased from 33.3 $mg.L^{-1}$ to 2.6 $mg.L^{-1}$ while sulphate remained constant at 15.5 ± 0.3 $mg.L^{-1}$ between one and three months of incubation (Table III.1.2). After seven months of incubation reductive conditions were still predominating and Fe(II) was present in the soil solution at 1.28 $mg.L^{-1}$, the SO_4^{2-} concentration was 4.8 $mg.L^{-1}$, and NO_3^- was 4.5 $mg.L^{-1}$.

a)

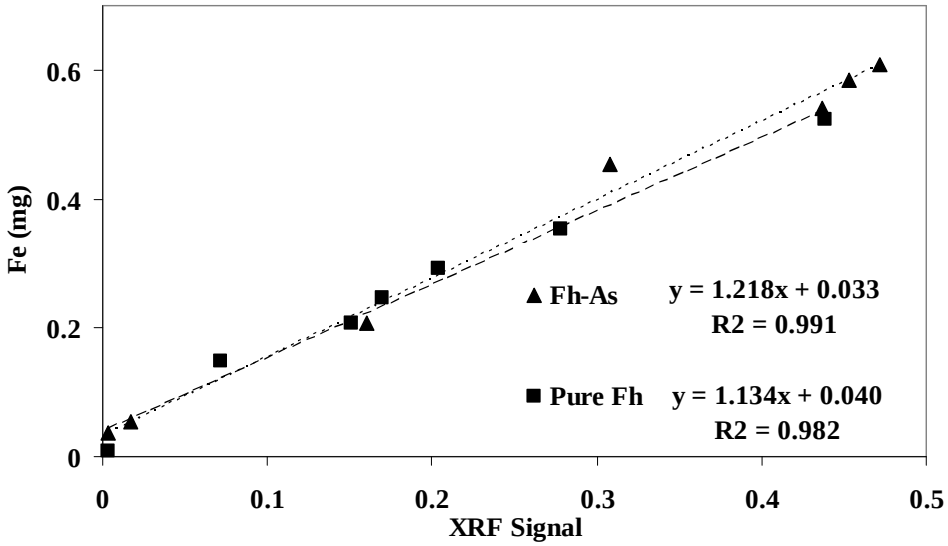

b)

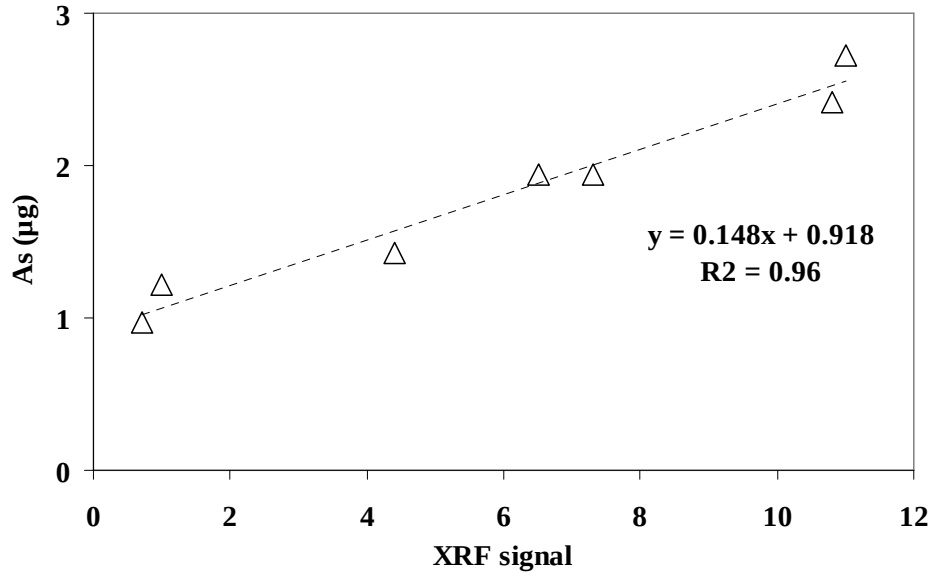

Figure III.1.2. a) XRF calibrations curves relating XRF signals to Fh amounts measured by complete dissolution for the two investigated Fe-oxides, pure Fh (continuous line) and Fh-As (discontinuous line), b) XRF calibrations curves relating XRF signals to As amounts measured by complete dissolution for Fh-As.

In the albic horizon soil solution a strong increase in the Fe(II) concentration (from 0.04 $mg.L^{-1}$ to 10.21 $mg.L^{-1}$) concomitant to a strong decrease of NO_3^- (from 12.7 $mg.L^{-1}$ to 1.2 $mg.L^{-1}$) and a strong decrease of sulphate (21.3 to 1.7 $mg.L^{-1}$) were observed during the first three months of incubation (Table III.1.2). However, a strong Fe(II) decrease - down to 0.23 $mg.L^{-1}$ - concomitant to a NO_3^- increase (2.4 $mg.L^{-1}$) was noticed after seven months.

Table III.1.2. Fe(II), NO_3^- and SO_4^{2-} concentrations in the soil solution during slide exposure, recording the redox state of the system through time.

	Concentration ($mg.L^{-1}$)			
	Organo-mineral horizon			
	t = 0	**1 month**	**3 months**	**7 months**
Fe(II)	0.21	0.69	2.58	1.28
SO_4^{2-}	15.8	15.5	15.2	4.8
NO_3^-	33.3	19.1	2.6	4.5
	Albic horizon			
	t = 0	**1 month**	**3 months**	**7 months**
Fe(II)	0.04	1.91	10.21	0.23
SO_4^{2-}	21.3	16.1	1.7	1.6
NO_3^-	12.7	13.7	1.2	2.4

1.3.4. Changes in Fe and As concentration on the iron-coated slides over time

Figure III.1.3 shows the dissolved amount of iron and As versus exposure times as a percentage of the initial metal mass. The comparison between the initial and the final Fe concentration measured by XRF allowed determining the dissolution of pure Fh and Fh-As in both organic and albic horizons of the investigated wetland soil. The Fe release from pure Fh increased as a function of the incubation time from 42% after one month to 51% and 58% after 3 and 7 months in the organo-mineral horizon. The Fh-As slide exhibited the same trend through time in the organo-mineral horizon, 15, 25 and 67% of Fe were dissolved after 1, 3 and 7 months, respectively. The As release correspond to 18, 19 and 57 % dissolved at 1, 3 and 7 month respectively.

Comparable Fe dissolution and As release kinetics were observed in the albic horizon (Fig. III.1.3). For the pure Fh, 19, 44 and 91% of Fe were dissolved after 1, 3 and 7 months, respectively. For, Fh-As, 45 and 74% of Fh was dissolved after 1 and 7 months of incubation, respectively. The As is released at 29 and 86 % after 1 and 7 months, respectively.

The dissolution rates for the pure Fh, Fh-As and associated As, were calculated for each slide at each sampling campaign (1, 3 and 7 months). Therefore, as an example, the rate at 3 months corresponds to the overall rate from 0 to 3 months. In order to facilitate comparison with previous studies, they were normalized to mol. m^{-2} s^{-1}. A surface area of 240 $m^2.g^{-1}$ was assumed, as found by BET for both pure and coprecipited As ferrihydrite suspension (Pedersen et al., 2006). The results are shown in Table III.1.3. In both soils the dissolution could be divided into two distinct steps, first a rapid one followed by a slower second one.

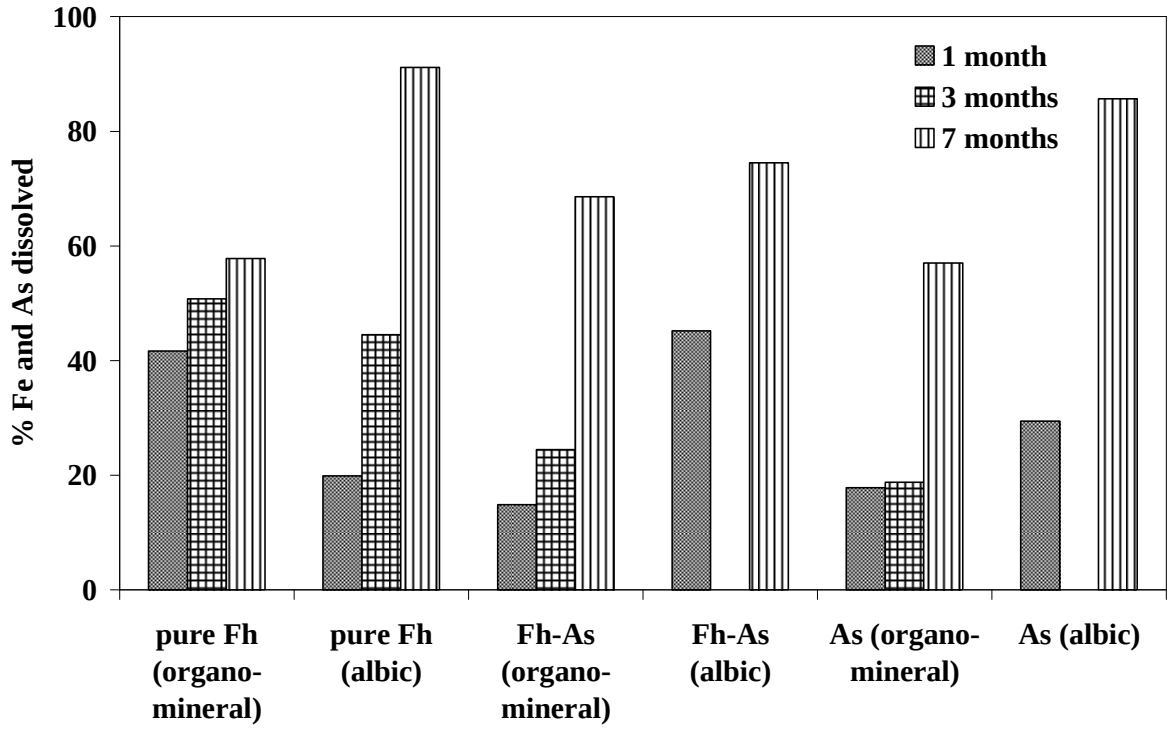

Figure III.1.3. Percentage of dissolved Fe a) and As b) on the different slides recovered from the both soil horizon, expressed as mass of metal recovered in percentage of initial mass of metal (determined by XRF).

Table III.1.3. Average dissolution rates of pure Fh, Fh-As and release of As from Fh-As in the two horizons during the first month and between the end of the first month and the seventh month. [a] : Dissolution rates were calculated for a surface area of 240 $m^2.g^{-1}$ (Pedersen et al., 2006) for each sampling campaign to taken into account the system heterogeneity.

Horizon	**Phase**	**Dissolution rate (mol $Fe.m^{-2}.s^{-1}$ and mol $As.m^{-2}.s^{-1}$)[a]**		
		1 month	**3 months**	**7 months**
Organo-mineral	**Pure Fh**	$1.2\ 10^{-11}$	$4.7\ 10^{-12}$	$2.3\ 10^{-12}$
	Fh-As	$4.3\ 10^{-12}$	$2.3\ 10^{-12}$	$2.7\ 10^{-12}$
	As (Fh-As)	$3.8\ 10^{-12}$	$4.0\ 10^{-12}$	$1.22\ 10^{-11}$
Albic	**Pure Fh**	$5.7\ 10^{-12}$	$4.3\ 10^{-12}$	$3.7\ 10^{-12}$
	Fh-As	$1.3\ 10^{-11}$	-	$3.1\ 10^{-12}$
	As (Fh-As)	$6.3\ 10^{-12}$	-	$2.1\ 10^{-11}$

1.3.5. SEM/EDS observations

The initial iron oxides exhibited a morphology characterized by 1- to 10-µm-long fractures (Fig. III.1.4) possibly formed as a consequence of the shrinking of the precipitates when the iron oxides were dried. The evolution of the morphology of the Fh and Fh-As surfaces was evidenced by SEM observations at each time step and is shown for the organo-mineral horizon in Fig. III.1.5 and for the albic horizon in Fig. III.1.6. After seven months of incubation, the slide colour became lighter, except for the pure Fh slide inserted in the albic horizon where after three months of incubation a black coloration occurred.

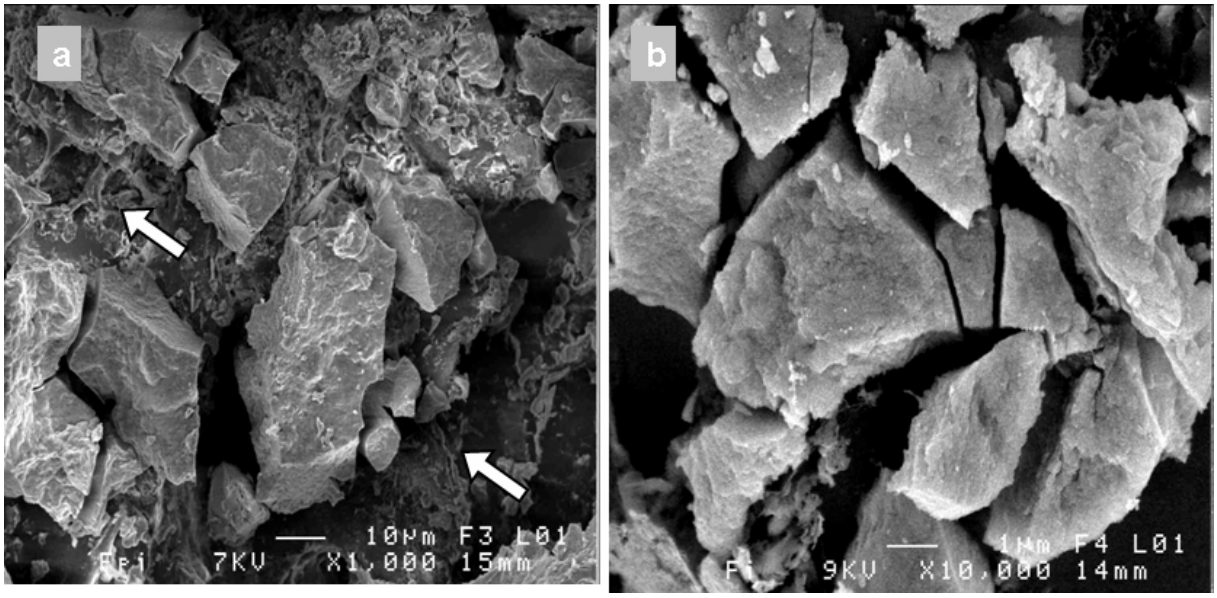

Figure III.1.4. SEM pictures of pure Fh on the slide before any contact with soil. a) magnification 1000 x and b) magnification 10000 x. The arrows indicate the three-dimensional structure of the bare PMMA.

After one month of incubation in the organo-mineral horizon, Fh and Fh-As slides were colonized by bacteria and biofilms covering the Fh and Fh-As particles (Figs. II.1.5a and II.1.5d). After three months, typical morphological features of progressive dissolution were observed on the Fe-oxide particle surface. The top layer was first dissolved, and then cavities appeared (Figs. III.1.5a to f). The formation of crusts occurred at the Fh surface during the third month and new phases were observed on the surface after the seventh month of incubation (Fig. III.1.5c). Newly formed micro-precipitates of 0.2 to 0.3 µm size also appeared on the Fh-As surface slide after seven months of incubation (Fig. III.1.5f). These micro-precipitates were mixed with Fh-As particles. EDS analysis evidenced that these new phases did not contain any sulphur in significant amount.

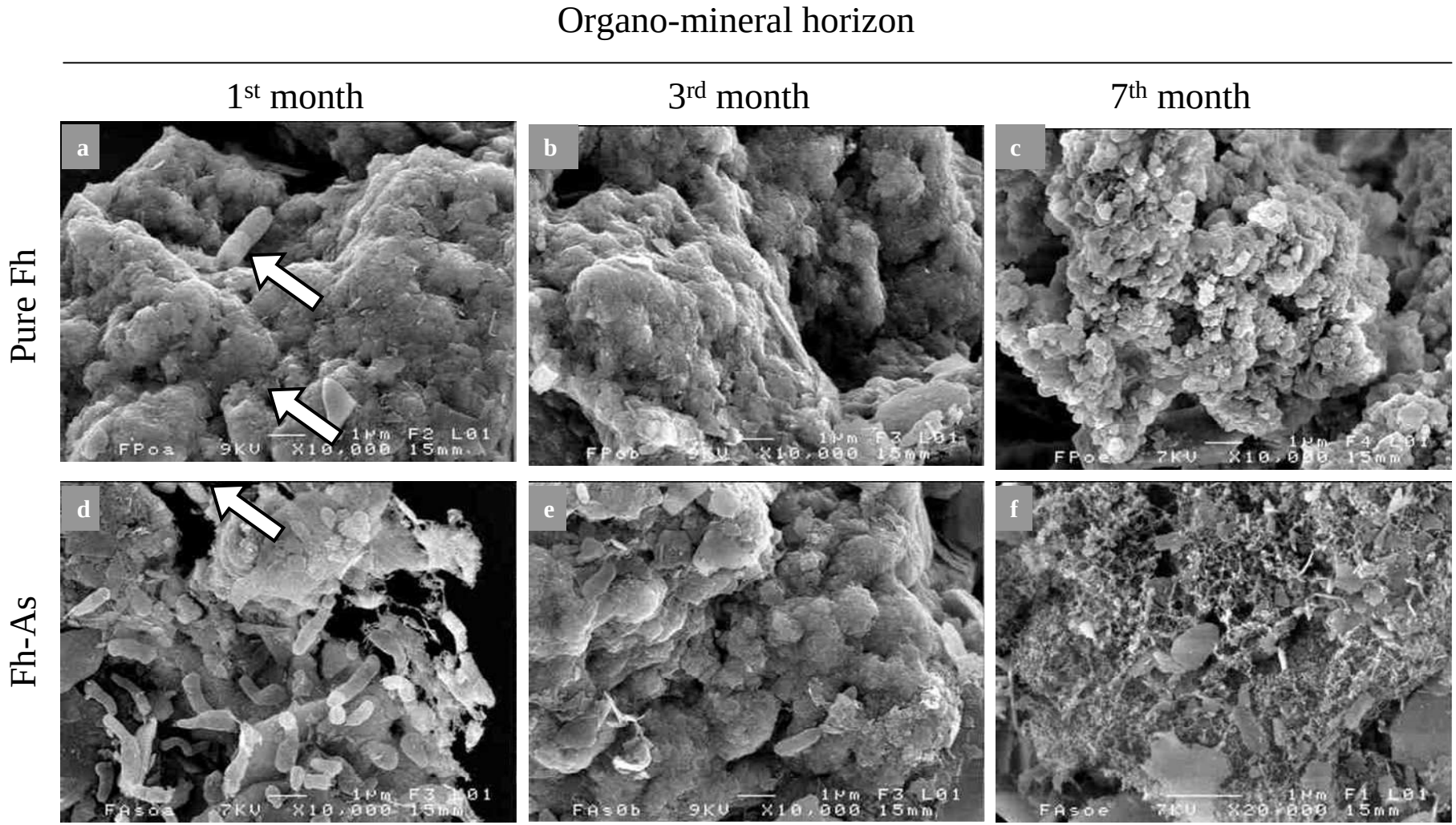

Figure III.1.5. SEM pictures of the morphological changes of pure Fh and Fh-As during exposure to the organo-mineral horizon: a), b) and c) plates covered with pure Fh and removed in after one, three and seven months, respectively. d), e) and f) Fh-As covered plates removed after one, three and seven months, respectively. The arrows indicate the bacteria and biofilms covering the pure Fh and Fh-AS.

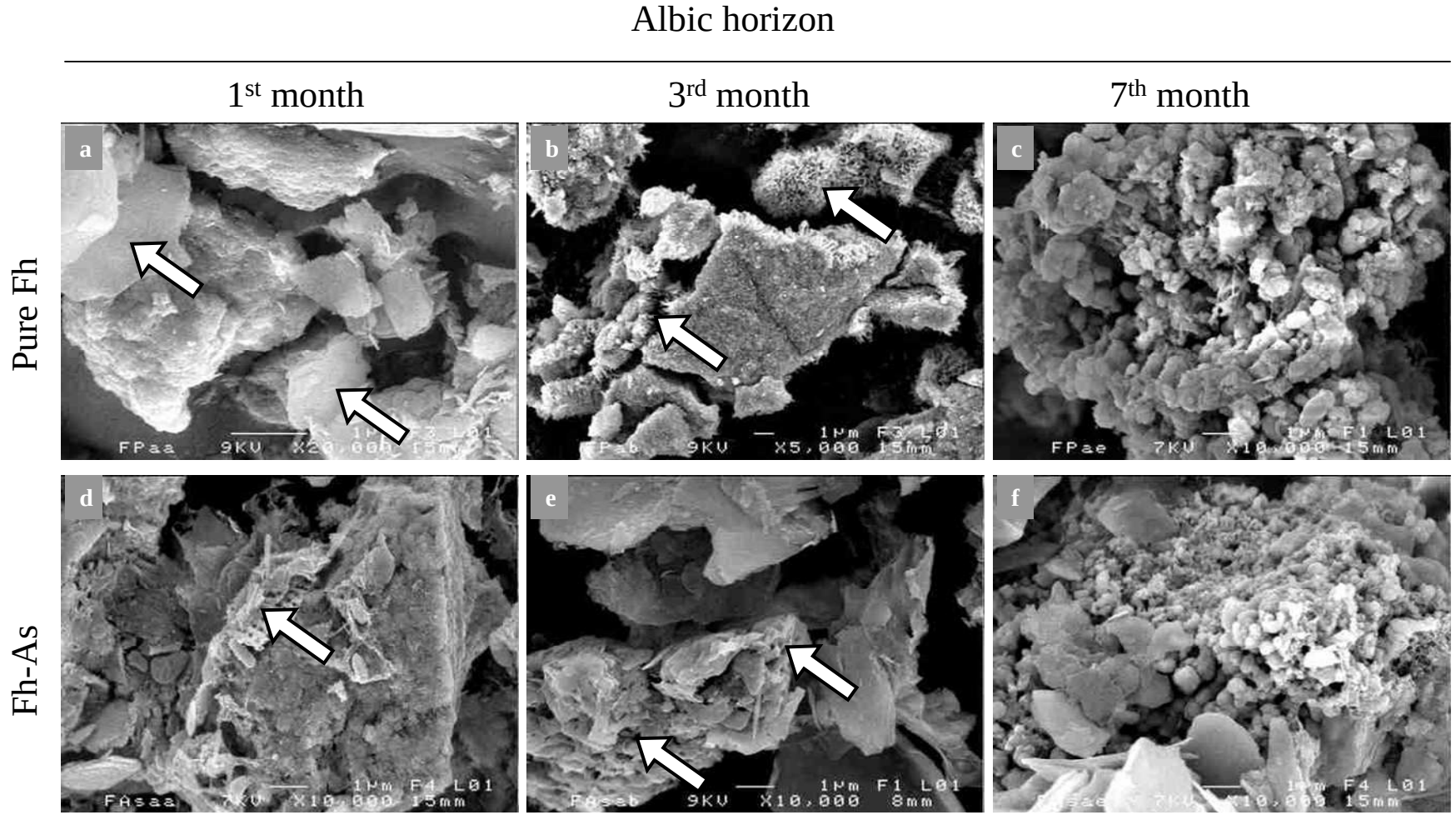

Figure III.1.6. SEM pictures of the morphological changes of pure Fh and Fh-As during exposure to the albic horizon: a), b) and c) SEM pictures of plates covered with pure Fh removed after one, three and seven months, respectively. d), e) and f) SEM pictures of plates covered with Fh-As removed after one, three and seven months, respectively. The arrows show soil mineral particles (6a and 6d), needles formed by sulphur and iron (6b) and cavities on the Fh-As surface (6e), respectively.

By contrast, after one month of incubation in the albic horizon, Fh and Fh-As slides were only sparsely colonized by bacteria (Fig. III.1.6) while large colonies were observed in the organo-mineral horizon (Fig. III.1.5). However, small soil particles (1-µm-long) were observed on the slide surfaces and determined by EDS (12.17% Al, 25.61% Si, 3.29% K and 1.24% Fe), providing evidence that interaction between the iron oxides and the soil mineral matrix occurred (Figs. III.1.6a and III.1.6d). The Fh morphology was modified after three months of incubation as evidenced by the SEM images which displayed typical morphological features corresponding to progressive dissolution. Again, the top layer was first dissolved, and then cavities and holes appeared (Figs. III.1.6b and III.1.6e). Moreover, small regular needles (0.4-µm-long) had been crystallized at the Fh surface (Fig. III.1.6b and III.1.7). SEM/EDS analysis provided the evidence that these needles were formed by sulphur and iron (4.1% of Fe and 0.5% of S), suggesting that precipitation of an iron sulphide occurred. After seven months of soil contact, the Fh slides also showed morphologically comparable needles (0.2- to 0.4-µm-long), mixed with micro-precipitates (Fig. III.1.6c). At the same time, the Fh-As slide exhibited an alteration on the surface of the iron oxides and the formation of small porous spheres (0.2 to 0.5-µm-diameter) was observed (Fig. III.1.6f). EDS analysis evidenced that both the micro-precipitates and the small porous spheres did not contain any sulphur in significant amount, but significant concentrations of Fe, C and O. This suggests that these formations might be secondary minerals formed out the dissolution products of the Fe-oxides. Furthermore, EDS analysis showed that the needles occurring on the slide after seven months did not contain any sulphur. This latter point strongly suggests that the iron- and sulphur-rich needles precipitated at an early stage were a metastable iron sulphide phase. This unstable iron sulphide phase disappeared after seven months of incubation within the soil.

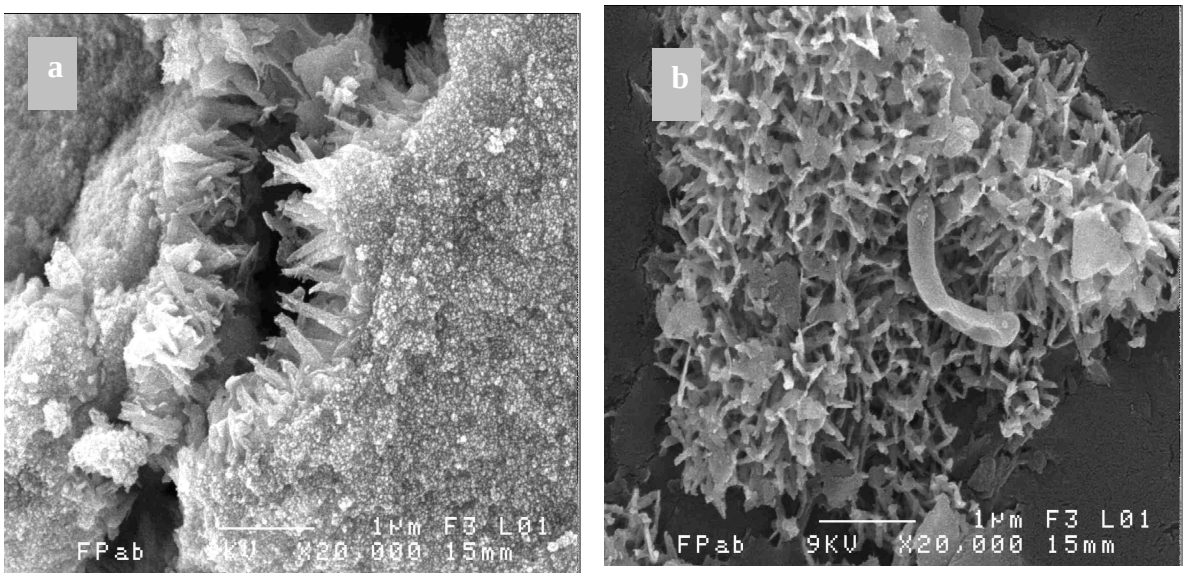

Figure III.1.7. SEM pictures of iron sulphide crystals after three months of incubation in the albic horizon. a) Transformation of pure Fh into iron sulphide. b) Iron sulphide mixed with bacteria and soil mineral particles.

1.4. DISCUSSION

1.4.1. Slide technique scope

The PMMA support method has previously been used to fix mineral particles in a pioneer study performed by Birkefeld et al. (2005). This study showed that (i) the polymer supports did not show any visible change over the incubation period of 18 months, that (ii) neither neutral nor acidic conditions affected its structure of the polymer and that (iii) the method allows easy exposure and recovery of mineral particles under environmental conditions. In this work, Fe-oxide particles were mechanically stable on the slides during seven months. A major concern of the validation of the method was that particles could be lost from the supports during exposure in the soil and the further analysis. The effect of sample handling was analyzed by means of an abrasive test which provided evidence that both pure Fh and Fh-As were not torn from the slides and released into the solution. This demonstrated that this method could be safely used to fix Fe-oxides on such supports to study their *in situ* behaviour in soils. Acid-mediated dissolution experiments carried out to perform XRF calibration curves showed that the dissolution of Fh and Fh-As increased following increasing HCl concentrations. As a consequence, a good mechanical stability of the Fe-oxides onto slides can be expected. This allowed us to establish XRF calibration curves for Fh and Fh-As. The occurrence of both small soil particles and intense bacterial colonization despite cleaning with anaerobic water showed that the Fe-oxides were in direct contact with soil and soil solution (Figs. III.1.6a and III.1.6d). Such supports covered with Fe-oxides seem therefore adequate for the *in situ* monitoring of reductive dissolution of a various set of iron oxides in natural soil matrices.

1.4.2. Dissolution rates

Iron-oxides dissolution rates were determined trough laboratory experiments involving chemical and/or biological reduction (Postma, 1993; Roden and Zachara, 1996; Paige et al., 1997; Roden, 2003; Pedersen et al., 2006) (Table III.1.4), but were never determined under field *in situ* conditions. Here, for the first time dissolution rates of ferrihydrite agglomerates were monitored in the field (Table III.1.3). The comparison between Table III.1.3 and III.1.4 provides evidence that the rates obtained in this study were mostly lower than the rates from chemical reduction experiments. However, they are similar to those determined in bacterial-mediated reductive dissolution studies (Roden et Zachara, 1996; Roden, 2003). This is quite a remarkable result considering all the factors known to affect dissolution rates. Firstly, it has already been proposed that bacteria cannot access the very tiny pores in the structure of the ferrihydrite agglomerates (Roden and Zachara, 1996; Roden, 2003, 2006). As a result, the dissolution rates measured for ferrihydrite were found to be dependent upon the aggregation state of the particles. Secondly, one of the important factors controlling the dissolution rates of iron oxides is the concentration of bacterial cells (e.g., Roden and Zacchara, 1996; Roden, 2003; Bonneville et al., 2004). The rates derived by Roden and Zacchara (1996) and Roden (2003) were obtained when the bacterial concentration was fixed at $2\ 10^8$ cells/ml. This concentration is far to be considered representative for the concentration of iron-reducing bacteria in soil. However, most field studies attempting to quantify the number of iron-reducing bacteria in soils have been able to characterize only those species, which can be cultured in the laboratory, using the most probable number method (Koretsky et al., 2003). Therefore, this point can be possibly reconsidered. Moreover, as in laboratory studies, the

initial dissolution rates were higher than later on (Postma, 1993; Roden and Zachara, 1996; Paige et al., 1997; Roden, 2003; Pederson et al., 2006). For instance, the pure Fh dissolution rate at the beginning was 2.9 to 5.8 (for the 3rd and 7th month) times higher in the organo-mineral and 1.4 to 1.5 (for the 3rd and 7th month) time higher in the albic horizon, than during the second part of the experiment. Initially, the fresh iron oxide agglomerates were easily accessible to the bacteria. However, over time, they became covered by the components of the soil.

Table III.1.4. Compilation of dissolution rates of pure and As-ferrihydrite estimated from chemical and biotic reductive dissolution experiments.

Oxide	Dissolution rate (mol Fe. m^{-2}. s^{-1})	Reducing agent	References
Ferrihydrite	$7.0\ 10^{-12}$	Bacteria	Roden et Zachara (1996)
	$2.0\ 10^{-12}$ $1.7\ 10^{-10}$	Bacteria Chemical reducer (Ascorbate)	Roden (2003)
	$1.2\ 10^{-8}$	Chemical reducer (Ascorbate)	Postma (1993)
	$3.3\text{-}4.1\ 10^{-8}$	Chemical reducer (Ascorbate)	Larsen and Postma (2001)
Ferrihydrite-As	$5.3\ 10^{-11}$	Chemical reducer (Ascorbate)	Pedersen et al. (2006)
	$1.8\text{-}8.0\ 10^{-11}$	Chemical reducer (Ascorbate)	Paige et al. (1997)

In addition, the Fe(II) concentration built up in the soil solution over the winter. Fe(II) has been shown to adsorb onto bacterial cells (Roden and Urrutia, 2002; Roden, 2003; Chatellier and Fortin, 2004), with the potential effect that this inhibits the reductive power of the bacteria. Some of the Fe(II) also probably readsorbed or reprecipitated onto the iron oxide surfaces (Appelo, 2002). All these factors mentioned above likely combined to reduce the dissolution rates of the Fe-oxides over the months.

Moreover, it must be notified that the dissolution rate of Fh is probably underestimated because of Fe re-precipitation as sulphide. The XRF method measures all iron on the slide surface whatever its speciation. It has been, however, assumed that all iron onto the slide surface was Fh to calculate the dissolution rate.

No significant difference between the rates obtained for the Fh and As-Fh systems was observed. It is likely that the ratio of As introduced in the iron oxides agglomerates (see Table III.1.5) was too low to induce major consequences.

Table III.1.5. Time-linked variation of the As/Fe ratio in both horizons.

	As/Fe (ratio in weight, mg/mg)		
	1 month	**3 months**	**7 months**
	Organo-mineral horizon		
Initial	$3.57\ 10^{-3}$	$4.04\ 10^{-3}$	$3.60\ 10^{-3}$
Final	$3.43\ 10^{-3}$	$4.34\ 10^{-3}$	$4.94\ 10^{-3}$
Final/Initial	0.96	1.08	1.37
	Albic horizon		
Initial	$4.46\ 10^{-3}$		$4.79\ 10^{-3}$
Final	$5.74\ 10^{-3}$		$2.70\ 10^{-3}$
Final/Initial	1.29		0.56

The combination of both total dissolved amounts (Fig. III.1.3) and dissolution rates through time (Table III.1.3) suggests that the weathering conditions were more intense in the albic horizon than in the organo-mineral horizon. This observation led us to propose that dissolution in both horizons probably involved different mechanisms with a mostly bacteria-mediated dissolution in the organo-mineral horizon, while abiotic mechanisms dominated in the albic horizon.

1.4.3. Reduction processes

Reduction processes occurring in natural soils depend on both abiotic and biotic factors. Abiotic controls include the geometry and cohesion of the soil matrix (Chenu and Stotzky, 2002). The surface area, shape, and spatial arrangement of soil particles and surface properties of iron particles are for instance of crucial importance. Chemical parameters, including the pH, can also affect the reduction of iron oxides. Biologically mediated processes involve microorganisms through direct and indirect mechanisms. Direct mechanisms involve close interactions between the iron-reducing bacterial cells and the solid surfaces of the Fe(III)-rich particles (Arnold et al., 1990). By contrast, in indirect mechanisms, microorganisms release reducing agents into the soil solution (Francis and Dodge, 1988).

The SEM pictures showed that the Fe-oxide particles placed in the organo-mineral horizon were highly colonized by bacteria and biofilms, suggesting that microorganisms played a key role in the involved processes. The coupled observation of (i) widespread bacteria and biofilm colonization on Fh particles, (ii) an alteration of the Fh surface and (iii) newly formed micro-precipitates, suggests that biological, physical and physicochemical processes occurred simultaneously. However, as elsewhere observed in analogous contexts, the observation of numerous bacterial colonies and biofilms occurrences allowed to assume that the reduction was mainly performed through a direct microbial reduction (Chenu and Stotzky, 2002; Lovley, 1993)**.**

Colonization of bacteria and biofilms on Fe-oxide particles was less important in the albic horizon. At the end of incubation (7^{th} month), the dissolution of Fh and Fh-As was higher in the albic horizon (Fig. III.1.3) despite the difference in their respective dissolution rates at the beginning of incubation. Because sulphide precipitation was only observed in the albic horizon (Fig. III.1.6b), the hypothesis is reinforced that the reduction conditions were more intense in the albic horizon. In the first month, the concentration of sulphate was high (Table III.1.2) and then decreased rapidly in both horizons, but nearly disappeared in the albic horizon after three months of incubation. The formation of iron sulphides during the third

month in the albic horizon was possible because sufficient ferrous ions were available to react with any H_2S produced (Germida et al., 1992).

1.4.4. Newly formed minerals

Two types of newly formed minerals were observed on the Fh slides. A yet unidentified Fe rich solid phase was observed on the slides recovered after 7 months (Figs. III.1.6b and III.1.6f). Most of these new phases were found in the albic horizon where the reductive conditions seem to have been more intense. SEM/EDS analyses allowed identifying a metastable iron sulphide on one of the two slides recovered from the albic horizon after three months. The occurrence of these new iron sulphides agrees with a previous study, where Charlatchka and Cambier (2000) observed the same sulphide precipitation within a soil after two months of flooding experiments at controlled pH (pH-6.2). As previously mentioned the apparently weaker reducing conditions prevailing in the organo-mineral horizon prevented any formation of iron sulphide in this horizon, although the iron sulfides seemed to grow directly on the iron oxides (Fig. III.1.6b and III.1.7). This observation supports a possibly indirect metabolic mechanism involving bacterial cells. Alternatively, an autocatalytic abiotic reaction might have developed from reactive nuclei forming spontaneously under the reductive and chemically favorable conditions of the soil.

1.4.5. Arsenic behaviour

XRF analyses provided the evidence that solubilisation of arsenic from Fh-As was lower than that of Fe in the organic horizon and higher in the albic horizon. Paige et al., (1997) and Pedersen et al. (2006) showed by studying the chemical reductive dissolution of Fh-As(V) with a ratio As/Fe similar to this study (0.005 against 0.006 (in mol)) that As is released in the solution after Fe(II). Apparently, As remains adsorbed onto the ferrihydrite surface until the surface area and thereby the site surface number is too small to contain all the As. It is important to note that As is believed to be adsorbed onto the ferrihydrite surface even during ongoing precipitation (as in this study) (e.g. Waychunas et al., 1993, Paige et al., 1997, Pedersen et al., 2006). Concerning, the albic horizon where As was more dissolved than Fe, an explanation could be that Fe is reincorporated onto the slide surface. A part of Fe(II) could be readsorbed or precipitated onto the slide. Many previous studies provided evidences that reductive dissolution of Fe-oxides was stopped by Fe(II) readsorption and saturation of the Fe-oxide surface sites, e.g. Appelo et al. (2002). Fe(II) readsorption is also favoured as compared to As readsorption (despite the valence, +3) due to its higher concentration in the solid hydration layer (Appelo et al., 2002). The formation of new minerals at the Fe-oxide surface results in a reincorporation of Fe onto the slide surface, increasing its concentration relative to As. In addition, Fe(II) is known to adsorb strongly onto bacterial and organic surfaces (Chatellier and Fortin, 2004), but As is not. Moreover, after soil incubation, various inorganic materials were observed to accumulate on the slide surface, commonly covering the Fh and clogging the fractures. In particular, particles with plate-like shapes typical of clays were numerous in the albic horizon and to a lesser extent in the organo-mineral horizon. The iron content of these mineral particles is taken into account by the XRF analysis and considered as Fe from ferrihydrite. All these mechanisms are not or to a lower extent involved in the organic horizon due to the release of organic compounds into the solution during the reduction process (Olivié-Lauquet et al., 2001; Grybos et al., 2007). This organic matter can complex Fe(II) and consequently inhibit the precipitation and readsorption processes.

Considering all these factors, we can predict that the As/Fe ratio should increase in the organo-mineral horizon and decrease in the albic horizon with time. Table III.1.5 displays the initial and final As/Fe ratio (in weight) on each slide and their evolution as a function of the incubation time. In the organo-mineral horizon the ratio increased, suggesting that Fe was more solubilised than As. By contrast, in the albic horizon, the As/Fe ratio decreased with the incubation time, which confirms that part of the released Fe was either reincorporated or supplied by soil particle (such as clays) on the slide surface.

1.5. CONCLUSIONS

This study showed that: (i) Fe-oxides can easily be fixed on inert supports and thus can be easily inserted and recovered from soils, (ii) that this new *in situ* method can be used to monitor Fe mobilization in soils during redox alternations, (iii) that it is possible to determine the reduction and dissolution kinetics and (iv) that the associated morphological and crystallographic changes of Fe-oxides can be evaluated as well.

The *in situ* monitoring experiments performed in the upper horizons of a wetland soil provided evidence that the reductive dissolution mechanisms are mostly bacteria-mediated with reductive dissolution rates comparable to previously published rates inferred from laboratory-based experimental studies. Iron sulphides and other micro-precipitates were formed only in the albic horizon after seven months of incubation in balance with a quasi dissolution of initial Fe-oxides.

Future studies dedicated to the identification of both the nature of the bacteria consortium involved in the reduction process and the nature of the secondary mineralogical phases are under progress. Kinetic laboratory studies of the trace metal release process that accompanied the Fe(III) reduction will be carried out both with amorphous ferrihydrite and more crystallized iron oxides (lepidocrocite) to study the role of iron oxide crystallinity.

2. DISSOLUTION REDUCTRICE DE LEPIDOCROCITE DOPEE EN AS(V) DANS UN SOL HYDROMORPHE : ETUDE CINETIQUE MENEE SUR LE TERRAIN

2.1. INTRODUCTION

Dans la partie précédente, nous avons mis en point une nouvelle méthode d'étude qualitative et quantitative *in situ* de la dissolution réductrice de la ferrihydrite dans le sol hydromorphique. Dans cette partie, la technique des supports précédemment validé a été appliquée à l'étude de la dissolution *in situ* de la lépidocrocite dans les mêmes horizons de sol. La lépidocrocite a été choisie pour ces différences cristallographiques avec la ferrihydrite (moins cristallisée) et pour sont ubiquité dans les sols.

2.2. MATERIELS ET METHODES

Cette étude axée sur la dissolution réductrice de lépidocrocite dopée en As(V), As(V)-lépidocrocite, a été menée dans le bassin versant de Kervidy-Naizin. Le bassin versant de Kervidy-Naizin est particulièrement bien adapté à l'étude *in situ* des processus de biodissolution et de bioréduction des oxydes de Fe. En effet, des cycles rédox impliquant le fer ont été mis en évidence dans les sols des zones humides de fonds de vallée de ce bassin, avec le développement d'épisodes de réduction du Fe en fin d'hiver et au printemps suivis de phases d'oxydation en été, suite à l'abaissement de la nappe (Durand et Torres, 1996 ; Bourrié et al., 1999 ; Molénat et al., 1999 ; Dia et al., 2000 ; Olivié-Lauquet et al., 2001).

Deux types de plaquettes recouvertes de lépidocrocite ont été utilisés dans cette étude. Des plaquettes identiques aux plaquettes recouvertes de ferrihydrite dopée en As (V) (voir partie III.1.2.2.) mais cette fois-ci recouvertes de As(V)-lépidocrocite. Vingt deux plaquettes ont été ainsi insérées dans les deux horizons organo-minéral et albique de la zone humide de Naizin-Kervidy. L'insertion des plaquettes dans les différents horizons a été réalisée selon la méthode décrite dans Fakih et al. (2008b) (Partie III.1.2.5). Ces plaquettes ont été incubées pendant une période variant entre 1 et 9 mois, en commençant à l'automne au moment de l'intensification des pluies et de la reprise des écoulements dans la zone humide. En parallèle à l'insertion des supports de 2 × 2 cm, des plaquettes longues de 40 cm recouvertes de lépidocrocite ont été introduites verticalement dans le sol de la zone humide de Naizin-Kervidy afin d'étudier, sans discontinuité géographique, l'impact de la nature des horizons du sol sur la réduction de l'As(V)-lépidocrocite. La partie supérieure de la plaquette était donc en contact avec l'horizon organo-minéral et la partie inférieure avec les horizons albique et rédoxique.

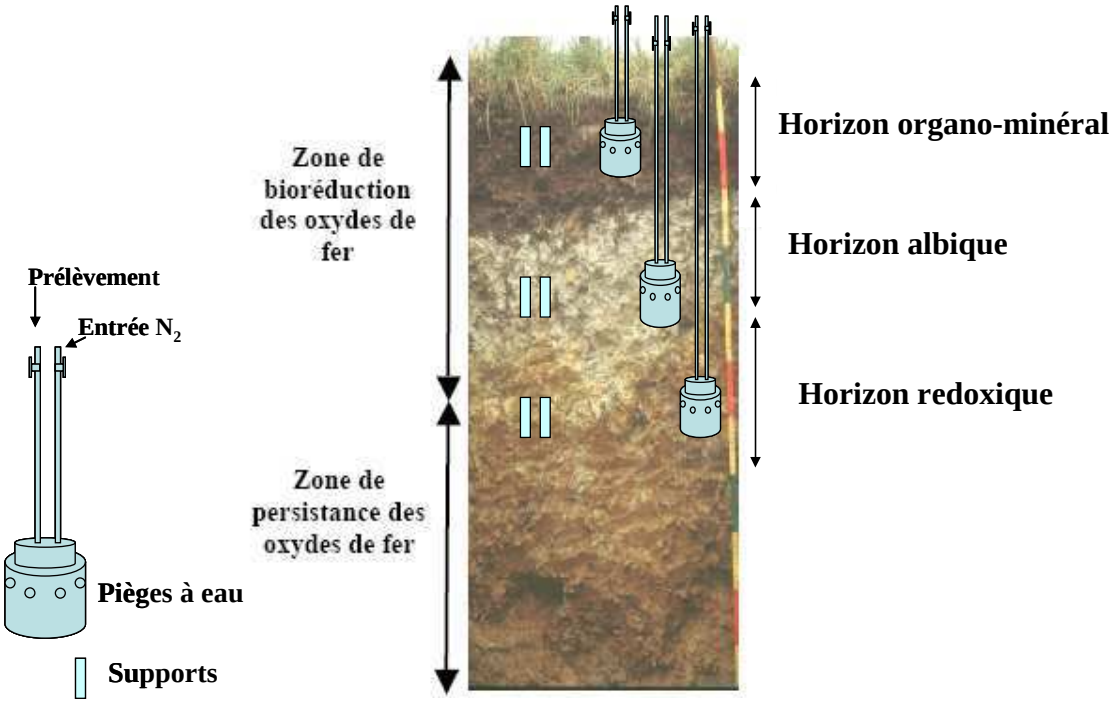

Figure III.2.1. Profil vertical d'un sol hydromorphe du bassin de Kervidy-Naizin montrant la variabilité des états rédox du fer avec la profondeur. La localisation des supports recouverts d'oxyhydroxydes de Fe et des pièges à eau est indiquée par les barres bleues.

Le suivi des paramètres physico-chimiques ainsi que les dosages des concentrations en cations, anions et Fe(II) ont été réalisés via des 'pièges à eau' insérés dans les différents horizons du sol (Bourrié et al., 1994) permettant les prélèvements en conditions anaérobiques (Fig. III.2.1). Les mesures de paramètres physico-chimiques et les dosages des concentrations élémentaires ont été effectués selon les protocoles préalablement décrits dans Fakih et al., (2008b) (Partie III.1.2.2).

2.3. RESULTATS

2.3.1. Longue plaquette

Après quatre mois d'incubation dans le sol, des précipités noirs, répartis de manière très hétérogène, ont été observés sur la longue plaquette (Fig. III.2.2). Dans l'horizon organo-minéral, la couleur orange de la lépidocrocite originelle a totalement disparue suggérant que la dissolution a été plus intense dans cet horizon que dans l'horizon albique (Fig. III.2.2). De plus, nous avons observé des débris de matière fixés à la plaquette dans l'horizon organo-minéral.

Ces précipités ont une forme circulaire qui peut faire penser à la forme des colonies bactériennes. Sur cette plaquette aucune analyse quantitative n'a été réalisée, en raison de sa taille non adaptée à l'analyse FRX (Taille acceptée pour les analyses : 2 × 2 cm).

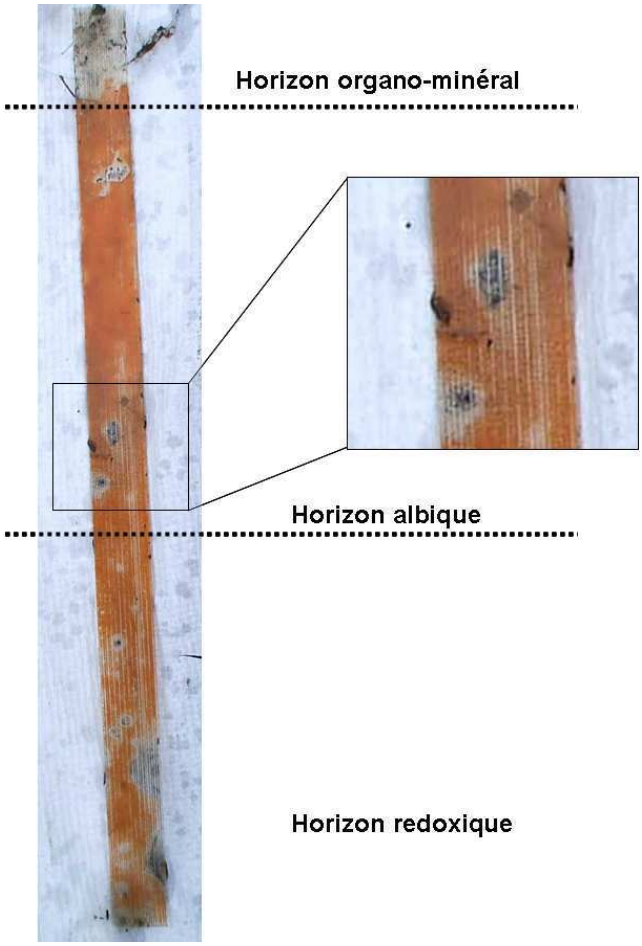

Figure III.2.2. Profil du sol montrant les trois principaux horizons du sol (organo-minéral, albique et rédoxique) et le positionnement des petites plaquettes et de la longue plaquette dans le sol. Les précipités noirs observés sur les plaquettes sont des phases néoformées.

2.3.2. Dissolution de la lépidocrocite et libération de l'As associé

A l'œil nu, et après cinq mois d'incubation, on peut voir une répartition hétérogène de la couleur orangée de la lépidocrocite suggérant une dissolution différentielle à la surface de la plaquette (Fig. III.2.3). Ceci laisse penser que la dissolution de la lépidocrocite dépend fortement des conditions physico-chimiques et certainement biologiques régnant dans les différents horizons de sol.

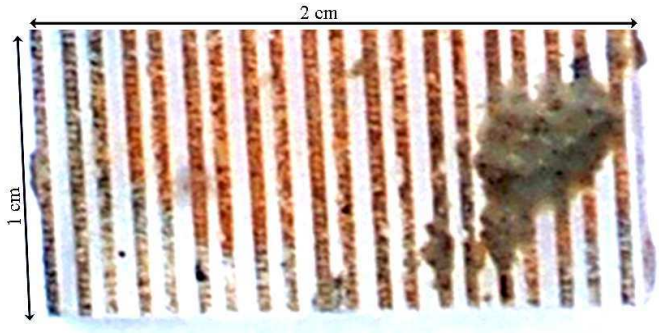

Figure III.2.3. Photo d'une petite plaquette incubée dans l'horizon organo-minéral.

La dissolution de la lépidocrocite ainsi que l'As associé a été présentée sous forme de pourcentages de dissolution rapportés à la masse initiale de Fe et d'As sur la plaquette. La Figure III.2.4a présente les pourcentages de dissolution du Fe et de l'As dans l'horizon organo-minéral après six mois d'incubation, 24,89% et 26,59% du Fe et 52,08% et 34,98% de l'As associé ont été respectivement dissous sur deux plaquettes insérées dans deux endroits différents au sein du même horizon. Après huit mois d'incubation, plus de 95% du Fe ont été dissous, enfin après neuf mois d'incubation 84,43% du Fe et 83,69% de l'As ont été dissous (Fig. III.2.4a).

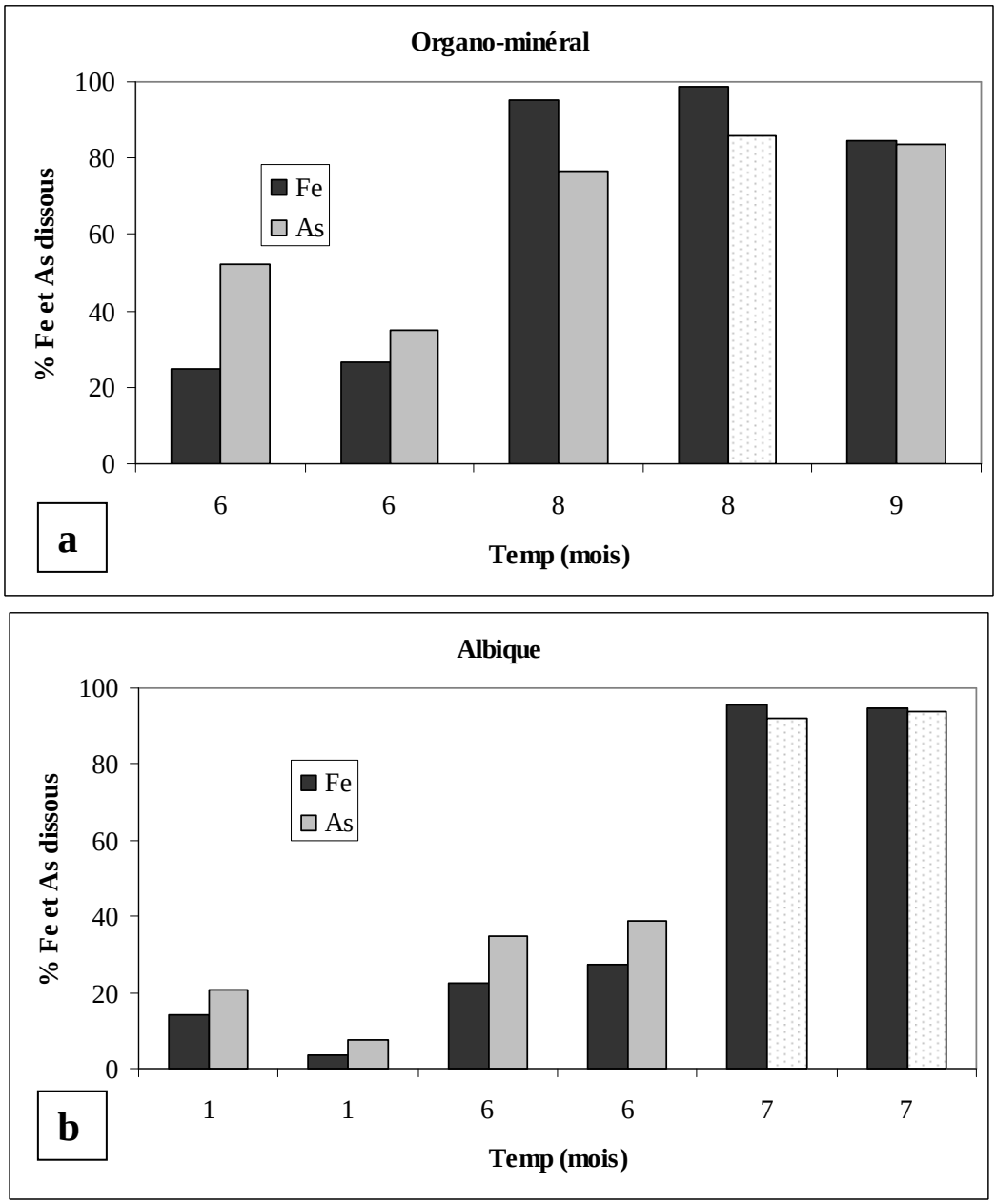

Figure III.2.4. Pourcentages de dissolution de Fe et d'As dans : a) l'horizon organo-minéral et b) l'horizon albique. Les pourcentages sont exprimés en masse de métal resté sur la plaquette par rapport à la masse initiale de métal présente avant incubation (les deux étant déterminées par FRX). Les colonnes blanches correspondent à des valeurs estimées pour le % de dissolution de l'As dans le cas où la quantité d'As restée sur la plaquette est inférieure à la limite de détection de FRX.

Pour l'horizon albique, après un mois d'incubation 13,91% et 3,51% du Fe et 20,81% et 7,47% de l'As associé ont été dissous. Après six mois d'incubation 22,49% et 27,20% du Fe et 35,01% et 38,62% de l'As ont été dissous. Enfin, plus de 90% du Fe ont été dissous après sept mois d'incubation. Les pourcentages de dissolution de l'As présentés dans la Figure III.2.4b dans les colonnes blanches sont des valeurs estimées, car la quantité d'As restée sur la plaquette était inférieure à la limite de détection de FRX.

Les taux de dissolution du Fe et de l'As ont été calculés en $mol.m^{-2}.s^{-1}$ afin de pouvoir être comparés aux données de la littérature (e.g. Fakih et al., 2008c ; Roden, 2003 ; Cooper et al., 2000 ; Larsen et Postma, 2001 ; Pedersen et al., 2006) (Tableau III.3.3). La surface spécifique utilisée est la même que celle déterminée par Pedersen et al. (2006), $139m^2.g^{-1}$, puisque la lépidocrocite-As(V) utilisée pour notre étude a été préparée selon le même protocole.

Après six mois d'incubation les taux de dissolution du Fe sont égaux ($\approx 0,21 .10^{-10}$ mol $Fe.m^{-2}.s^{-1}$) dans et au sein des deux horizons. Par contre, les taux de dissolution de l'As sont légèrement supérieurs ou égaux à ceux du Fe. Après six mois d'incubation, les taux de dissolution du Fe continuent à augmenter dans les deux horizons du sol. Au septième et neuvième mois, respectivement pour les horizons albique et organo-minéral, les taux de dissolution de l'As sont inférieurs à ceux du Fe (Tableau III.2.1).

Tableau III.2.1. Taux de dissolution de la lépidocrocite dopée en As dans les deux horizons du sol (organo-minéral et albique) en mol du Fe ou d'As en fonction du temps d'incubation et de la surface spécifique (ici $139m^2.g^{-1}$).

Organo-minéral	**Taux de dissolution mol (Fe ou As).$m^{-2}.s^{-1}.10^{-10}$**		**Albique**	**Taux de dissolution mol (Fe ou As).$m^{-2}.s^{-1}.10^{-10}$**	
Temps (mois)	**Fe**	**As**	**Temps (mois)**	**Fe**	**As**
8	0,59	0,35	6	0,19	0,22
8	0,61	0,40 [l.d.]	6	0,22	0,24
9	0,46	0,34	7	0,68	0,49 [l.d.]
			7	0,67	0,50 [l.d.]

[l.d.]: valeurs estimés (inférieurs à la limite de détection de FRX).

2.3.3. Observations réalisées par microscopie électronique

Les points marquants des observations réalisées par microscopie électronique sur la longue plaquette sont présentés dans la Figure III.2.5. Un biofilm bactérien recouvre les particules de lépidocrocite (Fig. III.2.5a, flèche blanche). Des néoformations de phases noires, constituées de petits cristaux de 50 à 150 nm de longueur, ont également été observées (Fig. III.2.5b).

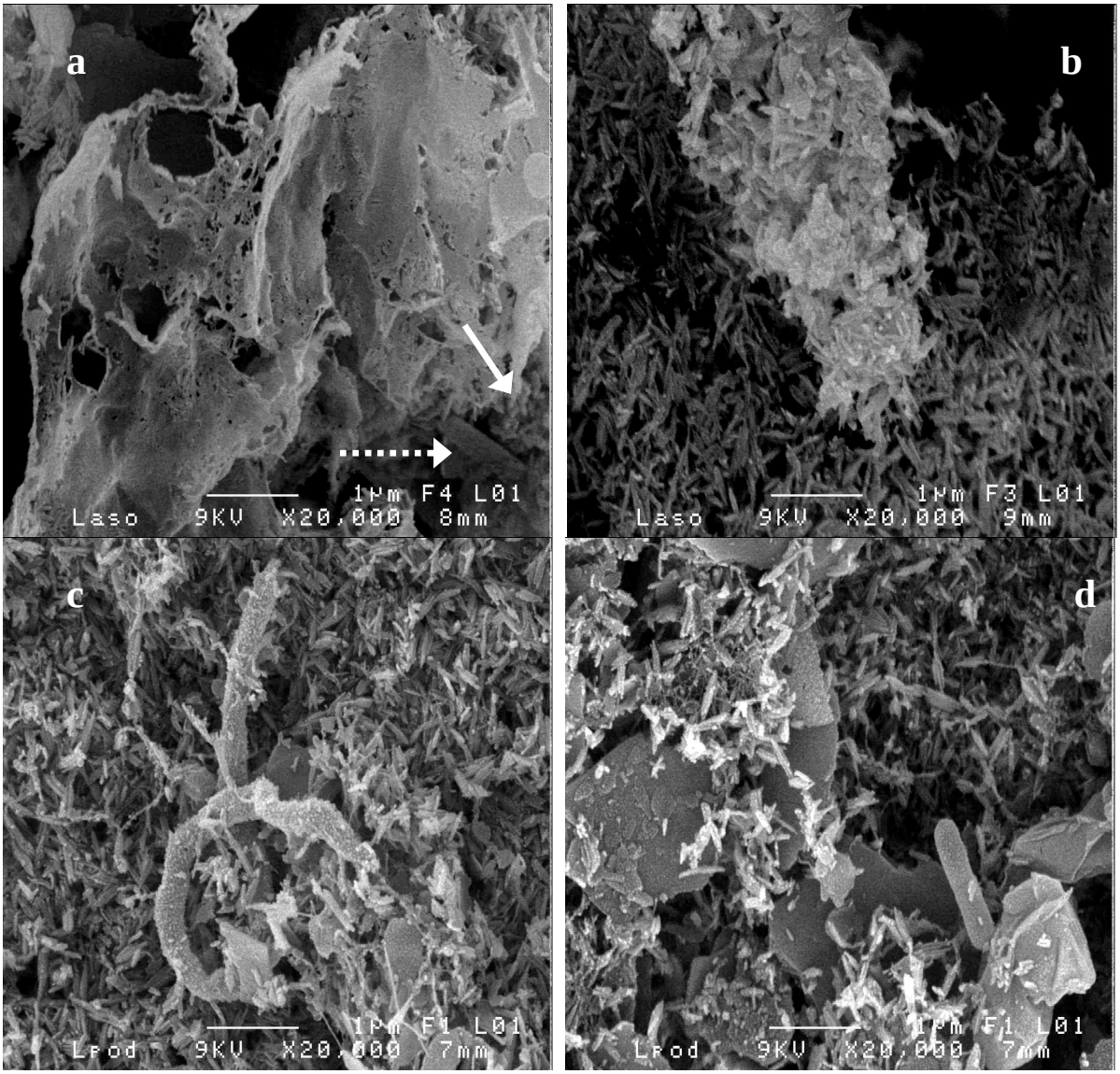

Figure III.2.5. Observation par microscopie électronique de la longue plaquette dans l'horizon organo-minéral après 4 mois d'incubation. La Figure III.2.5a montre la présence d'un biofilm qui couvre les oxydes et une colonisation bactérienne (flèche continue) montre les oxydes. La flèche en pointillé montre une bactérie. Les Figures III.2.5b et III.2.5c montrent la présence de bactéries et de particules de sol. La Figure III.2.5d montre la présence de phases néoformées de couleur noire.

L'autre partie de la plaquette (phases minéralogiques de couleur orange) a révélé des cristaux de lépidocrocite qui conservent leur forme originelle intacte (petit cristaux de 0.2 × 0.03 µm) (Fig. III.2.5b) et sur lesquels se trouvent des particules de sol et des bactéries (Figs. III.2.5c et III.2.5d).

Les principaux éléments observés sur les petites plaquettes d'As(V)-Lépidocrocite insérées dans l'horizon organo-minéral, sont synthétisés dans la Figure III.2.6.

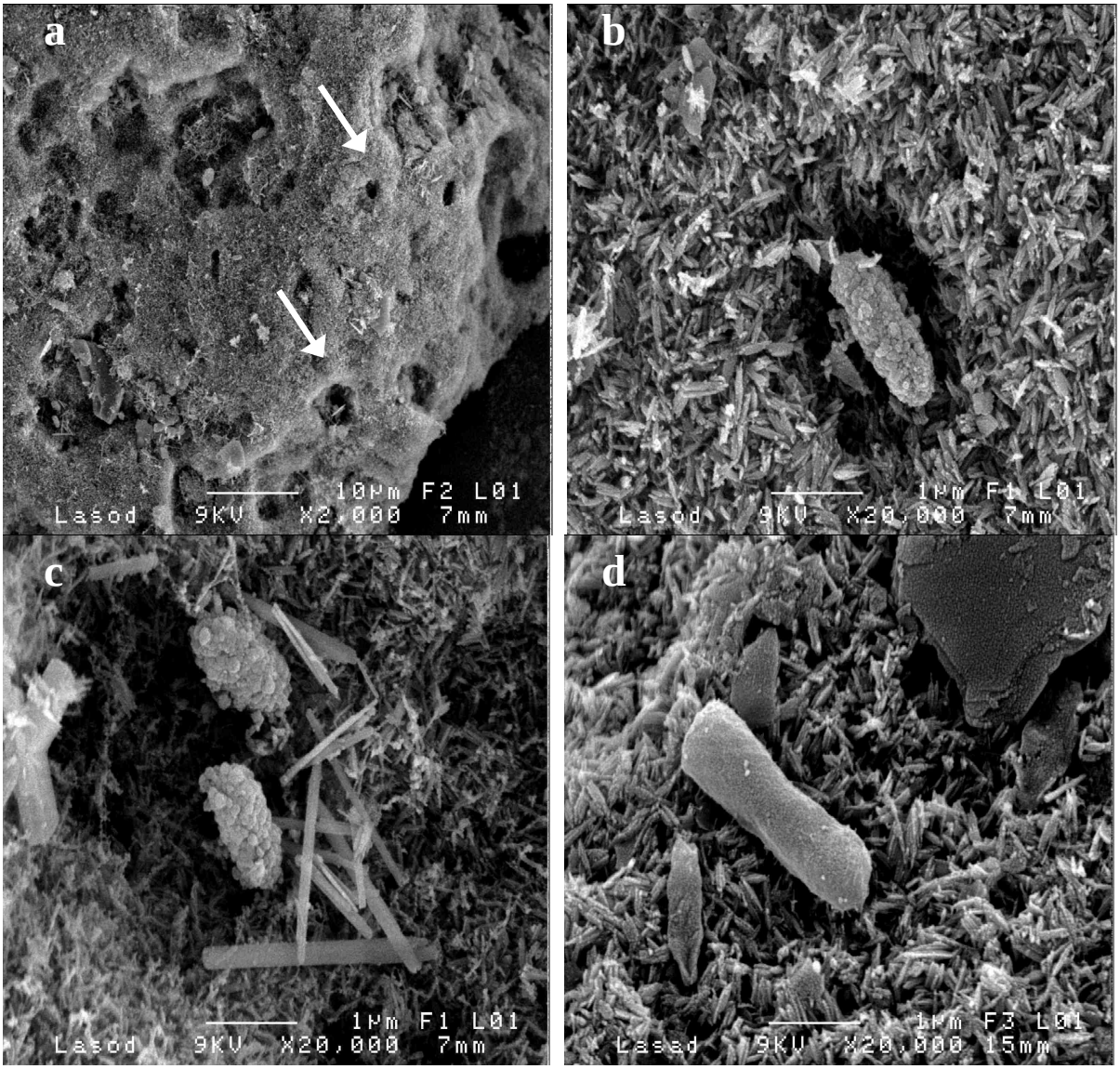

Figure III.2.6. Observation par microscopie électronique de la lépidocrocite dopée en As dans l'horizon organo-minéral Fig. III.2.6a), III.2.6b), III.2.6c) après 5 mois d'incubation. La Figure III.2.6d montre une photo de la lépidocrocite dopée dans l'horizon albique. On remarque la présence des particules du sol à la surface de la lépidocrocite.

Après cinq mois d'incubation, une importante altération de surface a été observée laissant apparaître des orifices de forme circulaire d'environ 2 à 10 µm de diamètre ou longitudinale (5 à 10 µm de longueur et de 2µm de largeur) (Fig. III.2.6a).

Une forte colonisation bactérienne a été observée à l'intérieur de ces orifices. Ces bactéries montrent une surface granuleuse (Figs. III.2.6b et III.2.6c) à laquelle adhèrent des phases minérales secondaires (Fig. III.2.6c). Deux phases, l'une amorphe, et l'autre cristallisée sont présentes dans ces orifices (Fig. III.2.6c). La phase amorphe se trouve en continuité avec la lépidocrocite alors que la phase cristallisée s'est déposée sur les cristaux de lépidocrocite. Cette phase cristallisée est formée de baguettes très fines de longueurs variant entre 1 et 2 µm.

L'observation des plaquettes incubées dans l'horizon albique a révélé des traces d'altération sensiblement différentes de celles observées pour les plaquettes insérées dans l'horizon organo-minéral. La colonisation bactérienne est négligeable et aucun orifice

comparable à ceux précédemment décrits n'a pu être mis en évidence. La lépidocrocite semble beaucoup moins altérée que dans l'horizon organo-minéral. Par contre, une forte présence de particules de sol en contact avec les cristaux de lépidocrocite a été notée (Fig. III.2.6d). De plus, les observations microscopiques ont montré que dans les deux horizons de sol, les cristaux de la lépidocrocite étaient altérés sur leur bords (Fig. III.2.7).

Contrairement à la longue plaquette aucune trace de minéraux secondaires de couleur noire n'est apparue sur les petites plaquettes après cinq mois d'incubation et ce, quel que soit l'horizon de sol considéré. Ce point important pose le problème de l'extrême hétérogénéité du sol, tant en terme de composition minéralogique, de densité ou de diversité bactérienne, que de présence de microsites aux conditions redox contrastées.

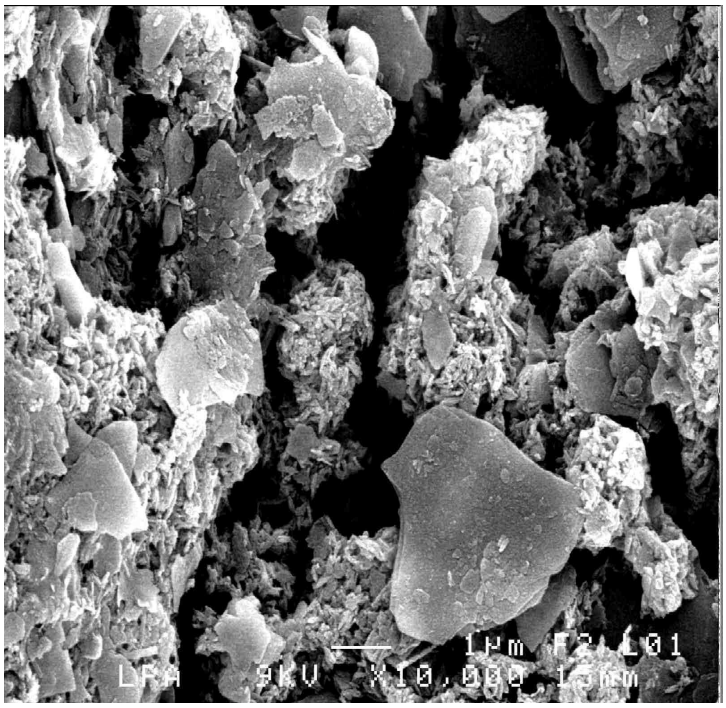

Figure III.2.7. Observation microscopique de la lépidocrocite dopée en arsenic sur la longue plaquette dans l'horizon albique. La flèche montre que les cristaux de la lépidocrocite sont rognés sur les bords.

2.4. DISCUSSION

2.4.1. Dissolution réductrice de la lépidocrocite

Malgré les fortes conditions réductrices régnant dans l'horizon albique (Tableau III.1.2), la dissolution de la lépidocrocite dopée en As après six mois d'incubation est comparable dans les deux horizons du sol (20 à 30 % du Fe et 35 à 50 % de l'As sont dissous). De même, les taux de dissolution calculés dans l'horizon organo-minéral sont plus importants que ceux de l'horizon albique. Plusieurs hypothèses peuvent expliquer ces résultats : (a) l'hétérogénéité du sol y compris au sein d'un même horizon, caractérisée par la présence de microsites aux conditions redox contrastées pourrait induire une hétérogénéité de dissolution des oxydes. Cette hypothèse est d'ailleurs soutenue par la présence des taches circulaires noires au sein de la matrice de lépidocrocite sur la longue plaquette en contact avec l'horizon albique (Fig.

III.2.2). En effet, cette plaquette offre une fenêtre continue sur les processus mis en jeu, et montre bien que les lieux actifs de dissolution réductrice et de formation de précipités secondaires sont distribués de manière extrêmement hétérogène. Les résultats obtenus dans les colonnes anaérobies suggèrent également la présence de sites plus actifs au sein des échantillons de sol. En effet, bien que les conditions redox globales de la solution de sol aient été supérieures aux conditions de précipitation de sulfures, il avait été possible d'identifier sur les plaquettes, la précipitation localisée de sulfures de fer secondaires (Fakih et al., 2008b, partie III.1.2.2). (b) Une activité bactérienne (en nature et quantité de cellules) différente au sein de chaque horizon pourrait également expliquer ces observations. Bien que l'horizon albique présente des conditions globalement plus réductrices que l'horizon organo-minéral, moins de cellules ont été observées sur les plaquettes insérées dans ce dernier. Ceci laisse penser que le nombre de cellules serait inférieur dans cet horizon. De plus, l'horizon organo-mineral, comme son nom l'indique, propose aux micro-organismes une matière organique en quantité et qualité supérieures à celles disponibles dans l'horizon albique et donc plus favorables au métabolisme bactérien. Enfin, l'horizon organo-mineral étant un horizon de surface de zone humide, il subit des alternances régulières de conditions rédox. Les communautés bactériennes sont donc adaptées non seulement à l'oxydation du fer mais également à sa réduction, et donc très réactives. L'horizon albique lessivé homogène moins organique et submergé une grande partie de l'année est probablement moins réactif vis-à-vis du Fe. (c) La dernière hypothèse repose sur le recouvrement important des cristaux de lépidocrocite pas les particules minérales du sol (ex. particules d'argiles) dans l'horizon albique (Fig. III.2.6d). Ces particules bloqueraient en partie l'accès des bactéries à la surface de l'oxyde et limiteraient donc la dissolution de la lépidocrocite dans cet horizon. Dans la partie non dissoute de la plaquette, les cristaux de la lépidocrocite semblent intacts, ce qui suggère que la dissolution se fait d'une manière hétérogène et de façon ponctuelle.

Si l'on compare les données de cette étude avec des études préalablement réalisées, d'autres paramètres semblent eux aussi jouer un rôle majeur. En effet, une augmentation du taux de dissolution a été observée jusqu'à $0{,}69.10^{-10}$ mol $Fe.m^{-2}.s^{-1}$ après six mois d'incubation, et ce, quel que soit l'horizon considéré. Mais, cette dissolution est inférieure à celle observée par Fakih et al. (2008c) obtenue dans en colonne anaérobie ($1{,}92.10^{-9}$ mol $Fe.m^{-2}.s^{-1}$) (Tableau III.3.4). Ceci suggère que les très fortes conditions réductrices obtenues en colonnes (Fakih et al., 2008c) (See supplementary section B.1), liées à une très forte colonisation bactérienne, ont significativement augmenté les taux de dissolution (Tableau III.3.2). Par contre, les taux de dissolution enregistrés ici sont plus élevés que ceux estimés par Pedersen et al. (2006) par réduction chimique à l'aide d'ascorbate ($1{,}34.10^{-11}$ mol $Fe.m^{-2}.s^{-1}$). L'activité bactérienne et biologique au sens large joue ici un rôle catalytique et amplificateur important, non observé dans l'étude de dissolution strictement chimique réalisée par Pedersen et al. (2006). Il a de plus été observé lors de l'étude réalisée avec de la ferrihydrite par Fakih et al. (2008b) (Tableau III.1.3) dans le même sol et avec les mêmes conditions d'incubation que les taux de dissolution de la lépidocrocite qui variaient de 0,17 à $0{,}69\ .10^{-12}$ mol $Fe.m^{-2}.s^{-1}$ étaient nettement inférieurs à ceux de la ferrihydrite qui eux, variaient de 2,3 à 12.10^{-12} mol $Fe.m^{-2}.s^{-1}$ (Fakih et al., 2008b) (Tableau III.1.3). Le caractère amorphe de la ferrihydrite comparé à la lépidocrocite plus cristallisée, favorise donc la dissolution réductrice de la ferrihydrite en conditions d'incubation équivalentes. Ceci implique que le degré de cristallisation de l'oxyde de fer impliqué est lui aussi, au même titre que l'hétérogénéité du sol, l'intensité des conditions réductrices, l'intensité et la diversité de l'activité des micro-organismes, un déterminant majeur de l'efficacité de la dissolution réductrice des oxyhydroxydes de fer, et donc de la libération des éléments traces qui leur sont potentiellement associés.

2.4.2. Colonisation bactériennes et néoformations

Les observations macroscopiques réalisées sur la longue plaquette ont montré la présence des taches noires réparties tout au long de la plaquette d'une manière hétérogène. Ces taches sont plus présentes dans l'horizon albique que dans l'horizon organo-minéral. De plus, la forme de ces taches ressemble à celle de colonies bactériennes (Fig. III.2.2). Malgré les fortes conditions réductrices dans l'horizon albique, la dissolution de la lépidocrocite dans l'horizon organo-minéral est totale et sans doute liée aux activités métaboliques qui y règnent (voir les débris de la matière organique attachés à la plaquette). La dissolution totale de lépidocrocite dans l'horizon organo-minéral et la présence des taches noires dans l'horizon albique mettent en évidence la présence de deux mécanismes de dissolution différents dépendant de l'horizon de sol considéré (Fakih et al. 2008b, partie III.1.4.3). Les observations macroscopiques couplées à l'observation par microscopie électronique à balayage dans l'horizon organo-minéral, montrant la présence de biofilms et de bactéries (Fig. III.2.5a), permettent de suggérer que les micro-organismes jouent un rôle important dans la dissolution du Fe et la mobilisation de l'As associé comme précédemment mis en évidence (Lovley et Phillips, 1987 ; Lovley, 1991, 1993 ; Wahid et Kamalam, 1993 ; Roden et Zachara, 1996 ; Chenu et Stotzky, 2002 ; Oremland et Stolz, 2003 ; Islam et al., 2004 ; Fakih et al., 2008b) (Partie III.1.4.3). L'hétérogénéité de la répartition de ces taches à la surface de la plaquette peut être expliquée par la présence de 'micro-sites' où les conditions réductrices sont probablement très intenses (Luo et al., 1999) activant ainsi la dissolution de la lépidocrocite. Ces taches noires correspondent à des phases néoformées. En se basant sur les études EDS de précipités noirs présents sur des petites plaquettes d'une expérience d'incubation réalisée au laboratoire (Fakih et al., 2008c) (Fig. III.3.7), on peut supposer que ces phases peuvent être divisées en deux groupes, stables comme la pyrite (Fakih et al., 2008b ; Charlatchka et Cambier, 2000 ; Blanchard et al., 2007) (Partie III.3.3.3) ou métastables comme la magnétite (Cooper et al., 2000 ; Lovley et al., 1987).

Les Figures III.2.6a et III.2.6b montrent la présence d'orifices formés à la surface de la lépidocrocite. Une forte présence bactérienne a été observée dans ces orifices (Fig. III.2.6b) ainsi que des nouvelles phases très bien cristallisées qui ressemblent à des cristaux de goethite (Fig. III.2.6c). Plusieurs études de dissolution réductrice bactériennes des oxydes de fer ont effectivement montré la formation de goethite comme produit secondaire de la dissolution réductrice d'oxyde de Fe (Fredrickson et al., 1998 ; Zachara et al., 2002 ; Glasauer et al., 2003 ; Shwertmann et Taylor, 1979).

2.4.3. Comportement de l'arsenic

Le pourcentage de dissolution de l'As est plus élevé que celui du Fe. Ces résultats peuvent être expliqués par deux hypothèses. (a) Plusieurs auteurs ont montré que la dissolution réductrice des cristaux de lépidocrocite se produisaitt principalement sur les bords long des ces cristaux. Or, ceux sont précisément sur les bords longs que les sites préférentiel d'adsorption de l'arsenic sont situés (Larsen and Postma, 2001; Pedersen et al., 2006). Si, ils sont détruits l'arsenic libéré par la dissolution de la lepidocrocite ne peut donc plus se réadsorber. (b) le rapport As/nombre de sites de surface de la lépidocorcite est très élevé et ne permet pas le réadsorption de l'arsenic. Néanmoins, après sept mois d'incubation, le pourcentage de dissolution du fer est inférieur à celui de l'arsenic. L'arsenic a pu précipiter ou s'adsorber (a) sur des phases secondaires, notamment les sulfures de fer (Bostick et Fendorf, 2003 ; Abraitis et al., 2004 ; Blanchard et al., 2007), (b) sur les particules d'oxydes de fer non

dissoutes (Dixit et Hering, 2003) et (c) sur les particules du sol collées sur la plaquette (Bowell, 1994 ; Bostick et Fendorf, 2003 ; Blanchard et al., 2007).

2.5. CONCLUSIONS

Quel que soit l'horizon du sol considéré, une dissolution réductrice de la lépidocrocite a eu lieu et a pu être quantifiée, de même que la libération de l'arsenic associé. Cette dissolution est fortement hétérogène en relation avec l'hétérogénéité même du sol et de la nature des horizons. Elle dépend vraisemblablement de la présence de micro-sites présents dans le sol et caractérisés par des conditions réductrices plus intenses, et de l'activité microbienne au sein des horizons. L'observation des petites plaquettes après cinq mois d'incubation a révélé une forte colonisation bactérienne et la présence de nouvelles phases cristallisées. La néoformation de goethite a pu être mise en évidence. Cette étude a également révélé, via l'observation d'orifices liés à une activité métabolique bactérienne à la surface de la lépidocrocite, que les mécanismes actifs de dissolution en conditions réductrices n'étaient pas les mêmes pour la lépidocrocite que ceux connus pour la ferrihydrite (Fakih et al., 2008b ; 2008c) (Partie III.3.4.2). Ce point est essentiel, dans la mesure où il souligne l'étroite relation existante, dans des conditions d'oxydo-réduction équivalentes, entre le degré de cristallisation et les processus physico-chimiques de dissolution mis en œuvre par les micro-organismes présents et métaboliquement impliqués dans le cycle du fer.

3. DISSOLUTION REDUCTRICE D'OXYDES DE FER (FERRIHYDRITE ET LEPIDOCROCITE) DOPES EN ARSENIC : ETUDE EN COLONNES AU LABORATOIRE

Mohamad Fakih
Mélanie Davranche
Aline Dia
Bernd Nowack
Guillaume Morin
Patrice Petitjean
Xavier Châtellier
Gérard Gruau

Cette partie correspond à un article soumis à la revue Chemical Geology 'Environmental impact of As(V)-Fe oxyhydroxide reductive dissolution: an experimental insight from *in situ* monitoring' (Juin 2008)

RÉSUMÉ

Des plaquettes acryliques recouvertes de ferrihydrite et lépidocrocite dopées en As(V) (As-Fh, As-Lp) ont été insérées dans un échantillon de l'horizon organo-minéral d'un sol de zone humide. Plaquettes et sol ont été incubés en condion anaérobie dans un système non conventionel (à l'équilibre) de colonnes anaérobies. Les plaquettes ont été prélevées à différents pas de temps. Des analyses de chaque support par fluorescence des rayons-X (FRX) et microscope électronique à balayage (SEM-EDS) ont permis de quantifier la dissolution des oxydes de fer, et la solubilisation de l'As et de suivre les transformations morphologiques et minéralogiques de chaque oxyde. Les taux calculés de dissolution du fer pour As-Fh et As-Lp ($2{,}02\ 10^{-9}$ et $1{,}92\ 10^{-9}$ mol Fe $m^{-2}.s^{-1}$, respectivement) sont plus élevés que ceux reportés dans la littérature pour des données de laboratoire et de terrain. Ceci peut être expliqué par une très forte colonisation bactérienne et l'apparition d'un épais biofilm à la surface des plaquettes qui traduisent une très forte activité biologique. Des minéraux secondaires riches en Fe et S apparaissent en surface des plaquettes et des particules d'oxydes. Aucun des minéraux secondaires communément identifiés par les études de laboratoire n'a pu être identifié. Ce resultat s'explique par la présence d'une forte concentration en anions inhibiteurs de la précipitation tels que des molécules organiques en solution. Ces inhibiteurs agissent soit, en maintenant le Fe(II) en solution par complexation soit, en empéchant sa réadsorption par blocage des sites de surface de l'oxyde. La proportion relative d'As(III) à la surface des plaquettes As-Fh augmente avec le temps alors que le rapport Fe/As chute. L'As(III) semble se réadsorber partiellement à la surface de la ferrihydrite non dissoute. Cependant, pour la lépidocrocite, le rapport Fe/As augmente, suggérant une plus faible réadsorption de l'As(III). Deux hypothèse peuvent expliquer ce résultat : (a) une indisponibilité des sites (fort rapport concentration en As/nombre de sites) ou (b) une destruction des sites d'adsorption de l'As à la surface des cristaux de la lépidocrocite réduite. La réduction et la réadsorption d'As semblent être le résultat d'une combinaison entre des réactions biologiques et chimiques dans laquelle les bactéries réductrices du Fe ou plus spécifiques à l'As réduisent l'As(V) en As(III).

ABSTRACT

Polymer slides covered by synthetic As-spiked ferrihydrite (As-Fh) or As-spiked lepidocrocite (As-Lp) were inserted into an organic-rich wetland soil in non conventional columns system under anaerobic conditions. Slide were recovered after different periods of time to evaluate (i) the impact of (bio)reduction on both Fe-oxide dissolution and secondary mineral precipitation and, (ii) the subsequent effects on As mobility. The calculated Fe dissolution rates for As-Fh and As-Lp were $2.02.10^{-9}$ and $1.92.10^{-9}$ mol Fe $m^{-2}.s^{-1}$, respectively, and were higher than what has been commonly reported in laboratory studies. Important bacterial colonization and occurrence of biofilm suggest the presence of biologically mediated processes. The newly formed minerals were mostly composed of Fe-sulphides. Fe(II) complexation by organic molecules in solution likely prevented formation of secondary Fe(II,III)-rich minerals. The relative proportion of As(III) increased with time on the As-Fh slides, and was combined with a decrease of the Fe/As ratio, suggesting a partial adsorption of As(III) onto minerals. By contrast, for lepidocrocite, the Fe/As ratio increased, suggesting that As(III) was less readsorbed due the lower available site number and the deletion of As adsorption sites on the reduced lepidocrocite surface. Reduction and subsequent As sequestration appeared to result from a coupled biotic-abiotic reaction pathway in which Fe or As reducing-bacteria allowed the reduction of As(V) to As(III).

3.1. INTRODUCTION

Iron (III) oxyhydroxides are of particular environmental relevance because they often occur as fine grained particles and exhibit high reactive surfaces (Tipping et al., 1981; Scheidegger et al., 1993; Kaplan et al., 1997; Fox and Doner, 2002). The Fe(II)/Fe(III) redox couple is an important electron-transfer mediator for many biological and chemical species. As a consequence, the stability of Fe(III) oxyhydroxides in soils exerts a major control on mobility of both organic (Avena and Koopal, 1998) and inorganic pollutants such as arsenic (Ahmann et al., 1997; Davranche and Bollinger, 2000a, b; Zobrist et al., 2000; Zachara et al., 2001; Fox and Doner, 2002; Davranche et al., 2003; Chatain et al., 2005).

The importance of microorganisms in the biogeochemical cycling of Fe is well-recognized (Lovley and Phillips, 1986b; Lovley, 1991; Lovley et al., 1991; Wahid and Kamalam, 1993; Roden and Zachara, 1996). Iron-reducing bacteria - which are ubiquitous in waterlogged soils and aquifers - couple the oxidation of organic matter with the reduction of various Fe(III) oxyhydroxides for their metabolism. A direct consequence of Fe(III) reduction is the associated trace metal release into soil solution (e.g. Schwertmann and Taylor, 1989; Lovley and Coates, 1997; Davranche and Bollinger, 2000a; Quantin et al., 2001; Zachara et al., 2001; Van Geen et al., 2004; Burnol et al., 2007). However, recent studies have shown that arsenic can efficiently adsorb onto mineral resulting from Fe-oxides bioreduction (Kocar et al. 2006; Wang et al., submitted), from Fe(II) promoted reduction of Fe-oxides (Pedersen et al. 2006), or resulting from the co-precipitation of Fe(II) and Fe(III) (Wang et al., 2008).

Arsenic is strongly adsorbed onto Fe-oxides (Manning et al., 1998; Raven et al., 1998; Dixit and Hering, 2003), which are probably the most important carriers of As in aquifers and soils (Morin et al., 2002b; Morin and Calas, 2006; Cancès et al., 2005; 2008). Arsenic occurs at concentrations exceeding drinkable levels in major aquifers in several parts of the world, especially in South Asia (Smedley and Kinniburgh, 2002; Islam et al., 2004, Van Geen et al., 2008). High As concentrations in subsurface waters result often from reductive dissolution of hydrous Fe-oxides and subsequent release of associated As (Nichson et al., 2000; Bose and Sharma, 2002; Van Geen et al., 2004).

Several laboratory studies reported that As(V) is mainly adsorbed onto Fe-oxide surfaces and is not incorporated into the crystal lattice, even during coprecipitation (Raven et al. 1998; Waychunas et al., 1993; Pedersen et al., 2006). These studies provided also evidence that As solubilisation rates and behaviour are dependent on both the mineralogical type of Fe-oxyhydroxide and its degree of crystallization. Pedersen et al. (2006) demonstrated through studies involving ferrihydrite and goethite submitted to chemical reduction that As(V) was not released before the surface site number became too small to adsorb all the available As. In the case of lepidocrocite, it has been reported that arsenic is mainly adsorbed on surface sites located on the (001) facets of the crystal (Cornell and Schwertmann, 2003), which are preferentially destroyed during reductive dissolution (Larsen and Postma, 2001). Recent studies showed that the transformation of Fe-oxides catalysed by Fe(II) under reductive conditions induces the production of more reactive solid phases such as magnetite, green-rusts, ferrous iron carbonate and amakinite which efficiently bind As(V) and As(III) (Kocar et al. 2006; Wang et al. 2008; Ona-Nguema et al., submitted; Wang et al. submitted). Formation of Fe(II,III) minerals may thus be important trapping mechanism for arsenic, notably in reducing environments where Fe concentration is sufficiently high to ensure over-saturation with respect to these minerals. Furthermore in organic rich-soil, organic compounds, including bacterial surfaces (Châtellier and Fortin, 2004), may complex Fe(II) and thus inhibit

the formation of secondary Fe(II,III) minerals. For instance, Pedersen et al. (2006) showed when using ascorbic acid as reducer instead of Fe(II) that arsenic was mobilized upon reduction of As(V)-ferrihydrite and As(V)-lepidocrocite. Moreover, arsenic may compete with a number of other anions as carbonates (Burnol et al., 2007; Stachowicz et al., 2007) and organic anions for surface sites on Fe-oxyhydroxydes (e.g. Bauer and Blodau, 2006; Slowey et al., 2007) or secondary Fe(II,III) minerals.

In the natural environment, the mineral soil matrix could also strongly influence the mechanism of the reductive dissolution and therefore the nature of the secondary mineral (for example, due to Fe(II) adsorption, the solubilisation of As). Until recently, it was extremely hard to gain an understanding of the involved processes in the natural environment. Studying mineralogical transformations of solids *in situ* in soils still remains a challenge. However, Fakih et al. (2008b) (Section III.1.2.1) developed a method inspired from Birkefeld et al. (2005) to monitor the transformation of Fe-oxides directly within soils and to quantify their reductive dissolution. Iron-oxides are precipitated onto acrylic slides which can be directly inserted into the soil. Iron-oxides particles can thereby interact with the surrounding soil components (minerals, organic matter and soil solution). Moreover the designed supports can be easily recovered from the soil matrix and the solid phases can subsequently be analyzed.

In the present study, we investigated the reductive dissolution of As-spiked ferrihydrite (As-Fh) and As-spiked lepidocrocite (As-Lp). A non conventional anaerobic column experiment was performed to stimulate reduction in a natural soil sample. Slides covered with either As-Fh or As-Lp were inserted directly into the soil (Fakih et al., 2008b, section III.1.2.5). The slides were recovered through time and then analyzed by XRF, SEM-EDS and X-ray Absorption Near Edge Structure (XANES). The aims of this study were (i) to determine the dissolution rates of two different types of Fe-oxides in a waterlogged organic-rich soil, (ii) to study the mineralogical evolution of the Fe-oxides and, (iii) to evaluate the impact of these evolutions on As release.

3.2. MATERIALS AND METHODS

All chemicals used were of analytical grade. The solutions were prepared with doubly de-ionised water (Milli-Q system, Millipore). The containers used were (i) soaked in 10% ultrapure HNO_3 for 48 h at 60°C to remove all possible contaminants sources, (ii) then rinsed with Milli-Q water for 24 h at 60°C, and (iii) finally dried at 30°C.

3.2.1. Iron oxide-covered slides

A technique based on slides coated by Fe-oxyhydroxides (Birkefeld et al., 2005; Fakih et al., 2008b) (Partie III.1.2.1) was used. The tool consists of small ($2 \times 2 \times 0.2$ cm) striated polymer plates covered by synthetic As(V)-ferrihydrite (As-Fh), or As(V)-lepidocrocite (As-Lp). The detailed methodology for the production of the slides, their characterization and the method validation are further detailed in Fakih et al. (2008b) (Section III.1.2). Both Fe-oxides, weakly crystallized 2-Line ferrihydrite and mildly crystallized lepidocrocite, were synthesized in the presence of As(V) (around 1 % in weight) according to the Schwertmann and Cornell protocol (2000). The final ratio As/Fe is 0.005 in mol/mol.

3.2.2. Soil sampling

The soil was sampled from an organic-rich soil horizon in a wetland located in the Kervidy-Naizin catchment (North western, France). This catchment is particularly well adapted to study Fe reductive dissolution because redox cycles involving Fe were highlighted in these soils (Dia et al, 2000; Olivié-Lauquet et al., 2001). The collected soil sample was dried at 30°C during 72 h, and then sieved to 2 mm. The total concentrations of major and trace elements were analyzed by ICP-MS (trace elements) and ICP-AES (minor elements) following a lithium metaborate fusion. The loss of ignition was measured as an indicator of the carbon content. The major element concentrations in the soil are given in Table III.3.1. The soil contained 1.03 wt% of Fe, 15.1 wt% of organic matter and 7.48 $\mu g.g^{-1}$ of As.

3.2.3. Experimental set-up

Columns suited for anaerobic conditions were designed to investigate the influence of soil reduction on the Fe-oxide dissolution (Fig. III.3.1). This technique was developed to allow the insertion of slides into a structured soil sample and to avoid the mechanical abrasion of oxides from slides that would occur in an equilibrium batch system under stirring. The anaerobic column can be described as follows: it consists of two reservoirs connected together by a flexible tygon tube of 0.2 mm internal diameter. The solution was continuously carried through the soil column using a peristaltic pump (Ismatec Ecoline) placed just before the entry into the upper reservoir (so-called 'soil' reservoir) (Fig. III.3.1). The solution circulated in closed system and the percolating solution reached a steady state. The columns were thus not a classical dynamic column system. Forty g of soil were filled into the soil reservoir which made of a 250 mL polypropylene centrifugation tube. Two horizontal perforated Teflon disks (69-µm-pore size) in between two woven nylon layers were placed at the column bottom. These disks retained the soil particles in the reservoir while allowing the percolation of the solution. The slides were inserted vertically into the soil. Eight hundred mL of anaerobic synthetic soil solution circulated from the lower reservoir (so-called 'solution reservoir'). This reservoir was a 1000 mL polypropylene bottle and was equipped with a rubber lid allowing solution sampling with a syringe, and two inputs/outputs for solution circulation. The chemical composition and the ionic strength of the synthetic solution were chosen to be comparable to the pore water composition in the Naizin wetland just at the beginning of the flooded period (30.71 $mg.L^{-1}$ of NaCl, 30.91 $mg.L^{-1}$ of $NaNO_3$ and 10.62 $mg.L^{-1}$ of Na_2SO_4 and pH =5.9). The solution percolated gently through the soil sample from the bottom of the column and returned back to the solution reservoir at the top of the column. The samples were continuously flooded during the experiments. The solution reservoir was continuously stirred using a 4-blade Teflon-covered magnetic stirrer to ensure solution homogeneity and to prevent particle settling and accumulation. The incubation experiments were performed at a constant temperature of 22 ± 0.6°C in a Jacomex glove box under purification (<10 ppm O_2 and H_2O). A 'reference' experiment was carried out without any Fe-oxide slides, while five experiments were performed with As-Lp slides and six with As-Fh slides.

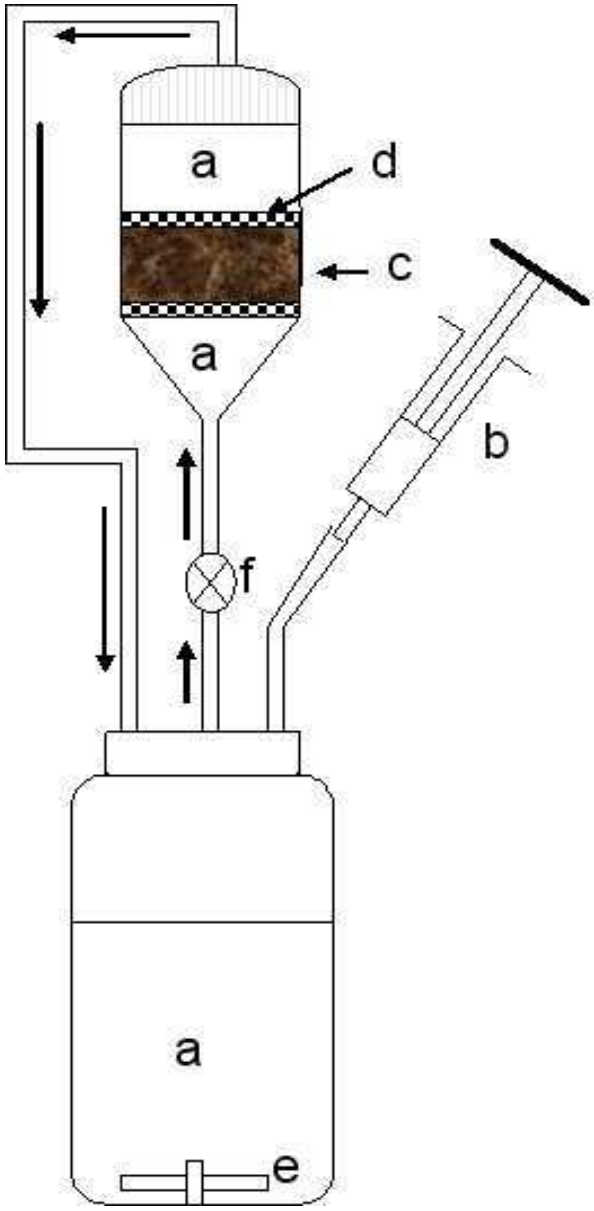

Figure III.3.1. Experimental column set-up. a) Soil solution, b) sampling syringe, c) soil sample inside which the iron oxide-covered slides were inserted, d) perforated Teflon disks, e) Teflon-covered magnetic stirrer and f) peristaltic pump.

Three slides were inserted vertically into the soil reservoir in form of a triangle. The Fe-covered side was turned towards the anaerobic column centre. The coated Fe-oxides did not chemically disturb the soil system because the amount of Fe on the slides was significantly lower than the total concentration of Fe in the soil (Table III.3.1). The slides were removed from the column after different time intervals distributed over two months. At each sampling time, one slide was dried under anaerobic conditions at the critical point for SEM observations (see section III.2.2.6). This procedure was required to observe possible organo-mineral associations and biological structures such as bacteria. A second slide was cleaned with water and dried at room temperature overnight for quantitative analysis by XRF. The third slide was cleaned and dried under anaerobic conditions for XANES analyses.

3.2.4. Soil solution sampling and chemical analyses

During the anaerobic flooding, about 5 ml of solution were sampled at each sampling time. The samples were filtered through a 0.2 µm cellulose acetate membrane (Millipore). They were divided into several aliquots for analysis of total metals and Fe(II), SO_4^{2-} and NO_3^-. Solution sampling and filtration were carried out in a Jacomex glove box under purification flow to prevent Fe(II) and As(III) oxidation. PH and Eh were measured in 1 mL of non filtered solution by InLab combined pH and redox electrodes. Measured Eh values were corrected to be presented relative to the standard hydrogen electrode. Fe(II) was quantified by the 1.10 phenantroline colorimetric method, AFNOR NF T90-017 (AFNOR, 1997) and analysed using an UV-visible spectrophotometer (UVIKON XS, Bio-Tek) with a precision of ±5%. NO_3^- and SO_4^{2-} concentrations were analysed by ion chromatography (Dionex, model X120), with a precision of about ±4%. Total concentration of major and trace elements were analyzed by an Agilent Technologies HP4500 ICP-MS instrument. Arsenic (III) was separated from As(V) in the soil solution using a Varian BondElut SAX in a Jacomex isolator glove box. Arsenic (V) was fixed, while As(III) was eluted and acidified with HNO_3 to avoid any precipitation. Arsenic (III) concentrations were then analysed by AAS (SOLAAR GF95 graphite furnace).

Table III.3.1. Total metal concentrations in the soil used for the column experiment (major and trace elements).

Major elements (%)	**Si**	**Al**	**Fe**	**Mn**	**Mg**	**Ca**	**Na**	**K**	**Ti**	**P**	**LOI**
	28	3,5	1,03	0,01	0,28	0.13	0.14	1.00	0.49	0.02	19,1
Trace elements ($\mu g,g^{-1}$)	**As**	**Cd**	**Co**	**Cr**	**Cu**	**Ni**	**Pb**	**Zn**	**REE**		
	7,48	0,29	5,38	76,61	8,52	17,01	22,53	38,78	128,27		

3.2.5. Determination of Fe amount on slide (XRF analysis)

XRF analyses of the slides were conducted before and after contact with the soil to determine the amount of Fe and associated As. The slide was analysed by XRF on a Spectro X-Lab 2000 (Germany) instrument following the methodology described in Fakih et al. (2008b) (Section III.1.2.3). Dissolved amounts of Fe and As were calculated from the difference between the initial and final concentrations analysed by XRF.

3.2.6. SEM/EDS Scanning Electron Microscopy with X-ray microanalysis

The slides devoted to the SEM/EDS observations were maintained under anaerobic conditions until they were brought to the SEM facility. SEM combined with Energy Dispersive X-ray Spectroscopy (EDS) was used to analyze surface mineral modifications as well as to identify the elemental composition of eventual secondary phases. Before insertion into the soil, a first series of samples was directly observed by SEM. This allowed a comparison of the morphology of the Fe-oxides before and after exposure to the soil. A second series of incubated slides was dried at critical point (Fakih et al., 2008b, section III.1.2.4). The slide surfaces were observed by SEM with a JEOL JSM-6301F Field Emission Gun Scanning Electron Microscope operating at 9kV after being coated with Au-Pd nano-

particles by cathodic deposition with a JEOL JFC 1100 sputter. The elemental composition of individual particles or agglomerates was investigated by Energy Dispersive X-ray Spectroscopy (EDS) using an Oxford Link-Isis Si/Li analyzer.

3.2.7. X-ray Absorption Near Edge Structure Spectroscopy (XANES)

X-ray absorption spectra were recorded at the As K-edge on the FAME beamline at the European Synchrotron Radiation Facility (ESRF, Grenoble, France). Photo-oxidation of As(III) under the x-ray beam was limited by recording all data at 10-15K using a liquid He cryostat, and moving samples automatically between each EXAFS scan. Energy was calibrated by using a double-transmission setup in which the As K-edge spectrum of the samples and that of a scorodite reference sample were simultaneously recorded. The absorption maximum of the As(V)-edge was chosen at 11875.0 eV. The redox state of As on the Fe-oxide slide samples was determined by linear least-squares fitting of XANES data, using linear combinations of XANES spectra of model compounds. Two relevant model compounds, cpp5 and cpp3, consisting of amorphous As(V)-Fe(III) and As(III)-Fe(III) co-precipitates (Morin et al., 2003), were used to fit the relative proportions of As(V) in the samples. Using this procedure, the accuracy of the As(III)/$\sum$As ratio is ±2% and components lower than 5% are not significant (Morin et al., 2003).

3.3. RESULTS

3.3.1. Soil solution composition during incubation

The chemical composition of the soil solution was similar for the reference experiment (without any slide) and the As-Fh and As-Lp slide experiments (Fig. III.3.2). Eh decreased rapidly from 370 mV to 175 mV during the first 72 h. After 1128 h, Eh decreased to -90 mV and finally raised up to 14 mV. The pH increased from 5.6 to 6.6 over the first 48 h, and then remained constant until the end of incubation (Fig. III.3.2a).

Iron (II) and acetate were produced as soon as the solution was NO_3^--depleted. Iron (II) and total Fe exhibited the same behaviour (Fig. III.3.2b). They increased up to 46.9 ± 1.6 $mg.L^{-1}$ after 1150 h. The acetate concentration rose up to approximately 230 $mg.L^{-1}$ at 750 h, and remained constant until the end of the experiment (Fig. III.3.2b). Although the concentration of SO_4^{2-} was stable for 72 h of incubation at 10.5 $mg.L^{-1}$, it decreased to negligible amounts during the next 260 h of incubation.

The measurement of the As(III) concentration cannot be considered as truly quantitative, because during the separation of As(V) from As(III), a significant amount of organic matter was retained on the filter. We cannot preclude that the retained organic matter might contain As(III) too. Therefore, the eluted part of As(III) cannot be considered as the total amount of As(III) occurring in solution. However, although not quantitative, the qualitative identification of As(III) is meaningful. After 504 h of incubation, As(III) was detected in the soil solution. The whole dataset can be found in the supplementary files (Section B1).

a)

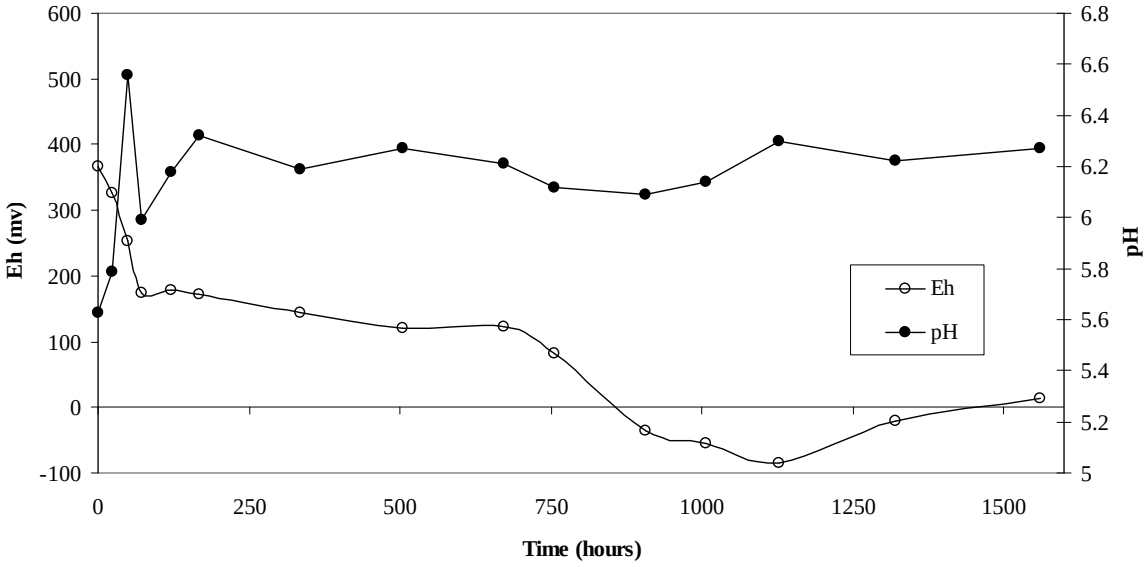

b)

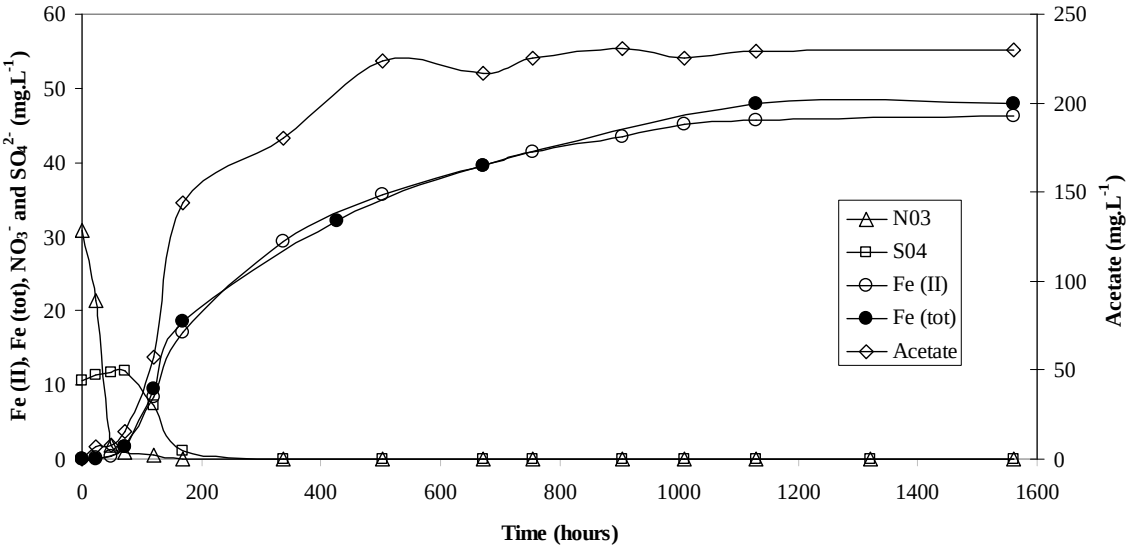

Figure III.3.2. a) Variations through the incubation time of a) pH and redox potential (Eh), b) Fe(II), total iron (Fe(tot)), acetate, sulphate (SO_4^{2-}) and nitrate (NO_3^-) concentrations in the reference column.

3.3.2. Iron-oxide dissolution and associated-As release

The amounts of Fe and As dissolved from the slides versus exposure times are reported as a percentage of the initial mass in Figures III.3.3a and III.3.3b. At the beginning, the dissolution of As-Fh started rapidly. After 336 h of incubation, Fe and As releases from the As-Fh slide were 57% and 35.6%, respectively (Fig. III.3.3a). By contrast, the dissolution of the As-Lp was slower, with 15.5% and 27.5% for Fe and As, respectively (Fig. III.3.3b). Iron and As dissolution from As-Fh slides continued to increase up to 86.8% after 888 h of incubation and then reached a steady state until the end of incubation. Concerning As-Lp, the percentage of dissolved Fe and As increased to 84.0% and 83.2%, respectively after 1560 h of

incubation without reaching any equilibrium. It has to be mentioned that the two last points corresponding to As for the As-Fh dissolution (sampled at 1248 and 1714 h) were lower than the XRF detection limit. The true values could be at least close to the lower XRF measured As signal for all As-Fh slides.

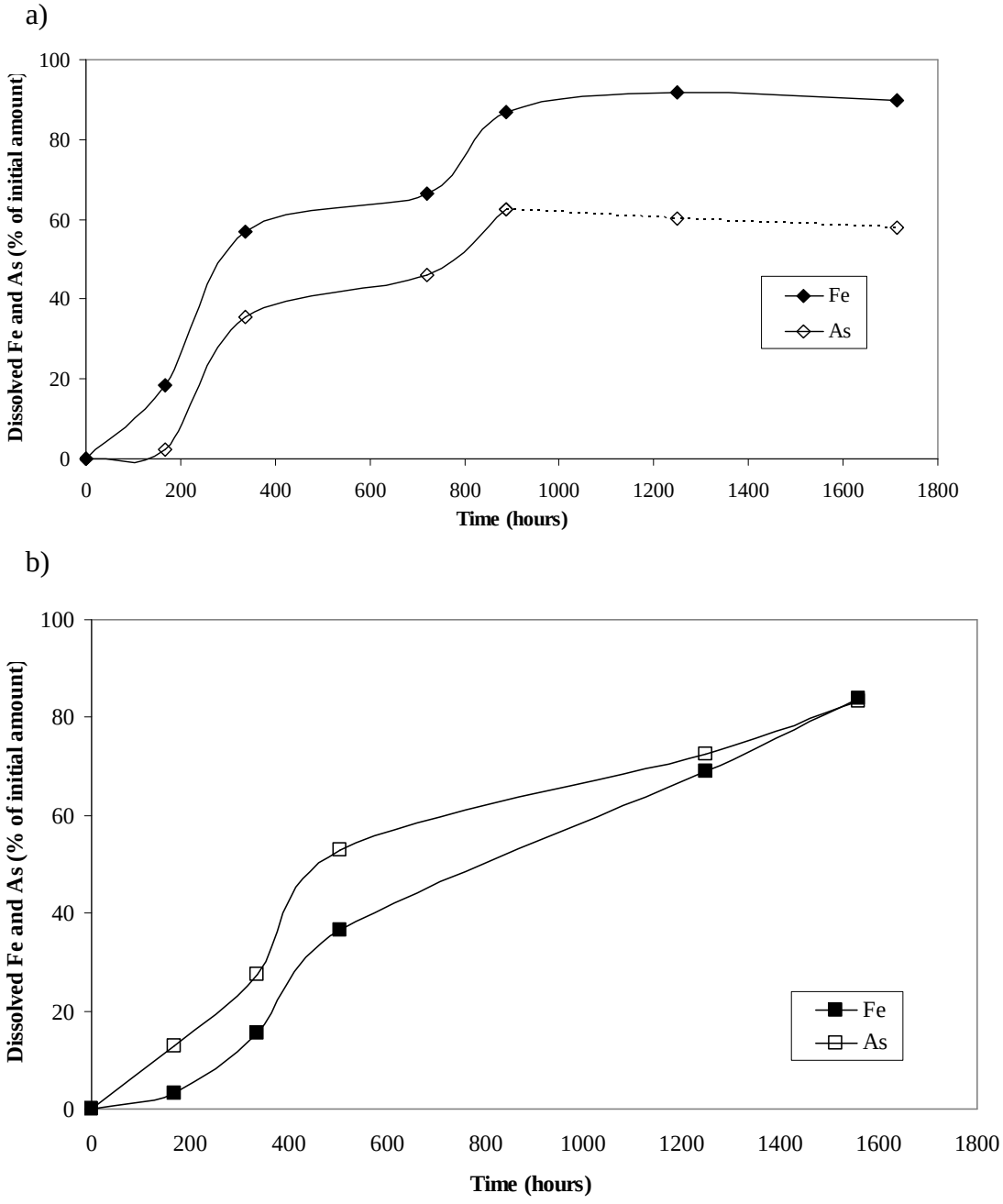

Figure III.3.3. Dissolved Fe and As from a) ferrihydrite and, b) lepidocrocite. Data are reported as percentages of the Fe and As amounts present on the slides after incubation as compared to their initial amounts before incubation.

We thus propose that these dissolved As amounts were higher or at least equal to 60.3% and 57.9%, respectively for the two considered sampling times. At first sight, the As release followed that of Fe. However, it was observed that the percentages of released As were always significantly higher than that of Fe for As-Lp, but lower for As-Fh.

a)

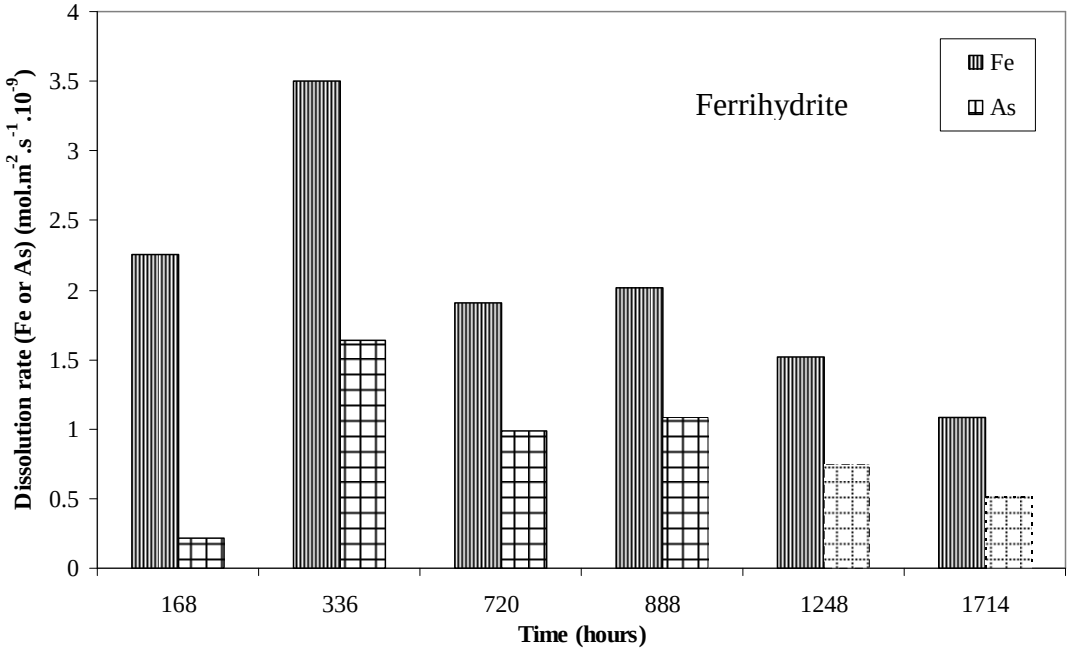

b)

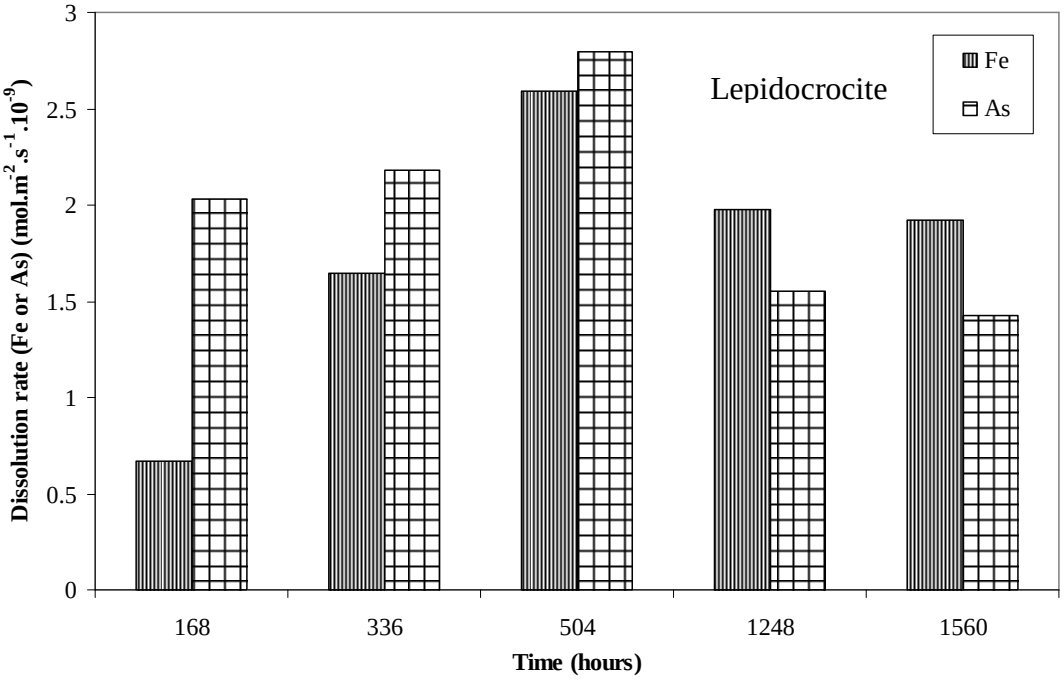

Figure III.3.4. Dissolution rates of ferrihydrite and lepidocrocite at different incubation times. Dissolution rates for ferrihydrite and lepidocrocite were calculated for a surface area of 240 and 139 $m^2.g^{-1}$, respectively (Pedersen et al., 2006).

In order to facilitate the comparison with previous studies, the dissolution rates were calculated in mol. m^{-2} Fe s^{-1} for iron and in mol. m^{-2} As s^{-1} for arsenic. BET surface area of 240 $m^2.g^{-1}$ for As-Fh (Cornell and Schwertmann 2003) and 139 $m^2.g^{-1}$ for As-Lp was assumed following Pedersen et al. (2006) since oxides were prepared with the same protocol (Table III.3.2). Iron and As dissolution rates of As-Fh increased until 336 h and decreased regularly

until the end of the experiment (Fig. III.3.4a). For As-Lp, Fe and As dissolution rates increased until 504 h, then decreased until the end of the experiment. During the onset, the As dissolution rate was higher than that of Fe. Afterwards As dissolution rate was smaller than that of Fe, probably due to a reincorporation of As onto the slide surface (Fig. III.3.4b). The whole dataset can be found in Table III.3.2.

Table III.3.2. Dissolution rates of ferrihydrite and lepidocrocite at different incubation times. Dissolution rates for ferrihydrite and lepidocrocite were calculated for a surface area of 240 and 139 $m^2.g^{-1}$, respectively (Pedersen et al., 2006)

	(As-Fh) Dissolution rate mol(Fe/As).m^{-2}.s^{-1}			**(As-L) Dissolution rate mol(Fe/As).m^{-2}.s^{-1}**	
Time (hours)	**Fe**	**As**	**Time (hours)**	**Fe**	**As**
0	0	0	0	0	0
168	$2.25\ 10^{-9}$	$2.15\ 10^{-10}$	168	$6.72\ 10^{-10}$	$2.03\ 10^{-9}$
336	$3.51\ 10^{-9}$	$1.64\ 10^{-9}$	336	$1.65\ 10^{-9}$	$2.18\ 10^{-9}$
720	$1.91\ 10^{-9}$	$9.86\ 10^{-10}$	504	$2.59\ 10^{-9}$	$2.80\ 10^{-9}$
888	$2.02\ 10^{-9}$	$1.90\ 10^{-9}$	1248	$1.97\ 10^{-9}$	$1.55\ 10^{-9}$
1248	$1.52\ 10^{-9}$	$7.46\ 10^{-10}$	1560	$1.92\ 10^{-9}$	$1.42\ 10^{-9}$
1714	$1.08\ 10^{-9}$	$5.21\ 10^{-10}$			

3.3.3. SEM/EDS observations

SEM micrographs of the As-Fh and As-Lp slides before incubation in soil are presented in Figures III.3.5a and III.3.5b. As-Fh occurred as more or less finely dispersed aggregates of particles of various size (Fig. III.3.5a). The biggest aggregates reached sizes of about 10 µm and were often separated by fractures (Fig. III.3.5a). The characteristic sizes of the smallest agglomerates were found to be less than 1 µm (Fig. III.3.5a). SEM micrographs of the initial As-Lp slide show small crystals (0.2 - 0.03 µm) (Fig. III.3.5b). They were regularly distributed on the slide stripes (Fig. III.3.5b).

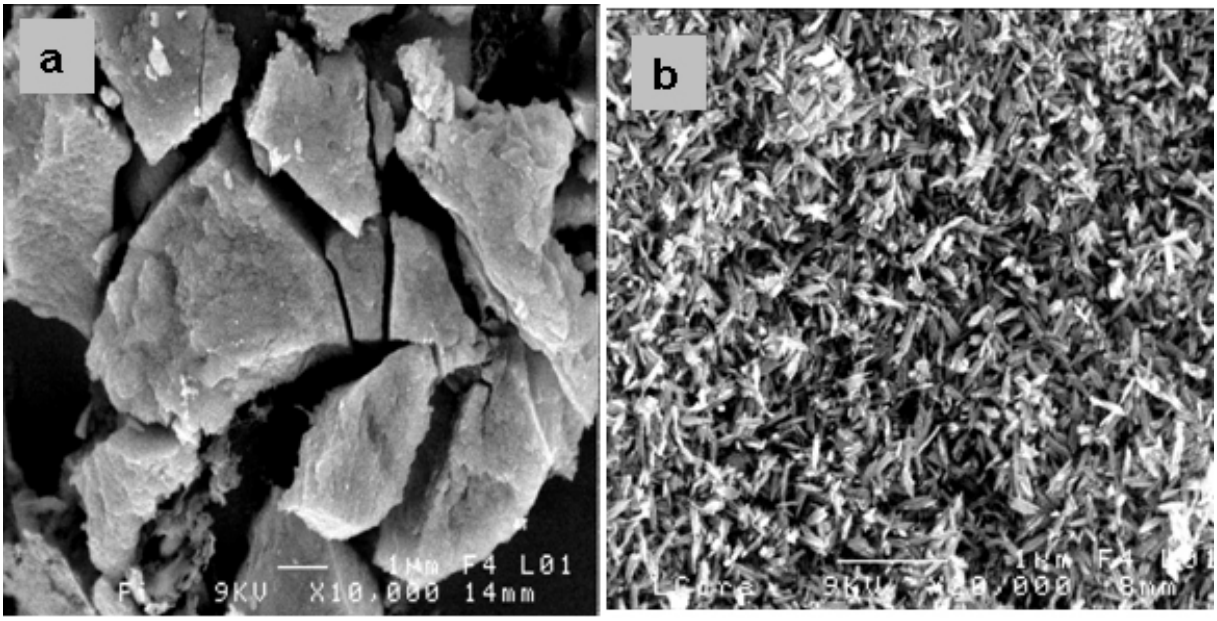

Figure III.3.5. SEM pictures of a) As-Fh and b) As-Lp before any contact with soil.

After incubation in the soil, SEM observations of the slides revealed the presence of different associations displaying systematic and clear differences between the As-Fh and As-Lp oxides. After 336 h of incubation, As-Fh slides were colonized by bacteria and biofilms (Fig. III.3.6a) and a light surface alteration with apparition of small cavities was observed (Fig. III.3.6a'). Small spheres (0.1 µm diameter) were detected on the top layer of the As-Fh surface (Fig. III.3.6a'). After 720 h, it was no more possible to observe the original structure of the As-Fh. By contrast, typical features (micro-cavities) of surface dissolution were observed. Microorganisms (Fig. III.3.6b) and fungi (Fig. III.3.6b') were always present and micro-precipitates appeared on the As-Fh surface (Figs. III.3.6b and III.3.6b'). In addition, starting at 720 h until the end of the incubation, black precipitates, which colour was unstable with time, were observed on slides as black dots (about 2-mm-wide) in the middle of the brown ferrihydrite particles. SEM analysis of these dots revealed amorphous agglomerates of about 0.1 µm diameter spheres (Fig. III.3.7a), while after 1248 h, needles (0.1-µm-long) covered by a thick biofilm were observed (Fig. III.3.7b). EDS analysis show that these micro-precipitates were Fe- and S- rich with an atomic Fe/S ratio equal to 18.4 ±9.4 and 1.8 ±0.6 after 720 and 1248 h, respectively. This latter point could suggest that FeS_2 (pyrite) formation occurred. After 1248 h, it became difficult to localize the Fe-oxide agglomerates upon SEM observation because 90% of Fe-oxide was dissolved (Fig. III.3.3a). Microorganisms were still present, and micro-needles (0.1-µm-long) mixed with soil particles and bacteria (Fig. III.3.6c) were observed. These needles were covered by biofilm (Fig. III.3.6c').

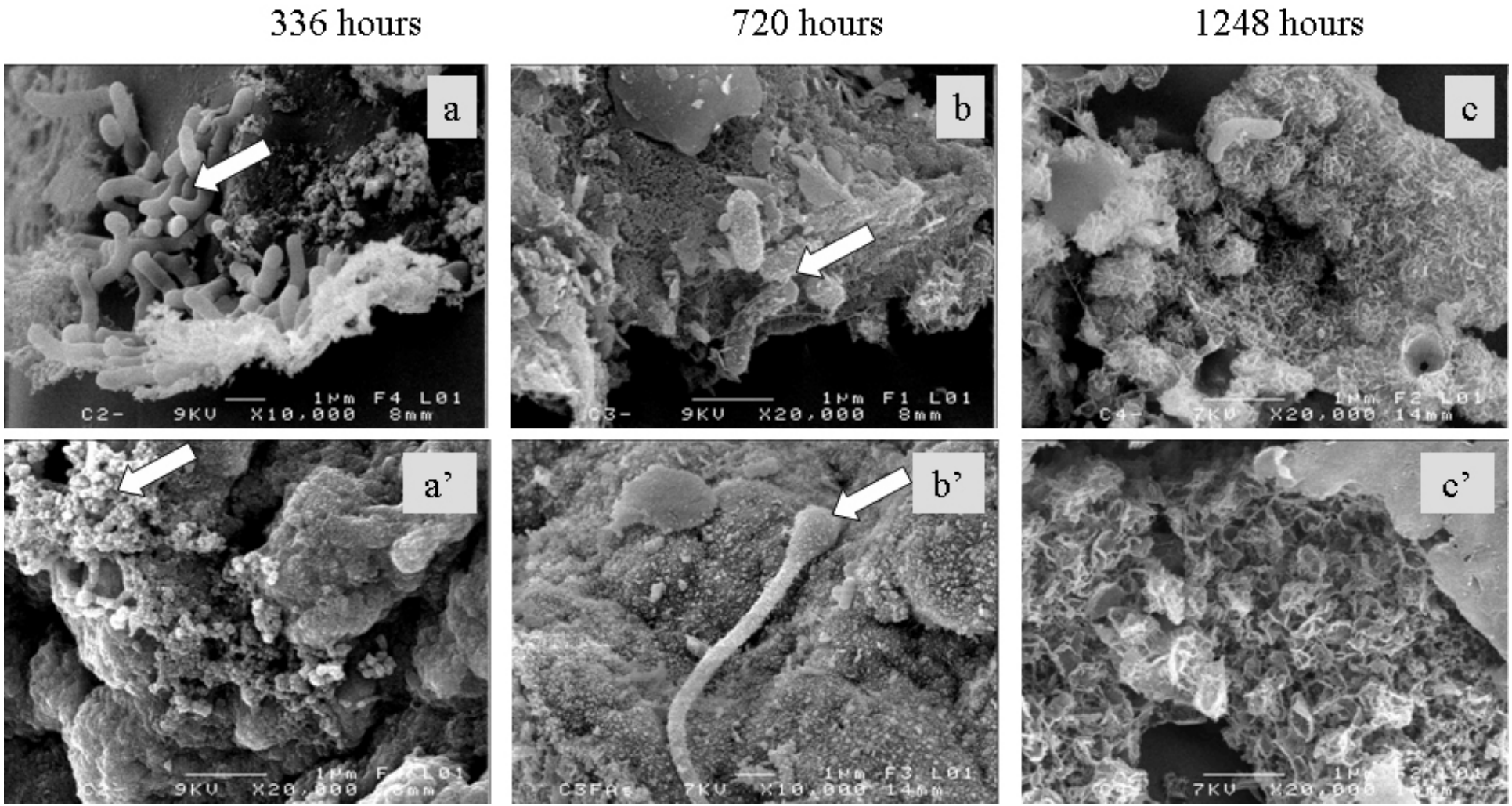

Figure III.3.6. Comparison between the morphological changes of As-Fh during incubation in soil as evidenced by SEM pictures. a, a'), b, b') and c, c') correspond to slides covered with As-Fh and incubated during 336, 720 and 1248 h, respectively. The arrows in a) and b), b'), and a') indicate the presence of bacteria, fungi and precipitates, respectively.

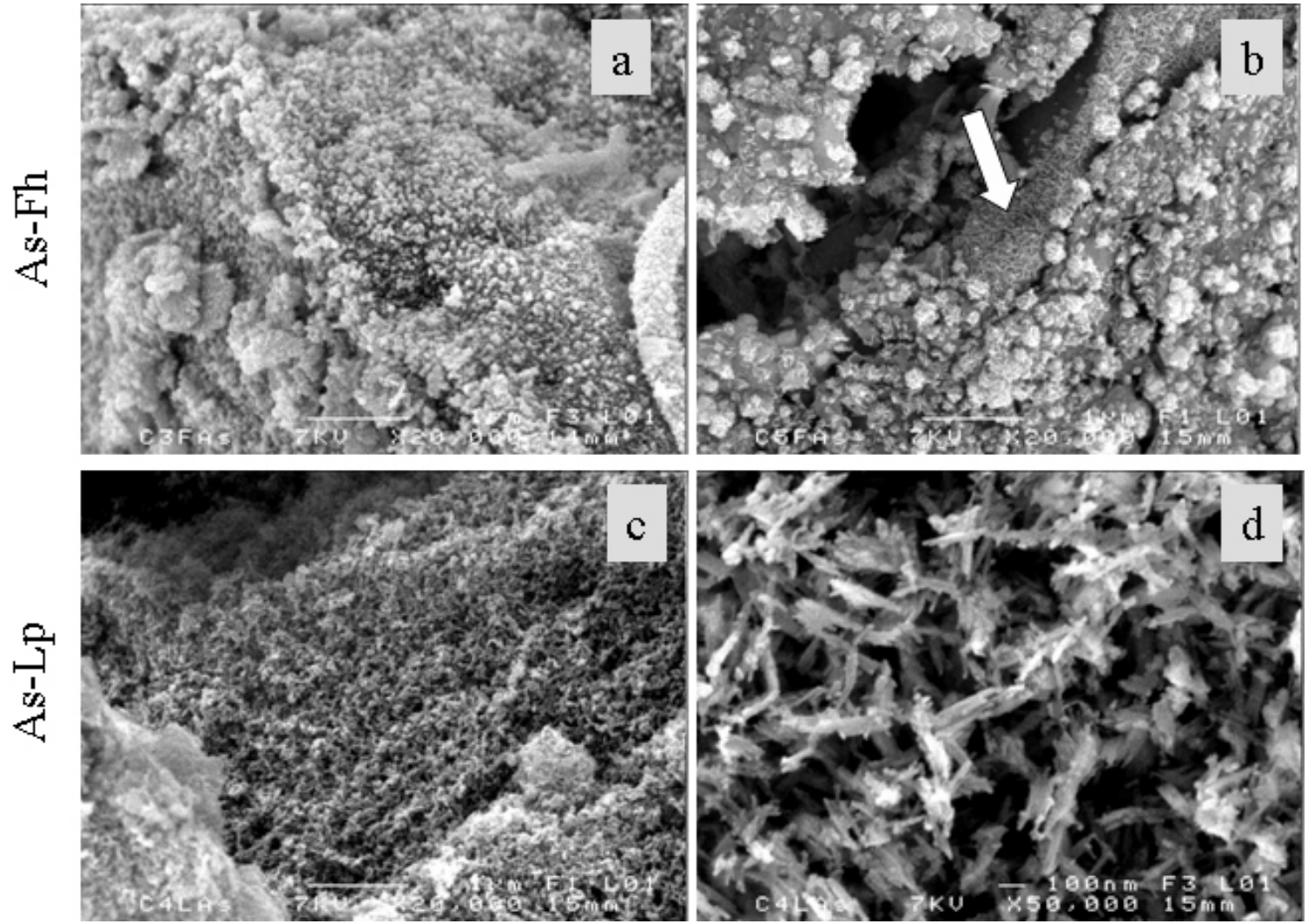

Figure III.3.7. SEM pictures of Fe-sulphides formed on the As-Fh slides after a) 720 h and b) 1248 h of incubation, respectively. The arrow shows the Fe-sulphide needles covered by a thick biofilm. c) and d) correspond to SEM pictures of Fe-sulphide on As-Lp slide after 1248 h of incubation.

The observation of As-Lp showed that after 168 h of incubation large cavities (from 1-µm- to 7-µm-long) - mixed by bacteria and soil particles - were formed at the surface (Fig. III.3.8). In these cavities, As-Lp was deteriorated (Fig. III.3.8). After 336 h, an important colonization by bacteria and biofilms was observed (Figs. III.3.9a and III.3.9a'). The arrow displayed in Figure III.3.9a' shows the presence of two bacteria types: (i) small (0.5- to 0.75-µm-long) with a smooth surface and (ii) large (1.5- to 2-µm-long) and with a granular surface. The shape of lepidocrocite shows a more connected structure, the large cavities disappeared, and the crystals were strongly out of shape. One can note that after 336 h, the slide surface was almost completely covered by biofilms, which limited the observable surface (Figs. III.39b and III.3.9b'). The black arrow in Figure III.3.9b' shows that the Fe oxide alteration was prevailing below the thick biofilm while bacteria and micro-precipitates were also observed at the surface. Finally, two different precipitates appeared after 1248 h (Figs. III.3.9c and III.3.9c'), showing aggregates of small spherical precipitates with diameters of about 0.1-µm. A new precipitate network was observed in close association with these small spherical precipitates (Fig. III.3.9c').

In addition, from 504 h until the end of the incubation, unstable black precipitates of dots of about 2-mm were observed in the middle of the orange pristine lepidocrocite, as evidenced for As-Fh slides. SEM observation of these dots revealed loose amorphous needles (0.2-µm-long) covered by a thick biofilm (Figs. III.3.7c and III.3.7d). EDS analysis revealed that they were Fe- and S-rich with a Fe/S atomic ratio equal 5.3 ±0.9 and 1.9 ±0.6 after 1248 and 1560 h, respectively.

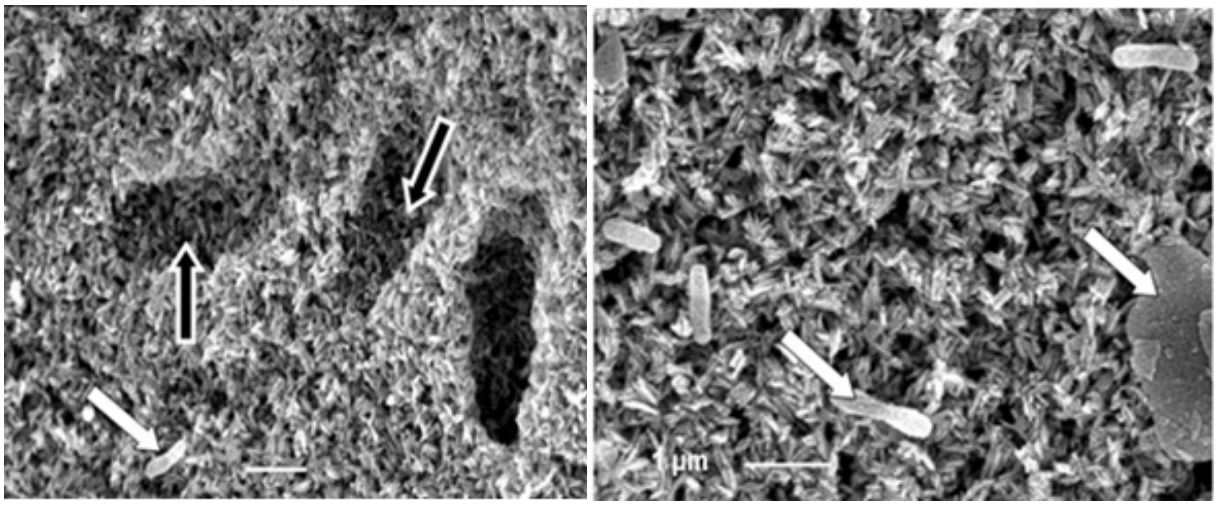

Figure III.3.8. SEM pictures of the surface alteration evidenced on lepidocrocite after 168 h of incubation in soil. The white arrows show bacteria or soil particles. The black arrows show Fe-oxide alteration features.

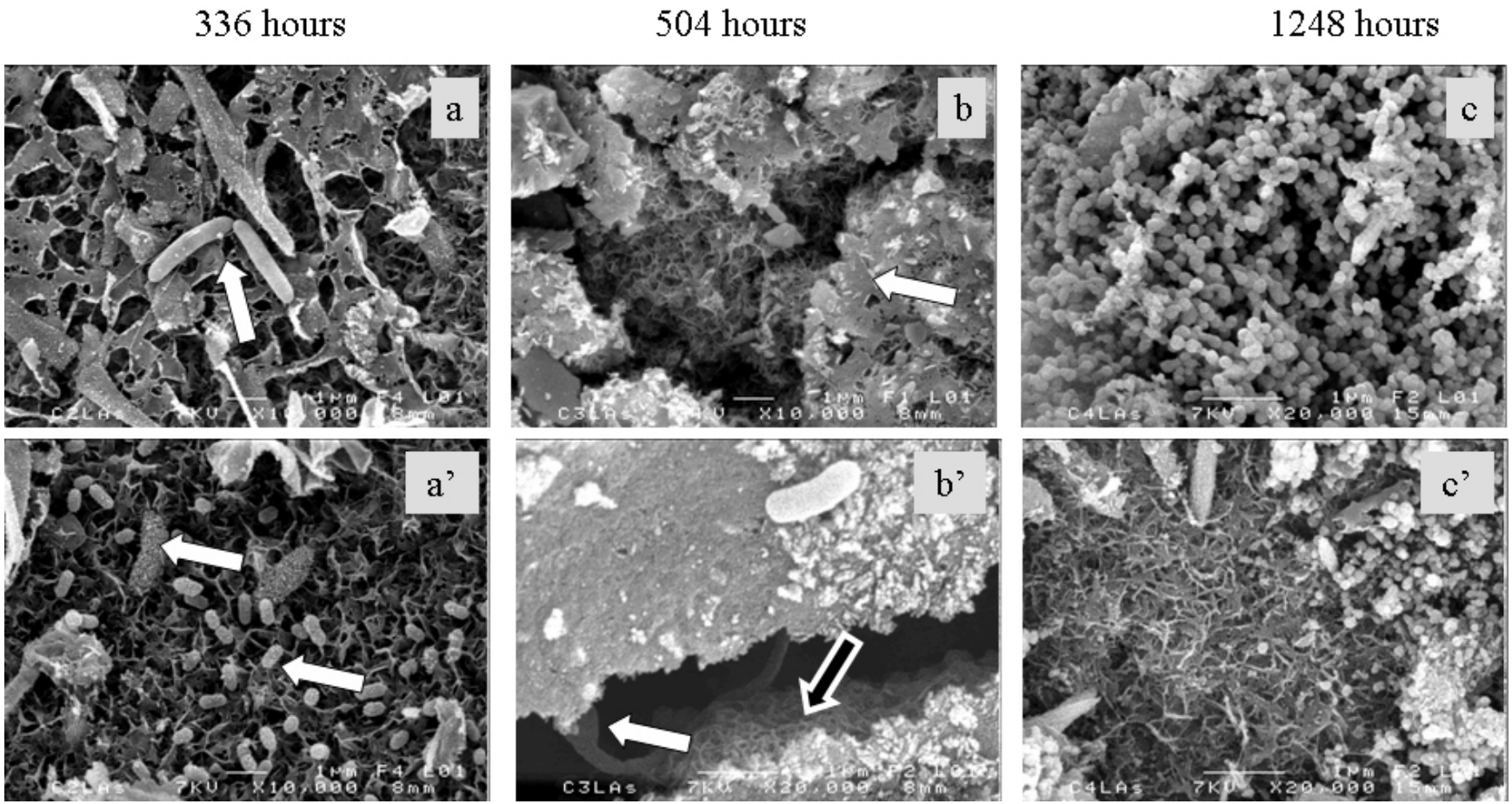

Figure III.3.9. Comparison between the morphological changes of As-Lp during incubation in soil as evidenced by SEM pictures. a, a'), b, b') and c, c') correspond to slides covered with As-Lp and incubated during 336, 504 and 1248 h respectively. The white arrows in 9a, 9a'), 9b) and 9b') show bacteria, biofilm and fungi, respectively. The black arrow in Fig. III.3.9b' shows the alteration of Fe-oxides covered by biofilms.

3.3.4. Redox state and As release during the transformation of Fe-oxides

Arsenic release during the reductive dissolution of ferrihydrite and lepidocrocite is shown in Figures III.3.3a and III.3.3b. Figure III.3.10 displays the amount of Fe relative to As released for both Fe oxides. The straight line represents a stochiometric release of As and Fe. For As-Fh, As was not released until 50% of the Fe-oxide had been dissolved. By contrast for As-Lp, As was rapidly released into solution in a proportion superior to that of Fe. The same results were obtained by Pedersen et al (2006) who studied the chemical (Ascorbate) reductive dissolution of As-Fh and As-Lp. The evolution of the Fe/As ratio for each slide and through time can be found in Table III.3.3.

Table III.3.3. Speciation of As in both Fe-oxides at different incubation times. nd refers to not determined.

As-Fh						
Time (h)	**Fe/As initial**	**Fe/As final**	**%As(V)**	**% As(III)**	**As(V) (µg)**	**As(III) (µg)**
	-		100.0	0.0		
168	237.90	199.05	-	-	-	-
336	245.0	163.8	73.1	26.9	1.1	0.4
720	258.5	160.0	44.0	56.0	0.7	0.9
888	262.5	92.8	-	-	-	-
1248	245.9	*50.0*	nd	nd	nd	nd
1714	239.7	*58.9*	-	-	-	-
As-Lp						
Time (h)	**Fe/As initial**	**Fe/As final**	**%As(V)**	**% As(III)**	**As(V) (µg)**	**As(III) (µg)**
0	-		100.0	0.0		
168	182.7	202.9	93.2	6.8	2.2	0.2
336	157.6	183.6	88.5	11.5	4.3	0.6
504	158.3	213.1	-	-	-	-
1248	178.7	201.4	95.5	4.5	0.7	0.0
1560	171.2	163.0	-	-	-	-

For As-Fh experiments, the Fe/As ratios decreased with increasing incubation time, suggesting that As is more readsorbed on the slide as compared to Fe. For the As-Lp oxide a slight increase of the Fe/As ratio was observed on each slide after 168 h. However, no significant change of the Fe/As ratio was noticed through time. Both observations suggest that by contrast to what has been observed for As-Fh, As was not readsorbed onto the As-Lp slide.

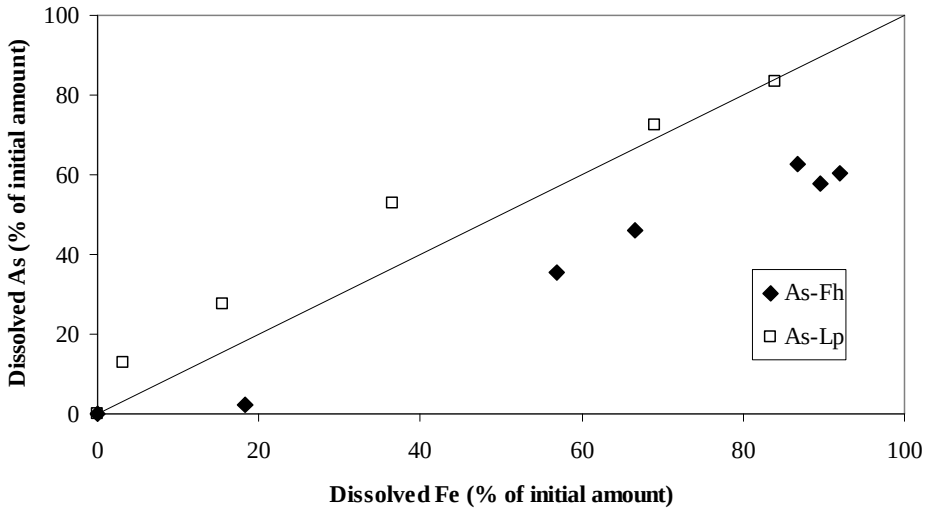

Figure III.3.10. Arsenic versus Fe release during reductive dissolution of As-Fh and As-Lp. The straight line corresponds to congruent release of As and Fe.

Arsenic K-edge XANES spectroscopy was used to determine the redox state of As after incubation in soil. The XANES spectra exhibit a well-resolved edge structure with an adsorption maximum at 11871.3 eV and 11875.0 eV, corresponding to As(III) and As(V), respectively (Fig. III.3.11). Before incubation, As occurred exclusively in the pentavalent form As(V), for both Fe-oxyhydroxydes. After 336 h, for As-Fh, 27% of the remaining As was present as As(III) (Table III.3.3). After 720 h, the proportion of As(III) on the slide increased up to 56 %. For the lepidocrocite, after 168 h only 7 % of As occurred as As(III), this proportion increased slightly up to 12% at 336 h (Table III.3.3).

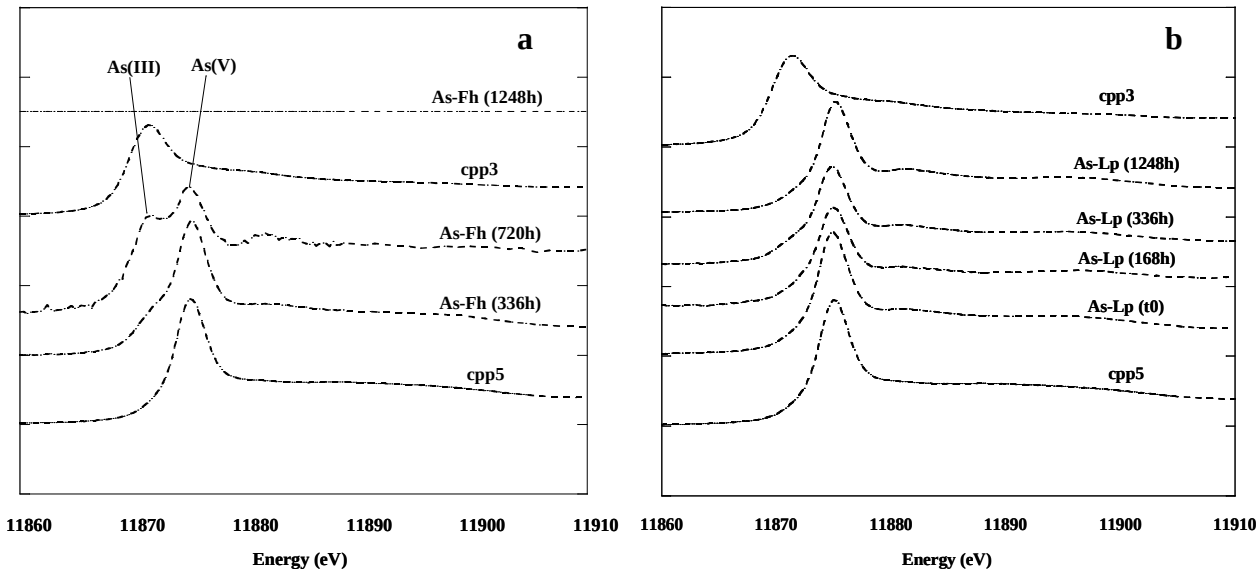

Figure III.3.11. As K-edge X-ray Absorption-Near-Edge Structure (XANES) spectra for slides after different incubation times, cpp 3 and cpp5 represent two relevant model compounds for As(III) and As(V)-doped-Fe-oxides respectively (Morin et al., 2003).

3.4. DISCUSSION

3.4.1. Reductive dissolution of Fe-oxide

During the incubation, the consumption of NO_3^- was followed by an increase of Fe(II) and acetate, and a decrease of SO_4^{2-} at lower Eh. This sequence was similar to that described in previous studies (Schwertmann and Taylor, 1989; Francis and Dodge, 1990; Lovley, 1991; Peters and Conrad, 1996; Lovley, 1997; Dassonville and Renault, 2002; Küsel et al., 2002; Grybos et al., 2007). The new experimental system thus allowed the development of anaerobic conditions and the subsequent Fe-oxide reductive dissolution. The acetate release was concomitant to the Fe(II) production. Acetate is derived from organic matter and is produced by the combined activity of fermentative and acetogenic bacteria which are known to be tightly linked to the microbial reduction of Fe(III) (Küsel et al., 2002).

The dissolution of As-Fh ceased at 90% of dissolved Fe after 1000 h (Fig. III.3.3). Moreover, the dissolution rates of the As-Fh strongly decreased with time (Fig. III.3.4). This can be explained by two processes: (i) oxides might be hidden by soil particles which made them inaccessible to microorganisms (Chenu and Stotzky, 2002; Fakih et al., 2008b) (Section III.1.4.3), (ii) adsorption and/or surface precipitation of biogenic Fe(II) might occur during the microbial reduction (Urrutia et al., 1998; Châtellier and Fortin, 2004). Initially, the fresh Fe-oxide agglomerates were easily accessible to bacteria, which justifies the strong Fe dissolution rate calculated at the beginning of the incubation. Later, the bacteria could not access to the very tiny pores of the ferrihydrite agglomerate structure (Roden and Zachara 1996; Roden 2003), which resulted in a decrease of the Fe dissolution rates.

By contrast, the dissolution of lepidocrocite did not stop and was delayed as compared to that of ferrihydrite. The iron dissolution rate for the As-Lp oxide was 2.13 times lower than that of As-Fh oxide 336 h and 1.78 times lower at the end of the incubation time. Several authors showed that poorly crystallised Fe(III)-oxides such as ferrihydrite are the favoured reducible forms of Fe(III) for microbial reduction (Munch and Ottow, 1980; Wahid and Kamalam, 1993; Roden and Zachara, 1996; Larsen and Postma, 2001). In the present study, the dissolution rates of the Fe-oxides were therefore controlled by their solubility relative to their mineralogical state.

Fe-oxide dissolution rates have been previously measured during laboratory experiments involving chemical and/or biological reduction (Postma, 1993; Roden and Zachara, 1996; Paige et al., 1997; Hansel et al., 2003; Roden, 2003; Pedersen et al., 2006) or under field *in situ* conditions (Fakih et al., 2008b, section III.1). They displayed a large range of variations as shown in Table III.3.4. The dissolution rates were highly dependent on both the selected bacterial species and the chosen experimental conditions. The calculated dissolution rates in this study (2.02×10^{-9} and 1.92×10^{-9} mol Fe m^{-2}. s^{-1} for As-Fh and As-Lp, respectively) are faster than the previously determined rates for bacterial and abiotic reductive dissolution (Table III.3.4). One of the more important factors controlling the dissolution rates of Fe oxides is the concentration of bacterial cells (Roden and Zachara, 1996; Roden, 2003; Bonneville et al., 2004). As shown in this study, a strong microbial colonization was observed in direct contact with the Fe oxides. The presence of several types of microorganisms colonizing the Fe oxide suggests that different types of combined mechanisms could be involved in the reductive process. This strong catalysis through biological activity could reinforce the effects of already strong reductive conditions (as evidenced by the low reported Eh values).

Table III.3.4. Compilation of published dissolution rates of pure ferrihydrite, As-Fh, pure lepidocrocite and As-Lp estimated from chemical, biotic reductive dissolutions and *in situ* experiments.

Oxide	Dissolution rate (mol Fe. m^{-2}. s^{-1})	Reducing agent	References
Ferrihydrite	2.3-12 10^{-12}	Autochthonous bacteria (*in situ* experiment)	Fakih et al. (2008b) (Table III.1.3)
	2.0 10^{-12}	Bacteria	Roden (2003)
	1.7 10^{-10}	Chemical reducer (Ascorbate)	
	7.0 10^{-12}	Bacteria	Roden and Zachara (1996)
	1.2 10^{-8}	Chemical reducer (Ascorbate)	Postma (1993)
	3.3-4.1 10^{-8}	Chemical reducer (Ascorbate)	Larsen and Postma (2001)
As-Ferrihydrite	2.02 10^{-9}	Autochthonous bacteria (Anaerobic soil column)	(This work)
	2.3-4.3 10^{-12}	Autochthonous bacteria (*in situ* experiment)	Fakih et al. (2008b) (Table III.1.3)
	5.3 10^{-11}	Chemical reducer (Ascorbate)	Pedersen et al. (2006)
	1.8-8.0 10^{-11}	Chemical reducer (Ascorbate)	Paige et al. (1997)
Lepidocrocite	4.6 10^{-11}	Bacteria	Roden (2003)
	7.9 10^{-11}	Bacteria	Cooper et al. (2000)
	4.6-7.3 10^{-9}	Chemical reducer (Ascorbate)	Larsen and Postma (2001)
As-Lepidocrocite	1.92 10^{-9}	Autochthonous bacteria (Anaerobic soil column)	(This work)
	1.34 10^{-11}	Chemical reducer (Ascorbate)	Pedersen et al. (2006)

3.4.2. Mineralogical modifications (SEM/EDS observations)

The occurrence of biofilms and the high microbial colonization of the ferrihydrite and lepidocrocite slides suggest that microorganisms played a key control in Fe and As mobilization through a direct microbial reduction mechanism as elsewhere evidenced (Lovley, 1993; Chenu and Stotzky, 2002; Oremland and Stolz, 2003; Islam et al., 2004). However, the two oxide types exhibited different dissolution patterns and associated mineralogical changes.

Pristine ferrihydrite was composed of aggregates spaced by fractures. After 336 h of incubation, typical morphological features of progressive dissolution were observed on the As-Fh particles surface. The processes involved in the dissolution of both Fe-oxide types were probably quite different. The aggregates of ferrihydrite were formed by an association of nano-crystals, easily reducible by bacteria when they were located at agglomerate surface. Roden and Zachara (1996) and Roden (2003) provided evidence that bacteria cannot access to the very tiny pores of the ferrihydrite agglomerate structure. Bacterial reduction of the ferrihydrite took therefore place on the whole exposed agglomerate surface.

By contrast, lepidocrocite was formed by non-agglomerated 2 µm crystals. Even if the lepidocrocite crystals were less reducible than the ferrihydrite nano-crystals, the porosity of the lepidocrocite layer allowed a better accessibility of bacteria. Therefore, in the first stage of reduction, the observed dissolution features were large cavities in the lepidocrocite layer. It has to be mentioned that so far to our knowledge, such pictures of the lepidocrocite bacteria-mediated reduction have never been published. Studies of the reductive dissolution of Fe-oxides were often performed in batch system where Fe-oxide particles were in suspension or in columns, which prevented any solid analysis to be done since the solid phase was unstructured (e.g. Roden and Urrutia, 1999, 2002; Larsen and Postam 2001, Hansel et al., 2003). In a second step, when the surface was entirely covered by biofilms and colonized by bacteria, the dissolution was revealed by an out of shape of lepidocrocite crystals. Larsen and Postma (2001) found that the mechanism for chemical reductive dissolution (Ascorbate-mediated) of lepidocrocite occurred along the c-axis by performing small pit in the fringe of the crystal. This phenomenon evidenced for chemical reduction is also expected to happen with bacteria-mediated reduction. Since lepidocrocite crystals were extended along the c-axis, the latter surface was probably more exposed to bacteria and therefore to dissolution.

Two types - needles and small spheres, of secondary minerals - were observed on the As-Lp slides and As-Fh slides, respectively. SEM/EDS analyses of the needles of both Fe oxides allowed identifying Fe sulphides. The formation of such Fe sulphides on the As-Fh slides was wider than on the As-Lp slides. The Fe/S ratios (1.8 and 1.9 ±0.6) were comparable for both types of Fe-oxides after 1248 h of incubation for As-Fh and 1560 h for As-Lp. The occurrence of Fe sulphides agrees with the previous study of Charlatchka and Cambier (2000), who observed Fe-sulphide precipitation within a soil after two months of flooding. Fakih et al. (2008b) observed also Fe sulphide on ferrihydrite-covered slides after three months of incubation in a natural soil (Section III.1.1.4.4). However, Fe-sulphide grains observed on As-Fh and As-Lp slides differ in morphology. SEM analysis of dots on the As-Fh slide revealed amorphous agglomerates of about 0.1 µm diameter spheres and, needles (0.1-µm-long) (Fig. III.3.7b). However, SEM observation of the dots on As-Lp slide revealed loose amorphous needles (0.2-µm-long) (Figs. III.3.7c and III.3.7d). This shape difference might be related to the influence of the texture of the original Fe-oxides on the dissolution pathway. The newly formed small sphere precipitates were not evenly spread over the slides, they are located in the black precipitates. Sulphide precipitation can be related to the consumption of dissolved SO_4^{2-}. However, such consumption is not expected to occur under the Eh conditions measured in the solution (Eh ≥ -100mV). Two hypotheses could explain this phenomenon: (i) Eh potentials were measured by a Pt electrode that is known to respond preferentially to metallic redox couple such as Fe(II)/Fe(III). Regards to the Fe(II) concentration in solution, the Eh potential was probably imposed by the Fe reduction; (ii) the precipitation of sulphides may also fingerprint the presence of local 'micro'-sites in soil characterized by an intense biogeochemical activity (Luo et al., 1999). In our experimental conditions, these 'micro'-sites might be more reducing than the bulk medium, thus allowing sulphate reduction to sulphide.

Biotic reductive dissolution of Fe-oxyhydroxides produces possibly several secondary minerals whose genesis and nature have been previously reported (Fredrickson et al., 1998,

Zachara et al., 2002; Glasauer et al., 2003). These minerals include magnetite ($Fe^{II}Fe_2^{III}O_4$), vivianite $Fe_3(PO_4)_2.nH_2O$, green rusts ($\left[Fe^{II}_{(6-x)}Fe^{III}_x(OH)_{12}\right]^{x+}\left[\left(A^{2-}\right)_{x/2}.yH_2O\right]^{x-}$), siderite ($FeCO_3$), ferrous carbonate hydroxide ($Fe^{II}{}_2(OH)_2CO_3$), and amakinite ($(Fe^{2+},Mg)(OH)_2$) (Lovley et al., 1987; Lovley and Phillips 1988; Mortimer and Coleman, 1997; Fredrickson et al., 1998; Cooper et al., 2000; Ona-Nguema et al. 2002, 2004, submitted; Zachara et al., 2002, Fredrickson et al., 2003). The nature of the secondary minerals is dominantly controlled by the concentration of aqueous Fe(II) and the presence of inhibitors, principally oxy-anions such as phosphate or carbonate (Couling and Mann, 1985; Zachara et al., 2002). These inhibitors limit the microbially-mediated Fe(II) readsorption required for the solid state changes of the primary Fe-oxides. In our experiment, none of these minerals, except sulphides, was identified at the Fe-coated slide surface. Previous studies have been mostly conducted in laboratory batch systems performed with a simple mixture of synthetic Fe-oxides, the required selected bacteria strain and the culture medium. Experimental conditions were always chosen to optimize the identification of secondary minerals. In the few cases where inhibitors were used, their concentrations were low enough to allow the evaluation of their impacts. However, in our experimental conditions, namely in a natural soil sample, organic oxy-anions ([acetate]>240mg.L^{-1}) could prevent the adsorption of Fe(II) by blocking the Fe-oxide surface sites and subsequently inhibit the previously cited mineral formation. Besides, Sun et al. (1999) evidenced that carboxylic acids can delay the transformation of ferrihydrite into more crystallized oxides. Cornell and Schwertmann (1979) suggested a model where carboxylate anions stabilize ferrihydrite by forming a binding between one or more units of ferrihydrite, preventing it from both aggregation and dissolution. Some of, these organic anions, in addition to their capacity to be adsorbed onto the Fe-oxide surface are strong complexing agents of Fe(II) ions, maintaining them in solution and preventing therefore their readsorption. In consequence, our results suggest that in organic-rich soil horizons, when Fe(II) is complexed by organic anions, and competes for sorption on the Fe(III)-oxides surface, the major secondary minerals are Fe-sulphides.

3.4.3. Consequences for As mobility

The comparison of the Fe/As ratio at initial and final stages showed that part of the released As was readsorbed on the As-Fh surface. This readsorption could be favoured by the dissolution of ferrihydrite which increased the specific area of the Fe-oxide (Munch and Ottow, 1980). In the case of As-Lp, our data showed that As(III) much less readsorbed on the remaining lepidocrocite. This difference between the As-Fh and As-Lp experiments can be explained by two processes. (i) The first point is related to the lower amount of available surface sites on Lp as compared to Fh in our experiments. The initial surface coverage on the As-Fh sample (0.5 µmol.m^{-2}) is much lower than that on the As-Lp sample (1.7 µmol.m^{-2}). According to the maximum site density of 3.7 µmol.m^2 for As(III) sorption onto Fe(III)-oxyhydroxides (Dixit and Hering,2003; Wilkie and Hering, 1996; Goldberg and Johnston, 2001), it can be inferred that the high initial As(V) loading on our As-Lp sample limited the readsorption of As(III), after partial dissolution of the Lp, as compared to our As-Fh sample which had a lower initial As(V) coverage. (ii) The second point is related to the Fe-oxide mineral structure. Cornell and Schwertmann (2003) showed that As(V) is adsorbed only on surface sites located along the *b*- and *c*-axes ((001) facets) of the lepidocrocite crystal. As evidenced by Larsen and Postma (2001) and expected to occur in our experiments, reductive dissolution of lepidocrocite was observed along the *c*-axis. This process increases the surface

site number, instead of eliminating surface sites for the adsorption or readsorption of As as reductive dissolution occurs (Larsen and Postma, 2001; Pedersen et al., 2006).

XANES analysis provided evidence for the partial reduction of As(V) to As(III) on both Fe-coated slide types, which increased with time. It has been shown that biotic reduction of As(V) to As(III) takes place after Fe(III) reduction, rather than occurring simultaneously, upon incubation of natural sediments (Islam et al., 2004) as well as upon As-Fh incubation in the presence of soil bacteria consortia (Burnol et al. 2007). The absence of As(V) reduction in abiotic experiments carried out in these studies have demonstrated that Fe(III) reducing bacteria played a major role in the subsequent reduction and release of As once the bioavailable Fe(III) had been used as an electron acceptor. It is thus likely that As(III) observed in our experiments originate from biotic reduction. Moreover, the speciation of As(III) on the Fe-oxide coated slide could include: (i) precipitation as a secondary phase. Arsenic sulphides as As_2S_3 have been identified in contaminated lakes (Soma et al., 1994) and wetlands (LaForce et al., 2000). However, thermodynamic equilibrium with arsenic sulphide minerals is achieved only in the presence of appreciable sulphur concentrations in highly sulphur-rich zones (Sadiq, 1997). (ii) Sorption on sulphide minerals (Bostick and Fendorf, 2003) or substitution in FeS_2 (Blanchard et al., 2007). Abraitis et al., (2004) showed that FeS_2 pyrite can incorporate up to ca. 10 wt% of As(III). Bostick and Fendorf, (2003) showed that As(III) sorption onto FeS and FeS_2 results in the formation of an FeAsS-like surface precipitate. In the present study, MEB-EDS analyses did not allow identifying the presence of such arseno-pyrite due to the low As concentration and the large EDS spot size. (iii) Finally, adsorption on the remaining Fe-oxide surface. The position of the As(III) shoulder in our XANES data (11871.3 eV) indicates that As(III) is coordinated to oxygen, since the more covalent bond to sulphur yield lower absorption energies (Bostick and Fendorf, 2003). Consequently, despite the lack of As-EXAFS data we can conclude that most of As(III) observed on the Fe-oxide slides is adsorbed onto the surface of the remaining Fe-oxide. According to the differences in the number of available surface sites between the Fh and Lp samples, such readsorption process is consistent with a higher amount of As(III) on the As-Fh than on the As-Lp slides. Reduction and subsequent immobilisation of As may have therefore resulted from a coupled biotic-abiotic reaction pathway in which (Fe or As) reducing-bacteria allowed the reduction of As(V) to As(III) that was subsequently mainly readsorbed onto remaining Fe-oxide surfaces. However, it is important to note that the readsorbed or precipitated fraction of As remains low as compared to the initial amount, probably less than 20 % for ferrihydrite and only a few % for lepidocrocite.

3.4.4. Environmental impacts

This study provided evidence that the reductive dissolution of Fe-oxides in organic rich soil horizons can involved a strong mobilization of Fe as Fe(II). A small fraction of Fe(II) precipitated with sulphur. Iron sulphides have been shown to be effective sorbents for a variety of toxic elements, including As, Cd, Cr, Cu, Hg and Pb (Bostick and Fendorf, 2003; Bostick et al., 2003; Doyle et al., 2004; Borah and Senapati, 2006; Ozverdi and Erdem, 2006). As a consequence, when reducing conditions prevail, part of these cations can be temporarily immobilized by sulphides in soils. However, wetland soils are subject to strong oxidizing/reducing alternations linked to the soil waterlogging. Under oxidizing conditions, sulphides can be transformed into sulphates, and subsequently adsorbed cations could be released into the soil solution or themselves transformed into sulphates (Ozverdi and Erdem, 2006). Such changes can represent an increased environmental danger for toxic trace metals occluded in sulphate minerals displaying high solubility. Therefore, the combination of

intensive Fe-oxide dissolution to the precipitation of sulphide secondary phases may increase the metal ion mobility in soil. Moreover, an important part of these trace elements could be eliminated from the soil solution to get into the hydrosystem when the water level decreases.

Iron-oxide reduction has also been suggested as a mechanism for As mobilization into groundwaters (Nickson et al., 2000; Bose and Sharma, 2002; Van Geen et al., 2004). This study confirms this hypothesis although the dissolution is not congruent as previously demonstrated by Pedersen et al. (2006). The present study also provides evidence that As(V) is reduced to the more toxic species As (III), which is observed to be strongly mobile in the anoxic soil solutions. Only a weak proportion of As(III) is sequestred by readsorption onto unreduced Fe-oxides and possibly on secondary Fe-sulphide minerals, especially when the iron-oxide has a low surface area. Therefore, wetlands and their waterlogged soils could be a non negligible source of As within soils, migrating first through soil solutions and then to the whole hydrosystem. Considering that wetlands supply oxic surface rivers, As could then be incorporated into the sedimentary floodplain, or carried further by the colloidal phase.

3.5. CONCLUSIONS

Several conclusions stem from this study, which allowed the monitoring of the reductive dissolution of two types of As-spiked Fe-oxyhydroxides (ferrihydrite and lepidocrocite) within a soil and the associated Fe and As release:

- the incubation of both As(V)-ferrihydrite and As(V)-lepidocrocite in soil columns under reducing conditions led to As release into solution.
- The reductive dissolution of lepidocrocite dissolved the As carrier site and resulted in As release. By contrast, the specific surface area of ferrihydrite remained relatively high, favouring As readsorption until the surface site number was low enough to allow As release. As release from ferrihydrite was therefore delayed as compared to As-spiked lepidocrocite.
- The secondary minerals were mostly composed of Fe-sulphides, probably due to the organic anion surface adsorption and/or Fe(II) organic complexation in solution that prevented the Fe(II) readsorption needed for the solid state transformation of the pristine Fe-oxides to occur.
- The reduction and the subsequent immobilisation of As were the result of a coupled biotic-abiotic reaction pathway in which (Fe or As) reducing-bacteria catalyzed the reduction of As(V) to As(III) which could be subsequently readsorbed onto the remaining unreduced Fe-oxides. By contrast, for lepidocrocite, As(III) was less readsorbed in response to the lower available surface site number and to the destruction of the As adsorption sites on the reduced lepidocrocite surface.

Future studies dedicated to the identification of both the nature of the bacteria consortium involved in the reduction process and the nature of the secondary mineralogical phases are under progress (EXAFS). NANOSIMS analysis will be dedicated to the imaging of the distribution of trace metals associated to either, Fe oxides or, soil particles after the reductive dissolution.

CONCLUSIONS GENERALES

IV. CONCLUSIONS GENERALES

Dans les zones humides et les environnements sédimentaires, l'alternance des épisodes de réduction et d'oxydation influe énormément sur la biogéochimie du fer et des contaminants associés. De plus, le cycle du fer influence à son tour la mobilité ou le piégeage, via des phases de réduction et/ou d'oxydation des éléments traces métalliques (potentiellement polluants) liés aux oxydes de fer.

Le cycle du fer est en grande partie sous contrôle des micro-organismes qui utilisent les oxydes de fer comme accepteurs d'électrons (minéralisation anaérobie de la matière organique) ou interviennent dans les processus d'oxydation/précipitation de ces oxydes. Il existe donc des relations majeures entre l'état d'oxydo-réduction du fer, la mobilité des contaminants, la nature du sol et les activités microbiennes (Zachara et al., 2001 ; Koopal et Avena, 1999). La connaissance des mécanismes d'oxydation et de réduction des oxydes de fer dans le sol est donc un préalable majeur à la compréhension (a) de la dynamique des éléments traces potentiellement polluants dans les sols et (b) de leur transfert vers les hydrosystèmes.

Ce travail de thèse, portant sur la biogéochimie du fer et des contaminants associés, s'est divisé en deux grands volets : la bio-oxydation et la bio-réduction. L'approche utilisée dans ce travail est une approche pluridisciplinaire, couplant géomicrobiologie, chimie et minéralogie. Cette étude s'est déroulée en couplant de l'expérimentation *in* (terrain) et *ex* (laboratoire) *situ*. Ce travail a permis d'apporter de nouveaux éclairages sur les relations existant entre l'activité des micro-organismes, la stabilité et la réactivité des oxyhydroxydes de fer et la mobilité de l'arsenic dans les sols et les eaux. Les principales conclusions concernant les deux volets de ce travail sont synthétisées ci-dessous.

La bio-oxydation

Le rôle des bactéries dans les processus d'oxydo-réduction du fer est de mieux en mieux connu (Lovley, 1991, 1997 ; Fortin et al., 1996 ; Emerson, 2000 ; Dassonville et Renault, 2002 ; Bonneville et al., 2004). Il reste néanmoins encore en partie élusif. Il a souvent été suggéré que les bactéries, du fait de la présence des groupements chimiques réactifs qui peuplent leur surface, catalysent l'oxydation du fer et la précipitation des oxydes de fer qui s'ensuit (Ferris et al., 1989). Pour tester cette hypothèse, nous avons réalisé des cinétiques d'oxydation du fer dans des conditions contrôlées de pH, de température, de concentration en oxygène et de conductivité, en présence et en absence de bactéries. Différents régimes de saturation de la surface des bactéries ont été testés. Les principaux résultats révélés par ces expériences sont :

- ✓ *Les bactéries retardent l'oxydation du Fe(II) plutôt que de la catalyser*

Les cinétiques d'oxydation abiotique du fer à un pH neutre, sont très rapides. Alors que l'oxydation des ions Fe^{2+} est inhibée en présence de bactéries soit, par adsorption des ions Fe^{2+} sur les sites de surface des membranes soit, par complexation aux molécules libérées par ces mêmes bactéries (polymères de surface ou produits de lyse des cellules). Les oxydations abiotiques sont caractérisées par un 'overshoot' important qui est dû à l'effet auto-catalytique (c.à.d. l'oxydation des ions Fe^{2+} par les oxydes de fer(III)), et qui se manifeste très peu de temps (voir Figure II.1.) après le début de la réaction d'oxydation. Les 'overshoots' sont maximums dans les systèmes abiotiques alors qu'ils diminuent en fonction de la concentration en cellules bactériennes dans les systèmes biotiques. La présence de bactéries diminue 'l'overshoot' et augmente aussi la durée de mise en équilibre du système, c.à.d. le temps nécessaire pour que les ions Fe^{2+} complexés à la surface des bactéries ou sur les polymères

qu'elles sécrètent, s'oxydent en Fe^{3+}. Dans le cas où les concentrations en cellules bactériennes sont élevées (c.à.d. nombre de sites de surface > nombre d'ion Fe^{2+}), tous les atomes de fer présents (Fe^{2+}, Fe^{3+} et oligomères de Fe(III)) sont adsorbés à la surface des bactéries ou complexés avec les molécules libérés par ces bactéries.

✓ *Les bactéries peuvent inhiber la cristallisation des oxydes de fer*

Les surfaces de bactéries, en favorisant l'adsorption des ions ferreux, retardent leur oxydation et leur précipitation. De plus, les oxydes formés sont moins cristallisés. Ces effets augmentent avec le rapport (bactéries/fer). Les cinétiques d'oxydation abiotique dans cette étude ont conduit à la formation de lépidocrocite. L'application de conditions expérimentales analogues sur les systèmes biotiques a conduit à la formation de lépidocrocite de moins en moins cristallisée en fonction de l'augmentation de la concentration en cellules bactériennes. Pour des concentrations très élevées en cellules bactériennes, les observations microscopiques et les analyses DRX ont montré qu'il n'y avait pas de formation d'oxydes de fer (Fig. II.1.1). Les atomes de fer se sont complexés sur les surfaces ou avec les molécules libérées par ces bactéries sous forme de Fe(II) ou Fe(III) monomériques ou Fe(III) polymériques.

✓ *Les bactéries ralentissent l'oxydation de Fe(II)*

L'oxydation des ions Fe^{2+} est un phénomène bien plus lent en conditions biotiques qu'en conditions abiotiques dans des conditions physico-chimiques équivalentes. De plus l'oxydation est plus rapide à pH 7,5 qu'à pH 6,5 alors que la plupart des ions sont adsorbés à la surface des cellules. Ceci suggère que (a) soit, l'oxydation a lieu rapidement dans la solution après désorption des ions de la membrane bactérienne (b) soit, les ions ferreux s'oxydent malgré leur adsorption à la surface des bactéries, ceci indique que leur oxydation dans la configuration d'ion adsorbé est dépendante du pH.

✓ *Implications pour le cycle du fer*

Le cycle du fer dépend essentiellement des réactions rédox, et des activités microbiennes (Fortin et Langley, 2005). Le fait que les bactéries puissent diminuer, voire inhiber la cristallisation des oxydes de fer, rend à la fois le fer plus mobile dans l'environnement, mais augmente aussi les surfaces spécifiques des oxydes de fer biogéniques et par conséquent favorise l'adsorption des éléments traces métalliques. Les oxydes de fer biogéniques sont donc des pièges mais aussi des sources potentielles des polluants métalliques. Par exemple l'arsenic possède une grande affinité pour les oxydes de fer amorphes et peut s'immobiliser à leurs surfaces. Cette technique est utilisée comme méthode de dépollution des eaux contaminés en arsenic (par exemple, ouest de Bengale en Asie) (Garelick et al., 2005 ; Charlet et Polya, 2006).

Notre étude a révélé, que malgré des conditions aérobiques constantes une proportion importante de fer reste adsorbée sous forme Fe(II) à la surface des cellules bactériennes. En fonction du pH, ce fer peut être libéré dans la solution. Les bactéries pourraient donc constituer un réservoir de fer non négligeable dans l'environnement.

Enfin, il est important de garder à l'esprit que le cycle du fer ne peut être interprété indépendamment de la présence non seulement des bactéries mais aussi des autres éléments. Si les oxydes de fer peuvent contribuer à la capture de divers éléments (phosphore, arsenic, métaux traces,…), ceux-ci peuvent aussi affecter les processus de précipitation du fer. Nous avons ainsi commencé une étude pour examiner conjointement l'oxydation du fer en présence à la fois de bactéries et de cadmium (cf. annexe). Celle-ci indique que si la précipitation des oxydes de fer a un impact sur la spéciation du cadmium, la réciproque peut aussi être vrai, dans la mesure où le cadmium peut favoriser la précipitation des oxydes en chassant les ions Fe^{2+} de la surface des bactéries. L'étude conjointe de systèmes complexes impliquant à la fois

des bactéries et plusieurs éléments permettra de mieux comprendre les interactions multiples qui peuvent se produire dans des environnements naturels complexes.

La bio-réduction

La bio-réduction du fer a été largement étudiée en laboratoire (Francis et Dodge, 1990 ; Zachara et al., 2001 ; Quantin et al., 2001, 2002). Les principaux paramètres influents tels que les paramètres physico-chimiques (pH, Eh, T), le nombre de cellules bactériennes, le type de matière organique donneur d'électrons et l'état de cristallisation des oxydes de fer, ont été mis en évidence. Cependant, ces expériences ont été menées dans des conditions bien contraintes de laboratoire. Il n'est pas certain que sur le terrain, où tous les paramètres jouent simultanément, et s'influencent les uns les autres, et où la solution de sol n'est pas à l'équilibre, les mêmes phases secondaires ou les mêmes rendements de dissolution puissent être obtenus. Pour pouvoir réaliser une telle étude sur le terrain, il a fallu résoudre plusieurs problèmes techniques tels que la récupération des oxydes de fer après leur insertion dans le sol naturel ou leur séparation de la matrice du sol. Pour cela, des plaquettes acryliques inertes ont été recouvertes d'oxydes de fer (ferrihydrite et lépidocrocite dopés ou non en As(V)) puis insérées directement dans les différents horizons d'un sol hydromorphe de zone humide (zone humide du bassin versant expérimental de Kervidy-Naizin, Bretagne, France). Après un temps donné de contact, les plaquettes on été analysées quantitativement et minéralogiquement afin (a) de mesurer la cinétique de dissolution réductrice des oxyhydroxydes de fer, (b) d'identifier les phases secondaires néoformées et (c) d'évaluer l'impact de la dissolution et de la reprécipitation des phases secondaires sur la mobilité de l'arsenic initialement associé aux oxyhydroxydes de fer. Les résultats majeurs se dégageant de cette étude de la bio-réduction sont résumés ci-dessous.

- ✓ *Nouvelle méthode in situ de suivi des oxydes de fer*

La technique des plaquettes acryliques recouvertes d'oxyhydroxydes de fer a montré son fort potentiel concernant l'étude qualitative et quantitative de la dissolution réductrice des oxyhydroxydes de fer et de son impact sur la mobilité des éléments traces associés. Elle a ainsi permis de : (a) déterminer des taux de dissolution dans le milieu naturel des oxyhydroxydes de fer et de l'arsenic associé, (b) d'identifier la nature des principales phases secondaires formées dans un sol naturel réduit.

- ✓ *Impact de la nature des oxydes de fer sur leur biodissolution*

La nature des oxydes de fer influent sur les processus et les vitesses de dissolution des oxydes. Il a, ainsi, été montré que la dissolution réductrice de la ferrihydrite était plus rapide que celle de la lépidocrocite. De plus, l'altération et la dissolution de la ferrihydrite se produisent en surface des agglomérats très denses formés par les nano-particules d'oxydes et se traduisent par un arrondissement global de la surface. Dans le cas de la lépidocrocite, constituée d'une 'couche' de cristaux de 0,1 µm de longueur empilés les uns sur les autres, la dissolution se traduit de deux manières : (a) les cristaux sont fortement altérés sur les côtés (Fig. III.2.5), (b) de profondes cavités colonisées par des bactéries apparaissent dans la couche de lépidocrocite (Fig. III.2.6).

- ✓ *Nature des phases secondaires*

Les phases secondaires issues des études de laboratoire portant sur la dissolution réductrice d'oxyhydroxydes de fer ont mis en evidence la présence d'amakinite, d'hydroxyde de carbonate ferreux, de magnétite, de pyrite, de rouilles vertes, de sidérite et de vivianite (Lovley et al., 1987; Lovley et Phillips 1988; Mortimer et Coleman, 1997; Fredrickson et al.,

1998; Cooper et al., 2000; Ona-Nguema et al. 2002 ; 2004 ; 2008 soumis; Zachara et al., 2002, Fredrickson et al., 2003). Cependant, dans ce travail, ce sont essentiellement des sulfures de fer plus ou moins cristallisés qui se sont formés, et ce, malgré des conditions globales de potentiel rédox non favorables (Eh ≈ 100 mV/ESH pour les Eh les plus faibles). La formation de sulfures de fer s'explique par la présence de sulfates dans la solution du sol et par un comportement hétérogène de la matrice du sol. Localement, les conditions de saturation en soufre et fer et les conditions rédox peuvent être plus favorables à leur précipitation (présence de micro-sites aux conditions rédox très contrastées). L'absence de phases secondaires de type sulfure dans les expériences de laboratoire précédemment réalisées s'explique grâce à deux éléments. Pour la plupart d'entres elles, ces expériences n'introduisaient pas de sulfates dans les solutions expérimentales. De plus, ces études ont montré que la nature des phases secondaires était contrôlée par le taux de réadsorption du Fe(II) à la surface des oxyhydroxydes de fer non encore dissous. Or, dans nos conditions expérimentales *in situ*, le Fe(II) est non seulement, en compétition avec un nombre conséquent d'anions et de cations pour l'adsorption sur les sites de surface des oxyhydroxydes mais en plus, les molécules organiques dissoutes peuvent le maintenir dans la solution par complexation.

✓ *Mécanismes bactériens de bio-réduction*

Les observations microscopiques ont montré une forte colonisation bactérienne en contact directe avec les oxydes de fer sur les plaquettes, suggérant que les micro-organismes jouent un rôle important dans les processus de réduction. La colonisation bactérienne, la présence de biofilms, l'altération de la surface des oxydes de fer et la précipitation de phases secondaires suggèrent que les processus biologiques, physiques et physico-chimiques se produisent simultanément. En début d'incubation, les oxydes de fer sont facilement accessibles aux bactéries, alors qu'en fin d'incubation, l'accessibilité des bactéries aux oxydes de fer devient difficile à cause de la présence des particules de sol. Ce dernier point est démontré par la chute de taux de dissolution (Fig. III.3.4). Par ailleurs, la nature du sol a un effet majeur sur les colonisations bactériennes qui sont plus présentes dans l'horizon organo-minéral que dans l'horizon albique.

✓ *Mobilisation de l'arsenic*

Une partie de l'arsenic associé aux deux oxyhydroxydes de fer a été réduit en As(III) comme l'ont montré les analyses XANES. Cet As(III) a été vraisemblablement réincorporé à la surface de la plaquette, très probablement par réadsorption sur l'oxyhydroxyde de fer non dissous comme le laisse penser l'épaulement obtenu sur les spectres XANES et suggérant une liaison As-O. Le processus de contrôle de la spéciation de l'arsenic semble donc être un couplage entre (a) une réaction de réduction biotique de l'As(V) (libéré dans la solution par dissolution des oxyhydroxyde) en As(III) par des bactéries réductrices de l'As et/ou du Fe et (b) une réaction de réadsorption. Le taux d'arsenic réadsorbé est plus important à la surface de ferrihydrite qu'à la surface de la lépidocrocite. La surface spécifique de la ferrihydrite est élevée, ce qui permet à l'arsenic de se réadsorber. Par contre, dans le cas de la lépidocrocite non seulement, le nombre de sites disponibles est moins important mais en plus, la dissolution des cristaux induit la destruction des sites préférentiels d'adsorption de l'arsenic qui ne peut plus se réadsorber.

✓ *Implications environnementales*

Cette étude a montré qu'en conditions naturelles les sulfures constituent la phase minérale secondaire majeure issue de la dissolution réductrice des oxyhydroxydes de fer. Or, les sulfures se comportent comme une phase puits capable de servir de réservoir temporaire ou

définitif de nombreux métaux traces comme l'As, Cd, Cr, Cu et Hg (Bostick et Fendorf, 2003, Bostick et al., 2003, Doyle et al., 2004, Borah et Senapati, 2006, Ozverdi et Erdem, 2006). Les sulfures de fer précipitent lorsque leur produit de solubilité est atteint, c'est-à-dire lorsque les concentrations en sulfures dissous (HS^-) issues de l'activité bactérienne sulfato-réductrice et celles en fer dissous ne sont plus compatibles avec le maintien de ces espèces à l'état dissous. Des sulfures particulaires de type mackinawite, greigite (FeS) apparaissent alors ; ils évoluent à terme vers d'autres sulfures de type pyrite (FeS_2). Les sulfures ainsi formés peuvent conduire à la génération de sulfures polymétalliques par substitution de sulfures de métaux moins solubles que le sulfure hôte initial. Le cadmium, par exemple, peut ainsi former des sulfures en s'échangeant avec le fer déjà précipité sous cette forme. De la même façon, le cuivre dont le sulfure est moins soluble que celui du cadmium peut, par substitution, conduire à l'apparition de sulfure de cuivre. Par ce processus, les sulfures sont des puits extrêmement actifs pour les éléments traces (Boust et al., 1999). Cependant, dans les sols hydromorphes faisant l'objet d'alternances rédox, les éléments métalliques peuvent s'adsorber aux sulfures de fer. Ces changements de conditions d'oxydo-réduction représentent donc un danger important pour l'environnement en raison de la grande solubilité des sulfates. Une partie importante des éléments traces peut donc ainsi être transférée de la solution du sol vers les hydrosystèmes.

Dans le cadre de cette étude, il a été montré que l'As(V) a été réduit en As(III), espèce beaucoup plus toxique et plus mobile. Une faible quantité de l'As(III) s'est réadsorbée sur l'oxyde de fer non encore réduit. Cependant, cette quantité d'As(III) réabsorbée est très faible au regard des concentrations initiales et on peut donc considérer que la majeure partie de l'arsenic a été libérée dans la solution sous forme d'As(III). Le processus de bio-réduction des oxydes de fer est donc un processus important de libération d'arsenic dans la solution de sol comme l'on déjà montré plusieurs auteurs à partir d'étude de laboratoire ou de suivis de terrain (McArthur et al., 2001, 2004 ; Akai et al., 2004 ; Islam et al. 2004 ; Hornemann et al., 2004). Les oxydes de fer peuvent donc être considérés comme des pièges à arsenic, on les utilise d'ailleurs comme tel en dépollution. Néanmoins, en présence de matière organique en condition anoxique ils se révèlent être des sources importante d'arsenic. C'est d'ailleurs la dissolution réductrice des oxyhydroxyde de fer riches en arsenic qui est soulignée comme étant le processus responsable de l'augmentation des teneurs en arsenic dans les eaux souterraines au Bengladesh et au Cambodge (Harvey et al., 2002). En effet, l'irrigation intensive liée au développement agricole au Bengladesh a entrainé une augmentation des teneurs en matière organique dans les eaux souterraines (Harvey et al., 2002). Dans ces eaux souterraines en présence de matière organique, les bactéries utilisent les oxyhydroxydes comme accepteur d'électrons, ceux-ci sont alors dissous et libèrent massivement leur charge en arsenic.

D'un point de vue plus général, comprendre les processus intervenant à l'interface solide-solution dans le sol (la 'critical zone' des Anglo-saxons), est un préalable indispensable à la préservation de la qualité des ressources que représentent les sols et l'eau. Cette compréhension des processus est également indispensable au développement de méthodes de dépollution-remédiation. Cette connaissance passe aussi bien, par une meilleure détermination des mécanismes et des taux de réactions biogéochimiques nécessaire aux modélisations que par, une meilleure connaissance des matériaux impliqués dans les processus. Ces dernières années, les techniques basées sur les micro-radiations synchrotron (EXAFS, XANES….), les techniques de génomique moléculaire et les sondes géophysiques ont permis de déterminer rapidement et plus précisément la composition des sols et sédiments naturels. Cependant, améliorer notre connaissance des processus biogéochimiques implique de connaitre l'interaction entre ces différents composants dans un sol 'vivant' et structuré parcouru par des flux d'éléments et d'énergie. Cette connaissance peut être partiellement atteinte par des

modèles couplant physique, chimie et biologie ou alors par des expérimentations *in situ* comme présentées dans ce travail. En effet, la technique des supports recouverts d'oxydes de fer ou d'un autre minéral peut permet d'améliorer nos connaissances quant à l'impact de la composition et du fonctionnement dynamique du sol sur la minéralogie des sols et sur les réactions biogéochimiques (nature et taux) mises en jeu. De plus, par sa capacité à isoler de la biomasse du sol des communautés spécifiques de micro-organismes, elle peut permettre de fournir des données sur leur nature et leur rôle dans les processus enclenchés.

PERSPECTIVES

V. PERSPECTIVES

Si cette étude a répondu aux objectifs fixés qui consistaient à évaluer le rôle de l'activité biologique et des réactions non métaboliques dans la dynamique du fer dans les sols, des aspects restent à explorer concernant, à la fois le volet bio-oxydation et le volet bio-réduction. Il serait, en effet, intéressant de:

- Coupler pour l'étude des mécanismes d'oxydation du fer à la surface des bactéries (a) des analyses par Spectroscopie Mössbauer afin de déterminer le degré d'oxydation et l'environnement électronique local du fer sur les parois cellulaires, (b) et des observations par Microscopie Electronique à Transmission (MET) afin de mieux visualiser la structure atomique des oxydes de fer biogéniques (intracellulaires ou extracellulaires) se formant en contact intime avec la matière organique bactérienne.
- Etudier les mécanismes et la cinétique d'oxydation du fer en milieu naturel. Bourcereau (2006) a montré que dans une chasse d'étang (Foret de Brocéliande, Bretagne, France), une quantité importante du Fe(II) rejeté dans le ruisseau sous-jacent s'oxydait en présence de bactéries (*Leptothrix*) sur des fibres nanocristallines constituées de polysaccharides (Fig. 1). Il serait intéressant de reproduire ce phénomène au laboratoire en présence de ces mêmes bactéries afin de comprendre les mécanismes de précipitation du fer.
- La technique des plaquettes recouvertes d'oxydes de fer a montré sa capacité à pouvoir isoler un consortium bactérien spécifique de la dissolution réductrice d'oxydes de Fe(III) et d'As(V). Il serait extrêmement intéressant de déterminer la nature de ces bactéries. En effet, la plupart des études de biodissolution réductrice des oxydes de fer ont été réalisées à l'aide de divers souches diverses de *Shewanella putrefaciens*. Or, ces bactéries ne sont pas des bactéries spécifiques des sols. L'étude des bactéries isolées sur les supports permettraient donc d'identifier les souches 'naturelles' du sol capables de réaliser non seulement, la bio-réduction du fer mais également, de mettre en évidence les associations bactériennes nécessaires à ce mécanisme. Les techniques de génomique à haut débit, ainsi que les puces à ADN pourraient fournir à ce titre des outils précieux. On pourrait imaginer une étude en deux temps avec une première étape consistant à localiser dans des échantillons in vitro, les micro-organismes responsables d'une activité métabolique particulière par des techniques basées sur l'hybridation des ARN. Dans un deuxième temps, les bactéries ainsi identifiées pourraient être d'autant plus facilement quantifiées et associées avec des minéraux marqueurs dans le milieu naturel qu'elles seraient associées à eux sur les plaquettes. Deux types de cibles ribonucléiques pourraient être envisagées pour le marquage : des ARN ribosomaux 16S ou des ARN messagers (codant pour une protéine directement impliquée dans la réduction du Fe(III) ou de l'As(V).
- Caractériser finement la minéralogie des phases secondaires formées :
  - par EXAFS, ce qui permettrait de déterminer le voisinage atomique du fer et de l'arsenic (-Fe-As, -S-As, -O-As) afin de savoir si l'arsenic est en priorité réabsorbé sur les oxydes de Fe ou lié au sulfures.
  - Par NanoSIMS, ce qui permettrait de réaliser une cartographie chimique fine des éléments à la surface des supports acryliques.

Le couplage NanoSIMS, EXAFS et XANES pourrait ainsi clarifier la nature des liaisons ainsi que les mécanismes impliqués dans la dissolution des oxydes et la formation des phases minérales secondaires.

- Appliquer cette méthodologie à d'autres minéraux riches en Fe(II) comme la magnétite, en les insérant, dans un premier temps, dans un sol réduit en colonnes de sol au laboratoire, ensuite en les réoxydant en aérobie, afin d'étudier la cinétique d'oxydation et ses conséquences (vitesses, quantités formées…). On pourrait également imaginer des études

d’alternances expérimentales d’oxydation et de réduction afin d’évaluer l’efficacité des processusopérants.

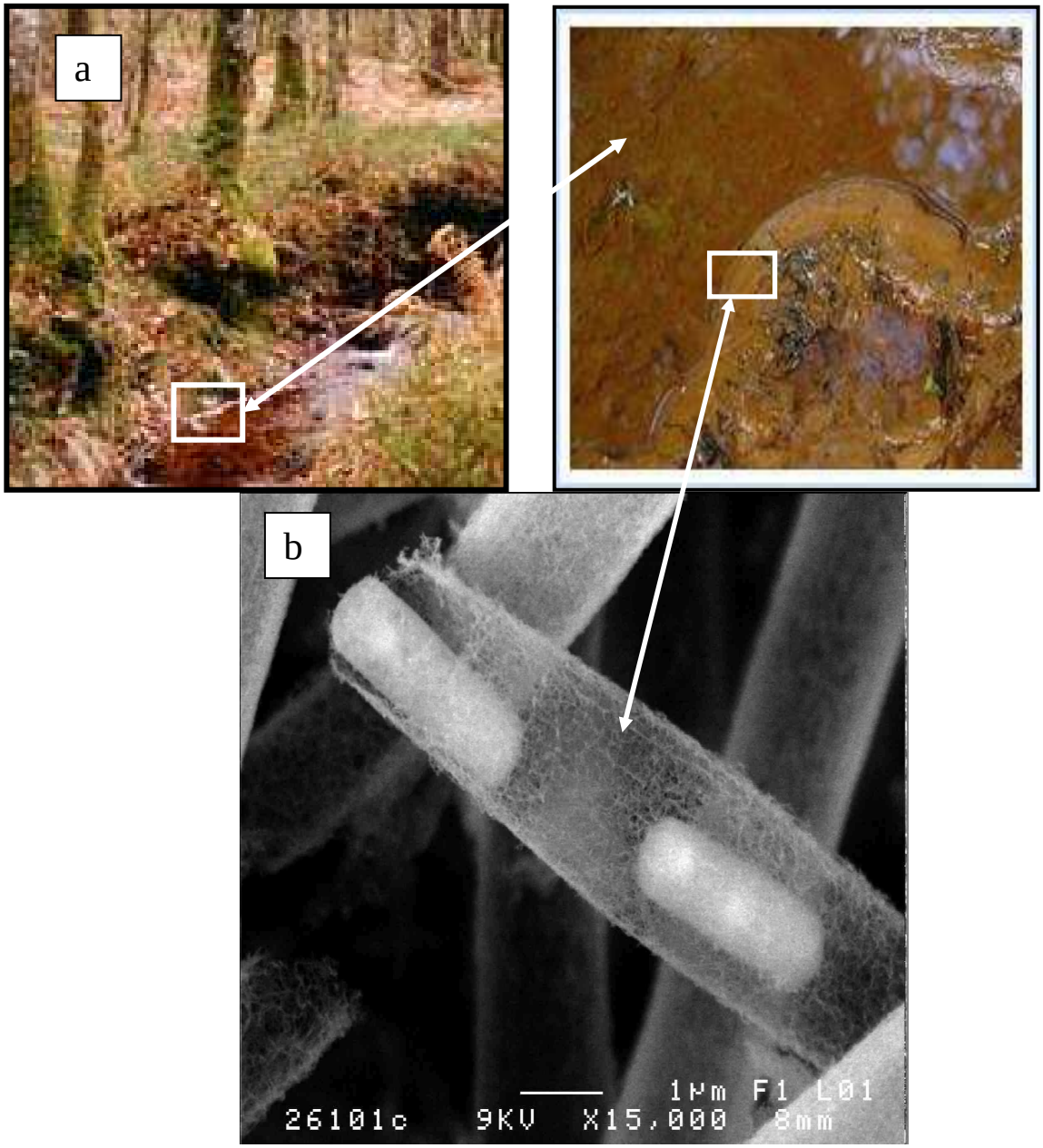

Fig. 1. a) Ruisseau du ‘Val sans retour’ dans la forêt de Brocéliande (Bretagne), très coloré, riche en oxydes de fer, montrant dans le détail de la photo, la présence de ces oxydes précipités sur les biofilms. b) Structure type de *Leptothrix* sur un échantillon de ce biofilm. La photo permet de visualiser la finesse des constructions nanocristallines de polysaccharides effectuées par les bactéries composant le biofilm responsable de l’immobilisation du fer.

TRAVAUX ANNEXES

A.1. Rôle de l'oxydation de Fe(II) dans la séquestration du cadmium par les surfaces bactériennes.

Xavier Châtellier
Mohamad Fakih
Christopher J. Daughney

Cette partie correspond à un article soumis à la revue Geochimica et Cosmochimica Acta, 'How the sorption and oxidation/hydrolysis of Fe(II) affects cadmium immobilization by *Anoxybacillus flavithermus* surfaces', (Août 2008)

RÉSUMÉ

Les isothermes d'adsorption du Cd ont été mesurées pour des cellules d'*Anoxybacillus flavithermus* exposées à des quantités croissantes de cations ferreux (Fe^{2+}) dans des suspension sous différents degrés d'oxydation. Les suspensions Cd-Fe-bactéries ont également été examinées par Microscopie Electronique à Balayage (MEB). La précipitation d'oxydes de fer a été ralentie dans des conditions de rapports (Fe/bactéries) faibles. L'adsorption de Cd a également été considérablement réduite. Les précipités d'oxydes de fer ont été formés sous des rapports (Fe/bactéries) élevés. L'adsorption de Cd a été également significativement réduite au début de l'oxydation quand le fer était partiellement oxydé. , Mais, à des stades plus avancés dans le processus d'oxydation et d'hydrolyse du fer, la capacité d'adsorption de Cd de la suspension a été en partie retrouvée. Nos résultats indiquent que les cations Fe^{2+} et Cd^{2+} sont en concurrence avec des affinités comparables pour les sites réactifs sur la paroi cellulaire bactérienne. Le rapport (Fe/bactéries), ainsi que la spéciation du fer jouent un rôle important sur l'adsorption de Cd sur la suspension fer-bactéries. On note également qu'alors que l'adsorption et l'oxydation/hydrolyse du fer affecte l'adsorption du Cd, l'inverse est également vrai, puisqu'il est observé que l'adsorption du Cd favorise la précipitation des particules d'oxydes de fer.

ABSTRACT

Cd^{2+} sorption isotherms were measured for *Anoxybacillus flavithermus* cells exposed to increasing doses of Fe^{2+} cations under different degrees of oxidation of the suspensions. The Cd-Fe-bacteria suspensions were also examined by Scanning Electron Microscopy. At low Fe/bacteria ratios, Fe-oxide precipitation was hindered and Cd sorption was significantly reduced. At high Fe/bacteria ratios, Fe-oxide precipitates were formed. In partly oxidized suspensions, Cd sorption was also significantly reduced, but at more advanced stages of the Fe oxidation/hydrolysis process, the Cd sorption capacity of the composite suspensions was partly recovered. Our results indicate that Fe^{2+} and Cd^{2+} cations compete with comparable affinities for the reactive sites on the bacterial cell walls and that the Fe/bacteria ratios as well as the Fe speciation are important controls on Cd sorption onto iron-bacteria composite suspensions. Interestingly, whereas Fe sorption and oxidation/hydrolysis affects Cd sorption, the opposite is also true, as Cd sorption was observed to promote the precipitation of Fe-oxide particles.

1.1. INTRODUCTION

Many studies have focused on the adsorption of metal cations by bacteria (e.g. Beveridge and Murray, 1980; Beveridge, 1989; Fein et al., 1997; Daughney et al., 2001; Borrok et al., 2004; Châtellier and Fortin, 2004; Daughney and Fortin, 2006) or by iron oxides (e.g. Dzombak and Morel, 1990; Venema et al., 1996; Hiemstra and van Riemsdijk, 1999; Buerge-Weirich et al., 2002). The adsorption of metals by both bacterial surfaces and iron oxides is dependent on pH and metal-to-sorbent concentration ratio, and may also be affected by ionic strength and the presence of competing sorbates. Many models have been developed to describe metal-bacteria and metal-iron oxide adsorption, often based on isotherms or surface complexation theory. The interest in developing quantitative model for these processes relates

to observed relationships between metal adsorption and metal transport, reactivity and toxicity (Langmuir, 1997).

Fewer studies have investigated metal partitioning in systems containing both bacteria and iron oxides. Small et al. (1999) performed a laboratory study and reported that *Shewanella alga* adsorbed more strontium than hydrous ferric oxide under the experimental conditions employed. In the iron-bacteria composite systems, there was an observable decrease in adsorption, in comparison with the pure bacterial systems, because the iron oxides were inferred to mask the bacterial surface binding sites. Kulczycki et al. (2005) observed similar behavior for the adsorption of cadmium and lead by composites of *Bacillus subtilis* or *Escherichia coli* and ferrihydrite. In contrast, a laboratory study performed using EXAFS spectroscopy indicated that the sorption of lead by composites of *Burkholderia cepacia* and goethite was dominated by the iron oxide at pH > 6 and that ternary complexes involving both phases were significant at low pH (Templeton et al., 2003). A few field studies have assessed metal ion binding by "biogenic" iron oxides formed by oxidation of Fe(II) in the presence of bacteria, and suggested that metal adsorption is governed by the bacterial component under the ambient conditions at the field site (Ferris et al. 1999, 2000; Martinez et al., 2004).

The aim of this investigation is to assess relationships between metal adsorption and 1) the ratio of total iron to biomass concentration and 2) the extent of the oxidation and hydrolysis of the Fe(II). Fe(II) is known to adsorb to bacterial binding sites (Châtellier and Fortin, 2004; Roden and Urrutia, 2002; Urrutia and Roden, 1998), and so we hypothesize that its presence will reduce the adsorption of other metal cations through competitive effects (e.g. Cotoras et al., 1992; Fowle and Fein, 1999). We also hypothesize that when iron oxides form, metal adsorption will decrease relative to iron-free controls, as observed in previous laboratory and field studies (Ferris et al. 1999, 2000; Small et al., 2001; Martinez et al., 2004). Overall then, the incremental oxidation, hydrolysis and precipitation of iron in the presence of bacteria might have a significant and previously unrecognized effect on the behavior of dissolved metals. To our knowledge, no previous studies have been designed to specifically assess relationships between metal adsorption and the ratio of soluble Fe(II) to iron oxide or the ratio of total iron to bacterial concentration.

The experiments conducted in this investigation are designed to mimic natural conditions where dissolved Fe(II) is diffusing from an anoxic environment into an oxic bacteria-bearing setting, leading to progressive oxidation of the iron while the oxygen concentration, conductivity and pH are essentially constant over time. The experiments are conducted using established protocols and previously studied reactants, in order to facilitate interpretation of results. Cadmium was selected as the sorbate because it is a common heavy metal contaminant, and because several previous studies have assessed its adsorption by bacteria (Fein et al., 1997; Daughney and Fein, 1998; Fowle and Fein, 1999; Daughney et al., 2001; Boyanov et al., 2003; Borrok et al., 2004) or iron oxides (Dzombak and Morel, 1990; Cowan et al., 1991; Ainsworth et al., 1994; Hiemstra and van Riemsdijk, 1999; Buerge-Weirich et al., 2002; Martinez et al., 2004). The experiments were performed using *Anoxybacillus flavithermus*, a thermophilic bacterium isolated from the main wastewater drain at the Wairakei Geothermal Power Station (North Island, New Zealand), because its surface characteristics and cadmium binding capacity have been recently described (Burnett et al., 2006a, b). Iron oxides and iron-bacteria composites were synthesized using a protocol developed by Châtellier et al. (Châtellier et al. 2001, 2004; Fakih et al., 2008a) (Section II.1.2.1), to ensure comparability with previously published results, and so that the immobilization of Cd could be measured while the iron oxidation/hydrolysis process was still taking place. Throughout this paper, we use the term "iron oxide" generically, without inference to mineralogy, crystallinity, particle size, or other properties (see Cornell and Schwertmann, 1996). We also use the term "iron-bacteria composite" to describe any mixture

of iron and bacteria, in order to avoid *a priori* assumptions about whether the iron is soluble or adsorbed, reduced or oxidized, monomeric or precipitated as iron oxide, or whether the iron oxide, if present, is coating cell surfaces or if it is not associated with the bacteria at all.

1.2. METHODS

1.2.1. Preparation of bacterial suspensions

Sixteen independent suspensions of *A. flavithermus* were prepared using a previously established protocol (Burnett et al., 2006a). The bacteria were pre-cultured in 5-mL volumes of autoclaved (121 °C, 20 min) trypticase soy broth (Becton Dickonson, USA). After growing for 24 ± 0.1 h at 60 °C, two 1-L volumes of autoclaved broth were inoculated, each with two 5-mL pre-cultures, and these were placed in an orbital mixer incubator (60 °C, 100 rpm) for an additional 24 ± 0.1 h. The two cultures were harvested in late stationary phase by centrifugation (6000*g*, 15 min), rinsed five times in 0.01 M $NaNO_3$ (the electrolyte used during the Cd adsorption experiments, in accordance with Burnett et al., 2006a), and mixed together. After each step in the rinse procedure, the bacteria were recovered by centrifugation and the supernatant was discarded. The bacteria were prepared with this growth protocol to ensure that the cells would be intact but not growing or dividing, with other characteristics as previously reported by Burnett et al. (2006a) (Table A.1). Finally, the cells were resuspended in 120 ml of 0.01 M NaCl (the electrolyte used during synthesis of the iron oxides, in accordance with Châtellier et al. 2001, 2004 and Fakih et al., 2008a, section II.1.2.1), and the biomass concentration was quantified by measurement of optical density at 600 nm. Three of the 16 cell suspensions (120 ml) were used to investigate Cd adsorption by the bacteria in the absence of added iron, whereas the remaining 13 cell suspensions were used in the synthesis of the iron-bacteria composite suspensions as summarized in Table A.2 and described in detail below.

Table A.1. Characteristics of *A. flavithermus* cells (after Burnett et al., 2006a).

Parameter	**Mean ± 2σ**
Cell length (μm)	3.89 ± 1.45
Cell Width (μm)	0.54 ± 0.18
Cell wall thickness (nm)	28.1 ± 7.4
Surface area (m^2 wet g^{-1}) (assuming cylindrical geometry)	7.9 ± 1.4
Ratio of dry biomass concentration (g L^{-1}) to optical density (600 nm)	0.5359
Ratio of wet to dry biomass concentration	6.7 ± 0.1
Cell wall functional group concentration ($\times 10^{-4}$ mol per dry g)	8.54 ± 2.0

Table A.2. Experimental conditions corresponding to each Cd sorption isotherm. n is the number of data points obtained for each experiment. In the columns indicating the total Cd concentration and the name of the suspension, the "*" indicates that the suspension was spiked with Cd using a solution neutralized at pH 5.5. In the columns indicating the name of the suspension, the sign "SEM" points at the two samples, which were exposed to Cd and then observed by Scanning Electron Microscopy. All suspensions were aged for 12 ± 5 h after the end of the addition of the $FeCl_2$ solution, except "fresh" suspensions. All suspensions were washed except "fresh", "not washed", and Fe-AF 10 suspensions.

Name of suspension	Synthesis, Iron-Bacteria Composites				Cd Adsorption Isotherms			
	pH	[AF] dry $g.L^{-1}$	$FeCl_2$ ml	ρ mg/dry g	[AF] dry $g.L^{-1}$	[Fe] $mg.L^{-1}$	[Cd] $mg.L^{-1}$	N
Blank 1	N/A	0	0	N/A	0.0	0.0	5	11
Blank 2*	N/A	0	0	N/A	0.0	0.0	5*	12
Blank 3*	N/A	0	0	N/A	0.0	0.0	5*	4
Blank 4*	N/A	0	0	N/A	0.0	0.0	1.5*	5
Blank 5*	N/A	0	0	N/A	0.0	0.0	5*	5
Blank 6*	N/A	0	0	N/A	0.0	0.0	1.5*	5
Blank 7*	N/A	0	0	N/A	0.0	0.0	5*	5
Blank 8*	N/A	0	0	N/A	0.0	0.0	1.5*	6
Blank 9*	N/A	0	0	N/A	0.0	0.0	5*	6
Fe 1	6	0	20	N/A	0.0	232	1	10
Fe 2	6.5	0	20	N/A	0.0	232	1	10
Fe 3	7	0	20	N/A	0.0	232	1	10
AF 1*	N/A	N/A	0	N/A	0.1	0.0	5*	12
AF 1*	N/A	N/A	0	N/A	0.4	0.0	5*	10
AF 1*	N/A	N/A	0	N/A	1.0	0.0	5*	12
AF 2*	N/A	N/A	0	N/A	0.1	0.0	5*	13
AF 2*	N/A	N/A	0	N/A	0.4	0.0	5*	13
AF 3*	N/A	N/A	0	N/A	1.0	0.0	5*	13
Fe-AF 0 (Blank)	6	0.36	20	62	0.4	25	0	12
Fe-AF 0 (Blank)	6	0.36	20	62	0.1	6.2	0	12
Fe-AF 1 (t=0)	6	0.36	20	62	0.4	25	5	6
Fe-AF 1 (t=10mn)	6	0.36	20	62	0.4	25	5	6
Fe-AF 1 (t=30mn)	6	0.36	20	62	0.4	25	5	6
Fe-AF 1 (t=1h)	6	0.36	20	62	0.4	25	5	6
Fe-AF 1 (t=3h)	6	0.36	20	62	0.4	25	5	6
Fe-AF 1 (t=6h)	6	0.36	20	62	0.4	25	5	5
Fe-AF 2	6	0.36	20	62	1.0	62	5	10
Fe-AF 2	6	0.36	20	62	0.4	25	5	10

Fe-AF 2	6	0.36	20	62	0.1	6.2	5	10
Fe-AF 2	6	0.36	20	62	0.03	1.9	5	10
Fe-AF 3	6	0.36	20	62	3.0	186	5	4
Fe-AF 3	6	0.36	20	62	1.0	62	5	10
Fe-AF 3	6	0.36	20	62	0.4	25	5	10
Fe-AF 3	6	0.36	20	62	0.1	6.2	5	10
Fe-AF 4*	6	0.36	20	62	1.0	62	5*	12
Fe-AF 4*	6	0.36	20	62	0.4	25	5*	12
Fe-AF 4	6	0.36	20	62	0.4	25	5	6
Fe-AF 4*	6	0.36	20	62	0.1	6.2	5*	12
Fe-AF 5	6	0.36	5	16	0.4	6.2	5	6
Fe-AF 5	6	0.36	5	16	0.1	1.6	5	6
Fe-AF 6 (SEM)	6	0.36	5	16	3.0	47	5	1
Fe-AF 6	6	0.36	5	16	0.4	6.2	5	12
Fe-AF 6	6	0.36	5	16	0.1	1.6	5	12
Fe-AF 7	6	0.36	5	16	3.0	47	5	4
Fe-AF 7	6	0.36	5	16	0.4	6.2	5	10
Fe-AF 7*	6	0.36	5	16	1.0	16	5*	12
Fe-AF 7*	6	0.36	5	16	0.4	6.2	5*	12
Fe-AF 7*	6	0.36	5	16	0.1	1.6	5*	11
Fe-AF 8*	6	0.36	10	31	1.0	31	5*	13
Fe-AF 8*	6	0.36	10	31	0.4	12	5*	13
Fe-AF 8*	6	0.36	10	31	0.1	3.1	5*	13
Fe-AF 9*	6	0.36	40	124	3.0	372	5*	6
Fe-AF 9*	6	0.36	40	124	1.0	124	5*	8
Fe-AF 9*	6	0.36	40	124	0.4	50	5*	13
Fe-AF 9*	6	0.36	40	124	0.1	12	5*	13
Fe-AF 10* (SEM)	6	0.36	5	16	0.36	5.6	5*	1
Fe-AF 11* (fresh)	6	0.44	10	25	0.4	10	5*	13
Fe-AF 11* (not washed)	6	0.44	10	25	0.4	10	5*	13
Fe-AF 11*	6	0.44	10	25	0.4	10	5*	13
Fe-AF 11*	6	0.44	10	25	1.0	25	5*	13
Fe-AF 11*	6	0.44	10	25	0.1	2.5	5*	13
Fe-AF 12* (fresh)	6	0.44	20	0 to 82	0.4	20	5*	2*

Fe-AF 12* (not washed)	6	0.44	20	82	0.4	20	5*	21 2
Fe-AF 12*	6	0.44	20	82	1.0	51	5*	12
Fe-AF 12*	6	0.44	20	82	0.4	20	5*	12
Fe-AF 12*	6	0.44	20	82	0.1	5.1	5*	12

1.2.2. Preparation of iron-bacteria composite suspensions

Altogether, 16 different suspensions were prepared (13 biotic experiments including bacteria, 3 abiotic experiments in the absence of bacteria). The first ten separate iron-bacteria composite suspensions are denoted in Table A.2 as Fe-AF 0 to Fe-AF 9. Each of these suspensions was prepared by starting with 500 ml of 0.01 M NaCl containing cells from two independently grown 1-L cultures of *A. flavithermus* (0.36 dry $g.L^{-1}$), as explained in section A.1.2.1. In each case, the cell suspension was adjusted to pH 6 using 0.1 M NaOH and then stirred continuously while a known total volume (5, 10, 20 or 40 ml) of $FeCl_2$ solution ($[Fe(II)] = 1.25 \times 10^{-2}$ M, $[HCl] = 2.50 \times 10^{-3}$ M) was added at a constant rate (0.05 ml/min, Metrohm model 776 automatic burette, Switzerland). During the addition of the $FeCl_2$ solution, the pH of the suspension was held constant at pH 6 via addition of 0.1 M NaOH controlled with a pH-stat autotitrator (Metrohm 736 GP Titrino, Switzerland). A high concentration of dissolved oxygen was maintained due to the slow rate of addition of the Fe(II) and by stirring the suspension, which remained in contact with the atmosphere. In addition to the ten iron-bacteria composite suspensions, three abiotic suspensions were prepared using the same protocol, denoted in Table A.2 as Fe 1 to Fe 3. These abiotic suspensions were prepared by starting with 500 ml of 0.01 M NaCl (without bacteria), to which 20 ml of $FeCl_2$ solution was slowly added at a constant rate of 0.05 ml/min while the pH was fixed at 6, 6.5, or 7 (Table A.2).

The solids (iron oxides or bacteria with associated iron and/or iron oxides) were harvested by centrifugation (6000*g*, 15 min) 12 ± 5 h after the end of the addition of the $FeCl_2$ solution. This time frame was selected based on practical considerations and on the measurements of pH and redox potential over time, which indicated that the oxidation and hydrolysis of the introduced iron could continue for several hours after the end of the addition of the $FeCl_2$ solution. The solids were then rinsed five times in 0.01 M $NaNO_3$ (the electrolyte used during the Cd adsorption experiments). After each step in the rinse procedure, the solids were pelleted by centrifugation and the supernatant was discarded. The iron-bacteria composites and the abiotic iron oxides were synthesized using this protocol in order to permit assessment of the degree of saturation of the bacterial surfaces with respect to introduced Fe(II).

Three additional iron-bacteria composite suspensions were prepared using variations of the protocol described above, in order to address certain research questions. In experiment Fe-AF 10 (volume of $FeCl_2$ added equal to 5 ml), the bacterial suspension was initially spiked with 5 $mg.L^{-1}$ of Cd (Cd Atomic Absorption standard solution, 1000 ppm Cd as $Cd(NO_3)_2$ in 0.5 M HNO_3, Merck, Germany) prior to the addition of any $FeCl_2$. In this experiment Cd was added to the background electrolyte in order to assess the effect of its presence during iron addition on the capacity of the iron-bacteria composites to adsorb Cd. In experiment Fe-AF 11 (volume of $FeCl_2$ added equal to 10 ml, bacterial concentration equal to 0.44 $g.L^{-1}$), the solids from 60 mL of the suspension were collected immediately following completion of the addition of the $FeCl_2$ solution. 17 h later, another 60 mL of the suspension was collected

again. These two samples were used immediately after collection and without any further treatment for Cd isotherm experiments at a bacterial concentration of 0.4 $g.L^{-1}$ (see Section A.1.2.4). The remainder of the solids from this synthesis were collected and rinsed as described above. Experiment Fe-AF 11 was thus designed to permit comparison of Cd adsorption by the "fresh" and "aged" iron-bacteria composites, as well as to evaluate the effect of the washing procedure on the Cd adsorption of the "aged" iron-bacteria composites. Finally, for experiment Fe-AF 12 (volume of $FeCl_2$ added equal to 20 ml, bacterial concentration equal to 0.44 $g.L^{-1}$), two 5-ml subsamples of the suspension were collected every 20 min for a total of 7 h, and used to assess the effects of the introduction, adsorption, precipitation and aging of the iron on Cd adsorption by the iron-bacteria composites at a bacterial concentration of 0.40 $g.L^{-1}$ (see Section A.1.2.4). 17 hours after the end of the addition of the $FeCl_2$ solution, the remainder of the solids were collected and rinsed as described above.

In this paper, we denote the Fe/bacteria ratio by the symbol ρ. The values of ρ investigated here range from 0 to 124 mg of Fe per dry g of bacteria (Table A.2).

1.2.3. Scanning Electron Microscopy

Seven selected samples of iron-bacteria composites, abiotic iron oxides and *A. flavithermus* cells (without added iron) were collected in microtubes, centrifuged, and washed five times in acetone (10 000 g, 10 min, 5°C), and then dried at the critical point (Balzers Instruments, CPD010, Liechtenstein). The samples were observed by SEM without metallization, using a JEOL JSM-6301F Field Emission Gun Scanning Electron Microscope operated at 9kV.

1.2.4. Cadmium adsorption measurements

Fifty-one Cd pH-adsorption isotherm experiments were performed using the solids from the various syntheses and at different cadmium-to-solid concentration ratios (0.01 M $NaNO_3$ was used as the diluent), following the method of Burnett et al. (2006b) (Table A.2, n>2). Each isotherm experiment involved solids from either one iron-bacteria synthesis (i.e. bacteria and associated iron and/or iron oxides present simultaneously), one abiotic synthesis (iron oxides only), or one suspension of pure bacteria (no added iron). In general, the solids were resuspended in 0.01 M $NaNO_3$ at a known concentration, and the suspension was spiked with a Cd Atomic Absorption standard solution (1000 ppm Cd as $Cd(NO_3)_2$ in 0.5 M HNO_3, Merck, Germany) to yield a final Cd concentration of 1.0 $mg.L^{-1}$ (the three abiotic iron oxides suspensions) or 5.0 $mg.L^{-1}$ (all other suspensions). Nine blank adsorption isotherm experiments, involving no solids at all, were also performed at Cd concentrations of 1.5 and 5.0 $mg.L^{-1}$. For some experiments, the Cd standard was first diluted to 55 $mg.L^{-1}$ and then adjusted to pH 5.5 ± 0.2 prior to addition to the suspension, in order to avoid possible alteration of the solids that might have resulted from the standard's acidity. Aliquots (5 ml) of the different suspensions were then transferred into polypropylene test tubes, and the pH of the suspension each test tube was adjusted to a different value (pH 3-8) using known amounts (<0.2 ml) of 0.01, 0.05 or 0.1 M NaOH or HNO_3. The test tubes were shaken for 1 h, except in the case of a preliminary kinetic experiment where the time of equilibration was varied. All Cd adsorption experiments were performed at 25 °C to ensure comparability with previously published results (e.g. Burnett et al., 2006a, b). Samples were then centrifuged (6000*g*, 15 min) and 3 ml of the supernatant was extracted, acidified and analysed for dissolved Cd by

flame atomic absorption spectrophotometry (FAAS) (Perkin-Elmer AAnalyst 800, Rodgau-Jügesheim, Germany) or for dissolved Cd and Fe by inductively coupled plasma optical emission spectroscopy (ICP-OES) (Thermo Electron Iris Intrepid II XDL, USA). The remaining 2 ml of each sample's supernatant were used for the measurement of the final equilibrium pH.

A slightly different procedure was used for the unwashed 60 ml aliquots sampled in experiment Fe-AF 11, which were split into 12 5-ml subsamples. For this experiment, the 5-ml subsamples of the iron-bacteria suspension that were used for the determination of the Cd adsorption isotherm were not rinsed, and hence the experiment was conducted with a background electrolyte of 0.01 M NaCl instead of 0.01 M $NaNO_3$. Each 5-ml subsample was spiked directly with Cd standard (pH ca. 5.5) to yield a total Cd concentration of 5 $mg.L^{-1}$ and a bacterial concentration of 0.40 $g.L^{-1}$. Various amounts of acid or base were added to the different 5-ml subsamples, as described above, to generate a Cd adsorption isotherm over the range $3 < pH < 8$. All samples were equilibrated for 1 h and then analyzed for final Cd concentration as described above.

In addition to the 51 adsorption isotherms, three additional Cd adsorption experiments were conducted using variations to the experimental protocol described above. First, Cd sorption was measured at a single pH (n=1) in experiment Fe-AF 6 at a bacterial concentration of 3 $g.L^{-1}$ (sample used for SEM, see Table A.2, final pH = 7.6). Second, in experiment Fe-AF 10, where Cd had been added prior to the Fe (see section A.1.2.2. and Table A.2, final pH = 6.0), Cd sorption was assessed in the supernatant at the end of the synthesis. Third, in experiment Fe-AF 12, two 5-ml subsamples of the iron-bacteria suspension were collected every 20 min (i.e. after addition of each ml of the $FeCl_2$ solution) for a total of 7 h, and once at the end of the synthesis, 17 hours after the end of the addition of the $FeCl_2$ solution. A small amount of 0.01 M NaOH (85 ± 15 µl) was added to one of the two subsamples collected at each time interval, in order to slightly increase its final pH, whereas the pH of the other subsample was not adjusted. Cd sorption was measured at the two pH values (n=2) as in experiment Fe-AF 11.

1.3. RESULTS AND DISCUSSION

1.3.1. Scanning Electron Microscopy

Figure A.1 displays characteristic SEM micrographs of the iron-bacteria composite suspensions. A micrograph of suspension AF 3, composed of *A. flavithermus* cells in the absence of any added Fe, is shown on Figure A.1a. The length and width of the cells appeared to be identical to the previous observations made by Burnett et al. (2006a), as given in Table A.1. The cells also appeared as devoid of any precipitates. They were partially translucent, as the electrons could penetrate the cells in the absence of a metallic coating. The cells of suspension Fe-AF 5, which was prepared with only $\rho = 16$ mg of Fe per dry g of bacteria, looked similar to those of the pure bacterial suspension AF 3. Notably, no precipitates were observed, but the cells were more opaque. In this sample, the introduced Fe was likely adsorbed at the surface of the cells as Fe^{2+} or Fe^{3+} monomers or oligomers. The Fe coating on the cell surfaces possibly contributed to their increased opacity. As ρ was increased to 25 mg/g (suspension Fe-AF 11), iron oxide precipitates became visible as scattered clumps of aggregated particles, which were most often in close association with the cells (Fig. A.1c).

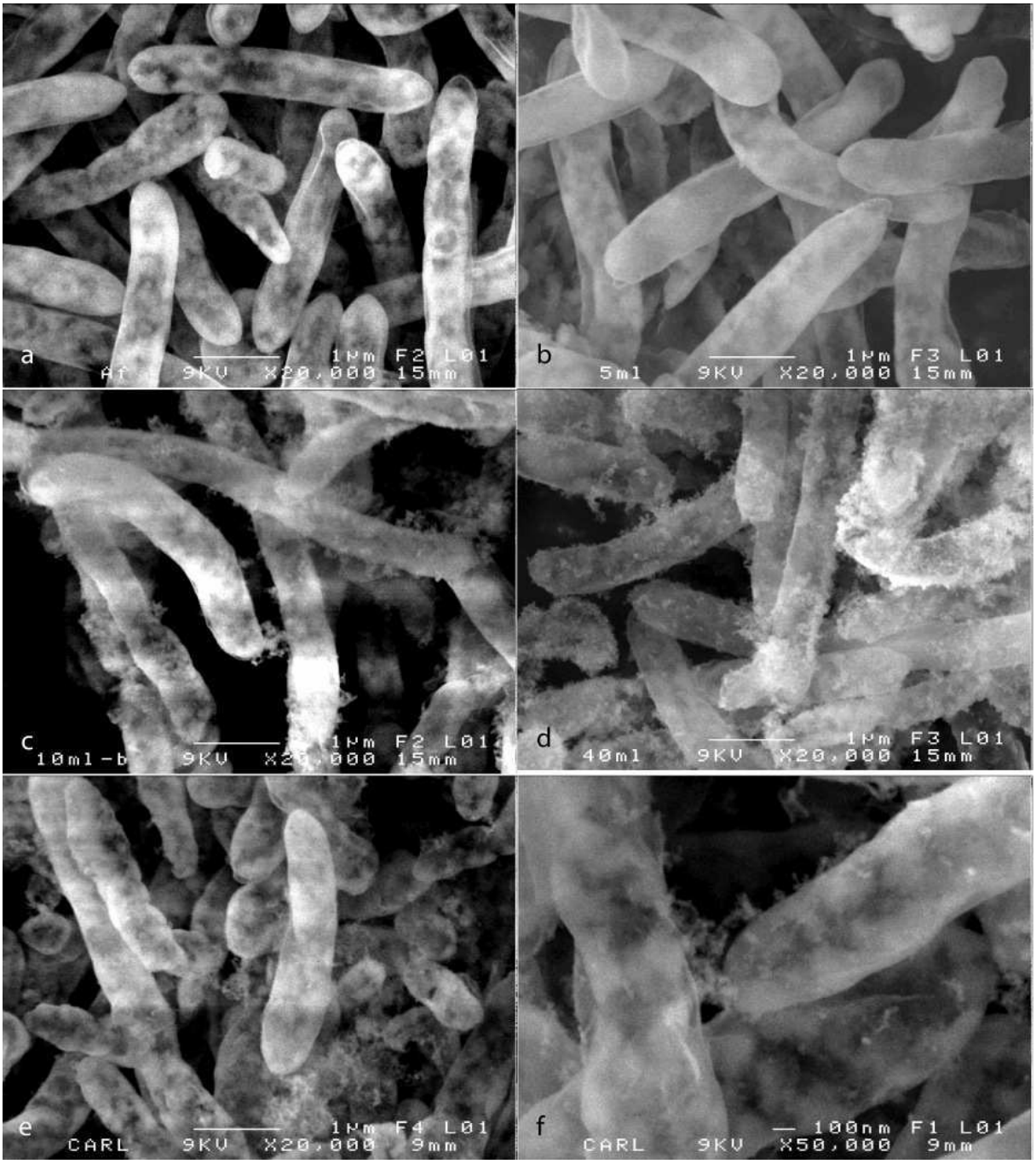

Figure A.1. SEM micrographs of suspensions AF-3 (a: no Fe), Fe-AF 5 (b: ρ = 16 mg/g), Fe-AF 11 (c: ρ = 25 mg/g), Fe-AF 9 (d: ρ = 124 mg/g), and Fe-AF 12 (e and f: ρ = 16 mg/g + 5 ppm Cd).

Under SEM observation, suspension Fe-AF 8 (ρ = 31 mg/g) looked similar to suspension Fe-AF 11 (micrographs not shown). For suspension Fe-AF 9 (ρ = 124 mg/g), the amount of iron oxide precipitates was noticeably larger (Fig. A.1d). The saturation of the cell surfaces was thus reached for a value of ρ between 16 and 25 mg of Fe per dry g of bacteria. For comparison, Fakih et al. (2008a) (Section II.1) reported that *Bacillus subtilis* cells were able to adsorb Fe^{2+} and inhibit the precipitation of iron oxide particles up to a value of ρ comprised between 21 and 80 mg of Fe per g of bacteria, which is similar to the range found here for *A. flavithermus* cells.

Two composite iron-bacteria suspensions were also observed by SEM after they had been exposed to Cd. In the first case, suspension Fe-AF 6 (ρ = 16 mg/g) was first synthesized and then spiked with 5 ppm Cd, at a bacterial concentration of 3 $g.L^{-1}$ (see Table A.2). After a one hour equilibration period, the suspension was sampled for SEM analysis. The bacterial cells were devoid of precipitates (micrographs not shown) and similar to those of suspension Fe-AF 5, where the Fe/bacteria ratio was identical. In this case, the presence of Cd did not lead to any apparent change in the amount of precipitated iron oxide. In the second case, suspension Fe-AF 10 (ρ = 16 mg/g) was first spiked with Cd at 5 ppm, and then exposed to Fe^{2+} cations, while the bacterial concentration was equal to 0.36 $g.L^{-1}$. In this second case, as can be seen on Figures A.1e and A.1f, some iron-oxide precipitates could be observed in the vicinity of the bacterial cells. The difference probably arises because although both cases correspond to the same Fe/bacteria ratio (ρ = 16 mg/g), in the second case there was much less bacteria relative to Cd, which could lead to a saturation of the cell surfaces with respect to Fe at an earlier ρ value.

1.3.2. Cd adsorption isotherms

1.3.2.1. Blanks

Blank experiments conducted without bacteria or iron oxide revealed an average Cd loss of 3 ± 3 % over the pH range 3 to 7 (number of Cd measurements n = 59). Blank experiments conducted with iron-bacteria composites but without added Cd did not show any release of Cd to solution (suspension Fe-AF 0, n = 24). For both types of blank experiment, there was no significant relationship between pH and amount of Cd detected in solution. We thus conclude that Cd loss and release in the blanks are negligible, and changes in Cd concentrations observed in other experiments can be interpreted in terms of adsorption by the bacteria and/or iron oxide.

1.3.2.2. Cd adsorption by abiotic iron oxides

Cd adsorption by the abiotic iron oxide was negligible below pH ca. 6.5 but increased sharply to 100% Cd loss by pH 7.5 (Fig. A.2). Similar results were obtained in each of the three abiotic isotherm experiments, with no systematic difference in Cd adsorption related to the pH of synthesis of the iron oxide. The pH at which the 100% loss of Cd was reached corresponds to the saturation limit of $CdCO_3$.

It is instructive to compare the data to a model prediction for Cd adsorption by iron oxides (Dzombak and Morel, 1990). The model prediction is in reasonable agreement with our data, indicating that little adsorption should occur below pH 6, with the adsorption reaching 100% by pH 7-7.5. The model over-predicts Cd adsorption slightly, possibly because the iron oxide synthesized in this investigation might not have quite as high a surface area and/or surface site density as assumed by Dzombak and Morel (1990). Alternatively, the complexation constants of the reactive sites of our nano-particulate iron oxides might be a bit different from those corresponding to larger particles. Nevertheless, the model prediction of Dzombak and Morel (1990) and the $CdCO_3$ saturation limit can be used to define an envelope, in the pH range 6-7, in which Cd adsorption by iron oxide might be significant in our experiments.

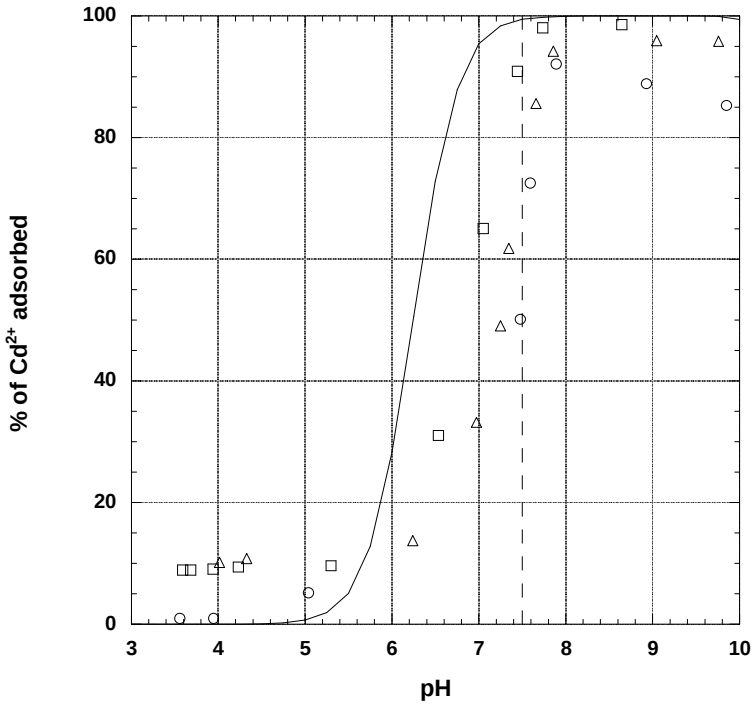

Figure A.2. Cd adsorption by abiotic iron oxides prepared at pH 6.0 (circles), 6.5 (squares), or 7.0 (triangles). The full line corresponds to the model according to Dzombak and Morel and the dashed line indicates the pH of otavite saturation.

1.3.2.3. Cd adsorption by *Anoxybacillus flavithermus*

Six Cd adsorption isotherms were obtained for the bacteria in the absence of any added iron. Cd adsorption by the bacteria increased with increasing pH and Cd-to-bacteria concentration ratio (Fig. A.3), as has been observed previously (Burnett et al., 2006b). The Cd adsorption data from independently grown cultures of the bacteria showed variability of ca. 5-10%. An equal or greater level of inter-culture variability in metal adsorption by bacteria has been previously observed for many different bacterial species and many different metals (e.g. Fein et al., 1997; Daughney et al., 2001; Ngwenya et al., 2003; Burnett et al., 2006b), which may simply reflect the quantitative reliability of this type of experimental data.

1.3.2.4. Cd Adsorption by Iron-Bacteria Composites: Effects of various details of the experimental protocol

The kinetic experiment (Fe-AF 1, ρ = 62 mg/g, 6 isotherms obtained after equilibration times t = 0, 10 min, 30 min, 1 h, 3 h and 6 h) indicated that Cd adsorption to the iron-bacteria composites was rapid, with equilibrium reached within 10 minutes at all pH values tested (data not shown). This rate of Cd adsorption is comparable to that observed for the bacteria alone (Burnett et al., 2006b). Average changes in Cd adsorbed for equilibration times between 10 minutes and 1 hour was less than ±3% for all pH values tested, whereas more significant changes in Cd adsorbed were sometimes observed after 3 or 6 hours, possibly due to cell lysis. Thus we selected 1 h as a reasonable and convenient duration of equilibration for all subsequent Cd isotherm experiments.

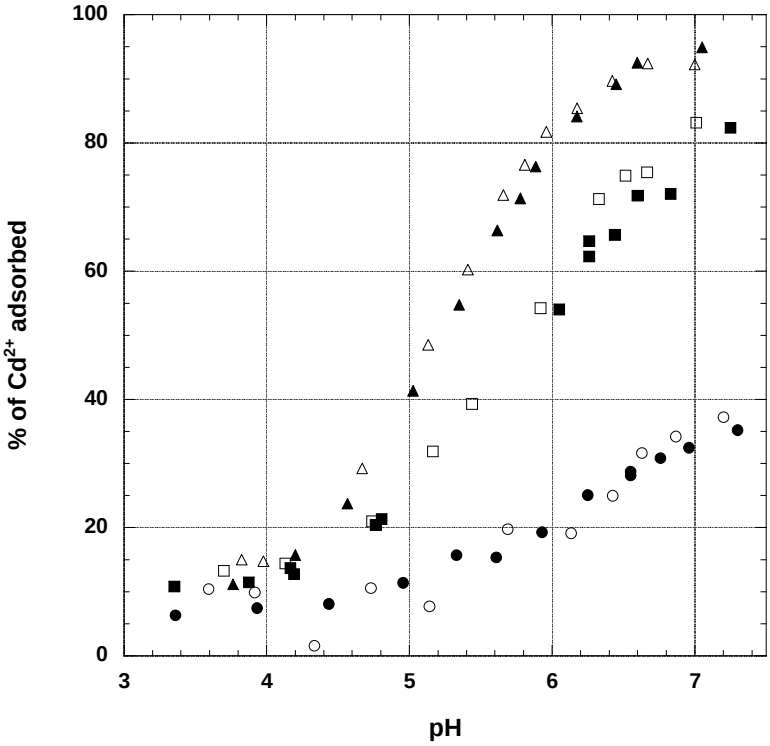

Fig. A.3. Cd adsorption by *A. flavithermus* AF 1* (open symbols) and AF 2*- AF 3* (full symbols) suspensions, at bacterial concentrations of 0.1 $g.L^{-1}$ (circles), 0.4 $g.L^{-1}$ (squares) and 1 $g.L^{-1}$ (triangles).

Cd adsorption by the bacteria-iron composites increased with increasing pH and Cd-to-bacteria concentration ratio (Fig. A.4), as also observed for the pure bacterial suspensions (Fig. A.3). Figure A.4a displays the Cd sorption isotherms obtained after an equilibration time of 1 h for suspensions Fe-AF 1 to Fe-AF 4, which were all prepared using ρ = 62 mg/g. For suspensions Fe-AF 2 (squares) and Fe-AF 3 (triangles) final Cd concentrations were measured using AAS. For suspension Fe-AF 1 (1 hour, empty circles), final Cd concentration was measured using ICP-MS instead of AAS. For experiments Fe-AF 1 to Fe-AF 3, the Cd was added as an acidic standard solution. For suspension Fe-AF 4, the Cd was added as an acidic solution (empty diamonds), or as a solution pre-neutralized at pH 5.5 (full diamonds, see section A.1.2.3). The variability between all these isotherms was equal to about 5-10%, i.e., it was not larger than the variability in the pure bacterial cultures (section A.1.3.2.3). A similar variability was obtained with ρ = 16 mg/g (suspensions Fe-AF 5 to Fe-AF 7, Fig. A.4b). Similar Cd adsorption was also observed for solids that had been aged for one day and then rinsed prior to the isotherm experiment, or aged for one day and used in the isotherm experiment without being rinsed (suspension Fe-AF 11, ρ = 25 mg/g, see Fig. A.5b). Overall then, these results show that the slight variations in experimental protocol had no significant effect on Cd adsorption.

1.3.2.5. Effect of changing the iron-bacteria ratio ρ on Cd adsorption

The striking result appearing clearly from Figure A.5 is that the iron to bacteria ratio of the composite had a significant effect on Cd sorption isotherms. For Cd sorption isotherms obtained for different ρ values and at bacterial concentrations of 1 $g.L^{-1}$, 0.4 $g.L^{-1}$ and 0.1 $g.L^{-1}$ respectively, the addition of iron to the bacterial suspensions generally led to a significant

reduction of the ability of the iron-bacteria composites to immobilize cadmium. The only exception to this general rule was observed for the isotherms performed at a bacterial concentration of 0.1 $g.L^{-1}$ and corresponding to $\rho = 62$ or $\rho = 124$ mg/g, between pH 7.0 and pH 7.5. For these two isotherms, it is possible that the contribution of the iron component led to an overall increase of the Cd sorption above pH 7. However, this hypothesis is backed by only two of our data points, which were close to the saturation limit of otavite, and so it won't be discussed further.

Interestingly, the effect of iron-bacteria ratio was not monotonous with increasing ρ values. The strongest reduction of Cd sorption was actually observed for the smallest ρ value tested here, i.e., $\rho = 16$ mg/g. On Figures A.5a, A.5b and A.5c, the Cd sorption isotherms of the pure bacterial suspensions (full circles) and of the iron-bacteria composite suspensions with $\rho = 16$ mg/g defined an envelope into which all other sorption isotherms fell. Upon increasing the ρ above 16 mg/g, Cd sorption increased and reached a maximum for $\rho = 62$ mg/g (diamonds). Then it decreased again and was similar, within experimental precision, for $\rho = 82$ and $\rho = 124$ mg/g. For example, the isotherm experiments conducted with biomass concentration of 0.4 dry $g.L^{-1}$ and with $\rho = 16$, 25, 31, 62, 82 and 124 mg/g showed Cd adsorption at pH 6 to be roughly 23%, 32%, 32%, 43%, 34% and 30% respectively (Fig. A.5b).

For comparison, about 55% Cd adsorption was observed at pH 6 for the bacteria in the absence of any added iron (Fig. A.3). These complex trends were observed at all three bacterial concentrations, and the magnitude of the effect exceeds experimental error (see Figures A.3 and A.4).

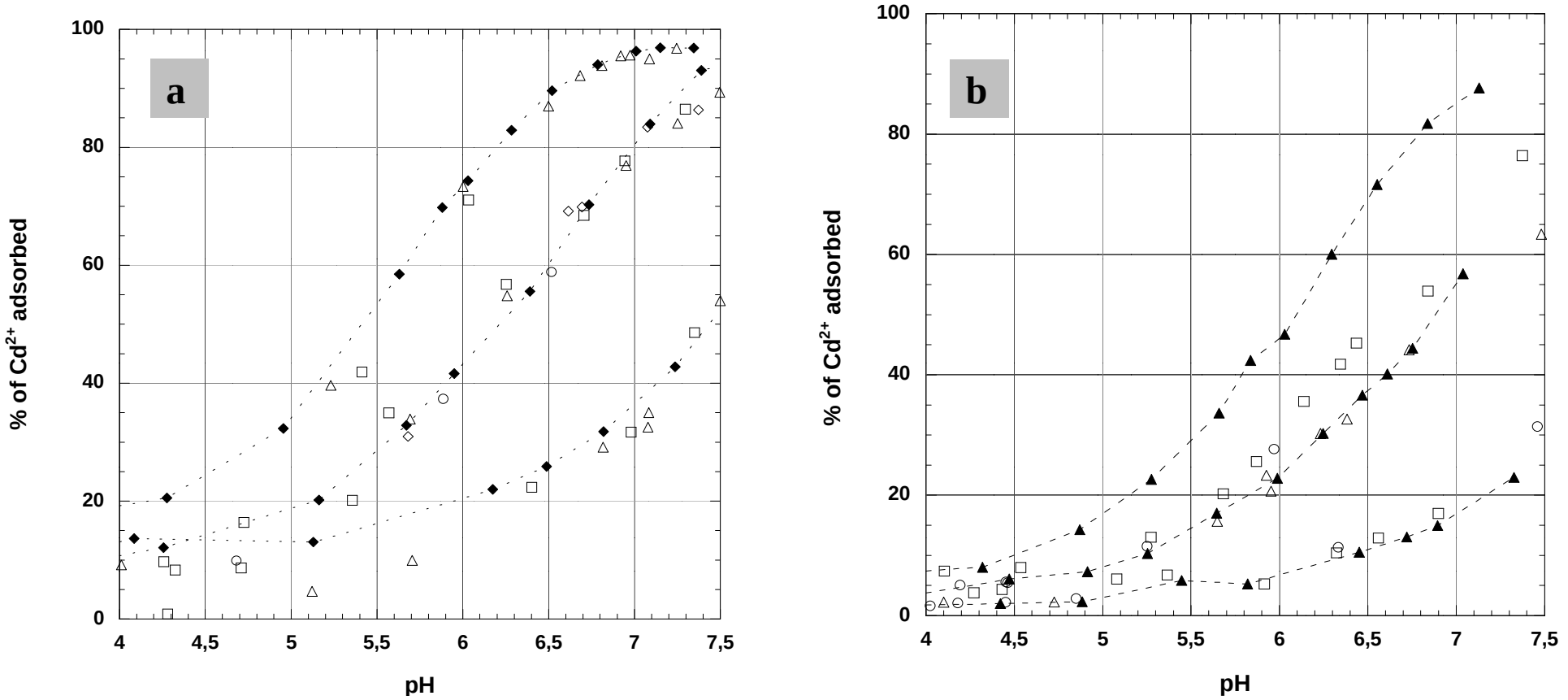

Figure A.4. Cd adsorption by iron-bacteria composites **a)** for ρ = 62 mg/g at bacterial concentrations of 0.1 $g.L^{-1}$, 0.4 $g.L^{-1}$ and 1 $g.L^{-1}$. Suspensions Fe-AF 1 (circles), Fe-AF 2 (squares), Fe-AF 3 (triangles), Fe-AF 4 (empty diamonds), and Fe-AF 4* (full diamonds and dotted line). **b)** for synthesis conditions of 16 mg Fe added per dry g bacteria at bacterial concentrations of 0.1 $g.L^{-1}$, 0.4 $g.L^{-1}$ and 1 $g.L^{-1}$. Suspensions Fe-AF 5 (circles), Fe-AF 6 (squares), Fe-AF 7 (empty triangles), and Fe-AF 7* (full triangles and dotted line).

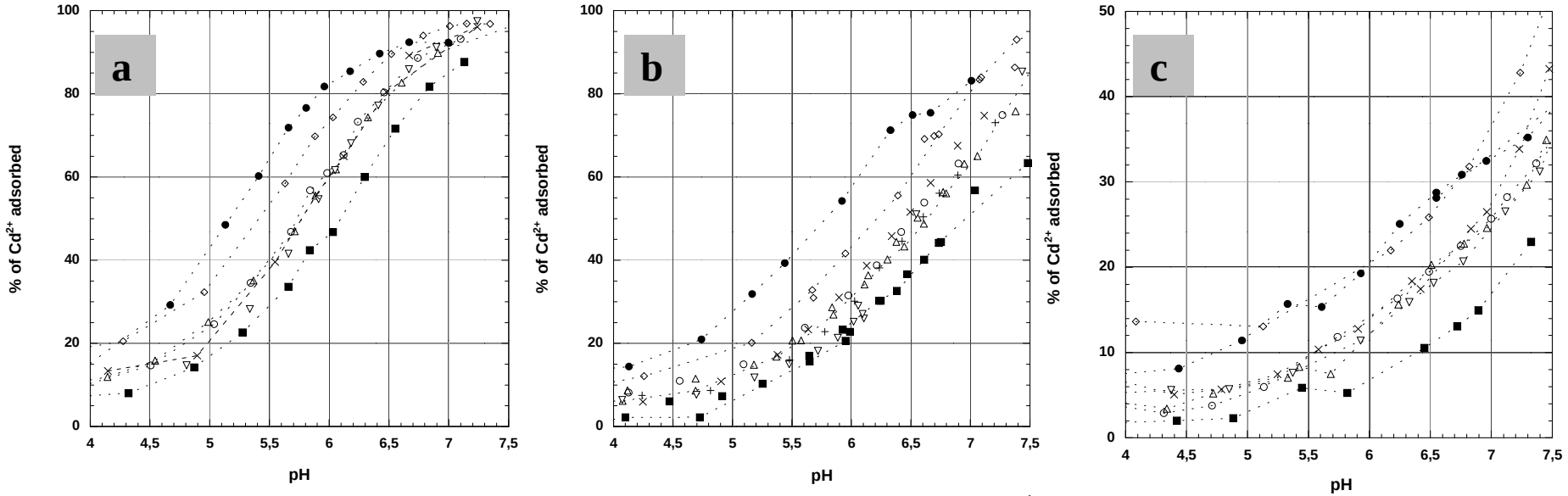

Figure A.5. Cd adsorption by iron-bacteria composites at a bacterial concentration **a)** of 1 $g.L^{-1}$ and for synthesis conditions of 0 (suspension AF 1, full circles), 16 (suspension Fe-AF 7*, full squares), 25 (suspension Fe-AF 11*, triangles), 31 (suspension Fe-AF 8*, circles), 62 (suspension Fe-AF 4*, diamonds), 82 (suspension Fe-AF 12*, upside-down triangles), and 124 (suspension Fe-AF 9*, crosses) mg of Fe added per dry g bacteria. **b)** of 0.4 $g.L^{-1}$ and for synthesis conditions of 0 (suspension AF 1, full circles), 16 (suspension Fe-AF 7 and Fe-AF 7*, full squares), 25 (suspension Fe-AF 11*, washed and not washed but aged, triangles; fresh and not washed, upside down triangles), 31 (suspension Fe-AF 8*, circles), 62 (suspension Fe-AF 4 and Fe-AF 4*, diamonds), 82 (suspension Fe-AF 12*, "+" signs), and 124 (suspension Fe-AF 9*, crosses) mg of Fe added per dry g bacteria. **c)** of 0.1 $g.L^{-1}$ and for synthesis conditions of 0 (suspension AF 1, full circles), 16 (suspension Fe-AF 7*, full squares), 25 (suspension Fe-AF 11*, triangles), 31 (suspension Fe-AF 8*, circles), 62 (suspension Fe-AF 4*, diamonds), 82 (suspension Fe-AF 12*, upside-down triangles), and 124 (suspension Fe-AF 9*, crosses) mg of Fe added per dry g bacteria.

1.3.3. Effect of the ongoing adsorption and oxidation/hydrolysis of Fe^{2+} on Cd sorption

1.3.3.1. Addition of base and pH changes

The experiments performed with suspension Fe-AF 12 allowed us to investigate the complex relationship between the ongoing adsorption and oxidation/hydrolysis of Fe on Cd sorption. As explained in section A.1.2.2., aliquots of the suspension were extracted periodically, two at a time, and used in a series of Cd sorption experiments (in which the Fe/bacteria ratio ρ was progressively increasing). For one aliquot of suspension extracted at each ρ value, no base was added and the suspension was simply spiked with the Cd standard (pH ca. 5.5). In the other aliquot, a volume 85 ± 15 µl of 0.01 N NaOH was added together with the Cd spike at the start of the 1 hour equilibration period (see section A.1.2.4). For simplicity we will refer in the following to the two kinds of aliquots as "B^-" (no base added) and "B^+" (base added) samples. The exact amount of base added as a function of ρ and the pH of the B^- and of the B^+ samples are given in Figure A.6. The pH of the B^- samples was close to 6, i.e., the pH of suspension Fe-AF 12 during synthesis; in other words, the addition of the Cd^{2+} cations and the equilibration period of 1 hour did not lead to significant change in pH, whether the sorption of the Cd^{2+} cations was taking place primarily onto protonated or onto deprotonated reactive groups. This indicates that the protons potentially released in solution by the Cd sorption were not sufficiently numerous to affect the pH measurably.

However, for $\rho > 40$ mg/g, a slight decrease of the pH from 6.0 down to 5.75 was observed. As observed by SEM (see section A.1.3.1), these systems were highly saturated in Fe with respect to the bacterial sorption capacity. It is well known that the oxidation of Fe(II) is enhanced by the presence of iron oxide nuclei (Williams and Scherer, 2004). Hence, since Cd sorption did not seem to induce a measurable pH change of the suspensions, the pH decrease observed for $\rho > 40$ mg/g was possibly due to a more pronounced oxidation and hydrolysis of the Fe(II) present in the suspension at the time of sampling.

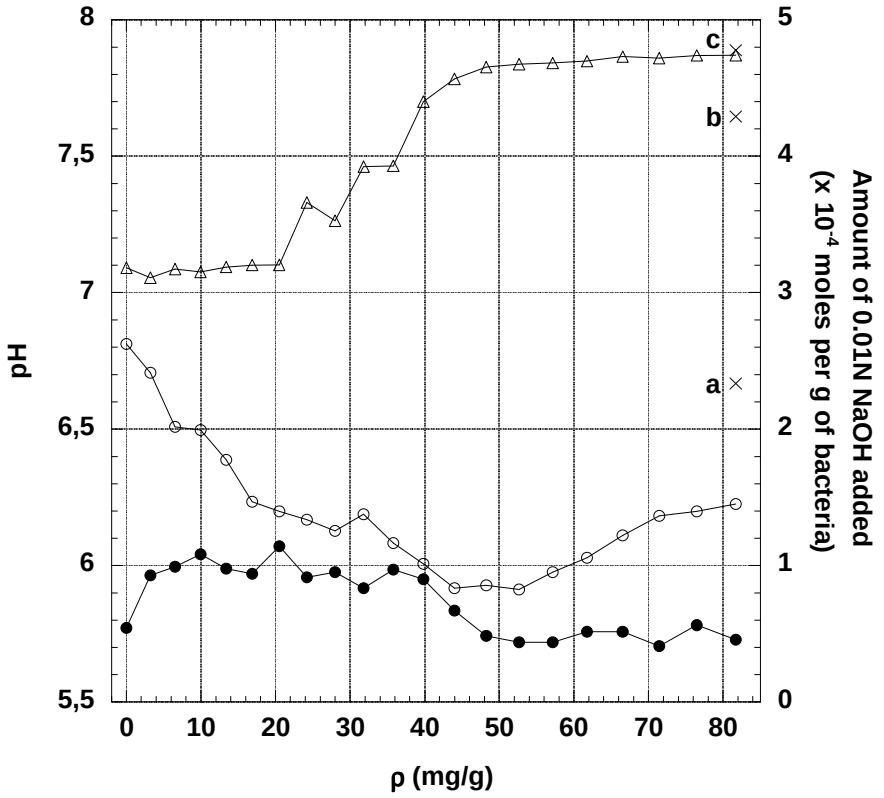

Figure A.6. pH as a function of ρ (experiment Fe-AF 12): vials without any addition of base (full circles), vials with addition of base (empty circles); aged suspension without (data point identified by letter a) or with (data point identified by letter b) addition of base. For the vials with base, amount of 0.01N NaOH added in 10^{-4} moles of OH^- per g of bacteria as a function of ρ for the fresh suspension (triangles), and for the aged suspension (data point identified by letter c).

In the B^+ samples, the pH was of course higher than in the B^- samples. However, the pH difference between both types of samples decreased from about one unit of pH down to almost zero when ρ increased from 0 to 40 mg/g, even though the amount of base increased by over 30% at the same time (Fig. A.6). This indicates that an increasing fraction of the base added was contributing to the reaction of oxidation/hydrolysis of the Fe(II) rather than to a pH change. Hence, the B^+ samples can be considered as similar to the B^- samples, with the main difference being, in addition to a slight variation of the pH, an increased amount of iron oxide precipitated. For at least the range $35 < \rho < 50$ (mg/g), we visually observed that the orange color of the B^+ samples was notably more intense than in equivalent B^- samples (pictures not shown). For $\rho > 50$ mg/g, the pH difference between the B^- and the B^+ samples increased again up to about 0.5 units of pH. This could be explained by diminishing concentrations of residual Fe(II) in the suspension (see section A.1.3.3.2.), as it was sampled at increased ρ values. At the large ρ values, the system was highly saturated in Fe such that the newly added Fe^{2+} ions were able to easily find reactive sites on the existing Fe oxides for a rapid oxidation/hydrolysis reaction.

1.3.3.2. Dissolved Fe concentrations

The measured dissolved Fe concentration is displayed on Figure A.7 (circles) for the B^- (full symbols) and for the B^+ (empty symbols) samples. The total amount of introduced Fe

was known, and so it was possible to calculate the concentration (triangles) and the percentage of immobilized Fe (squares). In the B^- samples, the dissolved Fe concentration initially increased from 0 to over 10 $mg.L^{-1}$, due to the progressive addition of $FeCl_2$, with dissolved Fe concentration reaching a maximum at a Fe/bacteria ratio ρ of about 40 mg/g. Concurrently, the concentration of immobilized Fe increased from 0 to about 6 $mg.L^{-1}$, indicating that not all of the added Fe remained in solution. The percentage of immobilized Fe (relative to total Fe) was not constant: it decreased from an initial value of over 40% to less than 30% as ρ increased from zero to ca. 20 mg/g. These results show that the dissolved Fe concentrations must be interpreted in terms of the changing total iron concentration in the system (due to continuous introduction of $FeCl_2$) as well as the equilibrium established between dissolved and adsorbed Fe ions. As ρ increased above 20 mg/g, the percentage of immobilized Fe began to increase, which likely indicates immobilization of an increasing fraction of the Fe in the form of sorbed Fe(III) monomers and/or of Fe(III) oxide precipitates. This result is consistent with the SEM micrographs (see section A.1.3.1 and Figure A.1), which show that the bacterial cell walls were likely saturated with adsorbed Fe(II) for ρ above ≈ 20 mg/g. As ρ increased above 40 mg/g, the observed decrease of the dissolved Fe concentration can only be explained by the immobilization of a significant and increasing fraction of the Fe in the form of Fe(III) oxide precipitates. However, the dissolved Fe concentration remained above 3 $mg.L^{-1}$, even up to ρ = 80 mg/g. Because Fe(III) is insoluble at pH 6, this indicates that a fraction of the Fe was still present as dissolved Fe^{2+} ions, even at large ρ values where Fe(III) oxide precipitation was occurring. Note that the final dissolved Fe concentration was close to zero after the system was aged overnight, indicating that the residual Fe(II) was eventually oxidized and precipitated as Fe(III) oxide (not shown on Figure A.7 for clarity).

The B^+ samples followed the same trends, except that the dissolved Fe concentration was systematically lower than in the B^- samples. The lower initial dissolved Fe concentration in the B^+ samples was initially likely related to the higher pH value, which would be expected to lead to a higher percentage of sorbed Fe^{2+} ions. As ρ increased from 0 to 20 mg/g, the pH difference between both types of samples rapidly decreased. However, there was a constant difference of about 25-30% between the percentages of immobilized Fe in the B^+ compared to the B^- samples. This indicates that the oxidation of the Fe was significantly enhanced in the systems to which base had been added. Above ρ = 40 mg/g, the difference between the percentages of immobilized Fe gradually decreased to about 10%. For ρ > 65 mg/g, the dissolved Fe concentration in the B^+ samples decreased to less than 1 $mg.L^{-1}$, indicating that there was little dissolved Fe(II) remaining.

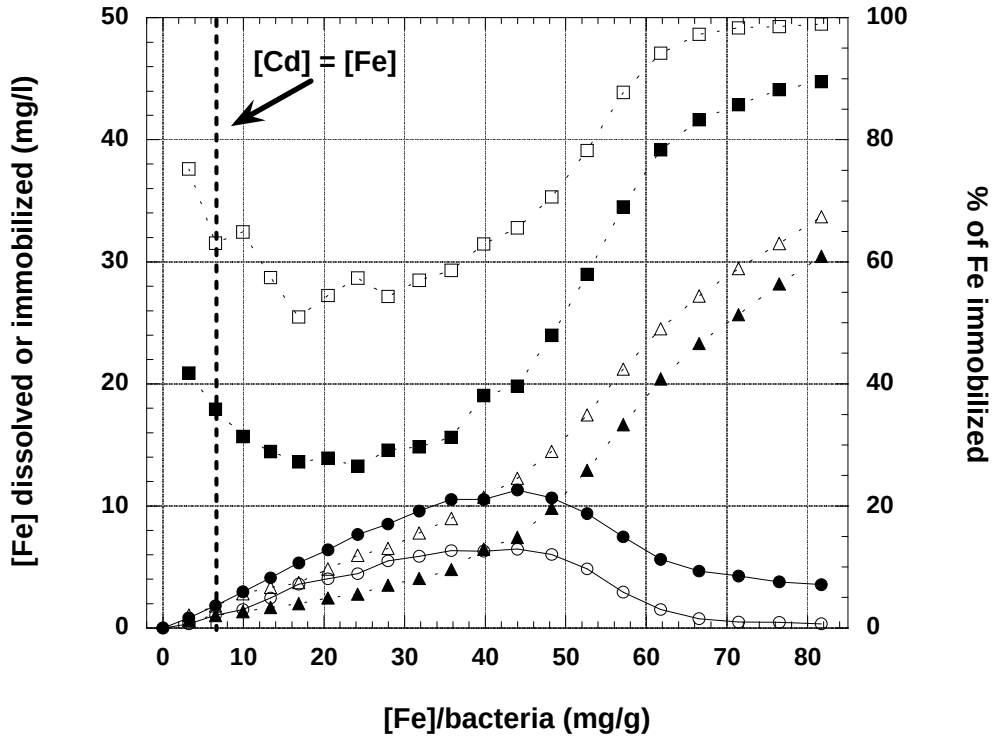

Figure A.7. Dissolved Fe concentration in the B^- (full circles) and in the B^+ (empty circles) samples in $mg.L^{-1}$. Immobilized Fe concentration in the B^- (full triangles) and in the B^+ (empty triangles) samples in $mg.L^{-1}$. Percentage of immobilized Fe in the B^- (full squares) and in the B^+ (empty squares) samples. The vertical dashed line indicates the value of the Fe/bacteria ratio at which the total molar concentrations of Fe and Cd are equal.

In summary, the results of the Fe concentration measurements displayed on Figures A.6 and A.7 demonstrate that the Fe(II)/Fe(III) ratio decreased as ρ increased and as base was added. Whereas Fe was mainly present as sorbed and dissolved Fe(II) at low ρ values in both the B^- and B^+ samples, it consisted of mainly sorbed and precipitated Fe(III) as ρ increased, especially in the B^+ samples. The behavior of Fe must be kept in mind during interpretation of the Cd sorption data described below.

1.3.3.3. Cd sorption at increasing ρ values and rates of the reaction of oxidation/hydrolysis

Figure A.8a displays the percentage of Cd adsorbed by the suspension at increasing ρ values. The concentration of bacteria was equal to 0.4 $g.L^{-1}$, and the pH was equal to 5.9 ± 0.2 in the vials were no base was added, and to 6.4 ± 0.5 in those where base was added, as is shown on Figure A.6. Under these conditions, the slope of the Cd pH-adsorption isotherm was quite high. As seen on Figure A.5b, for a bacterial concentration of 0.4 $g.L^{-1}$, the isotherm slope was 30 ± 5 % of adsorbed Cd per unit of pH, with only weak variations as a function of ρ. The variations of sorbed Cd observed on Figure A.8a were thus partly related to pH variations. To remove the effect of pH, we extrapolated the adsorbed Cd values to a pH of 6. The results are presented on Figure A.8b, using an estimated slope of 30% of adsorbed Cd per unit of pH, and removing the data corresponding to pH values outside of the 5.5-6.5 pH range. For clarity, error bars are not shown in Figure A.8b. But we estimate them at about ± 5% of adsorbed Cd at most, based on the precision of the AAS measurements, as well as on the

errors involved in the extrapolation of the data described above, but excluding other sources of variability discussed in section A.1.3.2.3., such as inter-culture variability.

The percentage of adsorbed Cd^{2+} cations at pH 6 decreased from about 45% to about 22% as the Fe/bacteria ratio increased from 0 to 20 mg/g (Figure A.8b and considering the vials without added base). This decrease was consistent with the decrease displayed in Figure A.5b as the Fe/bacteria ratio was changed from 0 to 16 mg/g (suspensions AF 1 and Fe-AF 7). In experiment Fe-AF 12, a further progressive increase of the Fe/bacteria ratio up to 82 mg/g did not affect the percentage of adsorbed Cd, which remained in the 20-25% range. This is apparently in contradiction with the results displayed in Figure A.5b, according to which the percentage of adsorbed Cd increased back to about 30-40%, as the Fe/bacteria was increased above 20 mg/g. The main difference between experiment Fe-AF 12 and the isotherms presented in Figure A.5b was that the composite suspension was sampled while the Fe^{2+} was being added. Hence, the Fe in the suspension was not fully oxidized, as discussed in section A.1.3.3.1 and A.1.3.3.2. As a consequence, it is likely that some of the Fe was present as dissolved and adsorbed Fe(II) species.

For the vials to which base had been added, the Cd sorption was much higher than in the absence of base, before the pH correction (Fig. A.8a). However, when the Cd sorption was extrapolated to pH 6, the Cd sorption followed the same trend as in the absence of added base up to a Fe/bacteria ratio of 58 mg/g. When the Fe/bacteria ratio was increased from 58 mg/g to 82 mg/g, the percentage of adsorbed Cd increased by 10%, up to about 32%. As we have discussed in sections A.1.3.3.1 and A.1.3.3.2, there was likely little Fe(II) left in the B^+ samples for $\rho > 65$ mg/g. Hence, it is normal that the results obtained for the B^+ samples for $\rho > 65$ mg/g are more consistent with those displayed on Figure A.5b than those obtained for the B^- samples.

The examination of the Cd pH-adsorption isotherm obtained for the fresh suspension Fe-AF 11 ($\rho = 25$ mg/g, Fig. A.5b) and its comparison with the pH adsorption isotherms of the same suspension, aged and either washed or non-washed (Fig. A.5b), led to conclusions in agreement with our conclusions here. The same degree of Cd sorption was observed for the fresh and for the aged suspension, except in the 5-6 pH range, where a slightly (ca. 5%) lower Cd sorption was observed for the fresh suspension, and the sorption isotherm overlapped with the sorption isotherm of the suspension prepared with $\rho = 16$ mg/g. We interpret this lower sorption by the residual presence of Fe^{2+} cations competing with the Cd for sorption on the reactive sites in the cell walls. Below pH 5, the small percentage of Cd sorption made it difficult to distinguish differences between the different suspensions. Above pH 6, the addition of a larger amount of base to reach a given pH in the fresh suspension was indicative that a fraction of the base added was used up to catalyze the oxidation/hydrolysis of the residual Fe(II) during the equilibration period for the Cd sorption.

It is interesting to note that the Cd concentration of 5 ppm used in this study is equivalent to a molar concentration of 44.5 μM. A similar molar Fe concentration is obtained for 2.5 ppm of Fe. In Figure A.8, the bacterial concentration was equal to 0.4 $g.L^{-1}$, which for 2.5 ppm Fe corresponds to $\rho = 6.2$ mg/g. At this still low value of ρ, we have discussed that most of the Fe was likely present in the sorbed Fe(II) state. According to Figures A.7 and A.8a, for $\rho = 6.2$ mg/g, the percentages of adsorbed Fe and Cd were equal to approximately 36% and 33% in the B^- samples, and to 63% and 55% in the B^+ samples, respectively. These numbers suggest that the sorption affinities of Fe^{2+} and Cd^{2+} cations are very similar. This similarity between the Fe^{2+} and Cd^{2+} sorption onto bacterial cells had already been inferred by Châtellier and Fortin (2004). It explains why the sorption of the Cd^{2+} cations was significantly hindered but not completely prevented by the presence of the introduced Fe(II), and why Cd sorption increased again when the competition with Fe(II) was removed as a result of its oxidation and hydrolysis.

1.4. CONCLUSION

We have demonstrated here that the sorption of Cd^{2+} cations by an iron-bacteria composite suspension is affected by the incremental oxidation, hydrolysis and precipitation of the iron. The magnitude of the effect on Cd sorption depends on the Fe/bacteria ratio ρ and also on the degree of oxidation and hydrolysis of the Fe(II). In general, the Cd sorption is lower for an iron-bacteria composite than for bacteria alone at the same bacterial concentration. Prior to the onset of precipitation of iron oxide, the decrease in Cd sorption is mainly due to a competition between the Fe^{2+} and the Cd^{2+} cations, which have comparable affinities for the available bacterial surface sites. Once the cell walls are saturated with adsorbed Fe^{2+}, addition of more iron (i.e. increase in ρ value) leads to the precipitation of iron oxide, which in turn promotes the desorption of Fe(II) from the bacterial surfaces and leads to its oxidation to Fe(III). This effect allows Cd adsorption to increase, but not to the same level observed in the absence of iron: Cd sorption remains limited relative to the iron-free case, because of residual Fe(II) or Fe(III) monomers sorbed onto reactive bacterial sites and/or because of a limited access to the bacterial reactive sites due to a masking effect of the iron oxide particles themselves. We also observed that the presence of Cd affected the Fe(II) sorption and oxidation process. By competing with Fe^{2+} cations for the reactive sites on the cell walls, the presence of Cd promoted iron oxide precipitation. In conclusion, the sorption of Cd^{2+} and the sorption, oxidation and hydrolysis of Fe^{2+} cations in the presence of bacteria are interrelated processes that affect each other significantly. More generally, our study demonstrates that the immobilization of metal cations at oxic/anoxic boundaries in natural or engineered environments can not be examined independently of the redox processes occurring at such boundaries, such as the oxidation and hydrolysis of Fe(II) diffusing from an anoxic environment.

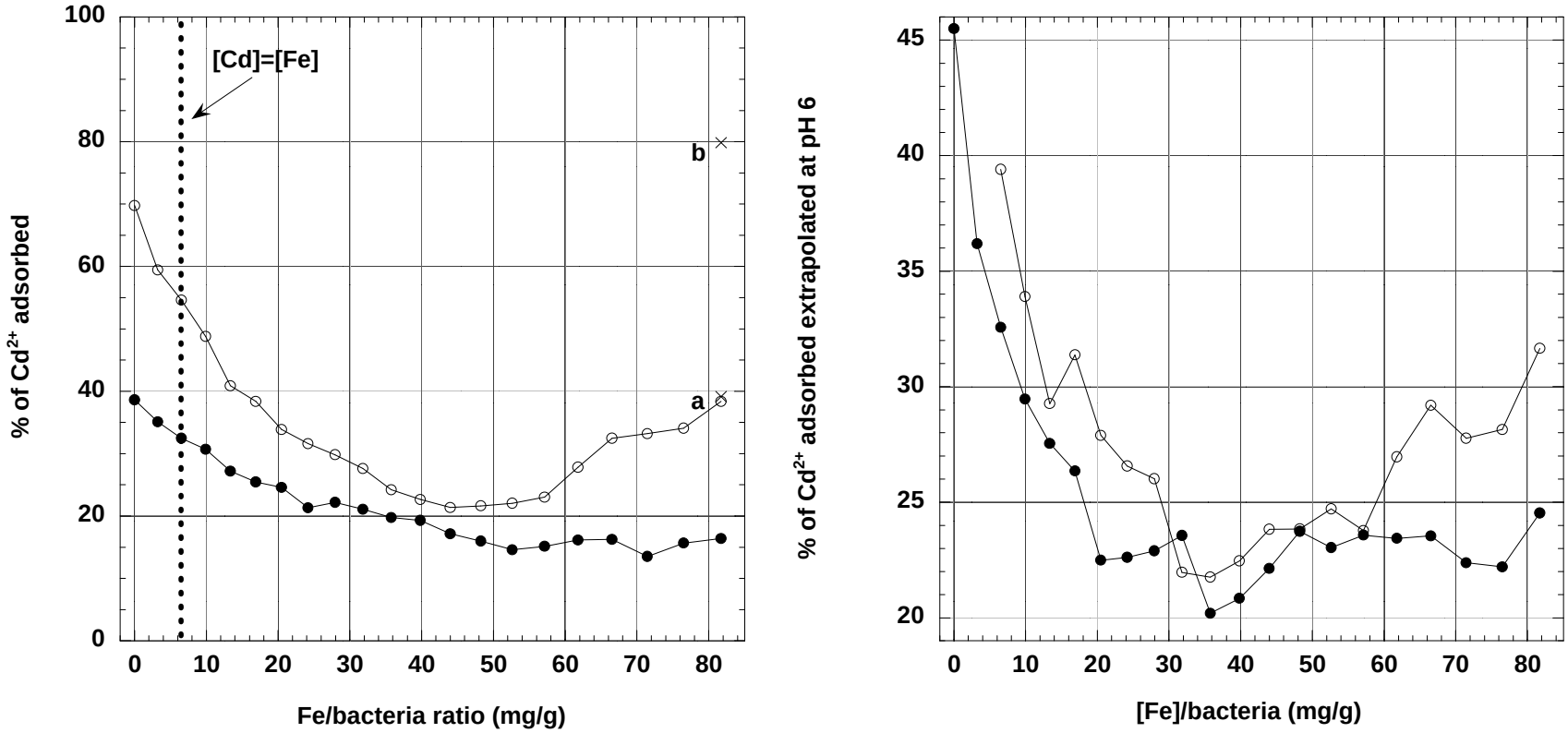

Figure A.8. Cd adsorption as a function of Fe/bacteria ratio (experiment Fe-AF 12) **a)** vials without any addition of base (full circles), vials with addition of base (empty circles). Aged suspension without (data point identified by letter a) or with (data point identified by letter b) addition of base. The vertical dashed line indicates the value of the Fe/bacteria ratio at which the total molar concentrations of Fe and Cd are equal. **b)** extrapolated at pH 6: vials without any addition of base (full circles), vials with addition of base (empty circles)

B.1. Variations through the incubation time of pH, redox potential (Eh), nitrate (NO_3^-), sulphate (SO_4^{2-}), acetate, Fe(II), total iron (Fe(tot)), and arsenic concentrations in the three columns (Reference, As-Fh and As-Lp.

Time (hours)	Reference	As-Fh	As-Lp	Reference	As-Fh	As-Lp	Reference	As-Fh	As-Lp	Reference	As-Fh	As-Lp
	pH			Eh (mV)			NO_3^- (mg.L^{-1})			SO_4^{2-} (mg.L^{-1})		
0	5.63	5.63	5.63	367	320	367	30.9	30.9	30.9	10.6	10.6	10.6
7	-	5.59		-	305	-	-	34.8	-	-	10.4	-
21	-	5.68		-	381	-	-	18.4	-	-	10.7	-
24	6.27		5.79	317	-	327	21.4	-	28.3	11.3	-	13.6
39	-	6.67		-	234	-	-	<d.l.	-	-	10.4	-
48	6.60		6.56	246	-	253	1.8	<d.l.	1.2	11.7	-	13.0
57	-	6.36	-	-	190	-	-	<d.l.	-	-	10.4	-
72	6.03	-	5.99	175	-	175	0.9	<d.l.	0.8	12.0	-	12.9
88	-	6.09	-	-	167	-	-	<d.l.	-	-	7.5	-
120	6.20	-	6.18	177	-	179	0.6	<d.l.	<d.l.	7.2	<d.l.	8.4
154	-	6.01		-	142	-	-	<d.l.	<d.l.	-	<d.l.	-
168	6.27	-	6.32	165	-	172	<d.l.	<d.l.	<d.l.	1.2	<d.l.	2.4
205	-	6.21	-	-	114	-	<d.l.	<d.l.	<d.l.	<d.l.	<d.l.	<d.l.
256.5	-	6.24	-	-	121	-	<d.l.	<d.l.	<d.l.	<d.l.	<d.l.	<d.l.
321	-	6.27	-	-	120	-	<d.l.	<d.l.	<d.l.	<d.l.	<d.l.	<d.l.
336	6.24	-	6.19	139	-	144	<d.l.	<d.l.	<d.l.	<d.l.	<d.l.	<d.l.
370.5	-	6.38	-	-	-	-	<d.l.	<d.l.	<d.l.	<d.l.	<d.l.	<d.l.
424	-	6.36	-	-	158	-	<d.l.	<d.l.	<d.l.	<d.l.	<d.l.	<d.l.
491.5	-	6.25	-	-	-3	-	<d.l.	<d.l.	<d.l.	<d.l.	<d.l.	<d.l.
504	6.25	-	6.27	125	-	121	<d.l.	<d.l.	<d.l.	<d.l.	<d.l.	<d.l.
542.5	-	6.26	-	-	-24	-	<d.l.	<d.l.	<d.l.	<d.l.	<d.l.	<d.l.
589.5	-	6.10	-	-	-26	-	<d.l.	<d.l.	<d.l.	<d.l.	<d.l.	<d.l.
660.5	-	6.06	-	-	-27	-	<d.l.	<d.l.	<d.l.	<d.l.	<d.l.	<d.l.
672	6.23	-	6.21	131	-	122	<d.l.	<d.l.	<d.l.	<d.l.	<d.l.	<d.l.
727.5	-	6.06	-	-	-69	-	<d.l.	<d.l.	<d.l.	<d.l.	<d.l.	<d.l.
756	6.18		6.12	101	-	83	<d.l.	<d.l.	<d.l.	<d.l.	<d.l.	<d.l.
851.5	-	6.02	-	-	21	-	<d.l.	<d.l.	<d.l.	<d.l.	<d.l.	<d.l.
898.5	-	-	-	-	-	-	<d.l.	<d.l.	<d.l.	<d.l.	<d.l.	<d.l.
906	6.12	-	6.09	-8	-	-36	<d.l.	<d.l.	<d.l.	<d.l.	<d.l.	<d.l.
990	-	6.23		-	21	-	<d.l.	<d.l.	<d.l.	<d.l.	<d.l.	<d.l.
1008	6.50	-	6.14	-27	-	-56	<d.l.	<d.l.	<d.l.	<d.l.	<d.l.	<d.l.

1128	6.70	-	6.30	-38	-	-86	<d.l.	<d.l.	<d.l.	<d.l.	<d.l.	<d.l.
1210.5	-	6.30	-	-	-17	-	<d.l.	<d.l.	<d.l.	<d.l.	<d.l.	<d.l.
1320	6.12	-	6.22	-11	-	-21	<d.l.	<d.l.	<d.l.	<d.l.	<d.l.	<d.l.
1402.5	-	6.27	-	-	100	-	<d.l.	<d.l.	<d.l.	<d.l.	<d.l.	<d.l.
1560	6.18	6.14	6.27	2	98	14	<d.l.	<d.l.	<d.l.	<d.l.	<d.l.	<d.l.
Time (hours)	**Reference**	**As-Fh**	**As-Lp**	**Reference**	**As-Fh**	**As-Lp**	**Reference**	**As-Fh**	**As-Lp**	**Reference**	**As-Fh**	**As-Lp**
	Acetate (mg.L^{-1})			**Fe(II) (mg.L^{-1})**			**Fe(tot) (mg.L^{-1})**			**Arsenic (µg.L^{-1})**		
0	<d.l.	<d.l.	<d.l.	<d.l.	<d.l.	<d.l.	<d.l.	<d.l.	<d.l.	<d.l.	<d.l.	<d.l.
7	-	<d.l.	-	-	0.38	-	-	-	-	-	-	-
21	-	<d.l.	-	-	0.76	-	-	0.39	-	-	0.93	-
24	6.6	-	4.3	0.14	-	0.19	<d.l.	-	-	-	-	-
39	-	30.4	-	-	1.28	-	-	-	-	-	-	-
48	7.6	-	8.6	0.38	-	0.61	-	-	-	-	-	-
57	-	14.2	-	-	2.27	-	-	2.00	-	-	4.15	-
72	15.5	-	22.1	1.76	-	1.94	1.60	-	1.53	4.41	-	4.29
88	-	48.8		-	5.88	-		-	-		-	-
120	57.6	-	72.9	8.28	-	9.37	9.46	-	8.80	13.76	-	13.22
154	-	114.0	-	-	14.75	-		15.38	-	-	17.28	-
168	143.7		159.6	17.08	-	17.39	18.59	-	16.63	21.05	-	19.59
205	-	134.8	-	-	19.56	-	-	21.76	-	-	23.47	-
256.5	-	166.5	-	-	25.36	-	-	25.90	-	-	26.83	-
321	-	195.5	-	-	29.54	-	-	28.98	-	-	28.83	-
336	180.0	-	214.4	29.36	-	30.90	-	-	30.95	27.70	-	28.46
370.5	-	191.4	-	-	33.55	-	-	33.25	-	-	31.39	-
424	-	218.0	-	-	35.94	-	32.20	35.74	-	-	33.95	-
491.5	-	259.0	-	-	37.72	-	-	38.41	-	-	37.26	-
504	224.0	-	259.3	35.70	-	39.20	-	-	-	-		-
542.5	-	239.6	-	-	38.36	-	-	41.26	-	-	39.45	-
589.5	-	242.8	-	-	40.91	-	-	39.59	-	-	38.92	-
660.5	-	251.0	-	-	38.49	-	-	42.50	-	-	42.82	-
672	216.8	-	242.9	39.59	-	48.81	39.50	-	45.76	-	-	38.76
727.5	-	244.6	-		40.68	-	-	48.84	-	-	51.18	-
756	225.3	-	254.0	41.48	-	49.13	-	-	-	-	-	-
851.5	-	253.6	-	-	43.37	-	-	-	-	-	-	-
898.5	-	-	-	-	44.57	-	-	-	-	-	-	-

906	230.3	-	256.0	43.50	-	52.07	-	-	-	-	-	-
990	-	-	-		44.18	-	-	53.58	-	-	54.33	-
1008	225.6	235.7	254.0	45.20	-	58.04	-	-	-	-	-	-
1128	229.0		248.0	45.70	-	61.53	48.00	-	-	38.02	-	-
1210.5	-	276.0	-	-	49.54	-	-	54.58	-	-	58.14	-
1320	-	-	243.0	-	-	61.13	-	-	58.40	-	-	38.10
1402.5	-	256.5	-	-	46.84	-	-	67.35	-	-	80.15	-
1560	230.1	-	252.0	46.20	-	64.19	48.00	-	-	-	73.19	-

d.l. detection limit

REFERENCES BIBLIOGRAPHIQUES

REFERENCES BIBLIOGRAPHIQUES

Abraitis, P.K., Pattrick, R.A.D., Vaughan, D.J., 2004. Variations in the compositional, textural and electrical properties of natural pyrite: a review. Int. J. Miner. Process. 74 : 41-59.

AFNOR. 1997 'Qualité de l'Eau, Méthodes d'Analyses 2, Elément Majeurs; Autres Eléments et Composés Minéraux.' Paris.

Ahmann, D., Krumholz, L.R., Hemond, C.H.F., Lovley, D.R., Morel, F.M., 1997. Microbial mobilization of arsenic from sediments of the Aberjona watershed. Environ. Sci. Technol. 31: 2923-2930.

Ainsworth, C.C., Pilon, J.L., Gassman, P.L., Van Der Sluys, W.G., 1994. Cobalt, cadmium, and lead sorption to hydrous iron oxide: Residence time effect. Soil Sci. Soc. Am. J. 58: 1615-1623.

Akai, J., Izumi, K., Fukuhara, H., Masuda, H., Nakano, S., Yoshimura, T., Ohfuji, H., Anawar, H.M., Akai, K., 2004. Mineralogical and geomicrobiological investigations on groundwater arsenic enrichment in Bangladesh. Appl. Geochem. 19(2): 215-230.

Akthar, N.M.D., Sastry, K.S., Mohan, P.M., 1996. Mechanism of metal ion biosorption by fungal biomass. BioMetals 9:21-28.

Anderson, C.R., Pedersen, K., 2003. *In situ* growth of Gallionella biofilms and partitioning of lanthanides and actinides between biological material and ferric oxyhydroxides. Geobiol. 1: 169-178.

Anderson, T.F., 1951. Techniques for the preservation of three-dimensional structure in preparing specimens for the electron microscope. Transactions of the New York Academy of Sciences 13: 130-134.

Appelo, C.A.J., Van der Weiden, M.J.J., Tournassat, C., Charlet, L., 2002. Surface complexation of ferrous iron and carbonate on ferrihydrite and the mobilization of arsenic. Environ. Sci. Technol. 36(14): 3096-3103.

Arnold, R.D., Hoffmann, M.R., Dichridtina, T., Picardal, F.W., 1990. Regulation of Dissimilatory Fe(III) Reduction Activity in Shewanella putrefaciens. Applied and Environ. Microbiol. 56: 2811-2817.

Avena, M.J., Koopal, L.K., 1999. Kinetics of humic acid adsorption at solid-water interfaces. Environ. Sci. Technol. 33(16): 2739-2744.

Avena, M.J., Koopal, L.K., 1998. Desorption of humic acids from an iron oxide surface. Environ. Sci. Technol. 32(17): 2572-2577.

Baker, B.J., Banfield, J.F., 2003. Microbial communities in acid mine drainage. FEMS Microbiol. Ecol. 44: 139-152.

Bauer, M., Blodau, C., 2006. Mobilization of arsenic by dissolved organic matter from iron oxides, soils and sediments. Sci. Total Environ. 354: 179-190.

Belkova, N.L., Zakharova, Ju.R., Tazaki, K., Okrugin, V.M., and Parfenova, V.V., 2004. Fe-Si Biominerals in the Vilyuchinskie Hot Springs, Kamchatka Peninsula, Russia. Int. Microbiol. 7: 193-198.

Belzile, N., Chen, Y.W., Wang, Z.J., 2001. Oxidation of antimony (III) by amorphous iron and manganese oxyhydroxides. Chem. Geol. 174(4): 379-387.

Benner, S.G., Hansel, C.M., Wielinga, B.W., Barber, T.M., Fendorf, S., 2002. Reductive dissolution and biomineralization of iron hydroxide under dynamic flow conditions. Environ. Sci. Technol. 36(8): 1705-1711.

Beveridge, T.J., Fortin, D., Ferris, F.G., 1997. Surface-mediated mineral development by bacteria. In: Banfield, J.F., Nealson, K.H. (Eds.), Geomicrobiology: Interactions Between Microbes and Minerals. Mineralogical Society of America. 35: 161-180.

Beveridge, T.J., 1989. Role of cellular design in bacterial metal accumulation and mineralization. Annu. Rev. Microb. 43: 174-171.

Beveridge, T.J., Doyle, R.J., 1989. Metal ions and bacteria, (eds.). Willey and Sons, New York.

Beveridge, T.J., Murray, R.G.E., 1980. Sites of metal deposition in the cell wall of *Bacillus subtilis*. J. Bacteriol. 141: 876-887.

Beveridge, T.J., Murray, R.G.E., 1976. Uptake and retention of metals by cell walls of *Bacillus subtilis*. J. Bacteriol. 127:1502-1518.

Birkefeld, A., Schulin, R., Nowack, B., 2007. *In situ* transformations of fine lead oxide particles in different soils. Environ. Pollut., 145(2): 554-561.

Birkefeld, A., Schulin, R., Nowack, B., 2006. *In situ* investigation of dissolution of heavy metal containing mineral particles in an acidic forest soil. Geochim. Cosmochim. Acta 70: 2726-2736.

Birkefeld, A., Schulin, R., Nowack, B., 2005. A new *in situ* method to analyze mineral particle reactions in soils. Environ. Sci. Technol. 39: 3302-3307.

Blanchard, M., Alfredsson, M., Brodholt, J., Wright, K., Catlow C.R.A., 2007. Arsenic incorporation into FeS2 pyrite and its influence on dissolution: a DFT study. Geochim. Cosmochim. Acta 71(3): 624-630.

Bonneville, S., Cappellen, P.V., Behrends, T., 2004. Microbial reduction of iron (III) oxyhydroxides: effects of mineral solubility and availability. Chem. Geol. 212: 255-268.

Borah, D., Senapati, K., 2006. Adsorption of Cd (II) from aqueous solution onto pyrite. Fuel 85: 1929-1934.

Borrok, D., Fein, J.B., Kulpa, C.F., 2004. Proton and Cd adsorption onto natural bacterial consortia: Testing universal adsorption behaviour. Geochim. Cosmochim. Acta 68: 3231-3238.

Bose, P., Sharma, A., 2002. Role of iron in controlling speciation and mobilization of arsenic in subsurface environment. Water Res. 36(19): 4916-4926.

Bostick, B.C., Fendorf, S., 2003. Arsenite sorption on troilite (FeS) and pyrite (FeS2). Geochim. Cosmochim. Acta 67: 909-921

Bostick, B.C., Fendorf, S., Helz, G.R., 2003. Differential adsorption of molybdate and tetrathiomolybdate on pyrite (FeS_2). Environ. Sci. Technol. 37: 285–291.

Bourcereau, L., 2006. Diversité et fonctions des microorganismes impliqués dans l'immobilisation du fer. Master 2 Bassins versants-eau-sols. Univ. De Rennes 1.

Bourrié, G., Trolard, F., Génin, J. M. R., Jaffrezic, A., Maître, V., Abdelmoula, M., 1999. Iron control by equilibria hydroxy-Green Rusts and solutions in hydromorphic soils. Geochim. Cosmochim. Acta 63: 3417-3427.

Bourrié, G., Maitre, V., Curmi, P., 1994. 2 types of seasonal-variations of dissolved iron in hydromorphic soils under temperate climate. Comptes Rendus de l'Academie des Sciences série II 318(1) : 87-92.

Bousserrhine, N., Gasser, U.G., Jeanroy, E., Berthelin, J., 1999. Bacterial and Chemical Reductive Dissolution of Mn-, Co-, Cr-, and Al-Substituted Goethites. Geomicrobiol. Jour. 16(3): 245 - 258.

Bousserrhine, N., 1995. Etude de paramètres de la réduction bactérienne du fer et application à la déferrification de minéraux industriels. Thèse en géomoicrobiologie et biochimie microbienne. Univ. de Nancy I.

Boust, D., Fischer, J.-C., Ouddane, B., Petit, F., Wartel, M., 1999. Fer et manganèse. Réactivités et recyclages. Fascicule N°9 du programme scientifique Seine-Aval. Editions IFREMER. Plouzané (France). 39 pages.

Bowell, R. J., 1994. Sorption of arsenic by iron oxides and oxyhydrox ides in soils. Appl. Geochem. 9: 279-286.

Boyanov, M.I., Kelly, K.M., Kemner, S.D., Bunker, B.A., Fein, J.B., Fowle, D.A., 2003. Adsorption of cadmium to Bacillus subtilis bacterial cell walls: A pH-dependent X-ray absorption fine structure spectroscopy study. Geochim. Cosmochim. Acta 67: 3299-3311.

Brady, P.V., Brady, M.V., Borns, D.J., 1997. Natural Attenuation: CERCLA, RBCA's, and the Future of Environmental Remediation. Lewis Publishers, Boca Raton.

Brown, G.E.J., Sturchio, N.C., 2002. An overview of synchrotron radiation application to low-temperature geochemistry and environmental science. In: P.A. Fenter (Editor), Application of synchrotron radiation in low-temperature geochemistry and environmental science. Rev. Min. Geochem. RIMG 49: 1-107.

Brown, G.E., Henrich, V.E., Casey, W.H., Clark, D.L., Eggleston, C., Felmy, A., Goodman, D.W., Gratzel, M., Maciel, G., McCarthy, M.I., Nealson, K.H., Sverjensky, D.A., Toney, M.F., Zachara, J.M., 1999. Metal oxide surfaces and their interactions with aqueous solutions and microbial organisms. Chem. Rev. 99(1): 77-174.

Buerge-Weirich, D., Hari, R., Xue, H., Behra, P., Sigg, L., 2002. Adsorption of Cu, Cd, and Ni on goethite in the presence of natural groundwater ligands. Env. Sci. Tech. 36: 328-336.

Bura, R., Cheung, M., Liao, B., Finlayson, J., Lee, B.C., Droppo, I.G., Leppard, G.G., Liss, S.N., 1998. Composition of extracellular polymeric substances in the activated sludge floc matrix. Wat. Sci. Technol. 37: 325-333.

Burnett, P.G., Heinrich, H., Peak, J.D., Bremer, P.J., McQuillan, A.J. Daughney, C.J., 2006a. The effect of pH and ionic strength on proton adsorption by the thermophilic bacterium Anoxybacillus flavithermus. Geochim. Cosmochim. Acta 70: 1914-1927.

Burnett, P.-G.G., Daughney, C.J., Peak, D., 2006b. Cd adsorption onto Anoxybacillus flavithermus: Surface complexation modeling and spectroscopic investigations. Geochim. Cosmochim. Acta 70: 5253-5269.

Burnol, A., Garrido1 F., Baranger, P., Joulian, C., Dictor, M.C., Bodénan, F., Morin, G., Charlet, L., 2007. Decoupling of arsenic and iron release from ferrihydrite suspension under reducing conditions: a biogeochemical model. Geochem. Trans. 8:12.

Cancès, B., Juillot, F., Morin, G., Laperche, V., Polya, D.,Vaughan, D.J., Hazemann, J.L., Proux, O., Brown, Jr.G.E., Calas, G., 2008. Change in arsenic speciation through a contaminated soil profile: a XAS based study. Sci. Total Environ. 397: 178-189.

Cancès, B., Juillot, F., Morin, G., Laperche, V., Alvarez, L., Proux, O., Hazemann, J-L, Brown, Jr. G.E., Calas, G., 2005. XAS evidence of As(V) association with iron oxyhydroxides in a contaminated soil at a former arsenical pesticide processing plant. Environ. Sci. Technol. 39: 9398-9405.

Chan, C.S., de Stasio, G., Welch, S.A., Girasole, M., Frazer, B., Nesterova, M., Fakra, S., Banfield, J.F., 2004. Microbial polysaccharides template assembly of nanocrystal fibers. Science 303: 1656-1658.

Charlatchka, R., Cambier, P., 2000. Influence of reducing conditions on solubility of trace metals in contaminated soils. Wat. Air Soil Poll. 118(1-2): 143-167.

Charlet, L., Polya, D.A., 2006. Arsenic in Shallow, Reducing Groundwaters in Southern Asia: An Environmental Health Disaster. Elements 2: 91-96.

Chatain, V., Sanchez, F., Bayard, R., Moszkowicz, P., Gourdon, R., 2005. Effect of experimentally induced reducing conditions on the mobility of arsenic from a mining soil. J. Haz. Mat. 122: 119-128.

Châtellier, X., Fortin, D., 2004. Adsorption of ferrous ions onto *Bacillus subtilis* cells. Chem. Geol. 212: 209-228.

Châtellier, X., West, M.M., Rose, J., Fortin, D., Leppard, G.G., Ferris, F.G., 2004. Characterization of iron-oxides formed by oxidation of ferrous ions in the presence of various bacterial species and inorganic ligands. Geomicrobiol. J. 21: 99-112.

Châtellier, X., Fortin, D., West, M.M., Leppard, G.G., Ferris, F.G., 2001. Effect of the presence of bacterial surfaces during the synthesis of Fe oxides by oxidation of ferrous ions. Eur. J. Mineral. 13: 705-714.

Chenu, C., Stotzky, G., 2002. Interactions between microorganisms and soil particles: An overview. In: P.M. Huang, J.-M. Bollag, N. Senesi (Editors), Interactions between soil particles and microorganisms. Impact on the terrestrial ecosystem. John Wiley & sons, New York. pp 3-41.

Chuan, M.C., Shu, G.Y., Liu, A., 1996. Solubility of heavy metals in a contaminated soil: effect of redox potential and pH. Wat. Air Soil Poll. 90: 543-556.

Cliff, J.B., Jarman, K.H., Valentine, N.B., Golledge, S.L., Gaspar, D.J., Wunschel, D.S., Wahl, K.L., 2005. Differentiation of spores of *Bacillus subtilis* grown in different media by elemental characterization using Time-of-Flight Secondary Ion Mass Spectrometry. Appl. Environ. Microbiol. 71: 6524-6530.

Cooper, C.D., Picardal, F.F., Coby, A.J., 2006. Interactions between Microbial Iron Reduction and Metal Geochemistry: Effect of Redox Cycling on Transition Metal Speciation in Iron Bearing Sediments. Environ. Sci. Technol. 40: 1884 -1891.

Cooper, D.C., Picardal, F., Rivera, J., Talbot, C., 2000. Zinc immobilization and magnetite formation via ferric oxide reduction by Shewanella putrefaciens 200. Environ. Sci. Technol. 34(1): 100-106.

Cornell, R. M., Schwertmann, U., 2003. The Iron Oxides: Structure, Properties, Reactions, Occurrence and Uses. VCH. Weinheim.

Cornell, R.H., Schwertmann, U., 1996. The iron-oxides. VCH Publ., Weinheim.

Cornell, R.M., Schwertmann, U., 1979. Influence of organic anions on the crystallization of ferrihydrite, Clay Clay Miner. 27: 402–410.

Cotoras, D., Viedma, P., Cifuentes, L., Mestre, A., 1992. Sorption of metal ions by whole cells of Bacillus and Micrococcus. Env. Tech. 13: 551-559.

Couling, S. B., Mann, S. 1985. The influence of inorganic phosphate on the crystallization of magnetite (Fe3O4) from aqueous solution. J. Chem. Soc., Chem. Commun. 23: 1713-1715.

Cowan, C.E., Zachara, J.M., Resch, C.T., 1991. Cadmium adsorption on iron oxides in the presence of alkaline-earth elements. Env. Sci. Tech. 25: 437-446.

Dassonville, F., Renault, P., 2002. Interactions between microbial processes and geochemical transformations under anaerobic conditions: a review. Agronomie 22(1): 51-68.

Daughney, C.J., Fortin, D., 2006. Mineral Adsorption and Absorption by Biological Cells. In Encyclopedia of Surface and Colloid Science, (A. Hubbard, Ed.), 2nd Edition, Marcel Dekker, New York, pp. 867 - 883.

Daughney, C.J., Fowle, D.A., Fortin, D., 2001. The effect of growth phase on proton and metal adsorption by *Bacillus subtilis*. Geochim. Cosmochim. Acta 65: 1025-1035.

Daughney, C.J., Fein, J.B., 1998. The effect of ionic strength on the adsorption of H^+, Cd^{2+}, Pb^{2+}, and Cu^{2+} by *Bacillus subtilis* and Bacillus licheniformis: a surface complexation model. J. Coll. Interf. Sci. 198: 53-77.

Daughney C.J., Fein J.B., Yee, N., 1998. A comparison of the thermodynamics of metal adsorption onto two common bacteria. Chem. Geol. 144: 161-176.

Davranche, M., Pourret, O., Gruau, G., Dia, A., Le Coz-Bouhnik, M., 2005. Adsorption of REE(III)-humate complexes onto MnO_2: Experimental evidence for cerium anomaly and lanthanide tetrad effect suppression. Geochim. Cosmochim. Acta 69(20): 4825-4835.

Davranche, M., Bollinger, J.-C., Bril, H., 2003. Effect of reductive conditions on metal mobility from wasteland solids: an example from the Mortagne-du-Nord site (France). Appl. Geochem. 18(3): 383-394.

Davranche, M., Bollinger, J.-C., 2000a. Release of Metals from Iron Oxyhydroxides under Reductive Conditions: Effect of Metal/Solid Interactions. J. Colloid Interf. Sci. 232(1): 165-173.

Davranche, M., Bollinger, J.-C., 2000b. Heavy Metals Desorption from Synthesized and Natural Iron and Manganese Oxyhydroxides: Effect of Reductive Conditions. J. Colloid Interf. Sci. 227(2): 531-539.

Deng, Y.W., Stumm, W., 1994. Reactivity of aquatic iron(III) oxyhydroxides implications for redox cycling of iron in natural-waters. Appl. Geochem. 9(1): 23-36.

Dia, A., Gruau, G., Olivié-Lauquet, G., Riou, C., Molénat, G., Curmi, P., 2000. The distribution of rare earth elements in groundwaters: Assessing the role of source-rock composition, redox changes and colloidal particles. Geochim. Cosmochim. Acta 64: 4131-4151.

Dixit, S., Hering, J.G., 2003. Comparison of arsenic(V) and arsenic(III) sorption onto iron oxide minerals: implications for arsenic mobility. Environ. Sci. Technol. 37: 4182-4189.

Doyle, C.S., Kendelewicz, T., Bostick, B.C., Brown, G.E. 2004. Soft X-ray spectroscopic studies of the reaction of fractured pyrite surfaces with Cr (Vl)-containing aqueous solutions, Geochim. Cosmochim. Acta 68: 4287–4299.

Doyle, R.J., Matthews, T.H., Streips, U.N., 1980. Chemical basis for selectivity of metal ions by the *Bacillus subtilis* cell wall. J. Bacteriol. 143: 471-480.

Durand, P., Torres, J.L., 1996. Solute transfer in agricultural catchments: the interest and limits of mixing models. J. Hydrol. 181:1-22.

Dzombak, D.A., Morel, F.M.M., 1990. Surface Complexation Modeling Hydrous Ferric Oxide. Wiley & Sons, NY.

Ehrenreich, A., Widdel, F., 1994. Anaerobic oxidation of ferrous iron by purple bacteria, a new-type of phototrophic metabolism. Appl. Environ. Microbiol. 60(12): 4517-4526

Elliott, H. A., Liberati, M. R. et Huang, C. P., 1986. Effect of iron oxide removal on heavy metal sorption by acid subsoils. Water, Air, & Soil Pollution, 27:379-389.

Emerson, D., 2000. Microbial oxidation of Fe(II) and Mn(II) at circumneutral pH. In Environmental Microbe-Metal Interactions, Lovley, D.R., Ed.; ASM Press: Washington, D.C.

Emerson, D., Weiss, J.V., Megonigal, J.P., 1999. Iron-oxidizing bacteria are associated with ferric hydroxide precipitates (Fe-plaque) on the roots of wetlands plants. Appl. Environ. Microbiol. 65: 2758-2761.

Emerson, D., Moyer, C.L., 1997. Isolation and characterization of novel iron-oxidizing bacteria that grow at circumneutral pH, Appl. Environ. Microbiol. 63: 4784–4792.

Ehrlich, H.L., 1996. How microbes influence mineral growth and dissolution. Chem. Geol. 132: 5-9.

Ehrlich, H.L., 1990. Geomicrobiology. Marcel Dekker, Inc., New York.

Fakih, M., Châtellier, X., Davranche, M., Dia, A., 2008a. *Bacillus subtilis* bacteria hinder the oxidation and hydrolysis of Fe^{2+} ions. Environ. Sci. Technol. 42: 3194-3200.

Fakih, M., Davranche, M., Dia, A., Nowack, B., Petitjean, P., Châtellier, X., Gruau, G., (2008b, En révision). A new tool for in situ monitoring of Fe-mobilization in soils. Appl. Geochem.

Fakih, M., Davranche, M., Dia, A., Nowack, B., Morin, G., Petitjean, P., Châtellier, X., Gruau, G., (2008c, soumis). Environmental impact of As(V)-Fe oxyhydroxide reductive dissolution: an experimental insight from *in situ* monitoring. Chem. Geol.

Fein, J.B., Daughney, C.J., Yee, N., Davis, T.A., 1997. A chemical equilibrium model for metal adsorption onto bacterial surfaces. Geochim. Cosmochim. Acta 61: 3319-3328.

Fein, J.B., Martin, A.M., Wightman, P.G., 2001. Metal adsorption onto bacterial surfaces: development of a predictive approach. Geochim. Cosmochim. Acta 65: 4267-4273.

Ferris, F.G., Hallberg, R.O., Lyvén, B., Pedersen, K., 2000. Retention of strontium, cesium, lead and uranium by bacterial iron oxides from a subterranean environment. Appl. Geochem. 15: 1035-1042.

Ferris, F.G., Konhauser, K.O., Lyvén, B., Pedersen, K., 1999. Accumulation of metals by bacteriogenic iron oxides in a subterranean environment. Geomicrob. J., 16: 181-192.

Ferris, F.G., Schultze, S., Witten, T.C., Fyfe, W.S., Beveridge, T.J., 1989. Metal interactions with microbial biofilms in acidic and neutral pH environments. Appl. Environ. Microbiol. 55: 1249-1257.

Fischer, W.R., 1988. Microbiological reactions of iron in soils. In: Stucki, J.W., Goodman, B.A., Schwertmann, U. (Eds.), Iron in Soils and Clay Minerals. Reidel, Dordrecht, pp. 715 749.

Fortin, D., Glasauer, S., Langley, R.S., 2007. Biominerals. Recorders of the past? In: Biomineralization. From Nature to Application, Vol. 4 of Metal Ions in Life Sciences, (A. Sigel, H. Sigel, R.K.O. Sigel (Eds)), John Wiley & Sons, Ltd., Chichester, UK (in press).

Fortin, D., Langley, S., 2005. Formation and occurrence of biogenic iron-rich minerals. Earth Sci. Rev. 72: 1-19.

Fortin, D., 2004. What biogenic minerals tell us. Science 303: 1618-1619.

Fortin, D., Beveridge, T.J., 2000. Mechanistic routes towards biomineral surface development. In Biomineralisation: From Biology to Biotechnology and medical Application (E. Baeuerlein Ed.), Wiley-VCH, Verlag, Germany, 294 p.

Fortin, D., Ferris, F.G., Scott, S.D., 1998. Formation of Fe-silicates and Fe-oxides on bacterial surfaces in hydrothermal deposits collected near the Southern Explorer Ridge in the Northeast Pacific Ocean. Am. Mineral. 83: 1399-1408.

Fortin, D., Ferris, F.G., 1998. Precipitation of iron, silica, and sulfate on bacterial cell surfaces. Geomicrobiol. J. 15: 309-324.

Fortin, D., Ferris, F.G., Beveridge, T.J., 1997. Surface-mediated mineral development by bacteria. In Geomicrobiology: Interactions between microbes and minerals; Banfield, J. F., Nealson, K.H., Eds.; Mineralogical Society of America: Washington D.C., 35: 161-180.

Fortin, D., Davis, B.S., Beveridge, T.J., 1996. Role of Thiobacillus and sulfate-reducing bacteria in iron biocycling in oxic and acidic mine tailings. FEMS Microbiol. Ecol. 21: 11-24.

Fortin, D., Leppard, G.G., Tessier, A., 1993. Characteristics of lacustrine diagenetic iron oxyhydroxides. Geochim. Cosmochim. Acta 57: 4391-4404.

Fowle, D.A., Fein, J.B., 1999. Competitive adsorption of metal cations onto two gram positive bacteria: Testing the chemical equilibrium model. Geochim. Cosmochim. Acta 63: 3059–3067.

Fox, P.M., Doner, H.E., 2002. Wetlands and aquatic processes - Trace element retention and release on minerals and soil in a constructed wetland. J. Environ. Qual. 31(1): 331-338.

Francis, A.J., Dodge, C.J., 1990. Anaerobic Microbial Remobilization of Toxic Metals Coprecipitated with Iron Oxide. Environ. Sci. Technol. 24: 373-378.

Francis, A.J., Dodge, C.D., 1988. Anaerobic Microbial Dissolution of Transition and Heavy Metal Oxides. Appl. Environ. Microbiol. 54: 1009-1014.

Fredrickson, J.K., Kukkadapu, R.K., Liu, C.K., Zachara, J.M., 2003. Influence of electron donor/acceptor concentrations on hydrous ferric oxide (HFO) bioreduction. Biodegradation 14: 91-103.

Fredrickson, J.K., Zachara, J.M., Kukkadapu, R.K., Gorby, Y.A., Smith, S.C., Brown, C.F.., 2001. Biotransformation of Ni-substituted hydrous ferric oxide by an Fe(III)-reducing bacterium. Environ. Sci. Technol. 35(4): 703-712.

Fredrickson, J.k., Zachara, J.M., Kennedy, D.W., Dong, H.L., Onstott, T.C., Hinman N.W., Li. Sm., 1998. Biogenic iron mineralization accompanying the dissimilatory reduction of hydrous ferric oxide by a groundwater bacterium. Geochim. Cosmochim. Acta 62(19-20): 3239-3257.

Freeze, R.A., Cherry. J.A., 1979. Groundwater. Prentice Hall, Inc.

Gadd, G.M., 1986. The uptake of heavy metals by fungi and yeasts: the schemistry and physiology of the process and applications for biotechnology. In: Eccles HH, Hunt S (eds) Immobilisation of ions by biosorption. Ellis Horwood, Chichester, UK, pp 135–147.

Gambrell R.P., Khalid R.A. et Patrick W.H.Jr., 1980. Chemical availability of Mercury, Lead, and Zinc in mobile bay sediment suspensions as affected by pH and oxidation-reduction conditions. Environmental Science and Technology, 14: 431-436.

Gao, Y., Mucci, A., 1999. Acid base reactions, phosphate and arsenate complexation, and their competitive adsorption at the surface of goethite in 0.7 M NaCl solution. Geochim. Cosmochim. Acta 65: 2361-2378.

Garelick, H., Dybowska, A., Valsami-Jones, E., Priest, N.D., 2005. Remediation technologies for arsenic contaminated drinking waters. J. Soils Sediments. 5(3): 182-190.

Germida, J.J., Wainwright, M., Gupta, V.V.S.R., 1992. Biochemistry of sulfur cycling in soil. In: G. Stotzky, J.-M. Bollag (Editors), Soil biochemistry. Marcel Dekker, New York. Vol 7, pp 1-53.

Glasauer, S., Weidler, P. G., Langley, S., Beveridge, T. J., 2003. Controls on Fe reduction and mineral formation by a subsurface bacterium. Geochim. Cosmochim. Acta 67: 1277-1288.

Goldberg, S., Johnston, C. T., 2001. Mechanisms of Arsenic Adsorption on Amorphous Oxides Evaluated Using Macroscopic Measurements, Vibrational Spectroscopy, and Surface Complexation Modeling. J. Colloid Interface Sci. 234 : 204-216.

Gordon, H.R., Clark, D.K., Brown, J.W., Brown, O.B., Evans, R.H., 1982. Satellite measurement of the phytoplankton pigment concentration in the surface waters of a warm core gulf-stream ring. J. Mar. Res. 40(2): 491-502.

Green, C.H., Heil, D.M., Cardon, G.E., Butters, G.L., Kelly, E.F., 2003. Solubilization of Manganese and Trace Metals in Soils Affected by Acid Mine Runoff. J. Environ. Qual. 32(4): 1323-1334.

Gruau, G., Dia, A., Olivié-Lauquet, G., Davranche, M., Pinay, G., 2004. Controls on the distribution of rare earth elements in shallow groundwaters. Wat. Res 38(16): 3576-3586.

Grybos, M., Davranche, M., Gruau, G., Petitjean, P., 2007. Is trace metal release in wetland soils controlled by organic matter mobility or Fe-oxyhydroxides reduction? J. Colloid Interf. Sci. 314: 490-501.

Guibal, E., Roulph, C., Cloirec, P.L., 1995. Infrared spectroscopic study of uranyl biosorption by fungal biomass and materials of biological origin. Environ. Sci. Technol. 29: 2496–2502.

Guine, V., Spadini, L., Sarret, G., Muris, M., Delolme, C., Gaudet, J.P., Martins, J.M.F., 2006. Zinc sorption to three gram-negative bacteria: combined titration, modeling, and EXAFS study. Environ. Sci. Technol. 40: 1806-1813.

Hansel, C. M.; Benner, S. G.; Neiss, J.; Dohnalkova, A.; Kukkadapu, R. K.; Fendorf, S., 2003. Secondary mineralization pathways induced by dissimilatory iron reduction of ferrihydrite under advective flow. Geochim. Cosmochim. Acta, 67(16): 2977-2992.

Harvey, C.F., Swartz, C.H., Badruzzaman, A.B.M., Keon-Blute, N., Yu, W., Ali, M.A., Jay, J., Beckie, R., Niedan, V., Brabander, D., Oates, P.M., Ashfaque, K.N., Islam, S, Hemond, H.F., Ahmed, M.F., 2002. Arsenic mobility and groundwater extraction in Bangladesh. Science. 298(5598): 1602-1606.

Hering, J.G., Kraemer, S., 1998. Environmental chemistry of trace metals. In: Macalady, D.L. (Editors), Perspectives in environmental chemistry. Oxford university press, New York Oxford. pp 57-74.

Hiemstra, T., van Riemsdijk, W.H., 1999. Surface structural ion adsorption modeling of competitive binding of oxyanions by metal (Hydr)oxides. J. Coll. Int. Sci. 210: 182-193.

Islam, F.S., Gault, A.G., Boothman, C., Polya, D.A., Charnock, J.M., Chatterjee, D., Lloyd, J.R., 2004. Role of metal-reducing bacteria in arsenic release from Bengal delta sediments. Nature 430(6995): 68-71.

Jackson, T.A., West, M.M., Leppard, G.G., 1999. Accumulation of heavy metals by individually analyzed bacterial cells and associated nonliving material in polluted lake sediments. Environ. Sci. Technol. 33: 3795-3801.

James, R.E., Ferris, F.G., 2004. Evidence for microbial-mediated iron oxidation at a neutrophilic groundwater spring. Chem. Geol. 212: 301-311.

Jenkinson, B.J., Franzmeier, D.P., 2006. Development and Evaluation of Iron-Coated Tubes that Indicate Reduction in Soils. Soil Sci. Soc. Am. Jour. 70: 183-191.

Jorgensen, S. S., Willems, M., 1987. The fate of lead in soils - the transformation of lead pellets in shooting-range soils. Ambio 16: 11-15.

Juste C., 1988. Appréciation de la mobilité et de la biodisponibilité des éléments en traces du sol. Science du sol, 26: 103-112.

Kaplan, D.I., Bertsch, P.M., Adriano, D.C., 1997. Mineralogical and physicochemical differences between mobile and nonmobile colloidal phases in reconstructed pedons. Soil Sci. Soc. Am. J. 61(2): 641-649.

Kappler, A., Newman, D.K., 2004. Formation of Fe(III)-minerals by Fe(II)-oxidizing photoautotrophic bacteria. Geochim. Cosmochim. Acta 68: 1217– 1226.

Kocar, B.D., Herbel, M.J., Tufano, K.J., Fendorf, S., 2006. Contrasting effects of dissimilatory iron(III) and arsenic(V) reduction on arsenic retention and transport. Environ. Sci. Technol. 40(21): 6715-6721.

Konhauser, K.O., Ferris, F.G., 1996. Diversity of iron and silica precipitation by microbial mats in hydrothermal waters, Iceland: Implications for Precambrian iron formations. Geology 24: 323- 326.

Koretsky, C.M., Moore, K.L. Lowe, C. Meile, T.J. DiChristina, P. Van Cappellen, 2003. Seasonal oscillation of microbial iron and sulfate reduction in saltmarsh sediments (Sapelo Island, GA, USA), Biogeochem. 64: 179–203.

Kukkadapu, R.K., Zachara, J.M., Smith, S.C., Fredrickson, J.K., Liu, C.X., 2001. Dissimilatory bacterial reduction of Al-substituted goethite in subsurface sediments. Geochim. Cosmochim. Acta 65: 2913-2924.

Kulczycki, E., Fowle, D.A., Fortin, D., Ferris, F.G., 2005. Sorption of cadmium and lead by bacteria-ferrihydrite composites. Geomicrob. J. 22: 299-310.

Küsel, K., Wagner, C., Trinkwalter, T., Gössner, A.S., Bäumler, R., Drake, H.L., 2002. Microbial reduction of Fe(III) and turnover of acetate in Hawaiian soils. FEMS Microbiol. Ecol. 40: 73-81.

LaForce, M.J., Hansel, C.M., Fendorf, S., 2000. Arsenic speciation, seasonal transformations, and co-distribution with iron in a mine waste-influenced palustrine emergent wetland. Environ. Sci. Technol. 34: 3937–3943.

Langmuir, D., 1997. Aqueous Environmental Geochemistry. Prentice-Hall, New Jersey.

Larsen, O., Postma, D., 2001. Kinetics of reductive bulk dissolution of lepidocrocite, ferrihydrite, and goethite. Geochim. Cosmochim. Acta 65(9): 1367-1379.

Liu, C., Zachara, J.M., Gorby, Y.A., Szecsody, J.E., Brown, C.F., 2001. Microbial reduction of Fe(III) and sorption/precipitation of Fe(II) on Shewanella putrefaciens strain CN32. Environ. Sci. Technol. 35: 1385-1393.

Lovley, D.R., 2000. Iron(III) and Mn(IV) reduction. In: Lovley, D.R. (Ed.), Environmental microbemetal interactions. ASM Press, Washington, D.C.

Lovley, D.R., 1997. Microbial Fe(III) reduction in subsurface environments. FEMS Microbiol. Rev. 20(3-4): 305-313.

Lovley, D.R., Coates, J.D., 1997. Bioremediation. of metal contamination. Current Opinion in Biotechnology 8: 285-289.

Lovley, D.R., 1993. Anaerobes into Heavy-Metal - Dissimilatory Metal Reduction in Anoxic Environments. Trends in Ecology and Evolution 8(6): 213-217.

Lovley, D.R., 1991. Dissimilatory Fe(III) and Mn(IV) reduction. Microbiol. Rev. 55: 259-287.

Lovley, D.R., Phillips, E.J.P., Lonergan, D.J., 1991. Enzymatic versus nonenzymatic mechanisms for Fe(III) reduction in aquatic sediments. Environ. Sci. Technol. 25: 1062-1067.

Lovley, D.R., Phillips, E.J.P., 1988. Novel mode of microbial energy metabolism: Organic carbon oxidation coupled to dissimilatory reduction of iron or manganese. Appl. Environ. Microbiol. 54: 1472-1480.

Lovley, D.R., Stolz, J.F., Nord, G.L.Jr., Phillips, E.J.P., 1987. Anaerobic production of magnetite by dissimilatory iron-reducing microorganism. Nature 330: 420-434.

Lovley, D.R., Phillips, E.J.P., 1986a. Availability of Ferric Iron for Microbial Reduction in Bottom Sediments of the Freshwater Tidal Potomac River. Appl. Environ. Microbiol. 52: 751-757.

Lovley, D.R., Phillips, E.J.P., 1986b. Organic Matter Mineralization with Reduction of Ferric Iron in Anaerobic Sedimant. Appl. Environ. Microbiol. 51(4): 683-689.

Luo, J., Tillman, R.W., Ball, P.R., 1999. Factors regulating denitrification in a soil under pasture. Soil Biol. Biochem. 31(6): 913-927.

Manning, B.A., Fendorf, S.E., Goldberg, S., 1998. Surface structures and stability of arsenic(III) on goethite: spectroscopic evidence for innersphere complexes. Environ. Sci. Technol. 32: 2383–2388.

Martinez, R.E., Pedersen, K., Ferris, F.G., 2004. Cadmium complexation by bacteriogenic iron oxides from a subterranean environment. J. Colloid. Interf. Sci. 275: 82-89.

Mavrocordatos, D., Fortin, D., 2002. Quantitative characterization of biotic iron oxides by analytical electron microscopy. Amer. Mineral. 87: 940-946.

Mayers, I.T., Beveridge, T.J., 1989. The sorption of metals to *Bacillus subtilis* walls from dilute solutions and simulated Hamilton harbour (Lake Ontario) water. Can. J. Microbiol. 35: 764-770.

McArthur, J.M., Ravenscroft, P., Safiulla, S., Thirlwall, M.F., 2001. Arsenic in groundwater: Testing pollution mechanisms for sedimentary aquifers in Bangladesh. Water Resour. Res. 37(1): 109-117.

McArthur, J.M., Banerjee, D.M., Hudson-Edwards, K.A., Mishra, R., Purohit, R., Ravenscroft, P., Cronin, A., Howarth, R.J., Chatterjee, A., Talukder, T., Lowry, D., Houghton, S., Chadha, D.K., 2004. Natural organic matter in sedimentary basins and its

relation to arsenic in anoxic ground water: the example of West Bengal and its worldwide implications. Appl. Geochem. 19(8): 1255-1293.
McBride, M.B., 1994. Environmental Chemistry of Soils. New York: Oxford University Press. 406 p.
Molénat, J., Davy, P., Gasuel-Odoux, C. Durand, P., 1999. Study of three subsurface hydrologic systems based on spectral and cross-spectral analysis of time. J. Hydrol. 222: 152-164.
Morin, G., Calas, G., 2006. Arsenic in soils, mine tailings, and former industrial sites. Elements 2: 97-101.
Morin, G., Juillot, F., Casiot, C., Bruneel, O., Personne, J.C., Elbaz-Poulichet, F., Leblanc, M., Ildefonse, P., Calas, G., 2003. Bacterial formation of tooeleite and mixed Arsenic (III) or Arsenic (V)-Iron(III) gels in the carnoulès acid mine drainage, France. A XANES, XRD, and SEM study. Environ. Sci. Technol. 37(9): 1705-1712.
Morin, G., Lecocq, D., Juillot, F., Calas. G., Ostergren, J. D., Ildefonse, P., Belin, S., Briois, V., Dillmann, P., Chevallier, P., Gauthier, C., Sole, A., Petit, P. E., Borensztajn, S., 2002a. Arsenic(V) adsorbé et pharmacosidérite dans un sol développé sur l'anomalie géochimique d'Échassière, Allier, France. Bull. Soc. Geol. France 173: 281-291.
Morin, G., Lecocq, D., Juillot, F., Calas, G., Ildefonse, P., Belin, S., Briois, V., Dillmann, P., Chevallier, P., Gauthier, C., Sole, A., Petit, P.E., Borensztajn, S., 2002b. EXAFS evidence of sorbed arsenic(V) and pharmacosiderite in soil overlying the Eschassières geochemical anomaly, Allier, France. Bull. Soc. Geol. Fr. 173: 281-291.
Morin, G., Ostergren, J., Juillot, F., Ildefonse, P.; Calas, G.; Brown, G. E. J., 1999. XAFS determination of the chemical form of lead in smelter-contaminated soils and mine tailings: importance of sorption processes. Am. Min. 84: 420-434.
Mortimer, R. J. G., Coleman, M. L., 1997. Microbial influence on the isotopic composition of diagenic siderite. Geochim. Cosmochim. Acta 61: 1705-1711.
Munch, J.C., Ottow, J.C.G., 1980. Preferential reduction of amorphous to crystalline iron-oxides by bacterial-activity. Soil Sci. 129(1): 15-21.
Ngwenya, B.T., Sutherland, I.W., Kennedy, L., 2003. Comparison of the acid-base behaviour and metal adsorption characteristics of a gram-negative bacterium with other strains. Appl. Geochem. 18: 527-538.
Nickson, R.T., McArthur, J.M., Ravenscroft, P., Burgess, W.G., Ahmed, K.M., 2000. Mechanism of arsenic release to groundwater, Bangladesh and West Bengal. Appl. Geochem. 15: 403–413.
Olivié-Lauquet, G., Gruau, G., Dia, A., Riou, C., Jaffrezic, A., Henin, O., 2001. Release of trace elements in wetlands: role of seasonal variability. Wat. Res. 35: 943-952.
Ona-Nguema, G., Morin, G., Wang, Y., Juillot, F., Guyot, F., Calas, G., Brown, Jr., G. E. (soumis). Influence of arsenic on the reduction of lepidocrocite and green rust into ferrous-carbonate hydroxide by Shewanella putrefaciens. Environ. Sci. Technol.
Ona-Nguema, G., Abdelmoula, M., Jorand, F., Benali, O., Géhin, A., Block, J.-C., Génin, J.M.R., 2002. Iron(II,III) hydroxycarbonate green rust formation and stabilization from lepidocrocite bioreduction. Environ. Sci. Technol. 36(1) : 16-20.
Ona-Nguema, G., Carteret, C., Benali, O., Abdelmoula, M., Génin, J.-M. R., Jorand, F., 2004. Competitive formation of hydroxycarbonate green rust I vs hydroxysulphate green rust II in Shewanella putrefaciens cultures. Geomicrobiol. J. 21(3): 79-90.
Ona-Nguema G., 2003. Biogenèse d'hydroxysels mixtes Fe(II-III) de type rouille verte en culture bactérienne (Shewanella putrefaciens). Thèse en Chimie et Microbiologie de l'Eau, Univ. de Nancy I.
Oremland, R.S., Stolz, J.F., 2003. The ecology of arsenic. Science 300(5621): 939-944.

Ozverdi, A., Erdem, M., 2006. Cu^{2+}, Cd^{2+} and Pb^{2+} adsorption from aqueous solutions by pyrite and synthetic iron sulphide, J. Hazard. Mater. 137: 626–632.

Paige, C.R., Snodgrass, W.J., Nicholson, R.V., Scharer, J.M., 1997. An arsenate effect on ferrihydrite dissolution kinetics under acidic oxic conditions. Water Res. 31(9): 2370-2382.

Pedersen, H.D., Postma, D., Jakobsen, R., 2006. Release of arsenic associated with the reduction and transformetion of iron oxides. Geochimica Cosmochimica Acta 70: 4116-4129.

Peters, V., Conrad, R., 1996. Sequential reduction processes and initiation of CH_4 production upon flooding of oxic upland soils. Soil Biol. Biochem. 28(3): 371-382.

Postma, D., 1993. The reactivity of iron-oxides in sediments - a kinetic approach. Geochim. Cosmochim. Acta 57(21-22): 5027-5034.

Pourret, O., Dia, A., Davranche, M., Gruau, G., Henin, O., Angée, M., 2007. Organo-colloidal control on major- and trace-element partitioning in shallow groundwaters: confronting ultrafiltration and modelling. Appl. Geochem 22: 1568-1582.

Pelmont, J., 1993. Bactéries et environnement. Adaptations physiologiques. Presses Universitaires de Grenoble.

Quantin, C., Becquer, T., Rouiller, J.H., Berthelin, J., 2001. Oxide weathering and trace metal release by bacterial reduction in a New Caledonia Ferralsol. Biogeochem. 53: 323-340.

Quantin, C., Becquer, T., Rouiller, J.H., Berthelin J., 2002. Redistribution of Metals in a New Caledonia Ferralsol After Microbial Weathering. Soil Sci. Soc. Am. J. 66: 1797-1804.

Rajot, J.L., 1992. Dissolution des oxydes de fer (hématite et goethite) d'un sol ferralitique des Llanos de Colombie par des bactéries ferri-réductrices. Thèse en Géomicrobiologie. Univ. de Nancy I.

Rancourt, D.G., Thibault, P.J., Mavrocordatos, D., Lamarche, G., 2005. Hydrous ferric oxide precipitation in the presence of nonmetabolizing bacteria: Constraints on the mechanism of a biotic effect. Geochim. Cosmochim. Acta 69, 553-577.

Randall, S.R., Sherman, D.M., Ragnarsdottir, K.V., Collins, C.R., 1999. The mechanism of cadmium surface complexation on iron oxyhydroxide minerals. Geochim. Cosmochim. Acta 63: 2971-2987.

Raven, K.P., Jain, A., Loeppert, R.H., 1998. Arsenite and arsenate adsorption on ferrihydrite: Kinetics, equilibrium, and adsorption envelopes. Environ. Sci. Technol. 32(3): 344-349.

Ricqlès, A., Livage, J., 2004. An introduction to biomineralisation: diversity and unity. Biomineralisation : Diversite et Unite 3(6-7): 435-441.

Roden E.E. 2006. Geochemical and microbiological controls on dissimilatory iron reduction C. R. Geosci. 338: 456-467

Roden, E.E., 2003. Fe(III) oxide reactivity toward biological versus chemical reduction. Environ. Sci. Technol. 37(7): 1319-1324.

Roden, E.E., Urrutia, M.M., 2002. Influence of biogenic Fe(II) on bacterial crystalline Fe(III) oxide reduction. Geomicrobiol. J. 19: 209-251.

Roden, E.E., Wetzel, R.G., 2002. Kinetics of microbial Fe(III) oxide reduction in freshwater wetland sediments. Limnol. Oceanogr. 47(1): 198-211.

Roden, E. E., Urrutia, M. M., 1999. Ferrous iron removal promotes microbial reduction of crystalline iron(III) oxides. Environ. Sci. Technol. 33: 1847-1853.

Roden, E. E., Zachara, J. M., 1996. Microbial reduction of crystalline iron(III) oxides: Influence of oxide surface area and potential for cell Growth Environ. Sci. Technol. 30: 1618-1628

Roden, E.E., Lovley, D.R., 1993. Dissimilatory Fe(III) reduction by the marine microorganism desulfuromonas-acetoxidans. Appl. Environ. Microbiol. 59(3): 734-742.

Rose, A.L., Waite, T.D., 2002. Kinetic model for Fe(II) oxidation in seawater in the absence and presence of natural organic matter. Environ. Sci. Technol. 36: 433-444.
Sadiq, M., 1997. Arsenic chemistry in soils: An overview of thermodynamic predictions and field observations. Water Air Soil Pollut. 93: 117-136.
Santana-Casiano, J.M., Gonzalez-Davila, M., Rodriguez, M.J., Millero, F.J., 2000. The effect of organic compounds in the oxidation kinetics of Fe(II). Mar. Chem. 70: 211-222.
Santo, L.Y., Doi, R.H., 1974. Ultrastructural analysis during germination and outgrowth of *Bacillus subtilis* spores. J. Bacteriol. 120: 475-481.
Scheidegger, A., Borkovec, M., Sticher, H., 1993. Coating of silica sand with goethite - preparation and analytical identification. Geoderma 58(1-2): 43-65.
Schultze-Lam, S., Fortin, D., Davis, B.S., Beveridge, T.J., 1996. Mineralization of bacterial surfaces. Chem. Geol. 132: 171-181.
Schwarz, O., 2002. Polymethylmethacrylate [PMMA]. In: O. Schwarz (Editor), Kunststoffkunde. Vogel Verlag, Würzburg. ISBN 3802319176.
Schwertmann, U., Cornell, R., 2000. Iron oxides in the laboratory. Preparation and characterization. Wiley Editors, New York. pp188.
Schwertmann, U., Cornell, R.M., 1991. Iron oxides in the Laboratory: preparation and characterization. Wiley-VCH, Weinheim, Germany.
Schwertmann, U., Taylor, R.M., 1989. Iron oxides. In: J.B. Dixon, S.B. Weed (Editors), Minerals in soil environments. ASA and SSSA, Madison, WI, pp. 379-438.
Schwertmann, U. Latham, M., 1986. Properties of iron oxides in some New Caledonian Oxisols. Geoderma 39: 105–123
Schwertmann, U., Taylor, R.M., 1979. Natural and synthetic poorly crystallized lepidocrocite. Clay Miner. 14: 285-293.
Sigg, L., Xue, H.B., Kistler, D., Sshonenberger, R., 2000. Size fractionation (dissolved, colloidal and particulate) of trace metals in the Thur River, Switzerland. Aquat. Chem. 6(4): 413-434
Slowey, A.J., Johnson, S.B., Newville, M., Brown, Jr.G.E., 2007. Speciation and colloid transport of arsenic from mine tailings. Appl. Geochem. 22: 1884-1898.
Small, T.D., Warren, L.A., Roden, E.E., Ferris, F.G., 1999. Sorption of strontium by bacteria, fe(III) oxide, and bacteria - Fe(III) oxide composites. Env. Sci. Tech. 33: 4465-4470.
Smedley, P.L., Kinniburgh, D.G., 2002. A review of the source, behaviour and distribution of arsenic in natural waters. Appl. Geochem. 17: 517-568.
Soma, M., Tanaka, A., Seyama, H., Satake, K., 1994. Characterization of arsenic in lake sediments by X-ray photoelectron spectroscopy. Geochim. Cosmochim. Acta 58: 2743–2745.
Spadini, L., Schindler, P.W., Charlet, L., Manceau, A., Ragnarsdottir, K.V., 2003. Hydrous ferric oxide: evaluation of Cd-HFO surface complexation models combining Cd-K EXAFS data, potentiometric titration results, and surface site structures identified from mineralogical knowledge. J. Colloid. Interf. Sci. 266: 1-18.
Stachowicz, M., Hiemstra, T., Van Riemsdijk, W.H., 2007. Multi-competitive interaction of As(III) and As(V) oxyanions with Ca^{2+}, Mg^{2+}, PO_4^{3-}, and CO_3^{2-} ions on goethite. J. Colloid Interf. Sci. 320: 400-414.
Straub, K.L., Schonhuber, W.A., Buchholz-Cleven, B.E.E., Schink, B., 2004. Diversity of ferrous iron-oxidizing, nitrate-reducing bacteria and their involvement in oxygen-independent iron cycling. Geomicrobiol. J. 21(6): 371-378.
Straub, K.L., Benz, M., Schink, B., Widdel, F., 1996. Anaerobic, nitrate-dependent microbial oxidation of ferrous iron. Appl. Environ. Microbiol. 62: 1458– 1460.
Stumm, W., Morgan, J.J., 1996. Aquatic Chemistry: Chemical Equilibria and Rates in Natural Waters, 3rd edition. Wiley-Interscience, New York, NY, p. 1040

Stumm, W., Morgan, J.J., 1970. Aquatic Chemistry, An Introduction Emphasizing Chemical Equilibria in Natural Waters, Wiley Interscience (1970), p. 583.

Sun T., Paige C.R., Snodgrass W.J. 1999. Combined effect of arsenic and cadmium on the transformation of ferrihydrite onto crystalline products, Journal of University of Science and Technology Beijing 6: 168–173.

Tamura, H., Kawamura, S., Hagayama, M., 1980. Acceleration of the oxidation of Fe2+ ions by Fe(III)-oxyhydroxides. Corros. Sci. 20: 963-971.

Templeton, A., Brown, G.E., 2003. Speciation of Pb(II) sorbed by Burkholderia cepacia/goethite composites. Environ. Sci. Technol. 37: 2166-2172.

Tipping, E., Woof, C., Cooke, D., 1981. Iron-oxide from a seasonally anoxic lake. Geochim. Cosmochim. Acta 45(9): 1411-1419.

Tobin, J.M., Cooper, D.G., Neufeld, R.J., 1990. Investigation of the mechanism of metal uptake by denatured Rhizopus arrhizus biomass. Enzyme Microb. Technol. 12: 591-595.

Trolard F, Tardy Y., 1989. A model of Fe^{3+}-kaolinite, Al^{3+}-goethite, Al^{3+}-hematite equilibria in laterites. Clay Minerals 24(1): 1-21.

Tüfekci, N., Sarikaya, H.Z., 1996. Catalytic effects of high Fe(III) concentrations on Fe(II) oxidation. Wat. Sci. Technol. 34: 389-396.

Urrutia, M.M., Roden, E.E., 1998. Microbial and surface chemistry controls on reduction of synthetic Fe(III) oxide minerals by the dissimilatory iron-reducing bacterium Shewanella alga. Geomicrobiol. J. 15: 269-291.

Van Geen, A., Zheng, Y., Goodbred, S., Horneman, J.R. A., Aziz, Z., Cheng, Z., Stute, M., Mailloux, B., Weinman, B., Hoque, M.A., Seddique, A.A., Hossain, M.S., Chowdhury, S.H., Ahmed, K.M., 2008. Flushing history as a hydrogeological control on the regional distribution of arsenic in shallow groundwater of the Bengal basin. Environ. Sci. Technol. 42: 2283-2288.

Van Geen, A., Rose J., Thoral S., Garnier J.M., Zheng Y., Bottero J.Y., 2004. Decoupling of As and Fe release to Bangladesh groundwater under reducing conditions. Part II. Evidence from sediment incubations, Geochim. Cosmochim. Acta 68: 3475–3486.

Venema, P., Hiemstra, T., van Riemsdijk, W.H., 1996. Multisite adsorption of cadmium on goethite. J. Colloid. Interf. Sci. 183: 515-527.

Viollier, E., Inglett, P.W., Hunter, K., Roychoudhury, A.N., Van Cappellen, P., 2000. The ferrozine method revisited: Fe(II)/Fe(III) determination in natural waters. Appl. Geochem. 15: 785-790.

Voegelin, A., Scheinost, A. C., Buhlmann, K., Barmettler, K., Kretzschmar, R., 2002. Slow formation and dissolution of Zn precipitates in soil - A combined column-transport and XAFS study. Environ. Sci. Technol. 36: 3749-3754.

Wahid, P.A., Kamalam, N.V., 1993. Reductive dissolution of crystalline and amorphous Fe(III) oxides by microorganisms in submerged soil. Biol. Fertil. Soils. 15(2): 144-148.

Wang, Y., Morin, G., Ona-Nguema, G., Menguy, N., Juillot, F., Olivi, L., Villain, F., Aquilini, G., Guyot, F., Bargar, J., Calas, G., Brown, Jr.G.E. (soumis). Multinuclear As(III) sorption on nano-Fe(OH)2 during bioreduction of As(V)-sorbed lepidocrocite by Shewanella putrefaciens. Geochim. Cosmochim. Acta.

Wang, Y., Morin, G., Ona-Nguema, G., Menguy, N., Juillot, F., Aubry, E., Guyot, F., Calas, G., Brown, Jr. G.E., 2008. Arsenite sorption at the magnetite-water interface during aqueous precipitation of magnetite. EXAFS evidence of a new surface complex. Geochim. Cosmochim. Acta 72: 2573-2586.

Warren, L.A., Haak, E.A., 2001. Biogeochemical controls on metal behavior in freshwater environments. Earth Sci. Rev. 54: 261–320.

Warren, L.A., Ferris, F.G., 1998. Continuum between sorption and precipitation of Fe(III) on microbial surfaces. Environ. Sci. Technol. 32: 2331-2337.

Waychunas, G.A., Rea, B.A., Fuller, C.C., Davis, J.A., 1993. Surface chemistry of ferrihydrite: Part 1. EXAFS studies of the geometry of coprecipitated and adsorbed arsenate. Geochim. Cosmochim. Acta 57: 2251–2269.

Wielinga, B., Bostick, B., Hansel, C.M., Rosenzweig, R.F., Fendorf, S., 2000. Inhibition of bacterially promoted uranium reduction: ferric (hydr)oxides as competitive electron acceptors. Environ. Sci. Technol. 34(11): 2190-2195.

Widdel, F., Schnell, S., Heising, S., Ehrenreich, A., Assmus, B., Schink, B., 1993. Ferrous iron oxidation by anoxygenic phototrophic bacteria. Nature 362(6423): 834-836.

Wightman, P.G., Fein, J.B., 2005. Iron adsorption by *Bacillus subtilis* bacterial cell walls. Chem. Geol. 216: 177-189.

Wilkie, J. A., Hering, J. G., 1996. Adsorption of arsenic onto hydrous ferric oxide: Effects of adsorbate/adsorbent ratios and cooccurring solutes. Colloids Surf., A 107: 97-110.

Williams, A.G.B., Scherer, M.M., 2004. Spectroscopic evidence for Fe(II)-Fe(III) electron transfer at the iron oxide-water interface. Environ. Sci. Technol. 38: 4782-4790.

Yeghicheyan, D., Carignan, J., Valladon, M., Le Coz, M. B., Le Cornec, F., Castrec-Rouelle, M., Robert, M., Aquilina, L., Aubry, E., Churlaud, C., Dia, A., Deberdt, S., Dupr, B., Freydier, R., Gruau, G., Henin, O., de Kersabiec, A. M., Mace, J., Marin, L., Morin, N., Petitjean, P., Serrat, E., 2001. A compilation of silicon and thirty one trace elements measured in the natural river water reference material SLRS-4 (NRC-CNRC). Geostand. Newslett- J. Geostand. Geoanal. 25: 465-474

Zachara, J.M., Kukkadapu, R.K., Fredrickson, J.K., Gorby, Y.A., Smith, S.C., 2002. Biomineralization of poorly crystalline Fe(III) oxides by dissimilatory metal reducing bacteria (DMRB). Geomicrobiol. J. 19: 179-207.

Zachara, J.M., Fredrickson, J.K., Smith, S.C. Gassman, P.L., 2001. Solubilization of Fe(III) oxide-bound trace metals by a dissimilatory Fe(III) reducing bacterium. Geochim. Cosmochim. Acta 65(1): 75-93.

Zhang, Y., Charlet, L., Schindler, P.W., 1992. Adsorption of protons, Fe(II), and Al(III) on Lepidocrocite (g-FeOOH). Colloids Surf. 63: 259–268.

Zobrist, J., Dowdle, P.R., Davis, J.A., Oremland, R.S., 2000. Mobilization of arsenite by dissimilatory reduction of adsorbed arsenate. Environ. Sci. Technol. 34(22): 4747-4753.